Compatibility of Seismic Hazard and Risk Calculations with Historical Observations

zur Erlangung des akademischen Grades eines

Doktors der Naturwissenschaften (Dr. rer. nat.)

von der KIT-Fakultät für

Bauingenieur-, Geo- und Umweltwissenschaften

des Karlsruher Instituts für Technologie (KIT)

genehmigte

Dissertation

von

M.Sc. Danhua Xin

aus Dancheng County, Zhoukou City, Henan Province, P.R. China

Tag der mündlichen Prüfung: 25.10.2019
Erster Gutachter: Prof. Dr. Friedemann Wenzel
Zweiter Gutachter: Prof. Dr. Mustafa Erdik

Zusammenfassung

Diese Dissertation befasst sich mit der Bewertung der Modellierung der Erdbebengefährdung und der Schäden durch Vergleich mit historischen Erdbeben und Schadensinformationen. Ina Cecic, Präsidentin der European Seismological Commission, bemerkt dazu: „Ich freue mich zu bemerken, dass wir die Aktivitäten für interdisziplinäre Aufgaben immer weiter ausdehnen und über die „reine“ Seismologie hinaus auf andere Bereiche vordringen, die im wirklichen Leben miteinander verbunden sind. Dies ist besonders wichtig für die Bereiche Bildung und Öffentlichkeitsarbeit, da nur das Bewusstsein für die Gefahren in unserer Umgebung und das Wissen darüber, was zu tun ist, langfristig Leben retten kann.“

In dieser Arbeit wird zunächst ein systematischer Rahmen für die flächenbezogene Bewertung der Qualität der seismischen Gefahrenkarten entwickelt. Seit vielen Jahrzehnten ist die Erdbebengefährdunskarte in den meisten Ländern ein zwingender Bestandteil der Konstruktionspraxis. Anstrengungen zur Beurteilung der tatsächlichen Qualität dieser Karten sind essentiell. Unterschiedliche Metriken und Kriterien werden angewendet und detailliert diskutiert. Ich untersuche diese Frage am Beispiel des Einflußes der Magnituden-Häufigkeit.

Zweitens wurden in den letzten vier Jahrzehnten zahlreiche Forschungsberichte und -dokumente veröffentlicht, die sich mit der Anfälligkeit von Gebäuden für Bodenbewegungen aufgrund von Erdbeben in China befassen, da eine umfassende Bewertung der seismischen Anfälligkeit von Gebäuden eine Schlüsselaufgabe der Erdbebensicherheits- und Schadensbewertung ist. Aus diesem Grund habe ich zuerst 69 Artikel und Dissertationen unter die Lupe genommen und untersuchte die Gebäudeschäden, die durch Erbeben in dicht besiedelten Gebieten entstanden sind. Sie stellen Beobachtungen dar, bei denen die makroseismischen Intensitäten gemäß der chinesischen offiziellen Seismic Intensity Scale bestimmt wurden. Aus diesen vielen Studien werden die mittleren Fragilitätsfunktionen (abhängig von der Makro-seismischen Intensität) für vier Schadensgrenzzustände von zwei am weitesten verbreiteten Gebäudetypen abgeleitet: Mauerwerk und Stahlbeton. Ich habe auch 18 Veröffentlichungen untersucht, die analytische Fragilitätsfunktionen (abhängig von der Spitzenbeschleunigung - PGA) für dieselben Schadensklassen und Gebäudekategorien bereitstellen. Auf diese Weise wird eine solide Fragilitätsdatenbank für seismisch gefährdete Gebiete auf dem chinesischen Festland erstellt, die sowohl auf Intensität als auch auf PGA basiert. Es wird ein umfassender Überblick über die Probleme bei der Bewertung der Fragilität für verschiedene Gebäudetypen gegeben. Ein notwendiger Vergleich mit internationalen Projekten mit ähnlichem Schwerpunkt wird durchgeführt. Basierend auf der neu gesammelten Fragilitätsdatenbank wird ein neuer Ansatz zur Ableitung der Intensität-PGA-Beziehung unter Verwendung der Fragilität als Brücke vorgeschlagen, und es werden optimierte Intensität-PGA-Beziehungen entwickelt. Dieser Ansatz führt zur Verringerung der Streuung in der traditionellen Intensitäts-PGA-Beziehung.

Drittens, für die Risikoanalyse wird der Gebäudebestand, der durch ein Erdbeben gefährdet ist benötigt. Diese Studie entwickelt einen Ansatz einesgeo-kodierten Bestandsmodells für Wohngebäude für das chinesische Festland durch. Hierbei werden die Daten der Volkszählung in einem 1 km × 1 km Rahmen als Proxy benutzt. Zur Bewertung der Modellleistung wird die in diesem Kapitel entwickelte Wohnfläche auf Bezirksebene mit Aufzeichnungen aus dem statistischen Jahrbuch verglichen. Es zeigt sich, dass die in dieser Studie entwickelte Grundfläche nach Bereinigung um einheitliche Baukosten durchaus mit der Grundflächenstatistik von Shanghai vergleichbar ist. Die Anwendung dieses Modells in der Risikoanalyse

des Erdbebens in Wenchuan M8.0 wird ebenfalls durchgeführt. Der auf der Grundlage dieses Expositionsmodells für Wohngebäude geschätzte Gesamtverlust entspricht in etwa dem Verlustwert, der aus Schadensmeldungen auf der Grundlage von Felduntersuchungen abgeleitet wurde. Diese Kongruenzen verdeutlichen die Robustheit des hier entwickelten Wohnungsbestandmodells. Schließlich wird die Schadensabschätzung mithilfe verschiedener Methoden durchgeführt und ein Vergleich mit Schäden angestellt, die aus Schadensmeldungen abgeleitet wurden. Zur Verbesserung des Verlustverteilungsmusters wird die Entwicklung eines regionalen Human Development Indexes vorgeschlagen. Sensitivitätstests werden durchgeführt, um die Auswirkungen jedes Faktors auf die Ermittlung des endgültigen Verlusts zu überprüfen.

Abstract

This thesis focuses on the evaluation of modelling seismic hazard and loss through comparison with historical earthquake and loss information, based on the long recording history and frequent occurrence of earthquakes in mainland China. Efforts are made to calibrate seismic hazard and risk model in a statistical way, and to figure out whether the historical damage information can effectively constrain the predicted results by various models. It's worth to note that, this kind of model calibration is not targeted at damage to individual building caused by specific earthquake, but at damage to groups of buildings in certain research area based on statistical analysis of historical earthquakes.

This work firstly presents a systematic frame for area-based assessment of seismic hazard map performance. Since seismic hazard map has been used in regulating engineering design practice in many countries for many decades, efforts in assessing how well these maps actually perform is essential. Different metrics and criteria are applied and discussed in detail. I study the effect of modelled earthquake sources as compared to historic earthquake sources.

Secondly, to better understand the susceptibility of the current buildings to be damaged in potential earthquake hazards in mainland China, a comprehensive evaluation of building seismic fragility is essential, which is also one key task of earthquake safety and loss assessment. Many research reports and papers have been published over the past four decades that deal with the vulnerability of buildings to ground motion caused by earthquakes in China. Therefore, I first scrutinized 69 papers and theses studying building damage for earthquakes occurred in densely populated areas. They represent observations where macro-seismic intensities have been determined according to the Chinese Official Seismic Intensity Scale. From these many studies the median fragility functions (dependent on intensity) are derived for four damage limit states of two most widely distributed building types: masonry and reinforced concrete. I also inspected 18 publications that provide analytical fragility functions (dependent on peak ground acceleration - PGA) for the same damage classes and building categories. Thus, a solid fragility database based on both intensity and PGA is established for seismic prone areas in mainland China. A comprehensive view of the problems posed by the evaluation of fragility for different building types is given. Necessary comparison with international projects with similar focus is conducted. Based on the newly collected fragility database, a new approach is proposed in deriving intensity-PGA relation by using fragility as the bridge and reasonable intensity-PGA relations are developed. This novel approach may allow to decrease the scatter in traditional intensity-PGA relation development, i.e., by further classifying observed macroseismic intensities and instrumental ground motions based on difference in building seismic resistance capability.

Thirdly, after the construction and evaluation of seismic hazards and the vulnerability of buildings to these seismic hazards, an evaluation of the currently exposed building stock value is also necessary. Therefore, a high-resolution residential building stock model for mainland China is further developed, by disaggregating administrative level census data into 1km×1km scale using population as the proxy. For evaluation of the model performance, floor area in districts of Shanghai developed in this study is compared with records from statistical yearbook. It turns out that, with certain adjustment the district level floor area developed in this study is quite consistent with that recorded in Shanghai statistical yearbook. Provincial level comparison of the modelled building stock value with that modelled in previous studies also validates the reliability of the model developed in this study. Furthermore, an application of the modelled

results in loss assessment of 2008 Wenchuan M8.0 earthquake is also conducted. The overall estimated loss based on the modelled residential building stock is quite approximate to the loss estimated from damage reports, which are based on field investigation and considered to be the most reliable source of damage information. These congruences convincingly validate the robustness of the residential building stock model developed here.

Finally, based on the hazard map constructed for Shanxi Rift System in Northern China, the vulnerability databased collected by extensive review of previous studies, and the country-wide building stock model developed, loss estimations in terms of both single earthquake scenario and multi-scenario are performed by using empirical method (using the macro-seismic intensity map as the hazard input) and analytical method (using the instrumental ground motion records as the hazard input). For single earthquake scenario, loss estimation results and distribution pattern are compared with that derived from damage reports based on post-earthquake field investigations. For multi-scenario based probabilistic loss, comparison is made between loss estimated from analytical method and from empirical method. Sensitivity tests of estimated loss to input parameters of the loss modelling chain are also conducted, e.g. by changing the parameters in hazard map construction, exposure model development and quantifying the consecutive change on modelled loss.

Acknowledgements

The four-year PhD study is approaching the end. For me it's the time to give a backward glance to the experiences during my stay here in Germany. Like water under the bridge, most trivial matters in daily life just showed up and gone with the wind. Luckily, there are also precious moments that will not fade away with time and will continue to affect my future style of work and study as well as my attitude towards life…

Time really flies! Four years ago, I went abroad for the first time and arrived at Karlsruhe all alone. Then my new journey in "seismic hazard assessment and loss estimation" began in Geophysical Institute of Karlsruhe Institute of Technology . At that time, I was a complete novice in this research area and also had quite limited training in how to do research. The old saying from the book "the Doctrine of the Mean" in China goes that "For doing research, one should read extensively, inquire prudently, think carefully, distinguish clearly and practice earnestly". With this philosophical thought as the guideline and under the supervision of Prof. Wenzel, I embarked on the road of my PhD research and dived into the ocean of knowledge from geology, seismology, structure engineering, economy and insurance industry. During this four-year's study, the achievements summarized in the Introduction chapter will not be possible without the patient supervison from Prof. Wenzel and Dr. James Daniell and the help from my collegue Frau Dick.

My sincere thanks first go to Prof. Wenzel. I want to thank you for your decision to accept me as your PhD student. The choice to shift my research direction from inner core to seismic hazard should be the most important decision I've made following my heart. And the support from Prof. Wenzel at the very beginning makes this choice being fruitful. In spite of those many methodologies Prof. Wenzel have formulized for my better understanding of the theory, the way how he supervises and inspires a student will be definitely inherited in my future career. I'm quite impressed by the anecdote that Prof. Wenzel tried to stimulate the courage of a former student to express her own idea by saying something wrong intendedly.

My sincere thanks also go to Prof. Mustafa from Bogaziçi University of Turky. I really appreciate the time he spent on reviewing my thesis and paper. His comments and suggestions also help deepen my understanding of issues related to seismic hazard and risk modelling. His strong and kind support increase my confidence to prepare and defend my PhD work. Additionally, I also want to sincerely thank Prof. Blum, Prof. Kohl, Prof. Andreas, Prof. Stempniewski and Prof. Schilling for being the members of my defense committee and their time spent on reviewing my PhD thesis. Specifically, Prof. Mustafa spared time from his busy schedule and flied all the way from Istanbul to Karlsruhe for my defense. I'm really grateful for his full support.

I want to thank James Daniell for his help in solving those technical difficulties that I encounter and could-not find a way out without his guidance. The advices from James in these cases can always help me out, sometimes it may be just the name a command, e.g. the VLOOKUP command in Excel is quite frequently used after being told to me by James. I also want to thank James for his PhD thesis, which is just like an encyclopedia and helps me so much in understanding the whole set of issues related to seismic loss estimation.

I'm also grateful to help from Hing-Ho Tsang. His short stay in the summer of 2016 helped me to clearly understand the puzzling concepts in seismic hazard assessment. Since for the explanation of some

technical terms, Chinese is the best language for me to understand and Hing-Ho helps clear out many of my puzzles. We've kept in touch since then and I believe this cooperation will be long-lasting.

I also want to thank Dr. Bin Li from Shanxi Earthquake Administration for sharing with me the data in his PhD thesis at the beginning of my PhD research. The importance of these data to me is just like the rice needed to cook meal. How to cook is up to me, but before cooking the rice should be available at first. Out of this reason, I also want to thank Dr. Weijin Xu from China Earthquake Administration for sharing the whole earthquake catalog he declustered for mainland China since 1000 A.D. The help of Shiyuan Wang from Sichuan Earthquake Administration in collection of county-level damage information of Wenchuan earthquake is also sincerely appreciated.

I also want to thank Dr. Hongjun Si from Seismological Research Institute Inc., Japan for accepting me as an intern and offering me the chance to be in charge of practical projects during my three-month exchange study in Tokyo, Japan. In regard of this, I want to specially thank Karlsruhe House of Yong Scientist (KHYS) to provide the research travel grant that covered all my expenses of meals and accommodations in Japan.

Besides research and study, the help and guide from Frau Kerstin Dick has made my stay abroad much easier than imagined. Thank you very much for sharing your travel experiences with me, teaching me German and translating my English abstract! I believe our friendship will continue even if I go back to China and looking forward to your visit to China!

I'm glad to have Shadi there as a good friend during my PhD study. Although we may disagree with each other in minor things, we can always find a way to reach the consensus and help each other out during the research. I'm grateful to Shadi's preparation of my PhD hat, which is designed with full care and mindfulness. Additionally, Mohsan and Sergio have worked hard to simulate the figure of my bicycle and the decoration in front of it, which is really touching, and I'll definitely take your great "artwork" back to China! I also want to thank Andreas Shaefer, Frau Virginia Roth, Frau Molina Cynthia, and Herr Rainer Plokarz for their care and help. Although besides Andreas, the others have left the institute, our time being together here were really warm and enjoyable. I also appreciate the chat with other Chinese colleagues, e.g. Tao Lei, Lingli Gao, Yudi Pan, Tan Qin, Tingting Liu, Lidong Bie and Yan Cai. The information they share within broaded my understanding of the job market in China and serves as good reference for me to locate my next destination in China.

I also want to thank the teachers during my master study in China, who have offered precious help during my application of the PhD position: Prof. Liangshu Wang, Prof. Mingjie Xu, Prof. Tao Wang and Prof. Xiaodong Song. I also want to thank my old friends. Although in these four years I mainly stay in Germany, but encouragements from friends really comfort me a lot especially when I'm tried and feeling frustrated. These friends I want to thank including those I met during my high school, undergraduate and master study, namely Zengxia Zhao, Xiaoxiao Sun, Runlian Pang, Lihua Tan, Ziwen Song, Wen Zhou, Mijian Xu, Lin Shao, Han Xia, Nannan Yang, Yingchun Lu, Liping Xu, Meihua Hao, Kun Wang, Hui Yu.

Finally, I want to thank my father and mother, for adopting me and supporting me to study until today. Without their supportm, I may still stay in the small village where I was born and where most of my childhood peers are still in. And my sister Danjie and brother Danwei, I want to thank you for taking care of yourselves and supporting me in your own way. I want to thank my boyfriend Xianrui Li, for our shared interests in study and life, and for your company from China to Germany, right now and in the future.

Contents

Figure list

Table list

Abbreviations

GMPE	Ground Motion Prediction Equation
PSHA	Probable Seismic Hazard Assessment
DS	structural/non-structural Damage State
LS	Limiting damage State
SA	Spectral Acceleration
PGA	Peak Ground Acceleration
PGV	Peak Ground Velocity
AAL	Average Annual Loss
LEC	Loss Exceedance Curve
UCC	Uniform Construction Cost
CAPRA	Comprehensive Approach to Probabilistic Risk Assessment
GHS	Global Human Settlement
GEM	Global Earthquake Model

Vorwort

In memory of the youth age,

Farewell to the time of being innocent,

Looking forward to the role of being a useful citizen.

Karlsruhe, in Sep. 2019

Danhua Xin

1 Introduction

1.1 Motivation

Increasing loss of human life and property due to earthquakes in past years have increased the demand of seismic risk analysis for people to be better prepared for potential threat. The rapid urbanization and building construction have increased the exposure of people and property to potential earthquake threat in the future. China, as the world's most populous nation, on one hand, is experiencing economic, social and urban change at unprecedented rates. One the other hand, devastating earthquakes have been recorded throughout Chinese history. For example, the Huaxian Mw8.0 earthquake that occurred in 1556 in Shaanxi province, killed an estimated 830,000 people, which is the highest known death toll resulting from an earthquake. To date, three of the top ten deadliest earthquakes and over 40% of all fatalities from earthquakes throughout the world have occurred within mainland China (Wong, 2014). With the centralization and increase of population near urban centers and megacities, earthquakes occur in these places will cause much more damage than in the past. Therefore, the quantification of seismic risk is extremely important.

Seismic risk model can play a key role in the following aspects: (i) to assess the potential seismic hazard and loss for a target area from both deterministic and probabilistic view; (ii) to support the long-term plan for seismic risk mitigation and preparedness; (iii) to prioritize decision making in emergence response and disaster management; and (iv) to optimize retrofitting strategies. Seismic risk modelling results provide the spatial distribution of expected damage and loss to exposed elements in an earthquake of different magnitudes. Key modules to derive such information include (i) hazard: which predicts the ground shaking distribution generated by potential earthquake; (ii) vulnerability: which establishes a relation between hazard and structural damage; (iii) exposure: which evaluates the stock value exposed to potential hazard.

Different researchers have applied different assumptions in modelled the seismic hazard, exposed stock value and their vulnerability. Therefore, uncertainty exists in every step of the risk modelling chain. In this regard, a comprehensive and deep-going understanding of each of these three modules are essential to better optimize the final modelled loss. This also outlines the focuses of this thesis.

As the output of the hazard module, a seismic hazard map predicts the effects of future earthquakes of different magnitudes based on the characterisation of the pattern and frequency of earthquake occurrence in specified sources and the use of ground-motion prediction equations (GMPEs) to quantify how shaking level varies with distance from the hypocentre. Seismic hazard map has been used for many decades as a tool to set the codes and standards for the structural design of buildings and infrastructure in many countries. Although hazard maps are used worldwide in making costly policy decisions for earthquake-resistant construction, whilst how well these maps actually perform is unknown (Brooks et al., 2016). In addition, there is no established formal procedure or standard for checking whether the hazard model is a reasonable reflection of the reality or not (Mak and Schorlemmer, 2016; Musson, 2004). Meanwhile, the "unexpected" occurrences of ground motions in the low hazard zones indicated by the PSHA map in a number of past earthquakes have triggered arguments and rebuttals on the performance of PSHA predictions (Frankel, 2003, 2013a, 2013b; Gülkan, 2013; Hanks et al., 2012; Stein et al., 2003, 2011, 2012, 2013; Stirling, 2012). In this regard, a systematic frame to conduct an area-based evaluation of the

performance of seismic hazard map will be explored and presented first in this thesis by using a long historical earthquake catalogue occurred in the test region of Shanxi Rift System of Northern China.

In the vulnerability module, the susceptibility of structure to ground shaking is depicted by a fragility curve. Building fragility curves, defined as expected probability of exceeding specific building damage state under given earthquake ground shaking, have been developed for different typologies of buildings. They are required for the estimation of fatalities and monetary losses due to building structural damage in seismic risk analysis. However, the application of the existing fragility curves has been considered as a challenging task, since different approaches and methodologies are spread across scientific journals, conference proceedings, technical reports and software manuals, hindering the creation of an integrated framework that could allow the visualization, acquisition and comparison between all the existing curves (Maio and Tsionis, 2015). In this regard, a comprehensive review of the available fragility curves that specially developed for Chinese buildings from 87 papers and thesis will be performed.

As to the exposure module, the modelling of building stock value and its spatial distribution across China is not readily available at high-resolution (e.g. 1km×1km scale). In those published studies related to building stock model development, e.g. Yang and Kohler (2008) and Hu et al. (2010), the simulation and evolution of building stock value (taking the mainland China as a whole) were designed and targeted for resource consumption and environmental impacts purposes, which cannot meet the needs of catastrophe modelling in risk analysis due to their coarse resolution. International projects e.g. PAGER (Jaiswal et al., 2010) and Gunasekera et al. (2015) also conducted global exposure modelling that covered the building stock value in mainland China. However, these global models cannot fully make use of the census data available in each country and usually assuming a uniform distribution of building stock value per capita for each province or even for each country, which might be convenient, but not realistic, especially for unevenly developed countries like China. Furthermore, the extent of the natural hazards, in most cases, are dependent on the geological structure (earthquakes) or along the riverside (floods), instead of being restricted to administrative boundary. In this regard, to better cope with this spatial mismatch between natural hazards and administrative boundary, a geo-coded building stock model with resolution of 1km×1km will be established and evaluated for mainland China.

After getting all the ingredients from hazard, vulnerability and exposure module ready, seismic loss estimations from both deterministic and probabilistic view are performed using techniques based on different ground motion indicators (namely macro-seismic intensity, peak ground acceleration, spectral acceleration and spectral displacement) and using various descriptions of monetary loss (e.g. net loss, gross loss, direct loss, indirect loss). One way to check the reasonability of seismic loss models is by comparison with real losses derived from post-earthquake surveys. However, a common problem in real loss values is that, for small earthquakes, the scattering of loss values is large; while for large earthquakes, the chance of its occurrence is very rare, thus hindering people to rely on each specific earthquake to calibrate the modeled loss, especially the multi-scenario based probabilistic loss. In this case, damage information of historical earthquakes is resorted to, to calibrate the losses estimated by different scholars and agencies. China has a long history of recording historical devastating natural disasters including major losses during earthquakes and associated secondary events, which can be dating back to 1831 B.C. (Gu, 1989). Such a lengthy data collection can be found only in a small number of places throughout the world and is of tremendous importance to seismologists, builders, engineers and economists. Based on this bunch of damage information, Daniell (2014) developed an empirical loss function for mainland China during his PhD study. The advantage of this loss function compared with others is its normalization of historical loss with socio-economic indicator (e.g. Human Development Index) and its calibration of damage functions

of previous events to relate to the present conditions. Therefore, the loss estimated based on the empirical loss function developed in Daniell (2014) will be used to evaluate losses estimated purely from modelled parameters. In this regard, a series of sensitivity tests will also be conducted from both deterministic and probabilistic view.

1.2 Achievement of this thesis

Hazard and loss estimation rely on models that are based on many (more or less) coarse assumptions. Measuring hazard and risk models against historic observations is rarely done but should be considered highly relevant as otherwise we simply have to believe in the models. Since the assessment of seismic loss requires three layers of information: hazard, exposure and vulnerability. Hazards refer to the occurrence probability of various natural disasters. Exposure captures the attributes of all exposed elements in terms of value, location and relative importance (e.g. critical facilities and infrastructure) to potential hazards. Vulnerability describes the susceptibility of those exposed elements to different hazards. Deep-going studies are conducted in each of these parts.

With focus on the Shanxi Rift System in Northern China, a new methodology is developed – based on an old idea – to check modelled hazard against the historic earthquake catalogue for various return periods, including a comparison with other hazard map performance evaluation methods found in the literature.

To have a thorough understanding of the susceptibility of exposed building property to potential seismic hazards, 87 recent papers and theses on fragility curves for major building types in mainland China are scrutinized, partly from field damage observations, partly from analytic evaluations. Compilation of these many papers provides a sound estimate of fragility curves for Chinese residential building stock available including their uncertainties. In addition, a noval approach is proposed to develop the relationship between Peak Ground Acceleration and macro-seismic Intensity based on the compiled fragility database. This part of work is submitted to *Natural Hazards and Earth System Sciences*.

Another important achievement of this study is the development of a country-wide exposure model for mainland China on a 1x1 km grid size from census data issued by the Chinese government. Comparisons of the modelled results with records from yearbook and from previous studies reveal the robustness and reliability of the exposure developed in this study. Most importantly, this model can be flexibly combined with seismic hazard map to assess potential risk and can be conveniently updated with the availability of new data.

Finally, modelled losses are evaluated based on comparison with the actual damage reports from post-earthquake investigations and based on the processing of the long-lasting records of damage information in mainland China, from both deterministic and probabilistic view.

1.3 Structure of this thesis

The thesis is structured as follows:

Chapter 1 briefly describes the motivation of this study; the contributions being achieved and the organization structure of this thesis.

In Chapter 2, an area-based test of seismic hazard maps is conducted to trade time with space by using a long historical earthquake catalogue, from which a database of peak ground acceleration (PGA) values was generated. Since seismic hazard map has been an element of good engineering design practice in modern countries for many decades. Efforts in assessing how well these maps actually perform is essential. Problems in current hazard map performance evaluation studies are summarized and discussed in detail. Different performance evaluation metrics and criteria are applied. In general, Chapter 2 presents a systematic frame for assessment of seismic hazard map performance.

In Chapter 3, a literature review of the currently available building fragility analysis for major building types in China is conducted by collecting information from hundreds of papers, thesis, book, reports, conference proceedings etc. From these many studies the median fragility functions (dependent on intensity and PGA) are derived for four damage limit states of two most widely distributed building types: masonry and reinforced concrete. A solid fragility database based on both intensity and PGA is thus established for seismic prone areas in mainland China. A comprehensive view of the problems posed by the evaluation of fragility for different building types is given. Necessary comparison with international projects with similar focus is conducted. Based on the newly collected fragility database, a new approach is proposed in deriving intensity-PGA relation by using fragility as the bridge and reasonable intensity-PGA relations are developed.

In Chapter 4, to better serve the risk analysis targeted at near-real-time post-earthquake mitigation and pre-earthquake allocation, an approach to develop the geo-coded grid-level residential building stock model for mainland China is introduced in detail, which is accomplished by disaggregating administrative level census data into 1km×1km scale using population as the proxy. Provincial-level based comparison of the modelled results with that from previous studies has achieved good consistency. For further evaluation of model performance, district level residential floor area developed in study is compared with records from statistical yearbook and high compatibility is observed. Finally, application of the modelled results in risk analysis by assuming the recurrence of 2008 Wenchuan Ms8.0 scenario earthquake further validates the robustness and reliability of the model. Additionally, limitations and future optimization direction are also outlined.

Chapter 5 performed the assessment of seismic loss by employing the hazard scenarios in Chapter 2, vulnerability curves in Chapter 3 and the residential building stock model developed in Chapter 4. The loss assessment was performed both for single scenario earthquake and for multi-scenario earthquakes by using empirical method and by analytical method. Sensitivity tests to quantify the sensitivity of estimated loss to parameters in hazard/vulnerability/exposure module were performed. Optimization direction for future loss assessment was also given. Sensitivity tests to figure out the impacts of input components on final estimated loss were discussed in detail as well.

Chapter 6 gives a summary of the work in this thesis.

Chapter 7 points out the limitations of this thesis and outlines the future optimization directions.

2 Area-based consistency check of probabilistic seismic hazard maps using historical earthquake records

2.1 Background introduction

2.1.1 Importance of seismic hazard assessment

Estimating the hazard of natural earthquakes is crucial for setting the codes and standards for the structural design of buildings and infrastructure, and more generally, for prioritizing risk mitigation efforts (Sørensen et al., 2012). Hazard maps predict the effects of future earthquakes of different magnitudes based on the characterisation of the pattern and frequency of earthquake occurrence in specified sources and the use of ground-motion prediction equations (GMPEs) to quantify how shaking level varies with distance from the hypocentre. Seismic hazard map has been used for many decades as a tool to display the spatial variation of hazard levels for good engineering design practice in modern countries. It is an integral component in building codes and standards for the design of critical structures such as dams, offshore structures, and nuclear power plants (Atkinson, 2007). Construction of such a hazard map entails multi-disciplinary information spanning from geology, geodesy, paleo-seismology, observed and modelled seismicity, as well as structural dynamics (Ward, 1994, 1995). Seismic hazard of a given location is described as the exceedance probability of various ground motion thresholds that are expected to occur in a given period, via a process called probabilistic seismic hazard assessment (PSHA). The most commonly adopted approach of PSHA was developed by Cornell (1968) and has been widely applied to engineering (e.g. McGuire, 1976, 1995).

2.1.2 PSHA map and its validation

PSHA calculations rely on several models and assumptions, such as the identification of seismic sources, their frequency-magnitude distributions, and the GMPEs (Tasan et al., 2014). There are two different types of uncertainties in the procedure: epistemic and aleatory. Epistemic uncertainties result from inadequate understanding and can be reduced by gathering more data or by refining the models. The logic-tree method is used to assign different weights to multiple models that are considered possible. Aleatory uncertainties are due to the intrinsic variability of nature and can be modelled but not reduced.

Hazard maps are used worldwide in making costly policy decisions for earthquake-resistant construction, whilst how well these maps actually perform is unknown (Brooks et al., 2016). It is not obvious how to validate a probabilistic statement on ground motion exceedance with a return period of 475 years. In addition, there is no established formal procedure or standard for checking whether the hazard model is a reasonable reflection of the reality or not (Mak and Schorlemmer, 2016; Musson, 2004). Meanwhile, the “unexpected” occurrence of ground motions in the low hazard zones indicated by the PSHA map in a number of past earthquakes has led to arguments and rebuttals on the performance of PSHA predictions

(Frankel, 2013a, 2013b, 2003; Gülkan, 2013; Hanks et al., 2012; Stein et al., 2003, 2011, 2012, 2013; Stirling, 2012). In this regard, Iervolino (2013) elaborated in detail why hazard maps cannot be validated by individual earthquakes.

The major obstacle in hazard map validation/confirmation/consistency-check is the incomparability between the short observation time in seismology (around 100 years at maximum for instrumental networks, and several centuries for historical intensity data) and the long recurrence intervals of large earthquakes. In addition, large earthquakes generate ground motions of long return periods which are of engineering interests: several hundreds of years at plate boundary locations and thousands of years or more in continental interiors. As illustrated in Beauval et al. (2008), for a meaningful comparison with a 20% uncertainty level, a minimum observational time window of 12000 years is required for estimating hazards corresponding to a 475-year return period at a single site. Thus, validation of the probabilistic hazard results at a site with actual instrumental records and even with historical intensities is hardly possible.

2.1.3 Area-based test to trade time with space

As the validation of seismic hazard at a site is scientifically impossible because of the short observation time as compared to the seismic cycle, efforts have shifted from validation at a specific site to PSHA map consistency-checks for an entire region. It requires trading time with space by combining multiple sites in space to compensate for the short period of ground motion records at each single site. This area-based technique was first proposed by Ward (1995). The hypothesis is that for a typical PSHA map showing ground motions to be exceeded with 10% probability at least once in 50 years, one should expect that the observed ground motions exceed the calculated threshold in around 10% of the area on the PSHA map. Based upon this assumption, the area-based approach has been adopted in a series of follow-on studies by using historical intensities or instrumental ground motion records (Atkinson, 2007; Brooks et al., 2016, 2017; Fujiwara et al., 2009; Mak and Schorlemmer, 2016; Mezcua et al., 2013; Miyazawa and Mori, 2009; Stirling and Gerstenberger, 2010; Stirling and Petersen, 2006; Tasan et al., 2014).

However, when testing PSHA map performance with actual records, the typically small set of observations makes the conclusion (whether a PSHA model under testing should be rejected by the observation data) very sensitive to minor variations in the observed dataset (Albarello and D'Amico, 2008; Stirling and Petersen, 2006; Tasan et al., 2014). Even though potential uncertainties were carefully considered, the area-based tests of the same PSHA model for the same study region can lead to quite contrasting conclusions even based on the same set of empirical intensity records (Stirling and Petersen, 2006) or instrumental ground motion records (Stirling and Gerstenberger, 2010). According to Mak et al. (2014), this could be due to the insufficient statistical power of the observation record length, which refers to the probability of a test to confidentially reject a PSHA model based on the observational dataset. The statistical power is calculated based on one predefined confidence interval (typically 95%) and two quantities: the ratio of the observed (true) to modelled annual rate of exceedance and the observation time-window length, counted as multiples of the return period. Mak et al. (2014) found out (in their Figure 2) that, even if the discrepancy between the true and the modelled hazard is huge, the use of short time window observations generally leads to a low probability to reveal such a discrepancy, thus leading to a false conclusion that the modelled hazard is consistent with the observation.

In addition to the aforementioned low statistical power of small observational datasets, the influence of the usually unknown site effects, caused by local soil conditions and reflected in the uncertainty of ground motion prediction equations (GMPEs), can significantly degrade the validation/confirmation of PSHA

results (Scherbaum et al., 2004). Another source of misfit, as mentioned in the discussion section of Stirling and Gerstenberger (2010), could be the handling of aftershock-generated ground motions in instrumental records, as aftershocks will almost certainly generate higher number of observed ground motions of lower levels in comparison with the forecasted exceedance rate (Mak and Schorlemmer, 2016). The PSHA methodology models both the occurrences of earthquakes and ground motions at a site as Poisson processes (Beauval et al., 2010), and is achieved by the removal of aftershocks from the earthquake catalogue. Thus, the predicted ground motion exceedance in the PSHA map is related to mainshock activities only, and ground motion records related to aftershocks should also be eliminated before conducting PSHA performance check. In Stirling and Gerstenberger (2010), the removal of aftershock-generated instrumental records led to the non-rejection of the PSHA model. However, in many previous studies, the elimination of aftershock-generated ground motions is either insufficient or simply undone. This is first of all due to the difficulty to differentiate ground motion records relating to mainshocks from those of aftershocks, and secondly, the data volume may shrink by over 50% if aftershock-related ground motions were completely eliminated.

2.1.4 The focus of this chapter

As discussed in the previous subsection, efforts of PSHA map validation/confirmation/consistency-check using historical intensity or instrumental ground motion records are inevitably affected by the short recording history, site effects and aftershocks. In this work, an area-based test of PSHA maps is conducted by using a long historical earthquake catalogue, from which a database of peak ground acceleration (PGA) values was generated. The acceleration database was calculated by combining the declustered historical earthquake catalogue with the same GMPE as used for constructing the PSHA map, to avoid uncertainty in relation to aftershocks and site effects. Thus, the actual occurrence probabilities of PSHA map predictions against probabilistic estimations can be instantly compared. In essence, the areal-based compatibility test is conducted between the PSHA map established based on a specific seismic source model with a specific GMPE and the historical earthquake catalogue only.

The test region chosen is the Shanxi Rift System, China, for which a 550-year and complete catalogue for $M \geqslant 5$ ("M" is the abbreviation of magnitude) earthquakes has been established (Xu and Gao, 2014). The PSHA models, in terms of PGA, were generated using open source software CRISIS2015 (Aguilar-Meléndez et al., 2017) for return periods of 101-year, 475-year, 975-year, 2475-year, corresponding to exceedance probabilities of 39%, 10%, 5% and 2% in 50 years, respectively.

For the construction of the PSHA map, the catalogue of historical earthquake activities was employed to derive the frequency-magnitude relationship of each area and fault source. It is further assumed that the events occur randomly in the source areas and along the faults, whereas the geography or the sequence of earthquakes do not constrain the PSHA prediction. Therefore, the acceleration database generated using the 550-year catalogue can be viewed as relatively independent information (Ward, 1995).

The same GMPE was used for generating the acceleration database from the historical catalogue and for constructing PSHA maps. This allows the full focus on checking the impacts of the catalogue-length and detecting the difference in the seismicity pattern on the performance of PSHA maps with different return periods.

2.2 Acceleration database construction

The Shanxi Rift System, located in the west of the North China Plain and in the east of the Ordos Block, is one of the most seismically active zones in China. The 1556 Huaxian M8.3 earthquake that caused over 800,000 fatalities, the deadliest known earthquake in human history, occurred there. Seismic hazard assessment for the Shanxi Rift System and its neighbouring areas was conducted in several studies previously (Li, 2015; Li et al., 2017; Liu et al., 2013; Xie et al., 2011). In this study, PSHA maps were constructed using the open source software CRISIS2015 (Aguilar-Meléndez et al., 2017), based on the work seismic source parameters developed in Li (2015; refer to Table 2 and Table 3 in his submitted paper 4). Generally, fours steps are followed to construct a PSHA map. Firstly, the identification of seismic sources (both area sources and fault sources), which are defined mainly based on geological structure and historical seismicity. Secondly, the frequency-magnitude distribution of earthquakes for each seismic source, modelled as the Gutenberg-Richter (G-R) relationship (Gutenberg and Richter, 1956). Thirdly, the development or selection of GMPE(s), which relates the ground motion at the site of interest to earthquake magnitude, distance to site and local site conditions. Finally, a hazard curve for each specific site can be established with contributions from all seismic sources being integrated.

In the database of Li (2015), the Shanxi Rift System was zoned into 28 area sources and 21 fault sources (Figure 2-1), every one of which was assumed to contain a sufficient number of seismic events for estimating the recurrence parameters required by the probabilistic method. In each seismic source, only M $\geqslant$5 earthquakes were used for two reasons. Firstly, multiple studies (Huang et al., 1994a, 1994b; Ren, 2011; Xu and Gao, 2014) suggested that the historical catalogue for M$\geqslant$5 earthquakes in the last 550 years (i.e. 1467-2017) occurred in Northern China is considered complete. Besides, earthquakes with magnitudes lower than 5 generally did not cause serious damage according to empirical observation (Wang et al., 2016), thus those events are of marginal engineering interest.

The maximum earthquake magnitude needs to be pre-defined in CRISIS2015 for each seismic source. For the fault sources, the maximum magnitude was derived from the empirical relationship between fault length (L) and maximum historical magnitude (Leonard, 2010; refer to Table 3 for Mw - L). Maximum earthquake magnitude in each area source was uniformly set as M6, with the assumption that M$\geqslant$6 earthquakes are mainly related to fault sources and earthquakes with M<6 are attributed to area sources as background seismicity. This assumption is based on the fact that previous disastrous earthquakes in the Shanxi Rift System mainly occurred within the fault segments (Figure 2-1).

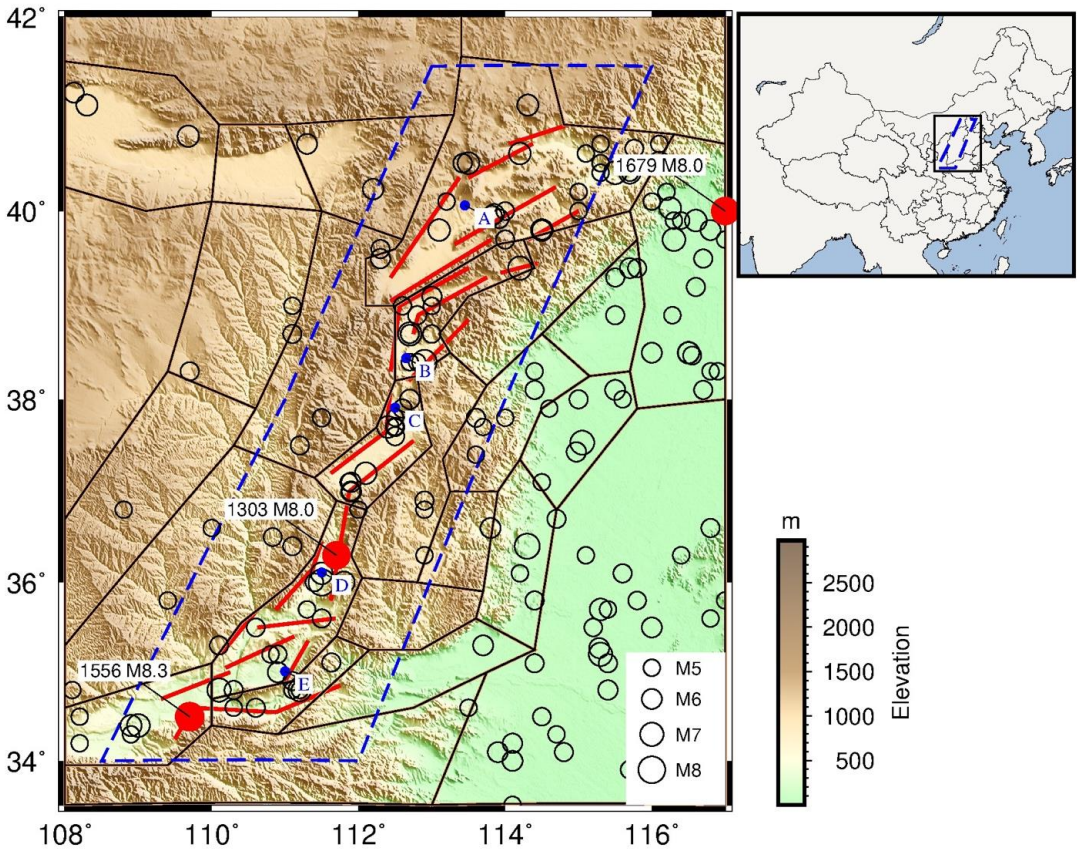

Figure 2-1: Topographic map of the study area modified after Li (2015). The 28 irregular brown polygons are the area sources and the 21 red lines are the fault sources used for generating the PSHA hazard map based on the database of Li (2015). Blue dash parallelogram is the Shanxi Rift System, which defines the range of PSHA map to be generated. The five blue dots (A, B, C, D, E) are the five key cities located in the Shanxi Rift System, namely Datong, Xinzhou, Taiyuan, Linfen and Yuncheng. Black hollow circles are the 150 M≥5 historical earthquakes in the 550-year declustered catalogue compiled by Xu et al. (2014). Among them, the red circles represent three historical M≥8 earthquakes, namely the Hongdong M8.0 earthquake in 1303, the Huaxian M8.3 earthquake in 1556 and the Sanhe-Pinggu M8.0 earthquake in 1679.

The GMPE adopted was taken from Yu et al. (2013; refer to Table 6), which is in terms of PGA and specially developed for the Fifth National Seismic Zonation Map of China that was issued in 2016. It should be kept in mind that GMPEs from other sources are also available, but Yu et al. (2013) was chosen to ensure that the same GMPE was used for generating the PSHA map and for constructing the acceleration database based on the historical catalogue. By doing this, the statistical uncertainty due to the misfits in relation to site amplification can be avoided. Hence, the focus could be put on the impact of catalogue-length and the difference in the seismicity pattern on the performance of PSHA maps with different return periods. The G-R relations of the 550-year historical catalogue and of the seismic source model for generating the PSHA maps are given in Figure 2-2, which will be discussed in detail in Section 2.5.1.

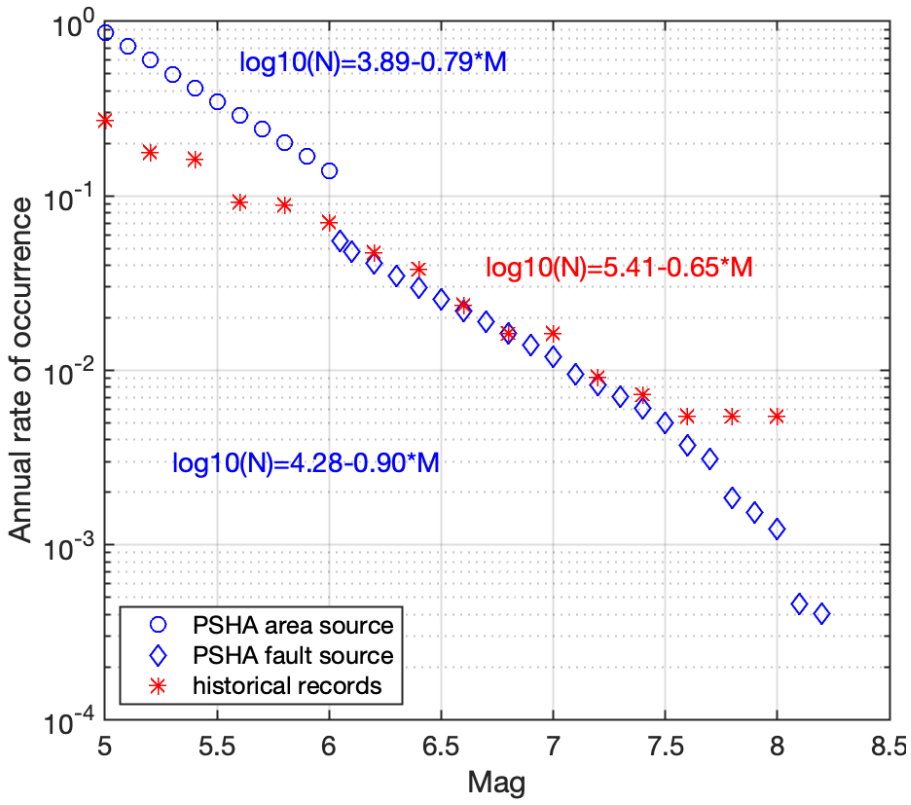

Figure 2-2: G-R relations of the 550-year historical catalogue (red) and of the seismic sources (both area source and fault source) adopted in PSHA construction (blue).

Finally, based on the source model parameters from Li (2015) and the GMPE from Yu et al. (2013), four PSHA maps in terms of PGA were constructed with 39%, 10%, 5% and 2% exceedance probability in 50 years. In other words, the PGA thresholds predicted in each map correspond to return periods of 101-year (Figure 2-3(a)), 475-year (Figure 2-4(a)), 975-year (Figure 2-5(a)) and 2475-year (Figure 2-6(a)), respectively.

In order to check the PSHA map performance, an acceleration database was synthetized directly from historical records (hereafter, the historical catalogue-based acceleration database) by using the catalogue compiled by Xu and Gao (2014), which is considered complete for M$\geqslant$5 events in the last 550 years (i.e., 1467-2017) in Northern China. Following the assumption of Poisson distribution that earthquakes occur randomly in time, aftershocks in this catalogue were removed using the well-known method of Gardner and Knopoff (1974), thus, there are only 150 M$\geqslant$5 mainshocks left in the historical catalogue. For simplicity, the depths of seismic source zones in the PSHA model and historical earthquake records were set as zero. It is noteworthy that the PSHA maps constructed in this study are mainly employed to illustrate the methodology but not intended for practical engineering application.

2.3 Methodology

The main focus of this work is to use an area-based method to check the consistency between PSHA maps and the acceleration database generated by the 550-year historical catalogue. This concept of area-based

PSHA map consistency check was first proposed by Ward (1995) and subsequently employed by Stirling and Petersen (2006), Albarello and D'Amico (2008), Fujiwara et al. (2009), Stirling and Gerstenberger (2010), Tasan et al. (2014), Mak and Schorlemmer (2016) and Brooks et al. (2016) based on the use of macro-seismic intensity or instrumental records. The detailed metrics and criteria employed to validate/compare/confirm PSHA performance vary from one study to another. As in previous studies, the basic assumption is also followed in this study that the observed likelihood of exceeding acceleration threshold on a PSHA map, when averaged over an area, should follow in proportion to the theoretically predicted likelihood.

The test region of the Shanxi Rift System was divided into 9501 equal-sized geocells, identified by index i, with dimension of 0.05° ×0.05° (approximately 5km×5km). For instance, at geocell i, the natural logarithmic value of PGA threshold in PSHA map with return period $T_{R1} = 101$ years is expressed as $z_{1,i}$; and likewise *k*=2,3,4 is assigned to return periods $T_{R2} = 475$-year, $T_{R3} = 975$-year, $T_{R4} = 2475$-year, respectively. The annual rate of exceeding PGA threshold $z_{k,i}$ in PSHA map at geocell i by historical catalogue-based acceleration database (using all N_C=150 historical M⩾5 earthquakes within the catalogue length $T_C = 550$-year) can be formulated as:

$$\lambda_{k,i}\left(IM \geq z_{k,i}\right) = \frac{1}{T_C}\sum_{n=1}^{N_C}\left[1 - \Phi\left(\frac{z_{k,i} - g(M_n, R_{i,n})}{\sigma}\right)\right] \tag{2.1}$$

where $g(M_n, R_{i,n})$ is the median logarithmic acceleration generated at geocell i by the n_{th} earthquake with magnitude M_n and distance $R_{i,n}$ (from the epicentre to the geocell); σ is the standard deviation of the GMPE developed in Yu et al. (2013) for Northern China, which is equal to 0.543 in natural logarithmic form; Φ is the normal distribution, indicating the probability that historical earthquake generated acceleration is lower than the PSHA map threshold $z_{k,i}$.

According to the assumption of Poisson distribution, at geocell i, the probability of exceeding PSHA predicted ground motion $z_{k,i}$ by historical catalogue-based acceleration database within 50-year is:

$$P_{k,i}\left(IM \geq z_{k,i}\right) = 1 - \exp\left[-\lambda_{k,i}\left(IM \geq z_{k,i}\right) \times 50\right] \tag{2.2}$$

For an area-based test, all the N_S geocells are taken as a whole. The average rate of exceeding PSHA map predicted thresholds (that varies across geocells) within 50-year is:

$$\bar{\lambda}_k = \frac{1}{N_S}\sum_{i=1}^{N_S}\lambda_{k,i}\left(IM \geq z_{k,i}\right) \times 50 \tag{2.3}$$

When taking all geocells as a whole, the corresponding average probability of exceedance, instead of averaging the exceedance probability of each geocell directly (which is of no physical meaning), should be derived from the average rate of exceedance $\bar{\lambda}_k$, that is:

$$\bar{P}_k = 1 - \exp\left(-\bar{\lambda}_k\right) \tag{2.4}$$

Strictly speaking there is no such a quantity as average probability in probability theory. For instance, $\bar{P}_k$ in Eq. (4) is not a probability but an estimate of a probability. Estimates can be averaged, whereas probabilities cannot. To avoid cumbersome wording, I stick here and further on to the notion of average probability.

Theoretically, for PSHA map with a return period of 101 years (*k*=1), the PGA threshold at each geocell on the map is expected to be exceeded with 39% probability within 50 years ($39\% = 1 - \exp\left(-50/101\right)$).

For PSHA maps of return periods 475-year, 975-year and 2475-year, the corresponding expected exceedance probabilities are 10%, 5% and 2%, respectively. To avoid confusion, hereafter the term "theoretical exceedance probability" will be restricted to the expected exceedance probability of 39%, 10%, 5% and 2% for PSHA maps with return periods of 101-year, 475-year, 975-year and 2475-year (k=2, 3, 4). Meanwhile, the term "observed exceedance probability" will be restricted to the actual probability of exceeding PSHA predicted ground motion thresholds by historic-record-based accelerations within 50 years.

If the input information (seismic source characterization, G-R relation, GMPE) for generating the PSHA maps were ideal and the historical catalogue was long enough (relative to the return period of the PSHA map considered), the "theoretical exceedance probability" and "observed exceedance probability" would be identical at all return periods. However, in real cases the probabilistic hazard models are never perfect due to the existence of aleatory and epistemic uncertainties, and the length of the historical catalogue is always limited. Therefore, the observed exceedance probability is expected to be reasonably close to the theoretical exceedance probability for short return periods, namely, 39% (101-year) and 10% (475-year), as these return periods are within the range of the catalogue length of 550 years. For long return periods like 975-year and 2475-year, the PSHA results are expected to be over-predicted, i.e. the average observed exceedance probability should likely be lower than the theoretical exceedance probability. Such effect is resulted from the fact that the G-R relation of the PSHA source model is usually derived by extrapolating to magnitude range beyond the empirically observed magnitude range of the historical records.

2.4 Results

The PSHA maps in terms of PGA with return periods of 101-year, 475-year, 975-year and 2475-year are plotted in panel (a) of Figure 2-3, Figure 2-4, Figure 2-5 and Figure 2-6, respectively. These maps show similar color patterns but with different thresholds. In each panel, the maximum ground motion threshold is annotated by its value, namely, 132, 460, 721 and 1109 (unit: cm/s^2) in the four PSHA maps. The PGA values for the five key cities in Shanxi Rift System as well as the maximum and minimum PGA thresholds in each PSHA map are summarized in Table 2-1 and plotted in Figure 2-7.

Table 2-1: The PSHA-predicted PGA values (plotted in Figure 2-7) at the five key cities (indicated by A, B, C, D, E in in Fig. 1) as well as the maximum and minimum PGA values with return period of 101-year, 475-year, 975-year and 2475-year.

City	A	B	C	D	E	Maximum PGA (cm/s^2)	Minimum PGA (cm/s^2)
Longitude	113.45	112.65	112.5	111.5	111		
Latitude	40.06	38.44	37.91	36.11	35.01		
Return Period (year)	PGA (cm/s^2)						
101	58.3	81.6	60.7	132	112	132	10
475	164	271	186	380	343	460	25
975	238	392	275	540	512	721	37
2475	359	578	421	793	794	1109	58

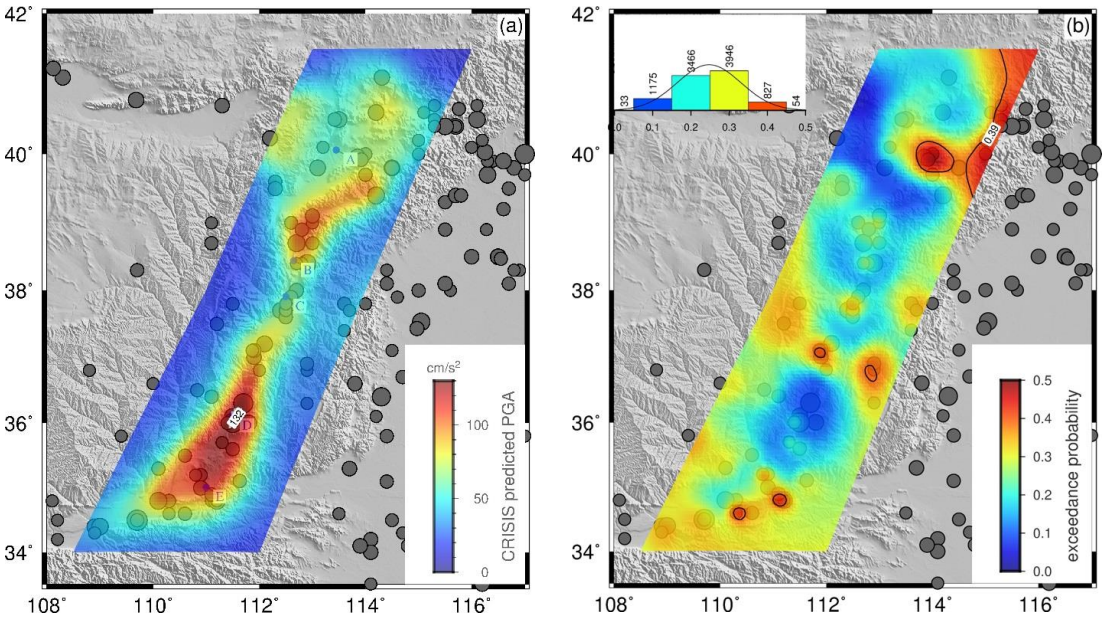

Figure 2-3: (a) PSHA map constructed by CRISIS2015 in terms of PGA with a return period of 101 years (39% in 50 years). The maximum value (132 cm/s^2) is annotated. (b) Distribution of the observed probability of exceeding PSHA-predicted PGA value at each geocell by the historical catalogue-based acceleration database. The black contour line indicates the benchmark exceedance probability of 39%. The histogram in the upper left corner summarizes the number of geocells within each probability range (there are 9501 geocells in total with dimensions of 5km×5km). The black line above the histogram is the corresponding normal distribution curve of these observed exceedance probability. Grey solid circles in both panels are the 150 M≥5 historical earthquakes in the 550-year catalogue.

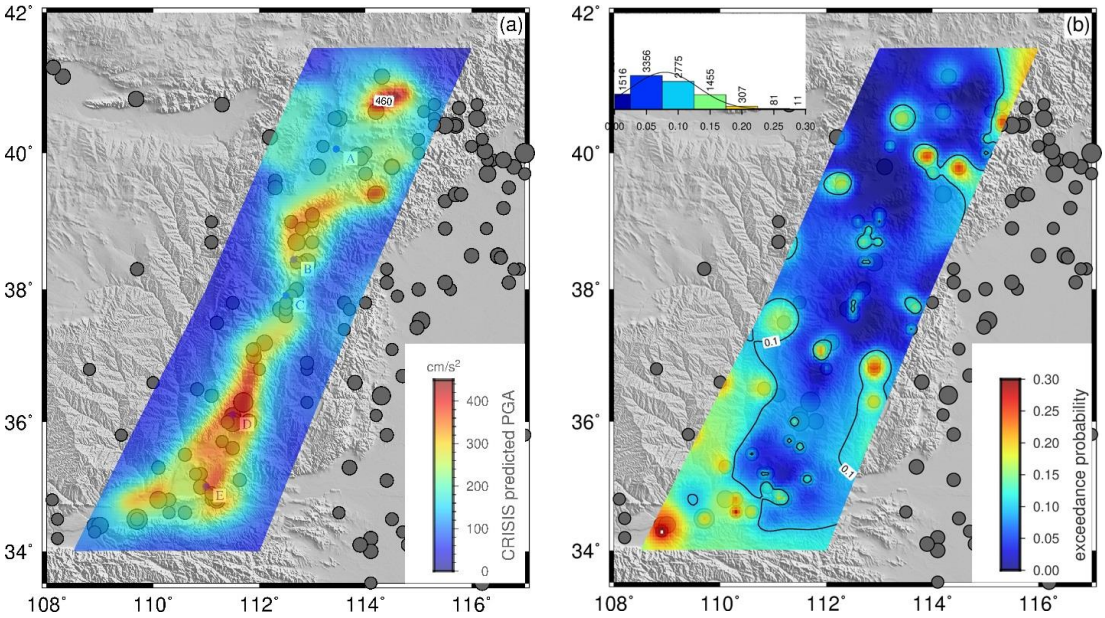

Figure 2-4: (a) PSHA map constructed by CRISIS2015 in terms of PGA with a return period of 475 years (10% in 50 years). The maximum value (460 cm/s^2) is annotated. (b) Distribution of the observed probability of exceeding PSHA-predicted PGA value at each geocell by the historical catalogue-based acceleration database. The black contour line indicates the benchmark exceedance probability of 10%. The histogram in the upper left corner summarizes the number of geocells within each probability range (there are 9501 geocells in total with dimensions of 5km×5km). The

black line above the histogram is the corresponding normal distribution curve of these observed exceedance probability. Grey solid circles in both panels are the 150 M≥5 historical earthquakes in the 550-year catalogue.

The distributions of the observed probability of exceeding PSHA map predicted ground motions within 50 years by the historical catalogue-based acceleration database (calculated by Eq. (2.2)) are shown in panel (b) of Figure 2-3 – Figure 2-6 for the four return periods. It is not surprising to see from these maps that the zones of higher observed exceedance probabilities generally cluster around the locations of historical earthquakes, as the accelerations used to compare with the PSHA map predictions are directly generated from those historical earthquakes. The contour lines in panel (b) of Figure 2-3 – Figure 2-6 represent the theoretical probability of exceeding the PGA threshold in the PSHA map within 50 years, namely, 39%, 10%, 5% and 2%. Ideally, if the PSHA results match perfectly with the predictions from historical records, it would be expected that all the geocells had the same colour as that of the theoretical exceedance probability of 39%, 10%, 5% and 2% in panel (b) of Figure 2-3 – Figure 2-6, respectively. However, it is not possible in reality. The distribution of observed exceedance probability at each geocell is statistically summarized in the histogram in each panel (b) of Figure 2-3 – Figure 2-6. The number above each bar in the histogram indicates the number of geocells within corresponding exceedance probability range. The normal distribution curve based on the observed exceedance probabilities of all geocells is also plotted on each histogram, with the average observed exceedance probability as the expectation value and the standard deviation as the sigma of the normal distribution.

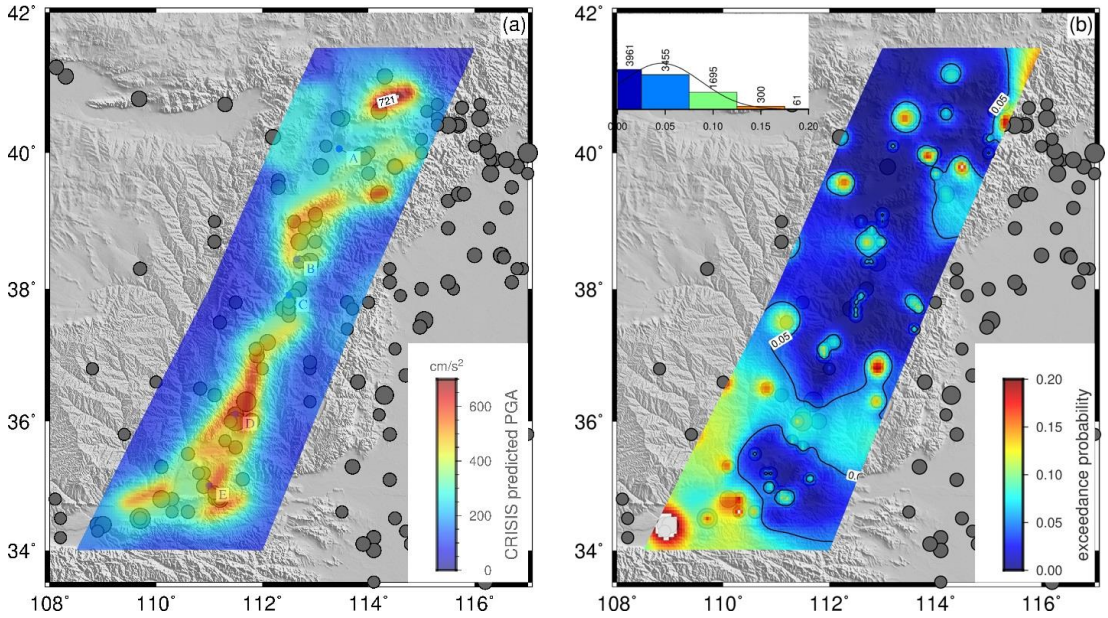

Figure 2-5: (a) PSHA map constructed by CRISIS2015 in terms of PGA with a return period of 975 years (5% in 50 years). The maximum value (721 cm/s^2) is annotated. (b) Distribution of the observed probability of exceeding PSHA-predicted PGA value at each geocell by the historical catalogue-based acceleration database. The black contour line indicates the benchmark exceedance probability of 5%. The histogram in the upper left corner summarizes the number of geocells within each probability range (9472 out of 9501 geocells are included in total for better visualization). The black line above the histogram is the corresponding normal distribution curve of these observed exceedance probability. Grey solid circles in both panels are the 150 M≥5 historical earthquakes in the 550-year catalogue.

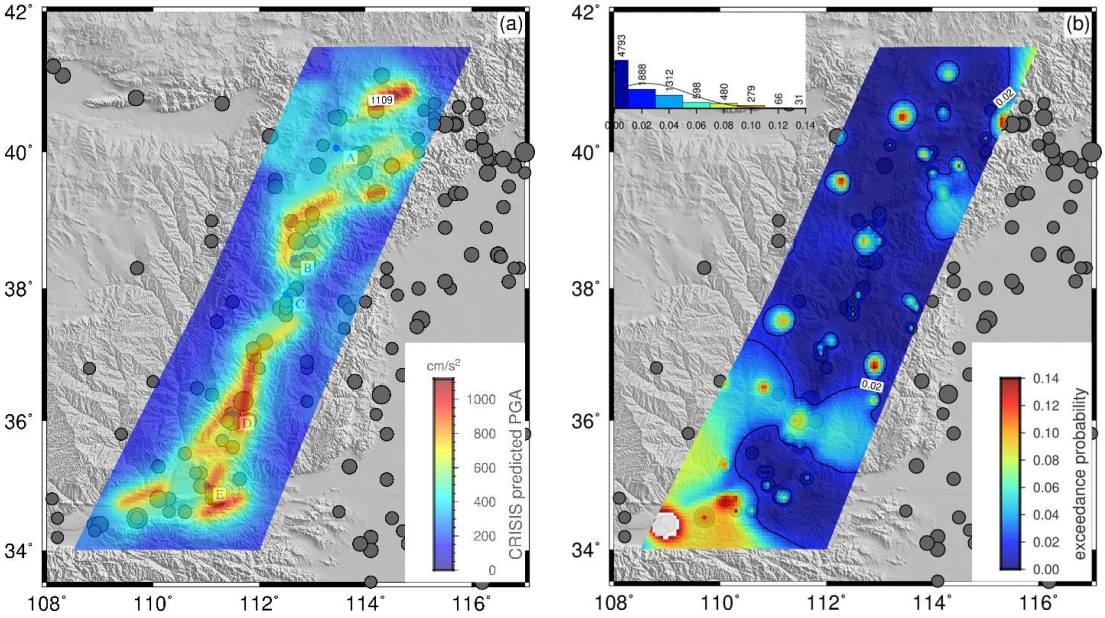

Figure 2-6: (a) PSHA map constructed by CRISIS2015 in terms of PGA with a return period of 2475 years (2% in 50 years). The maximum value (1109 cm/s^2) is annotated. (b) Distribution of the observed probability of exceeding PSHA-predicted PGA value at each geocell by the historical catalogue-based acceleration database. The black contour line indicates the benchmark exceedance probability of 2%. The histogram in the upper left corner summarizes the number of geocells within each probability range (9447 out of 9501 geocells are included in total for better visualization). The black line above the histogram is the corresponding normal distribution curve of these observed exceedance probability. Grey solid circles in both panels are the 150 M≥5 historical earthquakes in the 550-year catalogue.

It is clear from the histogram in panel (b) of Figure 2-3 – Figure 2-6 that, for return period 101-year as shown in Figure 2-3(b), the majority of the geocells have an observed exceedance probability lower than the theoretical exceedance probability of 39%, which indicates the relative over-prediction of the 101-year PSHA map compared with the predictions based on the historical catalogue-based acceleration database. For return period of 475-year as shown in Figure 2-4(b), the observed exceedance probabilities of geocells are more evenly centred around the theoretical exceedance probability of 10% with a slight leftward clustering, as revealed by the expectation value in the normal distribution function. For return period of 975-year as shown in Figure 2-5(b), the average exceedance probability is highly identical to the theoretical exceedance probability of 0.05, whilst the majority of the geocells has an exceedance probability that is obviously lower than the theoretical probability of 0.02 for return period of 2475-year as shown in Figure 2-6(b). However, the expectation value of the normal distribution curve in Figure 2-6(b) is slightly higher than 0.02. This is due to the higher weight of geocells with higher exceedance probability when averaging over the whole study region. The average observed exceedance rate and probability together with the theoretical exceedance rate and probability for each return period are summarized in Table 2-2.

Table 2-2: Area-based PSHA map performance evaluation criteria including average exceedance probability, the metrics M0, M1 proposed in Stein et al. (2015), , the relative metric M2 proposed in this study, and average exceedance rate for statistical power test in Mak et al. (2014).

Return Period (year)	Average Exceedance Rate (year^{-1})		Average Exceedance Probability		M0	M1	M2
	Theoretical	Observed	Theoretical	Observed			
101	0.495	0.290	0.39	0.252	0.038	0.027	7%

475	0.105	0.083	0.10	0.080	0.020	0.003	3%
975	0.051	0.048	0.05	0.047	0.003	0.002	4%
2475	0.020	0.024	0.02	0.024	0.004	0.001	5%

Note: M0, M1, M2 are three metrics used for assessing PSHA map performance. See text for further explanation.

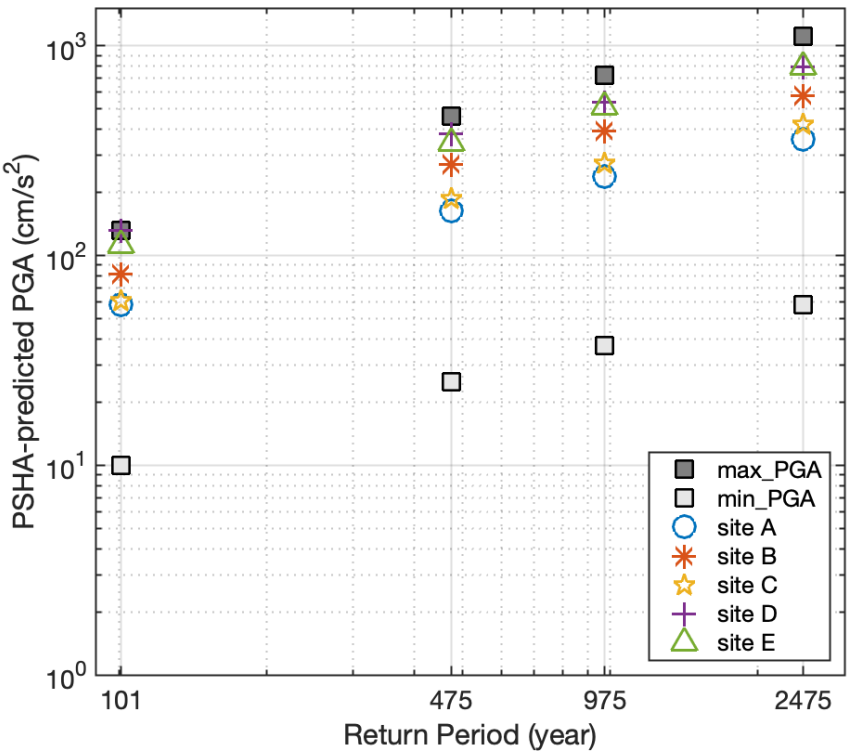

Figure 2-7: PGA values predicted by PSHA for four return periods (101-year, 475-year, 975-year and 2475-year) at the five key cities in the Shanxi Rift System as well as the maximum and minimum PGA predictions in each PSHA map.

2.5 Discussion

2.5.1 Source of discrepancy

As summarized in the area-based result in Section 2.4, compared with historical catalogue-based acceleration database, the PSHA map of 101-year return period is over-predicted and that of 475-year return period is slightly over-predicted. Meanwhile, the PSHA map of 975-year return period is consistent with the acceleration database, whereas the map is slightly under-predicted for 2475-year return period.

One possible explanation for such results is the difference in the earthquake distribution pattern between the seismic source model for PSHA and that implied by the historical records. It is noteworthy that for generating a PSHA map, the dataset of historical earthquake activities was only employed to obtain the frequency-magnitude relation of each area and fault source, whilst the geography or sequence of the earthquakes did not have a role in the PSHA (Ward, 1995). Previous studies on the comparison between probabilistic hazard estimates computed by the source-zone method and by the smoothed seismicity method (Beauval et al., 2006; Goda et al., 2013) indicated that the source-zone method tends to predict

higher probabilities of exceedance at low ground motion thresholds. This may help explain the over-prediction of PSHA map in this study for return periods of 101-year and 475-year. Furthermore, in the typical source-zone method, the effect of large earthquakes, that are capable of generating high levels of ground motions, is smoothed or divided into the whole fault source. This may lead to the fact that PSHA map tends to be under-predicted as compared with the actual accelerations generated by large earthquakes at higher return period (e.g. 2475-year).

In order to verify the explanation above, the frequency-magnitude (G-R) relations are derived and shown in Figure 2-2, both for the 550-year long historical catalogue and for the seismic source model in generating the PSHA maps. The source model includes fault sources and area sources; the G-R relation for $M \geqslant 6$ earthquakes is summed-up from all seismic fault sources and for $5 \leq M < 6$ earthquakes from all area sources. It is clearly seen from Figure 2-2 that, for relatively low magnitude events ($M < 6$), the PSHA source model exhibits higher occurrence frequency, whilst historical catalogue exhibits higher occurrence frequency for larger magnitude events ($M > 7.5$). These discrepancies in the frequency-magnitude relations at the two ends have then led to the over-prediction of PSHA map at relatively short return period (101-year and 475-year, as shown in Figure 2-3(b) and Figure 2-4(b)), and the under-prediction at longer return period (2475-year as shown in Figure 2-6(b)). One may argue that the G-R relation in PSHA is typically extrapolated to the magnitude range beyond the empirical magnitude range of the historical earthquake records, which would lead to over-prediction of the PSHA map at long return periods. In this study, the fact is that the historical catalogue has higher occurrence frequency for $M > 7.5$ earthquakes than in the seismic source model of PSHA, and the PSHA map of return period 2475 on average is under-predicted according to the area-based test (average exceedance probability for 2475-year is lower than its corresponding theoretical probability of 2%, as listed in Table 2-2).

Besides, it is noteworthy that the *b*-value of the G-R relation based on the historical catalogue is obviously too low (b=0.65). Although this is consistent with the findings from Ren et al. (2011), in which low *b*-values were also found in other regions of China, it remains an option that the historical catalogue at $M \geq 5$ level is not as complete as expected for the test region, despite the claims made in Xu and Gao (2014), Huang et al. (1994a, 1994b) and Ren (2011).

2.5.2 Varying criteria in assessment of PSHA map performance

As summarized in Table 2-2, according to the area-based test of using average probability as the indicator, PSHA map is over-predicted compared with the acceleration database based on the historical catalogue for return periods of 101-year and 475-year; but it is slightly under-predicted for return period of 2475-year and consistent at 975-year return period. Possible sources of discrepancies were discussed in Section 2.5.1. The next question is: Would the assessment conclusion of the over-/under-prediction of PSHA map change when other judgement criteria are used? Since in previous studies, various criteria/metrics have been proposed and applied in evaluating PSHA map performance (e.g. Albarello and D'Amico, 2008; Fujiwara et al., 2009; Mak and Schorlemmer, 2016; Tasan et al., 2014; Ward, 1995).

These methods can be briefly categorized into three types: the area-based metric type (Brooks et al., 2016, 2017; Stein et al., 2015), the fit of the 95% confidence interval or two-tail test type (e.g. Mak and Schorlemmer, 2016; Stirling and Gerstenberger, 2010; Stirling and Petersen, 2006; Tasan et al., 2014) and the likelihood method type, which is to pick up the most probable PSHA model based on actual observation (e.g. Albarello et al., 2015; Albarello and D'Amico, 2008). Beyond these methods, Mak et al. (2014) also

proposed the concept of statistical power to reveal how confident a PSHA model can be rejected by observational data.

Therefore, in the following part, metrics proposed by Stein et al. (2015) with certain modification are selected and will be firstly applied to illustrate an alternative way in assessing the performance of the PSHA maps. Then, the statistical power test proposed by Mak et al. (2014) will be performed to further figure out how "powerful" that the PSHA map can be concluded as inconsistent with the acceleration database generated from the historical catalogue.

2.5.2.1 Metrics in Stein et al. (2015)

The metric $M0 = |f - p|$ proposed in Stein et al. (2015) was firstly applied, where p refers to the theoretical probability of exceeding PSHA map predicted PGA thresholds within 50 years, namely 39%, 10%, 5% and 2% for return periods of 101-year, 475-year, 975-year and 2475-year, respectively; f is the average observed probability of exceeding PSHA map predicted accelerations by historical catalogue-based accelerations in 50 years, as calculated from Eq. (2.1)-(2.4) and listed in Table 2-2. Actually, the metric $M0$ is similar to the area-based criteria in Section 2.5.1 by comparing theoretical exceedance probability with average observed exceedance probability for each return period. The derived $M0$ values are listed in Table 2-2 for 5km×5km dimension geocells. As can be seen that, if $M0$ is used as the metric to assess the PSHA map performance, the discrepancy between PSHA map and historical catalogue-based acceleration database basically decreases with the increase in return period.

However, as pointed out in Stein et al. (2015) and Brooks et al. (2016), the limitation of using the metric $M0$ lies in that a map with exceedances at exactly as many sites as predicted ($M0 = 0$) could still significantly over-predict or under-predict the level of shaking, since no spatial variation among geocells are considered. Therefore, they also proposed another metric $M1$, which is defined as the average square misfit between the maximum observed and predicted shaking at each site in the study region. From my point of view, the accelerations predicted in PSHA map are only the thresholds with certain exceedance probability, but not the maximum acceleration for that specific site, as emphasized in Beauval et al. (2010) in a comment on the work of Miyazawa and Mori (2009). Hence, instead of directly comparing PSHA predicted acceleration and the maximum observed acceleration at each of the geocells, I have modified the calculation of $M1$ by measuring the average of square misfit between the observed exceedance probability at each geocell with the corresponding theoretical probability for each return period, namely $M1 = \sum_{i=1}^{N_S} \frac{(P_{k,i}-p)^2}{N_S}$, where $P_{k,i}$ is the observed exceedance probability at geocell i as defined in Eq. (2.2) and p has the same meaning as that in metric $M0$. The $M1$ values are also listed in Table 2-2 for 5km×5km dimension geocells.

Based on $M1$, the misfit between PSHA map predictions and historical catalogue-based accelerations also decreases with the increase in return period. The discrepancy for the return period of 101-year remains to be the largest.

Both $M1$ and $M0$ metrics indicate that the absolute discrepancy for the return period of 101-year seems to be much higher than that for the other three return periods. However, the theoretical probability of exceeding PSHA acceleration thresholds within 50 years actually decreases rapidly with the increase in return period, e.g. from 39% of 101-year to 2% of 2475-year. Thus, a more reasonable quantification metric for calibrating the discrepancy between the PSHA map and the historical catalogue-based accelerations should also take such rapid decrease of theoretical exceedance probability into consideration. Therefore, a third metric $M2 = M1/p$ is proposed, which measures the spatial variation of exceedance probability

misfit relative to the corresponding theoretical probability. The values of $M2$ are also listed in Table 2-2 for 5km×5km dimension geocells. From the changes of $M2$, it is clear that the discrepancy between PSHA map and historical records generated acceleration databases, although remains the largest for 101-year, but not that exaggerated compared with other three return periods.

So far, the discrepancies measured by the metrics above are all in terms of exceedance probability, which might be less straightforward for cross-comparison compared with using ground motion as the indicator. Therefore, to better illustrate how far the PSHA predictions deviate from the historical catalogue-based accelerations, the difference in PGA between PSHA map and historical catalogue-based acceleration databases are roughly derived. This is achieved by multiplying the maximum PGA thresholds (as listed in Table 2-1 and shown in Figure 2-7) with the values of *M2* for each return period. Finally, the difference in PGA is approximated to be 9, 13.5, 18.6 and 55 (cm/s^2) for return periods of 101-year, 475-year, 975-year and 2475-year, respectively. This difference in terms of the ground motion level can thus provide more direct impression on how far the PSHA predictions deviate from the historical catalogue-based accelerations.

2.5.2.2 Statistical power test in Mak et al. (2014)

Besides the metric method used in Stein et al. (2015) and Brooks et al. (2016, 2017), previous studies (Mezcua et al., 2013; Stirling and Gerstenberger, 2010; Stirling and Petersen, 2006; Tasan et al., 2014) also referred to the confidence interval or one/two tail test to assess the consistency between PSHA map and observation data. This stems from the widely applied assumption that the exceedance rate/frequency of PSHA map predictions follows a Poisson process. Therefore, a Poisson probability density distribution can be established, with the PSHA map modelled hazard (in terms of exceedance rate) as the expectation value. In addition, a confidence interval (e.g. 95%) with an upper-bound exceedance rate and lower-bound exceedance rate can also be determined. In those confidence interval tests, the judgement is made as follows: If the observed rate of ground motion exceedances falls within the boundary of the predefined confidence interval, the model is regarded as consistent with the observation; otherwise, the model is rejected by the observation.

However, as argued in Mak et al. (2014), even if the actual hazard is different from that being modelled, there is still a probability that the observed rate of exceedance does not exceed the boundaries of the confidence interval, thus failing to reveal the discrepancy and generating the false comfort that the PSHA map prediction is consistent with observation. Therefore, they proposed the concept of statistical power test, which is defined as the probability that the PSHA model can be confidently rejected by observation. If the statistical power is over 90%, then the discrepancy between modelled hazard and observed hazard is obviously high and the PSHA model is considered to be rejected by observation data.

To conduct the statistical power test, three parameters are needed: the ratio of the observed to the modeled annual rate of exceedance, the historical earthquake records length (accumulated over all observed sites) and the range of confidence interval (here 95% is used). The average observed exceedance rates for each return period (as defined in Eq. (2.3)) are given in Table 2-2 for 5km×5km dimension geocells. Correspondingly, the modelled/theoretical exceedance rates for each return period are also given in Table 2-2, which is simply the ratio between observation time window (i.e. 50-year in this study) and each return period, namely 0.5, 0.11, 0.05 and 0.02. It is clear that the ratio between the observed and modelled annual rate of exceedance is unaffected by the length of observation time.

Based on sensitivity tests, the average observed exceedance rate for geocells with coarser resolution (e.g. 25km×25km and 50km×50km) remains the same as that for 5km×5km dimension geocells for each return period. To better illustrate the statistical power test, four coarser PSHA maps with 25km×25km dimension were generated in Shanxi Rift System. Then the statistical test was applied to the 397 geocells with dimension of 25km×25km. Since the historical catalog length is 550-year, the cumulative length of historical records is thus calculated by multiplying 550 with 397 (number of geocells). More calculation details can refer to Mak *et al.* (2014). As shown in Figure 2-8, the area of the shaded region indicates the probability that the observed exceedance rate falls outside of the confidence interval of the theoretical/modelled exceedance rate. The statistical power is defined as the percentage of the shaded area in the Poisson distribution of the observed exceedance rate, which is 100%, 99%, 12% and 53% for return periods of 101-year, 475-year, 975-year and 2475-year, respectively. The higher the statistical power, the higher confidence that the PSHA model can be rejected by the observation. For return periods of 101-year and 475-year, the PSHA maps are rejected by the observation data, given that the statistical power is approaching 100%. For 975-year, the discrepancy between the PSHA map and the observation is quite low; while for 2475-year, it is difficult to draw a conclusion, since the probability to reveal the discrepancy between PSHA map and observation is only of moderate level.

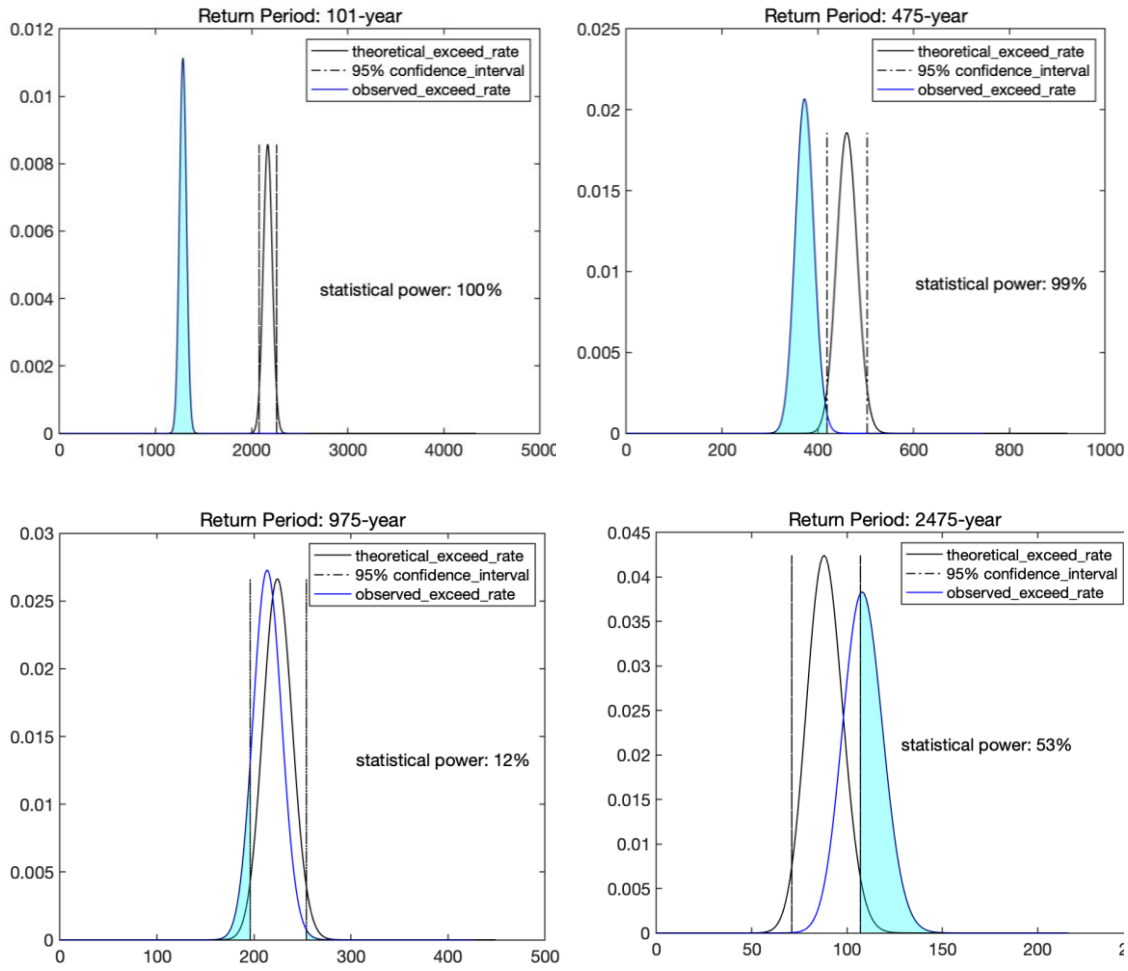

Figure 2-8: Statistical power test based on average exceedance rate for geocells with dimensions of 25km×25km at return periods of (a) 101-year (b) 475-year (c) 975-year (d) 2475-year. Following the assumption of Poisson distribution, the statistical power refers to the probability that the observed exceedance rate (blue curve) falls outside of the

95% confidence interval (black dash-dotted line) of the theoretical exceedance rate (black curve). Mathematically it equals to the area of the shaded region.

However, it should be noticed that the shape of the Poisson distribution in the statistical power test is very sensitive to the cumulative length of records, which is related to the number of geocells used. When the dimension of the observation geocells is further enlarged, e.g. to 50km×50km, and only 105 geocells are available in the research area, then the cumulative length of historical records is 550×105 years. Following the same calculation process as that for 25km×25km dimension geocells, the refreshed statistical power for return periods of 101-year, 475-year, 975-year and 2475-year for 50km×50km dimension geocells is 100%, 59%, 8% and 18% (as shown in Figure 2-9). In this case, only PSHA map for return period of 101-year can be rejected. Consistency between PSHA map for return period of 475-year and the observation turns to be difficult to conclude. PSHA maps of 975-year and 2475-year gain improved probability/confidence to conclude that PSHA map is consistent with observation.

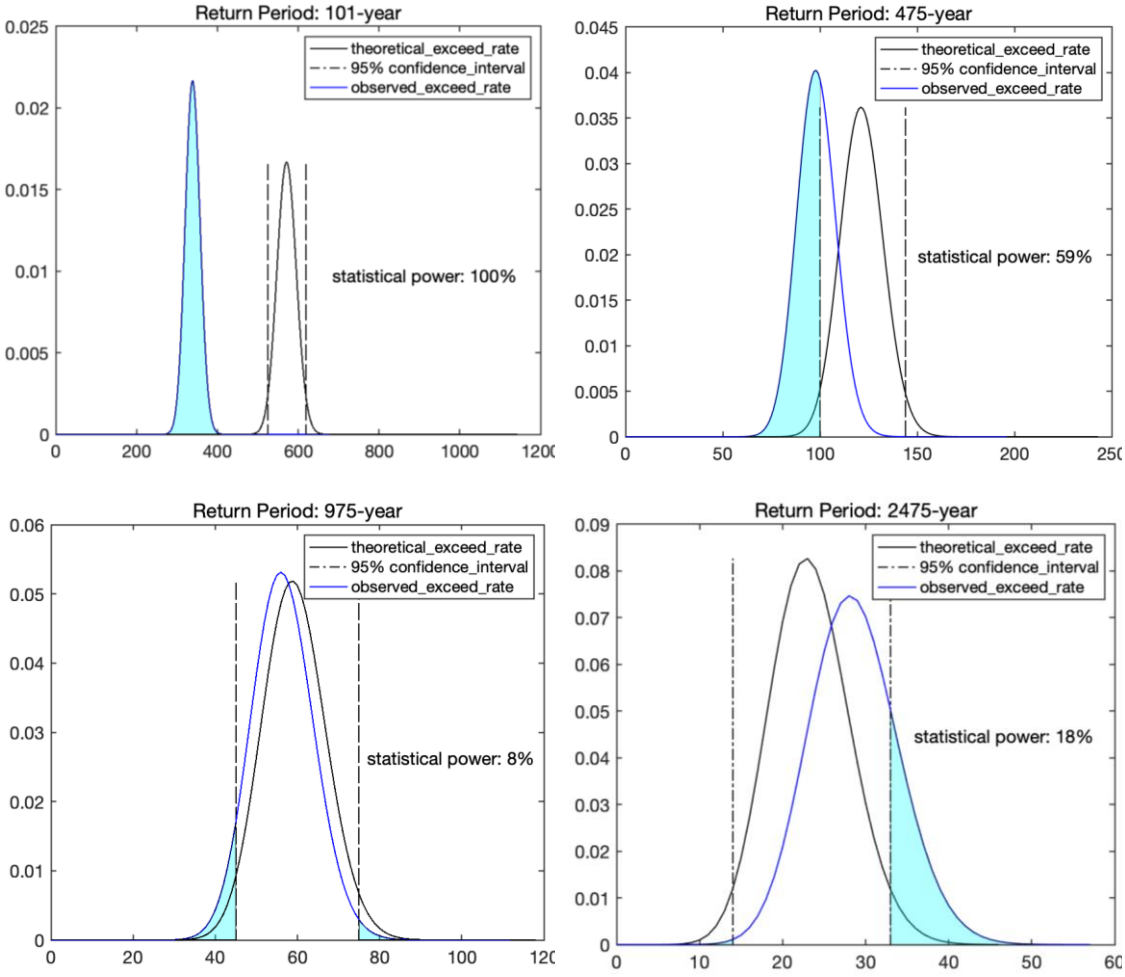

Figure 2-9: Statistical power test based on average exceedance rate for geocells with dimensions of 50km×50km at return periods of (a) 101-year (b) 475-year (c) 975-year (d) 2475-year. Following the assumption of Poisson distribution, the statistical power refers to the probability that the observed exceedance rate (blue curve) falls outside of the 95% confidence interval (black dash-dotted line) of the theoretical exceedance rate (black curve). Mathematically it equals to the area of the shaded region.

Hence, based on the statistical power test for geocells with dimension of 25km×25km and 50km×50km, the shared conclusion is that PSHA map of 101-year is rejected by historical observation; while PSHA map of 975-year is highly consistent with historical observation. For return period 475-year and 2475-year, the consistency between PSHA and historical catalogue-based acceleration database hinges on the dimension/number of the geocells used in PSHA map. Correspondingly in real cases, it depends on the number of observation sites.

2.6 Conclusion

To assess PSHA map performance, an area-based test of PSHA maps was conducted by using a long historical earthquake catalogue, from which a database of peak ground acceleration (PGA) values were generated. The historical catalogue was declustered and the same GMPE was used in construction of the PSHA maps and in generating the historical catalogue-based acceleration database, to avoid uncertainty in relation to aftershocks and site effects and to examine the role of the seismic source model only. Four PSHA maps with 39%, 10%, 5%, 2% exceedance probability within 50-year in terms of peak ground acceleration (PGA) were constructed using CRISIS2015. The PGA thresholds predicted in each map thus correspond to return period of 101, 475, 975 and 2475-year, respectively.

The PSHA map performance was firstly assessed by comparing the theoretical exceedance probability with observed probabilities of exceeding the PSHA predictions by the historical catalogue-based accelerations within 50-year. Histogram of observed exceedance probability for each return period was shown. Representative performance assessment metrics proposed in previous studies, e.g. Stein et al. (2015) were applied with necessary modification. The statistical power test of Mak et al. (2014) were also conducted for geocells with varying dimensions. Generally, PSHA map of return period 101-year has the largest discrepancy with historical catalogue-based accelerations and 975-year the smallest. Possible sources of the discrepancy from seismicity distribution pattern were discussed in detail. A main cause might be related to the difference in frequency-magnitude relation of the 550-year historical catalogue and of the seismic source model used in PSHA map construction. The differences in exceedance probabilities were also approximately converted to differences in PGA values for straightforward cross-comparison.

This work sheds light on the usage of judgement criteria in area-based test to assess PSHA map performance, since the performance of PSHA map hinges on the metric used and may change with the dimension of geocells or number of observation sites. Furthermore, the comparison of PSHA map with historical catalogue-based acceleration database in this study has totally avoided contaminations from aftershocks and from site effects, caused by local soil conditions and reflected in the uncertainty of GMPE. These effects are difficult to handle when testing PSHA maps with actual instrumental records or empirical intensities, but should be dealt with special caution, since they may degrade the conclusion on seismic hazard map's performance, as revealed by the work of Stirling and Petersen (2006) and Stirling and Gerstenberger (2010).

2.7 Data/Code availability

The open source software CRISIS2015 (Aguilar-Meléndez *et al.,* 2017) in calculating PSHA map is available from https://sites.google.com/site/codecrisis2015/home (last accessed July 2019). The seismic source parameters from Li (2015) was provided by Dr. Bin Li through personal request. The historical earthquake catalogue from Xu and Gao (2014) was provided by Dr. Weijin Xu through personal request. Some figures were plotted using Generic Mapping Tools (Wessel and Smith, 1998) from http://gmt.soest.hawaii.edu/home (last accessed July 2019).

3 Review of fragility analyses for major building types in China with new implications for intensity-PGA relation development

3.1 Background introduction

Field surveys after major disastrous earthquakes have shown that poor performance of buildings in earthquake affected areas is the leading cause of human fatalities and economic losses (Yuan, 2008). The evaluation of seismic fragility for existing building stocks has become a crucial issue due to the frequent occurrence of earthquakes in the last decades (Rota et al., 2010). Building fragility curves, defined as expected probability of exceeding specific building damage state under given earthquake ground shaking, have been developed for different typologies of buildings. They are required for the estimation of fatalities and monetary losses due to building structural damage. The development of fragility curves can be divided mainly into two approaches: empirical methods and analytical methods. Empirical methods are based on post-earthquake surveys for groups of buildings and considered to be the most reliable source, because they are directly correlated to the actual seismic behavior of buildings (Maio and Tsionis, 2015). Numerous post-earthquake investigations have been conducted for groups of buildings to derive the empirical damage matrices. A damage matrix is a table of predefined damage states and percentages of specific building types at which each damage state is exceeded due to particular macro-seismic intensity levels. However, as pointed out by Billah and Alam (2015), empirical investigations are usually limited to particular sites or seismo-tectonic/geotechnical conditions with abundant seismic hazard and lack generality. Moreover, they usually refer to the macro-seismic intensity, which is not an instrumental measure but is based on a subjective evaluation (Maio and Tsionis, 2015). By contrast, analytical methods are based on static and dynamic nonlinear analyses of modelled buildings, which can produce slightly more detailed and relatively more transparent assessment algorithms with direct physical meaning (Calvi et al., 2006). Therefore, analytical methods are conceived to be more reliable than empirical results (Hariri-Ardebili and Saouma, 2016). Nevertheless, variations in the different practices of analytical fragility studies, such as selection of seismic demand inputs, use of analysis techniques, characterization of modelling structures, definition of damage states thresholds as well as usage of damage indicators by different authorities, can create discrepancies among various analytical results even for exactly the same building typology. In addition, analytical fragility studies for groups of buildings are computationally demanding and often technically difficult to perform.

Despite the limitations of each fragility analysis method, both empirical and analytical fragility curves are essential in conducting seismic risk assessment. However, the application of the existing fragility curves has been considered as a challenging task, since different approaches and methodologies are spread across scientific journals, conference proceedings, technical reports and software manuals, hindering the creation of an integrated framework that could allow the visualization, acquisition and comparison between all the existing curves (Maio and Tsionis, 2015). In this regard, the first purpose of this study is to

describe and examine available fragility curves, specially developed for Chinese buildings from 87 papers and theses using empirical and analytical methods. The median fragility functions from these previous research findings for the main building types in seismic prone areas in mainland China are then outlined and compared with international projects with similar focus.

Furthermore, based on the empirical and analytical fragility database collected, the second purpose of this work is to propose a new approach in deriving intensity-PGA relation by using fragility as the bridge. The main concern behind this attempt is that intensity-PGA relation is quite essential in seismic hazard assessment, while traditional practices in deriving such a relation are generally region-dependent and have large scatter (Caprio et al., 2015). Traditionally, intensity-PGA relations are developed using instrumental PGA records and empirical intensity observations within the same geographical range. In this chapter, I try to establish intensity-PGA relation using fragility as conversion media. Formally, this is achieved by the elimination of the fragility values from the fragility–intensity and from the fragility–PGA relation. Theoretically, reasonable results should emerge if the building types used in analytic fragility analyses and those investigated in the empirical field surveys are close enough.

This study is organized as follows. In Section 3.1, the necessity of fragility database construction and the pros and cons of main fragility analysis methods are briefly introduced. In Section 3.2, a literature review of fragility studies in mainland China and related concepts are provided. Section 3.3 presents the discrete fragility database extracted from reviewed papers and theses. In Section 3.4, median empirical and analytical fragility curves are derived for major building types in seismic prone areas in mainland China. Comparisons with international projects with similar focuses are also conducted in this section. In Section 3.5, it is introduced in detail the new approach in developing intensity-PGA relation by using fragility as bridge, which is quite comparable with relation developed by traditional practice. In Appendix and Code/Data availability, accesses to supplementary documents mentioned in the context are provided.

3.2 Review of building fragility studies in mainland China

3.2.1 Empirical method

As documented in Calvi et al. (2006), the first application of empirical method to investigate building fragility at large geographical scale was carried out in the early 1970s. In mainland China, since the 1975 Haicheng M7.5 earthquake, around 112 post-earthquake surveys have been conducted for M≥4.7 earthquakes (Ding, 2016). Currently, the main processes in post-earthquake field investigation and macro-seismic intensity determination in mainland China basically follow the workflow proposed by Hu (1988) based on the field work of Tonghai earthquake in the 1970s (Wang et al., 2007). In this workflow, the key concept of “average damage index” is introduced. That means, in each post-earthquake field survey unit (village/town/street), the number of different types of buildings in each damage state are firstly investigated; median damage index of five damage states D5, D4, D3, D2, D1 as defined in GB17742-2008 are used in later on calculation, namely 0.93, 0.70, 0.43, 0.20, 0.05 for these five damage states respectively. For each building type in each field survey unit, the corresponding average damage index is derived by summarizing the products of percentage of building in each damage state and its damage index. Generally, there should be one or two predefined reference building types, thus the average damage index of other surveyed building types can be further scaled to the damage index of the reference building type. In the end, the overall average damage index for each survey unit is calculated by summarizing the products of each

building type's scaled damage index and that building type's weight in the survey unit. Once the average damage index in the survey unit is determined, the corresponding macro-seismic intensity can be directly derived from the predefined empirical relation between macro-seismic intensity and damage index of reference building type (GB17742-2008). In mainland China, currently three reference building types are used to determine macro-seismic intensity: (1) Type A: wood-structure, soil/stone/brick-made old building; (2) Type B: single- or multi-storey brick masonry without seismic resistance; (3) Type C: single- or multi-storey brick masonry sustaining shaking of intensity degree VII. A detailed building structural damage state description for judgement of macro-seismic intensity scale in China is given in Appendix Table A (a non-official translation of the latest version of China seismic intensity scale: GB17742-2008).

Given the importance of building fragility in seismic risk assessment and loss mitigation, in total I reviewed 87 existing fragility analyses from papers and theses for the main building typologies in seismic prone areas in mainland China. It's worth to note that, in Ding (2016), a very detailed collection of empirical fragility database was provided for 112 M≥4.7 events since the 1975 M7.5 Haicheng earthquake based on available post-earthquake surveys. However, due to the lack of building seismic resistance capability information in this database, it is not suitable for the later-on fragility analysis. Thus, I did not use this database and instead collected my own empirical fragility database from individual publications and M.S./Ph.D theses. In mainland China, the main building types of concern are masonry and reinforced concrete (RC) buildings (Sun and Chen, 2009), given the wide distribution of masonry in rural and township areas and the increasing popularity of RC buildings in urban areas. Historical earthquakes that caused serious building damage mainly occurred in seismic prone provinces including **Sichuan** (Chen et al., 2017; Gao et al., 2010; He et al., 2002; Li et al., 2015; Li et al., 2013; Sun et al., 2013; Sun et al., 2014; Sun and Zhang, 2012; Ye et al., 2017; Yuan, 2008; Zhang et al., 2016), **Yunnan** (He et al., 2016; Ming et al., 2017; Piao, 2013; Shi et al., 2007; Wang et al., 2005; Yang et al., 2017; Zhou et al., 2007; Zhou et al., 2011), **Xinjiang** (Chang et al., 2012; Ge et al., 2014; Li et al., 2013; Meng et al., 2014; Song et al., 2001; Wen et al., 2017), **Qinghai** (Piao, 2013; Qiu and Gao, 2015), **Fujian** (Bie et al., 2010; Zhang et al., 2011; Zhou and Wang, 2015) and **other seismic active zones** (A, 2013; Chen, 2008; Chen et al., 1999; Cui and Zhai, 2010; Gan, 2009; Guo et al., 2011; Han et al., 2017; He and Kang, 1999; He and Fu, 2009; He et al., 2017; Hu et al., 2007; Li, 2014; Liu, 1986; Lv et al., 2017; Ma and Chang, 1999; Meng et al., 2012; Meng et al., 2013; Shi et al., 2013; Sun and Chen, 2009; Sun, 2016; Wang et al., 2011; Wang, 2007; Wei et al., 2008; Wu, 2015; Xia, 2009; Yang, 2014; Yin et al., 1990; Yin, 1996; Zhang and Sun, 2010; Zhang et al., 2017; Zhang et al., 2014; Zhou et al., 2013). The main outputs of these post-earthquake surveys are empirical damage probability matrices (DPMs), which can be used to derive the discrete conditional probability of exceeding predefined damage limit states under different macro-seismic intensity degrees. That is, for the DPMs, macro-seismic intensity degree is usually used as the ground motion indicator. In mainland China, detailed definition of each intensity degree is provided in Chinese Official Seismic Intensity Scale GB17742-2008 (see the non-official English translation in Appendix Table A).

3.2.2 Analytical method

As summarized in Introduction section, the main drawback of empirical method lies in the subjectivity on allocating each building to a damage state and the lack of accuracy in the determination of the macro-seismic intensity affecting the region (Maio and Tsionis, 2015). Furthermore, the interdependency between macro-seismic intensity and damage as well as the limited or heterogeneous empirical data are commonly identified as the main difficulties to overcome in the calibration process of empirical approaches (Del Gaudio et al., 2015). By contrast, analytical methodologies produce more detailed and

transparent algorithms with direct physical meaning, that not only allow detailed sensitivity studies to be undertaken, but also allow for the straightforward calibration of the various characteristics of the building stock and seismic hazard (Calvi et al., 2006). Different from the empirical fragility that is directly collected from post-earthquake survey, the derivation of analytical fragility curve is often based on nonlinear fine-element analysis. Popular analytical methods include push-over analysis (Freeman, 1998; Freeman, 2004), adaptive push-over method (Antoniou and Pinho, 2004), and incremental dynamic analysis (IDA) (Vamvatsikos and Cornell, 2002; Vamvatsikos and Fragiadakis, 2010). Within these approaches, most of the methodologies available in literature lie on two main and distinct procedures: the correlation between acceleration or displacement capacity curves and spectral response curves, as the well-known HAZUS or N2 methods (FEMA, 2003; Fajfar, 2000), and the correlation between capacity curves and acceleration time histories, as proposed in Rossetto and Elnashai (2003).

The major steps in using analytical methods to study building fragility include: the selection of seismic demand inputs, the construction of building models, the selection of damage indicator and the determination of damage limit state criteria (Dumova-Jovanoska, 2000). To combine empirical post-earthquake damage statistics from actual building groups with simulated/analytical damage statistics from modelled building types under consideration, quite a few studies deriving analytical fragility curves for masonry and RC buildings in mainland China were examined. The analysis techniques in these studies vary from static push-over analysis or adaptive push-over method (Cui and Zhai, 2010; Liu, 2017), to dynamic history analysis or incremental dynamic analysis (Liu et al., 2010; Liu, 2014; Liu, 2014; Sun, 2016; Wang, 2013; Yang, 2015; Yu et al., 2017; Zeng, 2012; Zheng et al., 2015; Zhu, 2010) as well as based on necessary statistical assumptions (Fang, 2011; Gan, 2009; Guo et al., 2011; Hu et al., 2010; Zhang and Sun, 2010).

3.2.3 Damage state definition

As predefined, building fragility curve describes the exceedance probability of specific damage state given an ensemble of earthquake ground motion levels. To describe the susceptibility of building structure to certain ground motion level, four damage limit states are used: slight damage (LS1), moderate damage (LS2), serious damage (LS3) and collapse (LS4). These four limit states divide the building into five structural damage states, namely negligible (D1), slight damage (D2), moderate damage (D3), serious damage (D4) and collapse (D5). The relation between damage limit states and structural damage states is illustrated by Figure 3-1. Hereafter, fragility curves in this study specifically refer to the probability of exceeding four damage limit states (LS1, LS2, LS3, LS4) under different ground motion levels.

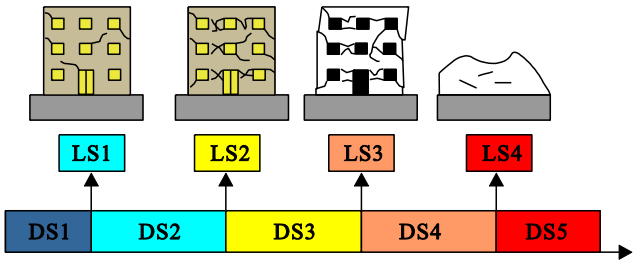

Figure 3-1: Corresponding Relation between structural damage states (DS1, D2, D3, DS4, DS5) and limit states (LS1, LS2, LS3, LS4) (modified from Wenliuhan et al., 2015).

Standard definitions of building structural damage states have been issued in different countries and areas. In the European Macro-seismic Scale 1998 (EMS1998) proposed by European Seismological

Commission (ESC), five grades of structural damage are defined: negligible to slight damage (Grade 1), moderate damage (Grade 2), substantial to heavy damage (Grade 3), very heavy damage (Grade 4) and destruction (Grade 5). In the HAZUS99 Earthquake Model Technical Manual, developed by Department of Homeland Security, Federal Emergency Management Agency of the United States (FEMA) in 1999, generally four structural damage classes are used for all building types: slight damage, moderate damage, extensive damage and complete damage. Other damage state classifications like MSK1969 proposed by Medvedev and Sponheuer (1969) and AIJ1995 (Nakamura, 1995) in Japan issued by Architectural Institute of Japan are summarized in Table 3-1. In mainland China, the latest standard GB17742-2008 was issued in 2008 by China Earthquake Administration (CEA), in which detailed damage to structural and non-structural components are defined for each damage state (Table 3-2).

Table 3-1: Example of major damage states classification methods (modified after Rossetto and Elnashai, 2003).

<table>
<tr><td>vulnerability</td><td>HAZUS1999</td><td>EMS1998</td><td>MSK1969</td><td>AIJ1995</td><td>China2008</td></tr>
<tr><td colspan="3">0</td><td colspan="3">no damage</td></tr>
<tr><td>10</td><td rowspan="3">slight damage</td><td rowspan="2">Grade 1</td><td rowspan="2">D1</td><td rowspan="2">Light</td><td>D1</td></tr>
<tr><td>20</td><td>D2</td></tr>
<tr><td>30</td><td>Grade 2</td><td>D2</td><td rowspan="2">Minor</td><td>D3</td></tr>
<tr><td>40</td><td rowspan="3">moderate damage</td><td rowspan="3">Grade 3</td><td rowspan="3">D3</td><td rowspan="2">D4</td></tr>
<tr><td>50</td></tr>
<tr><td>60</td><td>Moderate</td></tr>
<tr><td>70</td><td rowspan="3">extensive damage</td><td rowspan="3">Grade 4</td><td rowspan="4">D4</td><td rowspan="3">Major</td><td rowspan="3">D5</td></tr>
<tr><td>80</td></tr>
<tr><td>90</td><td rowspan="2">complete damage</td></tr>
<tr><td>100</td><td>Grade 5</td><td>Partial col-</td></tr>
</table>

Table 3-2: Detailed definition of building damage states in GB17742-2008, China.

Damage state	Structural damage	Non-structural damage	Performance-based Description
D1	Negligible	Cracks only in *very few* non-structural compo-	No need to repair, instant use
D2	*Very few* components have visible cracks	Obvious cracks can be found	No need to repair or after slightly repairing, can be used directly
D3	*A few* components have slight cracks, *very few* have obvious cracks	*Most* components have serious damage	Certain repair work should be done before continued use
D4	*Most* components have serious damage, *a majority* have obvious cracks	*Most* components partially destroyed	The damage is difficult to repair
D5	*The majority* components have serious damage, the building structure is close to collapse or already collapsed	Non-structural components are *commonly* destroyed	To repair the building back to normal is impossible

Notes about qualifiers: "very few": <10%; "a few": 10%-50%; "most": 50%-70%; "majority": 70%-90%; "commonly": >90%.

In empirical method, fragility curve is derived from damage probability matrices (DPMs) based on post-earthquake field surveys. DPMs describe the proportions of buildings in each structural damage state (D1,

D2, D3, D4, D5) at given intensity scale, and can be used to derive the probability of exceeding each damage limit state $P[LS_i]$ (*i*=1,2,3,4), as illustrated in Eq. (3.1):

$$P[LS_i] = 1 - P[D_i]\ (i = 1); \quad P[LS_i] = P[LS_{i-1}] - P[D_i]\ (i = 2 \dots N) \tag{3.1}$$

where *N* refers to the total number of damage limit states (here *N*=4); for each building type, $P[D_i]$ refers to the proportion of building in each structural damage state *i*.

In analytical method, fragility curve is derived by Eq. (2), with the assumption that building response to seismic demand inputs follows the lognormal distribution:

$$P[LS|S_d] = \Phi\left[\frac{1}{\beta_{LS}} \ln\left(\frac{S_d}{S_{C|LS}}\right)\right] \tag{3.2}$$

where $P[LS|S_d]$ is the probability of being in or exceeding damage limit state *LS* due to ground motion indicator S_d (e.g. the inter-storey displacement, spectral acceleration, peak ground acceleration etc.); $S_{C|LS}$ refers to the median value of damage state indicator at which the building reaches the threshold of the damage state *LS*; β_{LS} represents integrated uncertainties from seismic demand input, building capacity and model uncertainty, generally within the range of 0.6-0.8; $\Phi[\ ]$ is the normal cumulative probability distribution.

3.3 Fragility database analysis

3.3.1 Building typology and seismic resistance level classification

During the past four decades, more than 2000 M≥4.7 earthquakes have occurred in mainland China and its neighbouring areas (Xu et al., 2014). Up to 2014, post-earthquake field surveys have been conducted for at least 112 damaging earthquakes that occurred in the densely populated areas in mainland China, since the 1975 M7.3 Haicheng earthquake (Ding, 2016). These damaging earthquakes mainly clustered in seismic prone provinces in southwestern China (e.g. Sichuan, Yunnan) and western China (e.g. Xinjiang Uygur, Tibet, Qinghai), as shown in Figure 3-2. The main building types in these areas are featured by masonry, reinforced concrete (RC), brick-wood, soil, stone as well as chuandou-timber (a typical building type with timber frame in mountainous area of Tibet, Qinghai and Sichuan). Due to the limitation in fragility data abundance, I mainly focus on studying the seismic fragility of the two most widely distributed building types: masonry and RC buildings (Sun and Chen, 2009). Masonry buildings are mainly composed of brick and concrete. RC buildings include building structures such as RC core wall, frame structure and frame-shear wall.

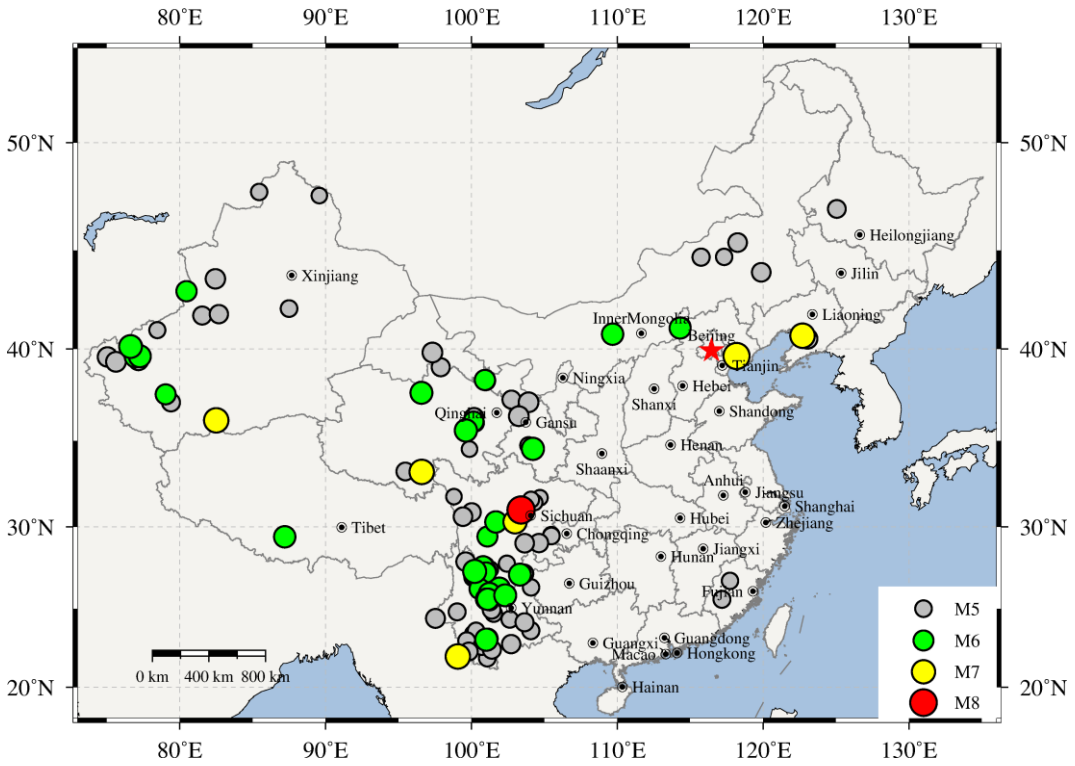

Figure 3-2: The distribution of earthquakes occurred in mainland China and its neighboring area, for which field surveys were conducted. Detailed earthquake catalogue can be found from the online supplement, which is newly compiled based on Ding (2016) and Xu et al. (2014).

The seismic resistance level of masonry and RC buildings is further divided into two classes: level A and level B. The assignment of seismic resistance level in this study is mainly based on supplementary information given in each scrutinized literature, including building age, construction material, seismic resistance code at construction time, load-bearing structure etc. Given the changes in building quality and corresponding code standard over the past four decades in China, buildings constructed in different ages though with the same nominal resistance level of each period, are reassigned with different seismic resistance levels according to the latest standard. The referred grouping criteria is given in Table 3-3 (*more building classification details can be found from the online supplement in Data/Code availability section*). Generally, "level A" includes buildings with seismic resistance level assigned as pre/low/moderate-code, and "level B" includes buildings assigned as high-code.

Table 3-3: Divisions of seismic design level for Chinese buildings (modified after Lin et al., 2010).

Seismic Resistance Design Level (PGA)	Construction Age			
	before 1978	1979-1989	1989-2001	After 2001
IX (0.4g)	pre-code	moderate-code	high-code	high-code
VIII (0.3g)	pre-code	moderate-code	moderate-code	high-code
VIII (0.2g)	pre-code	low-code	moderate-code	high-code
VII (0.15g)	pre-code	low-code	low-code	moderate-code
VII (0.10g)	pre-code	pre-code	low-code	low-code
VI (0.05g)	pre-code	pre-code	pre-code	low-code

3.3.2 Outlier check

After grouping the empirical and analytical fragilities based on building type (masonry and RC) and seismic resistance level (A and B) in Section 3.3.1, the empirical fragility database based on macro-seismic intensity (Figure 3-3) and analytical fragility database based on PGA (Figure 3-4) for four damage limit states (LS1, LS2, LS3, LS4) are thus constructed (*data can be found from the online supplement*). The Y-axis "fragility" of Figure 3-3 and Figure 3-4 refers to the exceedance probability of each damage limit state at each ground motion level. As can be clearly seen, the scatter of fragilities vary across building types and seismic resistance levels. For empirical fragilities, the scatter may relate to the uneven abundance of damage data for buildings investigated in post-earthquake field surveys, the subjective judgement of damage states as well as the rough division of building structure types. For analytical fragilities, the scatter may come from the difference in the selection of seismic demand inputs, the use of analysis techniques, the detailing of the modelled building structure, the definition of damage state as well as the difference in damage indicators used by different researchers. Thus, before deriving consecutive building fragility curves from these discrete fragility data in Figure 3-3 and Figure 3-4, the outliers need to be firstly removed from these originally collected datasets.

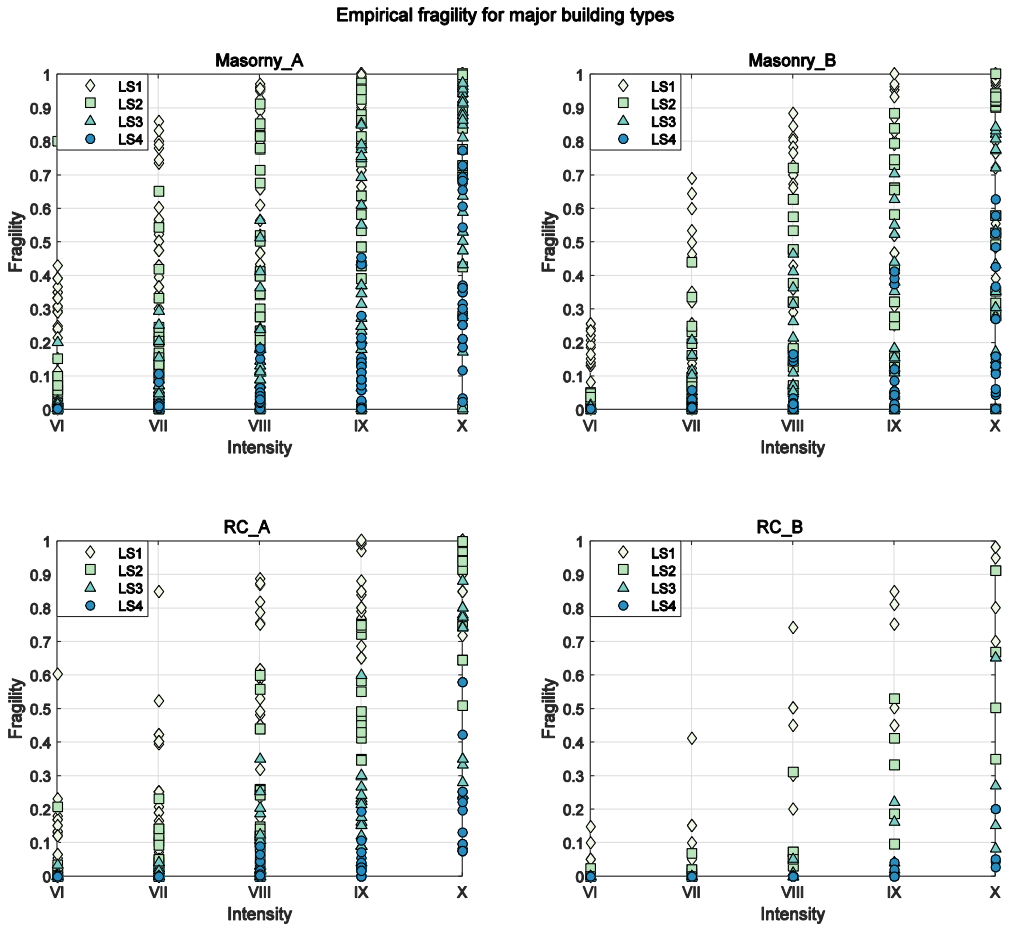

Figure 3-3: The distribution of empirical fragility data from post-earthquake field surveys, depicting the relation between the exceedance probability of each damage limit state (LS1, LS2, LS3, LS4) at given macro-seismic intensity levels. The fragility datasets are grouped by building types (masonry and RC) and seismic resistance levels (A and B).

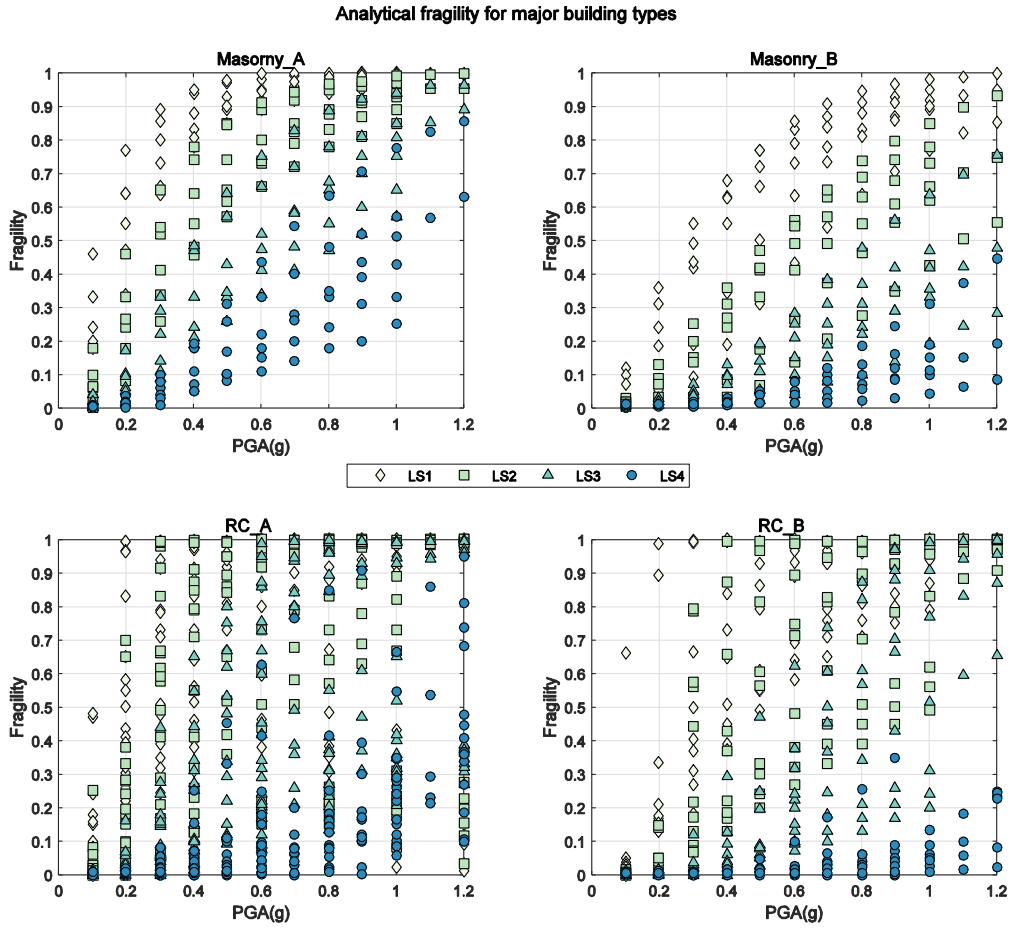

Figure 3-4: The distribution of analytical fragility data derived from non-linear analyses, depicting the relation between the exceedance probability of each damage limit state (LS1, LS2, LS3, LS4) at given PGA levels. The fragility datasets are grouped by building types (masonry and RC) and seismic resistance levels (A and B).

To figure out the outliers in the originally collected fragility database, the box-plot check method was applied. For each building type (Masonry_A, Masonry_B, RC_A, RC_B) and in each damage limit state (LS1, LS2, LS3, LS4), the corresponding series of fragility data was sorted from the lowest to the highest value. Three quantiles (Q_1, Q_2, Q_3) were used to divide each fragility series into four equal-sized groups and they correspond to the 25%, 50% and 75% quantile value in each series. A discrete fragility value (Q_i) was assigned as an outlier if $Q_i - Q_3 > 1.5 \times (Q_3 - Q_2)$ or $Q_1 - Q_i > 1.5 \times (Q_2 - Q_1)$. The box-plot check results are shown in Figure 3-5 for empirical fragility data and in Figure 3-6 for analytical fragility data.

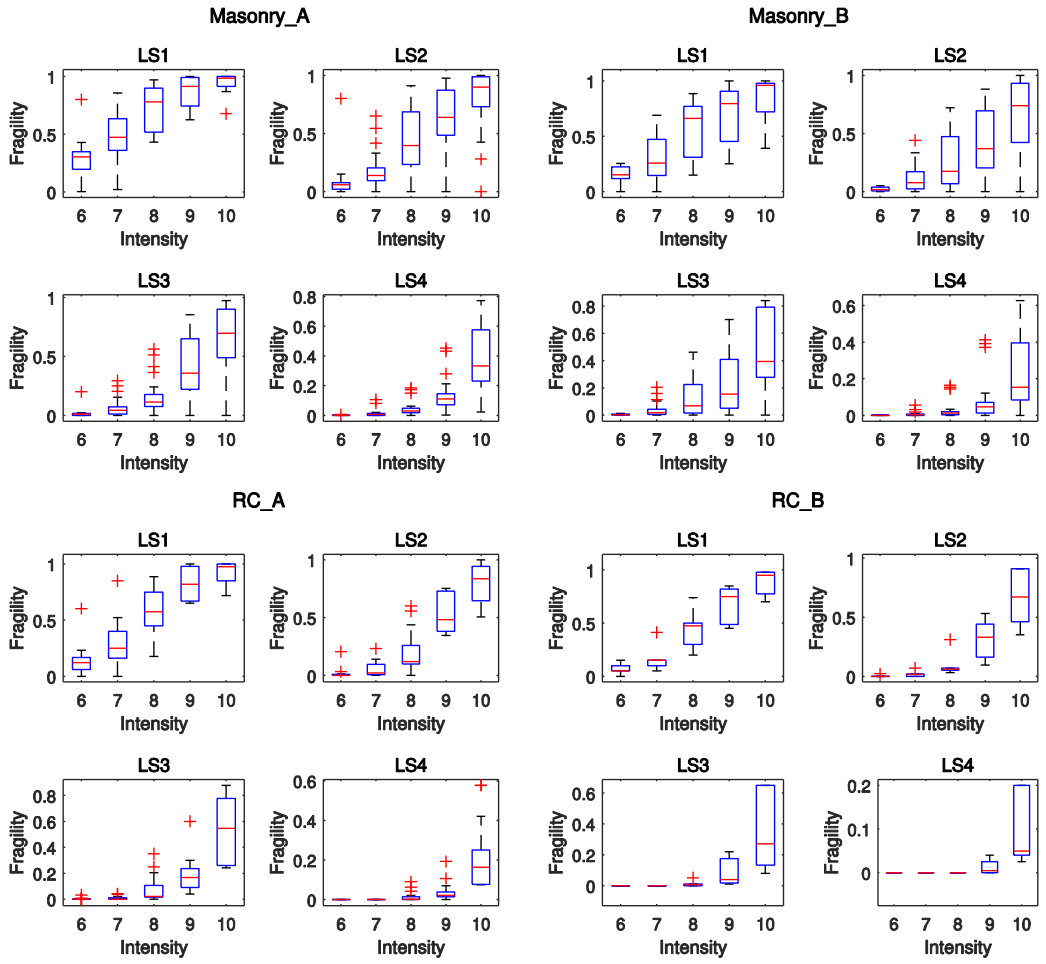

Figure 3-5: Outlier-check using box-plot method for empirical fragility data. Five macro-seismic intensity levels are used to classify the original fragility datasets: VI, VII, VIII, IX, X. "A" and "B" represent the pre/low/moderate-code and high-code seismic resistance level, respectively (more classification details are available from online supplement). LS1, LS2, LS3, LS4 are the four damage limit states. Outliers are marked by red crosses and red lines within each box indicates the 50% quantile fragility value.

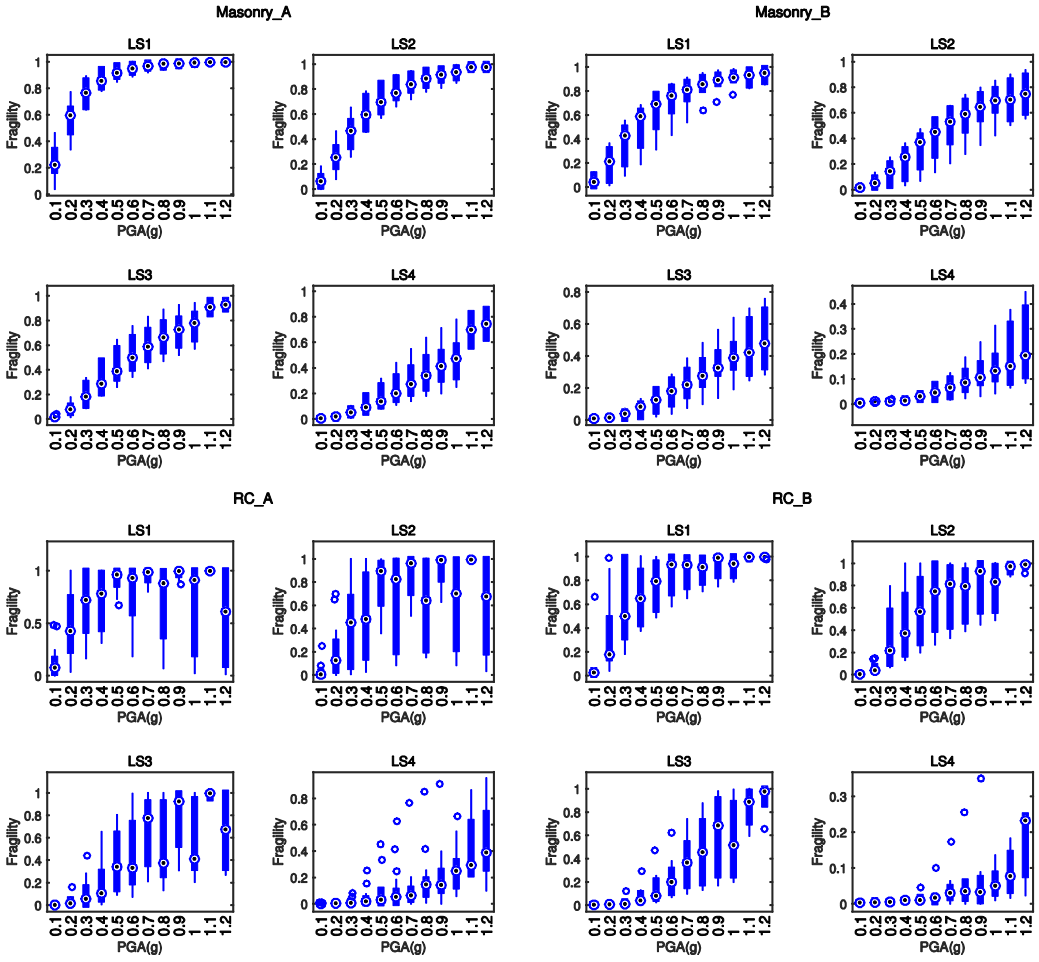

Figure 3-6: Outlier-check using box-plot method for analytical fragility data. Twelve PGA levels are used to group the discrete analytical fragility datasets: 0.1-1.2 g. "A" and "B" represent the pre/low/moderate-code and high-code seismic resistance level, respectively (more classification details are available from online supplement). LS1, LS2, LS3, LS4 are the four damage limit states. Outliers are marked by blue hollow circles and blue dot within each box indicates the 50% quantile fragility value.

3.4 Derivation of representative fragility curves

After removing outliers, details of the remaining fragility dataset (e.g., the number of data points, median and standard deviation of these data) for each damage state of each building type are plotted in Appendix Figure C1-C4 and summarized in Appendix Table B. It is worth to iterate that, as aforementioned in the Introduction section, the organization of this study is centred on two focuses. The first one is to construct a comprehensive fragility database for Chinese buildings from 87 papers and theses using empirical and analytical methods, which is one key component of seismic risk assessment. Based on the empirical and analytical fragility database collected, the second focus is to propose a new approach in deriving intensity-PGA relation by using fragility as the bridge. In this regard, a representative fragility curve should be firstly derived for each damage state of each building type, and I refer to use the median fragility values to derive such a curve.

3.4.1 Median fragility curve

To derive a representative fragility curve for each damage limit state (LS1, LS2, LS3, LS4) of each building type (Masonry_A, Masonry_B, RC_A, RC_B), the median values (50% quantile) of each fragility series in Figure 3-5 and Figure 3-6 are used. Cumulative normal distribution is assumed to fit the discrete median empirical fragilities and log-normal distributions is assumed to fit the discrete median analytical fragilities. For each damage limit state of each building type, the parameters μ_{LS} and σ_{LS} in the consecutive fragility curve can be regressed following Eq. (3.3):

$$P(X|LS) = \Phi\left[\frac{X_{int}-\mu_{LS}}{\sigma_{LS}}\right] \quad or \; P(X|LS) = \Phi\left[\frac{1}{\sigma_{LS}}\ln\left(\frac{X_{PGA}}{\mu_{LS}}\right)\right] \tag{3.3}$$

where $P(X|LS)$ represents the exceedance probability of each damage limit state *LS* given ground motion level X (X refers to X_{int}, namely macro-seismic intensity in terms of empirical fragility; and X refers to X_{PGA}, namely PGA in terms of analytical fragility).

The median fragility curves derived from empirical data and from analytical data are plotted in Figure 3-7 and Figure 3-8, respectively. As can be clearly seen from Figure 3-7 and Figure 3-8, there are two obvious trends: (1) for the same building type (masonry or RC), the higher the seismic resistance level (A<B), the lower the building fragility, which applies for all damage limit states; (2) for the same seismic resistance level, RC building has lower fragility than masonry building, which also applies for all damage limit states. These two trends indicate the reliability of the newly collected fragility database, the reasonability of the criteria in grouping building types and seismic resistance levels, as well as the suitability of using median fragility values to develop representative fragility curves for further analysis. However, some extra abnormality is also noteworthy, e.g. in the median fragility curve developed for LS4 of "RC_B" in Figure 3-8, the probability to exceed LS4 damage limit state remains 0 even when PGA is higher than 0.8 g, which is obviously not the case in reality. Detailed source of such abnormality and its effect on the intensity-PGA relation to develop will be discussed in Section 3.5.3.

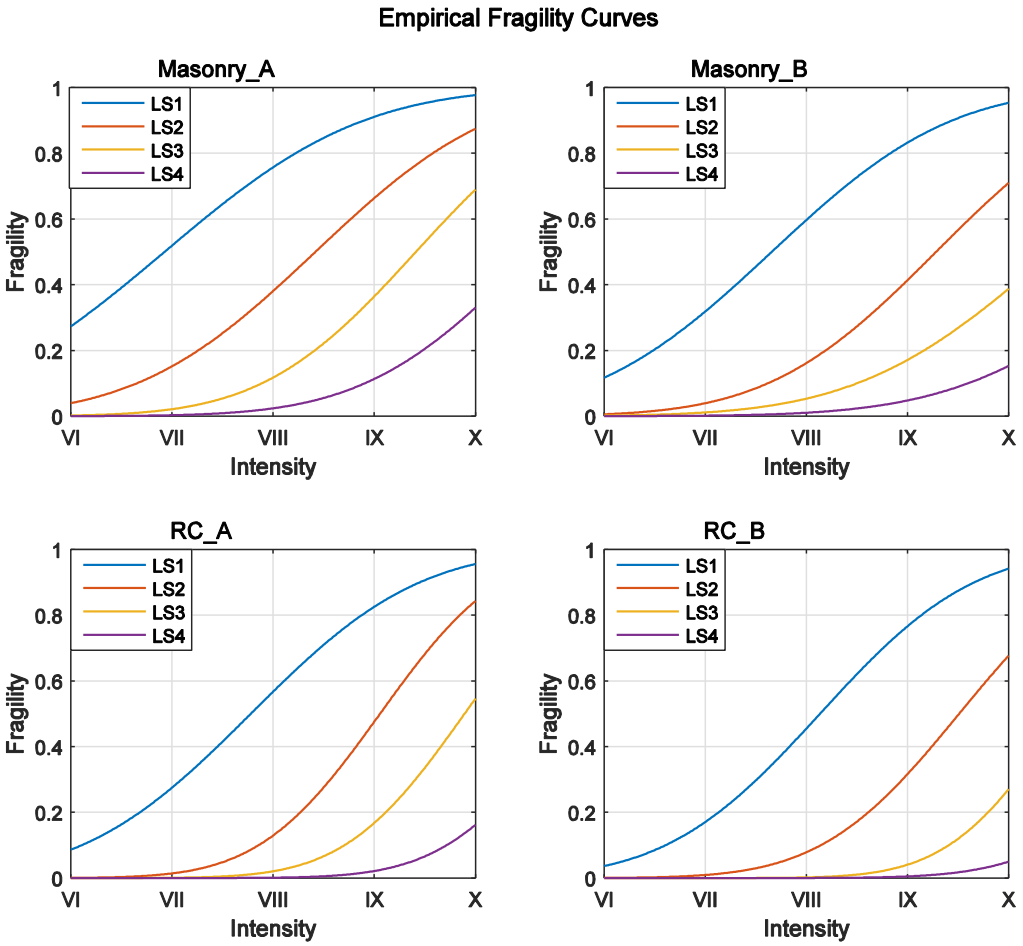

Figure 3-7: Median fragility curves derived from empirical fragility datasets, which depict the relation between macro-seismic intensity and exceedance probability of each damage limit state (LS1, LS2, LS3, LS4) for masonry and RC building types (Note: these median fragility curves are of varying robustness; see Section 3.4.1 and Section 3.5.3 for more details).

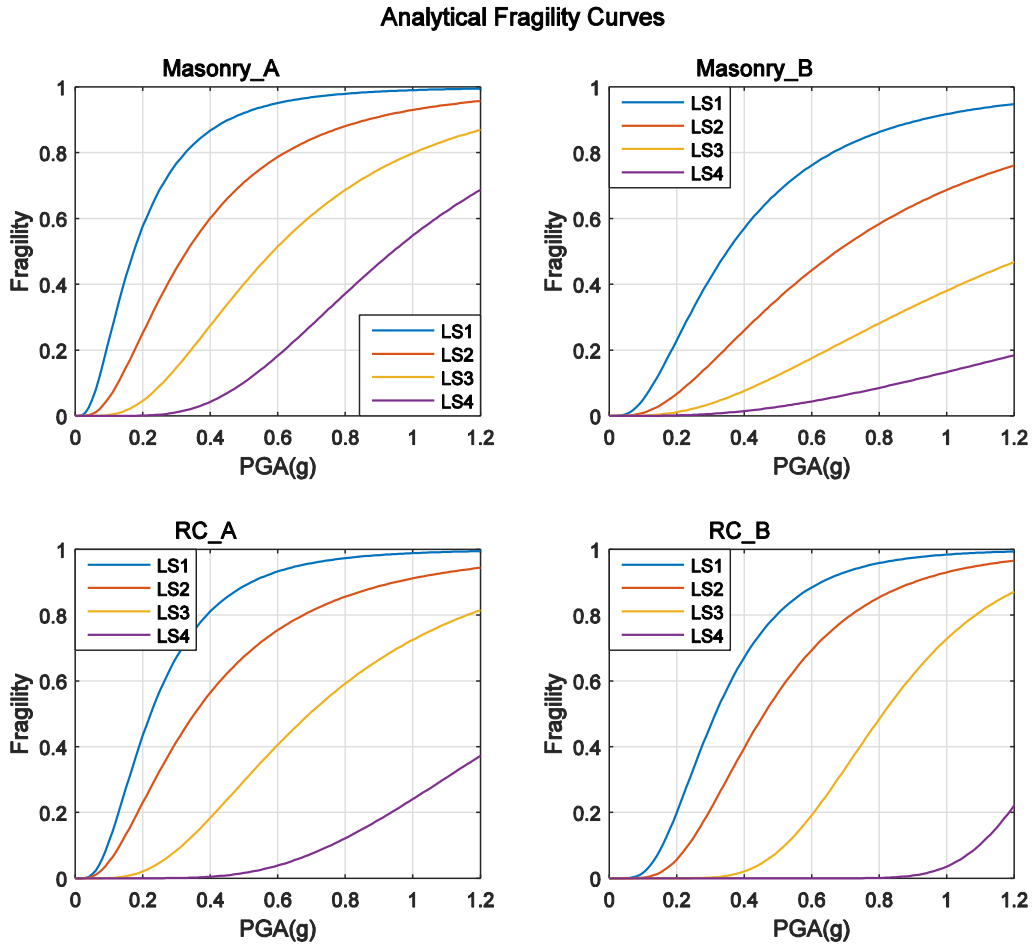

Figure 3-8: Fragility curves derived from analytical fragility datasets, which depict the relation between PGAs (unit: g) and exceedance probability of each damage limit state (LS1, LS2, LS3, LS4) for masonry and RC building types (Note: these median fragility curves are of varying robustness; see Section 3.4.1 and Section 3.5.3 for more details).

Mathematically, the goodness of fit of the consecutive fragility curve regressed from the discrete median fragilities can be measured by statistical indicator R^2 (Draper and Smith, 2014). Higher R^2 value indicates a better fit of the regressed fragility curve, since it is defined as the ratio between *SSR* and *SST: SSR* is the ***s**um of **s**quares of the **r**egression* ($SSR = \sum_{i=1}^{n}(\hat{y}_i - \bar{y}_i)^2$), and SST is the ***t**otal **s**um of **s**quares* ($SST = \sum_{i=1}^{n}(y_i - \bar{y}_i)^2$); y_i refers to the original discrete fragilities for each damage limit state, $\bar{y}_i$ refers to the mean fragility, $\hat{y}_i$ refers to the predicted fragility by the fitted fragility curve. As shown in Table 3-4, the R^2 values are generally above 0.95, which indicates the normal or lognormal distribution assumption in Eq. (3.3) is very suitable to match the discrete fragility datasets. Noticeably, there are also three low R^2 values (≤0.8) in Table 3-4 for damage limit state LS1, LS2, LS3 of building type "RC_A", which may indicate the low quality (e.g. high scatter) of the originally collected fragility data. As can be cross validated from Figure 3-4 and even better Figure 3-6, the analytical fragility data for "RC_A" are more scattered than for other building types. This thus directly leads to the low R^2 values in fitting the median fragility curve for damage limit state LS1, LS2, LS3 of "RC_A".

Table 3-4: The median fragility curve parameters regressed from empirical and analytical fragility data.

data_source	build_type	fort _level	damage_state	μ_{LS}	σ_{LS}	R^2
Empirical	masonry	A	LS1	6.926	1.539	0.99
			LS2	8.418	1.378	1
			LS3	9.412	1.189	1
			LS4	10.57	1.298	1
		B	LS1	7.658	1.393	0.98
			LS2	9.283	1.298	0.99
			LS3	10.43	1.505	0.99
			LS4	11.59	1.553	1
	RC	A	LS1	7.779	1.304	1
			LS2	9.057	0.9367	1
			LS3	9.893	0.9269	1
			LS4	10.95	0.9626	1
		B	LS1	8.135	1.191	1
			LS2	9.511	1.067	1
			LS3	10.54	0.8831	1
			LS4	11.77	1.075	1
Analytical	masonry	A	LS1	0.1732	0.7512	1
			LS2	0.33	0.7512	1
			LS3	0.5862	0.6383	0.99
			LS4	0.9416	0.4983	0.97
		B	LS1	0.3499	0.7573	1
			LS2	0.6743	0.8101	1
			LS3	1.281	0.8125	1
			LS4	2.595	0.8581	0.99
	RC	A	LS1	0.223	0.6615	**0.80**
			LS2	0.353	0.7699	**0.77**
			LS3	0.694	0.6111	**0.73**
			LS4	1.404	0.4818	0.98
		B	LS1	0.315	0.539	0.99
			LS2	0.46	0.5269	0.99
			LS3	0.811	0.346	0.95
			LS4	1.374	0.1763	0.91

Note: "**fort_level**" **A** & **B** represent the pre/low/moderate-code and high-code seismic resistance level, respectively; "**damage_state**" LS1, LS2, LS3, LS4 represent the four damage limit states: slight, moderate, serious-, collapse, respectively; "μ_{LS}" and "σ_{LS}" are the regression parameters between intensity/PGA and the corresponding fragilities of each damage limit state; $\boldsymbol{R^2}$ indicates the fitness quality of the regressed median fragility curve, as plotted in Figure 3-7 and Figure 3-8.

3.4.2 Fragility curve comparison with international projects

Given the import role of fragility curve for future seismic risk assessment and loss estimation especially in seismic prone areas, the empirical and analytical fragility database derived from 87 individual papers and theses are constructed. The median and standard deviation of the fragility series for each damage state of each building type are plotted in Appendix Figure C1-C4 and listed in Appendix Table B. To derive new intensity-PGA relation by using fragility as the bridge, the median fragility curves for masonry and RC building types with seismic resistance levels A and B are regressed, as shown in Figure 3-7 and Figure 3-8. However, the robustness of these median fragility curves varies across damage states and building types, as will be discussed in detail in Section 3.5.3. Here, to better place such a review work, it is worth to compare it with international projects with similar focus. Therefore, I also checked the fragility outputs from several international projects, including PERPETUATE, SYNER-G, PAGER, HAZUS and GEM. Based on the fragility curve robustness analysis in Section 3.5.3, median fragility curves developed for building type "Masonry_A" are of relatively highest robustness. Thus, the comparison of the median fragility curves in this chapter with these international projects (in terms of PGA) will be based on "Masonry_A" building

type only. To avoid over complexity, the scatter attached to each fragility curve is not taken into account in this comparison.

3.4.2.1 PERPETUATE project

The main goal of European PERPETUATE project was to develop European guidelines for evaluation and mitigation of seismic risk to cultural heritage assets, applicable in the European and other Mediterranean countries. As written in their project homepage, the risk assessment of heritage buildings requires the assessment of both architectonic and artistic assets contained in them, which needs improvement in methods of analysis and assessment procedures rather than in intervention techniques for common buildings and infrastructures. Besides that, a verification approach in terms of displacement rather than in terms of strength is more reliable and effective for heritage building. However, the fragilities collected in this study are mainly for general masonry and RC buildings and mainly in terms of macro-seismic intensity or PGA, not displacement. Therefore, the fragility outputs from PERPETUATE project and this study are not so comparable.

3.4.2.2 SYNER-G project

European SYNER-G project focused on reviewing fragility for masonry and RC buildings in Europe, including the collection of existing fragility functions, building recategorization, and harmonization of intensity measure and limit states. In the final output of SYNER-G project, fragility curves were given in terms of PGA, with some of them converted from macro-seismic intensity or spectral acceleration (SA) (Crowley et al., 2011a; Crowley et al., 2011b; Kaynia et al., 2013; Pitilakis et al., 2014). Comparisons between mean fragility curves developed in SYNER-G project (Crowley et al., 2011b; refer to Table 6.3 and Table 6.5) with the median analytical fragility curves developed in this study for "Masonry_A" building type are plotted in Figure A5. It is noteworthy that, in SYNER-G outputs, the typically four damage limit states were further harmonized into two: yielding damage state (LS2) and collapse state (LS4).

As can be seen from Figure C5, the fragility in SYNER-G project for typical European masonry buildings is much higher than "Masonry_A" in this study. The discrepancy of masonry building fragility between SYNER-G (Silva et al., 2014) and this study is potentially related to the following factors. Firstly, the difference in use of ground motion indicator (part of SYNER-G's PGA-related fragility curves are converted from intensity, SA related fragility curves; the analytical fragility curves in this study are purely PGA-related) may play a role. Besides that, difference in building classification is difficult to accurately calibrate but certainly contributes to the final fragility discrepancy. Furthermore, the harmonization of damage limit states in SYNER-G project (from four to two) makes the fragility difference between these two damage states subtle (as shown in Figure C5), and also hinders the fragility comparison for each damage limit state accordingly. Lastly, in SYNER-G project, the mean fragility curves are provided; but in this study, median fragility curves are developed for nominally similar masonry buildings. In all, these differences combined together lead to the fragility discrepancy for general masonry buildings' fragility curves in this study and those in SYNER-G project.

3.4.2.3 PAGER project

The ongoing PAGER project (Prompt Assessment of Global Earthquakes for Response) of United States is an automated system specialized in estimating the seismic ground shaking distribution, the number of people and settlements exposed to that severe shaking, and the scale/range of possible fatalities and economic losses. For these purposes, vulnerability functions are used, which are different from the fragility functions I focus on in this study. The main difference lies in that, vulnerability functions can be derived

either directly from historical damage information, or indirectly from fragility function combined with consequence functions, which describe the probability of loss given a level of performance (e.g. collapse damage state). Thus, direct comparison between the outputs of PAGER project and this study is not available.

3.4.2.4 HAZUS project

The ongoing HAZUS project of United States, is developed and updated to provide local, state and regional officials with the tools necessary to plan and stimulate efforts to reduce risk from earthquakes and to prepare for emergency response and recovery from an earthquake (FEMA, 2003; FEMA, 2008). HAZUS offers a series of fragility curves for typical building types based on HAZUS building taxonomy. Here for comparison with fragility curves in this study for "Masonry_A", I extracted HAZUS fragility curves developed for two specific masonry building types: mid-rise reinforced masonry bearing walls with wood or metal deck diaphragms (RM1M) and high-rise reinforced masonry bearing walls with precast concrete diaphragms (RM2H) from HAZUS Earthquake Technical Manual (refer to Table 5.16a-d). These fragility curves are based on median spectral displacement of the damage state of interest and an assumed demand spectrum shape that relates spectral response to PGA. The reference spectrum used to derive HAZUS fragility curve represents ground shaking of a large-magnitude (i.e. M≈7.0) western United States earthquake for soil sites (e.g. site class D) at site to source distances of 15km or greater.

Comparisons between the fragility curves of HAZUS for "RM1M, RM2H" and those developed in this study for "Masonry_A" are plotted in Figure C6 (RM1M) and Figure C7 (RM2H). In HAZUS four code levels (pre/low/moderate/high) are provided; but in this study, only two seismic resistance levels "A" and "B" are assigned to the analytical fragilities extracted from individual literature (*more details can be found from online supplement*). As can be seen from Figure C6 and Figure C7, the median fragility of "Masonry_A" in this study is basically between the median fragility of high-code and moderate-code of "RM1M" and "RM2H" building types, which indicates the compatibility between HAZAU and this study's median fragility curves for general masonry buildings, compared with the mean fragility curves in SYNER-G project.

3.4.2.5 GEM project

The ongoing Global Earthquake Modelling (GEM) project, is motivated to "serve the public good in a collaborative, credible, open and transparent manner, and to make risk assessment inclusive to create a holistic culture of awareness and resilience, bringing a once-scarce resource available to all sectors and beneficiaries". GEM project has integrated outputs from three other European projects: SHARE, SYNER-G and NERA. SHARE focused on seismic hazard harmonization in Europe and covers all of Europe and the Maghreb countries. The hazard model is developed with the OpenQuake Engine. SYNER-G partners developed an unified methodology and tools for systemic vulnerability assessment in Europe. NERA focused on the creation of a European research infrastructure for risk assessment and mitigation. Besides the fragility outputs from SYNER-G project, GEM online fragility database also integrates fragility curves from HAZUS (Yepes-Estrada et al., 2016). Therefore, the comparison with GEM fragility curves developed for European and American building types will not be repeated. For mainland China, the fragility curves integrated in GEM database is solely from Tang et al. (2011) developed for Chinese schools, and only for RC building with spectral acceleration (SA) as the ground motion indicator. To avoid uncertainty introduced from converting SA to PGA, the comparison with fragility curves in Tang et al. (2011) is also skiped.

3.5 New approach in deriving intensity-PGA relation

Intensity-PGA relation has an important application in seismic hazard assessment, since the use of macro-seismic data can compensate for the lack of ground motion records and thus help in reconstructing the shaking distribution for historical events. Traditionally, intensity-PGA relations are developed using instrumental PGA records and macro-seismic intensity observations within the same geographical range (Bilal and Askan, 2014; Caprio et al., 2015; Ding et al., 2014; Ding, 2016; Ding et al., 2017; Ogweno and Cramer, 2017; Worden et al., 2012). These relations are generally region-dependent and have large scatter (Caprio et al., 2015). In this section, I propose a new approach in deriving intensity-PGA relation based on the newly collected empirical and analytical fragility database. For each building type and each damage limit state, an empirical fragility curve (exceedance probability vs. macro-seismic intensity) and an analytic fragility curve (exceedance probability vs. PGA) are available, as derived from the median fragilities in Section 3.4.1. By eliminating the same fragility value, the corresponding pair of macro-seismic intensity and PGA can be derived. Thus, for a series of fragility values, the corresponding intensity-PGA relation can be further regressed based on the paired intensities and PGAs. Ideally, the overlap of all these regressed intensity-PGA relations would be expected, regardless of the difference in building type, seismic resistance level and damage state.

3.5.1 Difference between this new approach and previous practices

Compared with this new approach in intensity-PGA relation development, previous practices directly regressed intensity and PGA datasets within the same geographical range, but no further classification of datasets was conducted, as based on building type or damage state in this study. The lack of further classification of PGA and intensity datasets may explain why the previously derived intensity-PGA relations generally have high scatter. The reason lies behind is that, although macro-seismic intensity is a direct macro indicator of building damage, higher instrumental ground motion (e.g., PGA) does not necessarily mean higher damage to all buildings. Instead, damage is more determined by the seismic resistance capacity of different building types. Thus, further division of intensity and instrumental ground motion records based on affected building types should promisingly help decrease the scatter of regressed intensity-PGA relation.

Furthermore, local site effect also contributes to the amplification of instrumental peak ground motions (PGA or SA), when combining intensity and PGA datasets from areas with different geological background together. This in turn increases the scatter of regressed intensity-PGA relation. In this regard, it is worth to emphasize that, in this newly collected PGA-related analytical fragility database, the PGA parameter is not the real instrumental records as used in regressing traditional intensity-PGA relation, but the input PGA records used in experimental fragility analysis (push-over analysis, incremental dynamic analysis, dynamic history analysis etc.). Therefore, the regional dependence (here I mainly refer to site condition), which contributes to the scatter of traditional Intensity-PGA relation, is not a source of uncertainty in the newly developed relation.

3.5.2 Derivation of initial intensity-PGA relation

As a tentative approach, here the relation between intensity and PGA is derived by using median fragility as the bridge for each damage limit state of each building type. It is deeply aware that uncertainty is inherent in every single step of empirical and analytical fragility analyss. However, the trial of using the

median fragility as the bridge to develop intensity-PGA relation, more importantly, aims at providing a new approach in this regard compared with traditional practice, not to backwards reduce the uncertainties (building structure, seismic demand inputs, computation methods etc.) in deriving empirical and analytical fragility. By using Eq. (3.3) for PGA-fragility and intensity-fragility respectively and eliminating fragility as variable, the following relations can be derived:

$$\ln(PGA) = \alpha + \beta * Int,$$

$$with\ \alpha = \ln(\mu_{PGA}) - \frac{\sigma_{PGA}}{\sigma_{Int}} * \mu_{Int,}\ \beta = \frac{\sigma_{PGA}}{\sigma_{Int}} \tag{3.4}$$

In which, the parameters μ_{PGA}, μ_{Int}, σ_{PGA}, σ_{Int} are taken from Table 3-4 with values varying across building types and damage limit states.

These intensity-PGA relations are plotted in Figure 3-9 (grouped by building types) and Figure 3-10 (grouped by damage limit states). Theoretically, higher damage states can occur only at higher intensities or PGA values. For instance, a LS4 damage state at intensity III would not happen, as reflected by the curves in Figure 3-9 and Figure 3-10: LS1 have the lowest PGA or intensity starting point, while LS4 has the highest. Thus, the intensity-PGA curve is truncated at fragility values above 1%. Ideally, it would be expected that all intensity-PGA relations overlap with each other, whether grouped by building type or by damage state. As a matter of fact, for building type "Masonry_A" and "Masonry_B" in Figure 3-9, the four intensity-PGA curves of four damage limit states do coincide very well. Meanwhile, the discrepancy in intensity-PGA relations of "RC_A" for damage states LS1, LS2, LS3 in Figure 3-9 is also not surprising, given the relatively high scatter in the original analytical fragility datasets of "RC_A" (as discussed in Section 3.4.1 and verified by Appendix Figure C1-C4).

3.5.3 Source of abnormality in intensity-PGA curves

For building type "RC_A" and "RC_B" in Figure 3-9, it is clear that for the same intensity levels, the corresponding PGA values of damage limit state LS4 are much higher than that of damage limit states LS1, LS2, LS3. For fixed fragility value, this may due to the underestimation of intensity by the median empirical fragility curve in Figure 3-7, or the overestimation of PGA by the median analytical fragility curve in Figure 3-8, or a combination of both effects. In this regard, damage data scarcity at higher damage limit states may contribute to the abnormal high PGA values of LS4 in Figure 3-9. When reviewing the fragility data collection process, it is clear that the construction of empirical fragility database requires the combination of damage statistics from multiple earthquake events that cover a wide range of ground motion levels. Generally, large magnitude earthquakes occur more infrequently in densely populated areas, thus damage data tend to cluster around the low damage states and ground motion levels. This limits the validation of high damage states or ground motion levels (Calvi, 2006). According to Yuan (2008), those seriously damaged buildings in earthquake affected area are mainly masonry buildings, not so many RC buildings. Therefore, the cause of the abnormal high PGA values of damage state LS4 for "RC_A" and "RC_B" can be attributed to the relative scarcity of damage data at higher intensity/PGA level, especially for RC buildings.

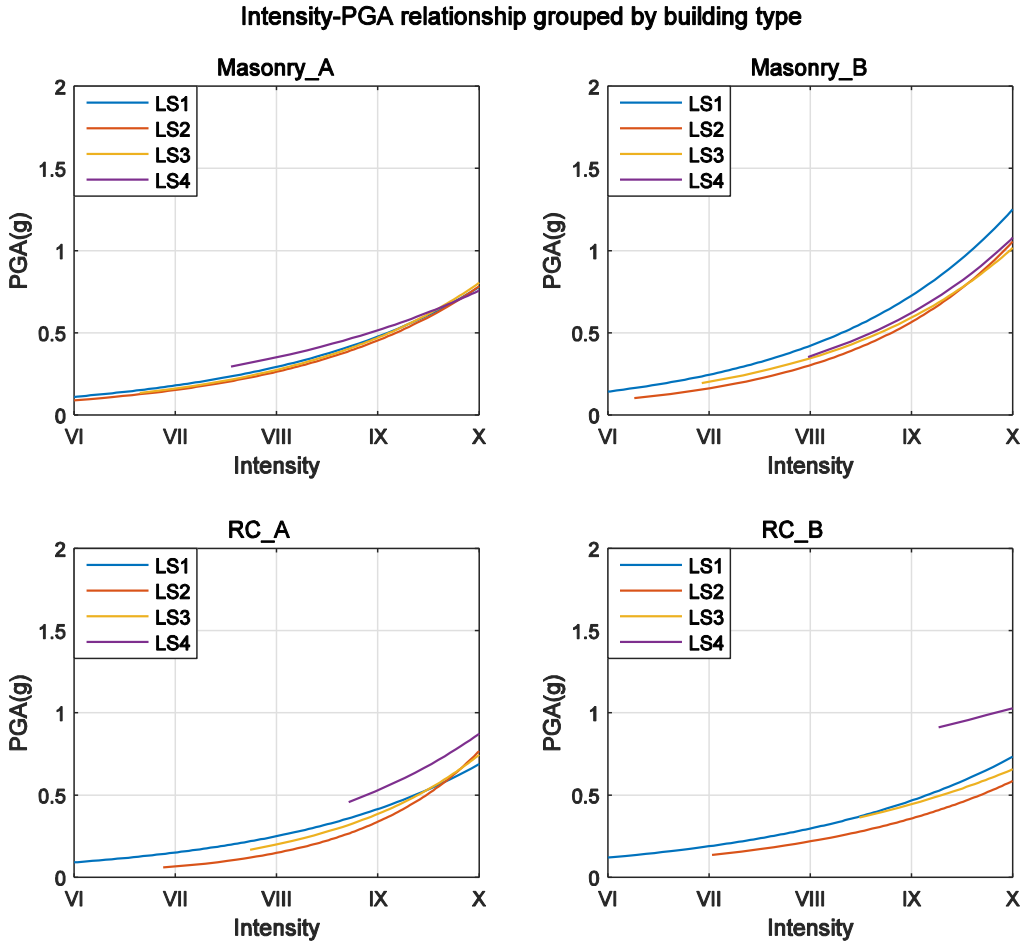

Figure 3-9: Intensity-PGA relations grouped by building types. Only intensity and PGA values with truncated exceedance probability ≥1% for each damage limit state of each building type are plotted, since higher damage states can appear only for higher intensities or PGA values (see Section 3.5.2 for more details).

As to building type "Masonry _A" and "Masonry _B" in Figure 3-9, for the same intensity level, the PGA values revealed by four damage states of "Masonry_B" are generally higher than that in "Masonry_A". This can be more clearly seen from Figure 3-10, in which the intensity-PGA relations are grouped by damage limit states. How to explain this abnormal phenomenon that given the same intensity level, the PGA values revealed by "Masonry_B" are generally higher than that by all the other three building types? In fact, compared with "Masonry_A", buildings assigned as type "Masonry_B" generally have much higher seismic resistance capacity. In this study, level "A" refers to buildings assigned as pre/low/moderate-code seismic resistance capacity, and level "B" refers to buildings assigned as high-code (*building classification details can be found on the online supplementary material*). That is, according to the grouping criteria in Table 3-3, buildings assigned as "Masonry_B" mainly refer to those built after 2001 with seismic resistance level VIII and above. This is obviously a very high code standard. Thus, for the same ground motion level, the damage posed on "Masonry_B" should be much slighter than on "Masonry_A". Therefore, for the same PGA level, the corresponding intensity revealed by "Masonry_B" should be lower than by "Masonry_A".

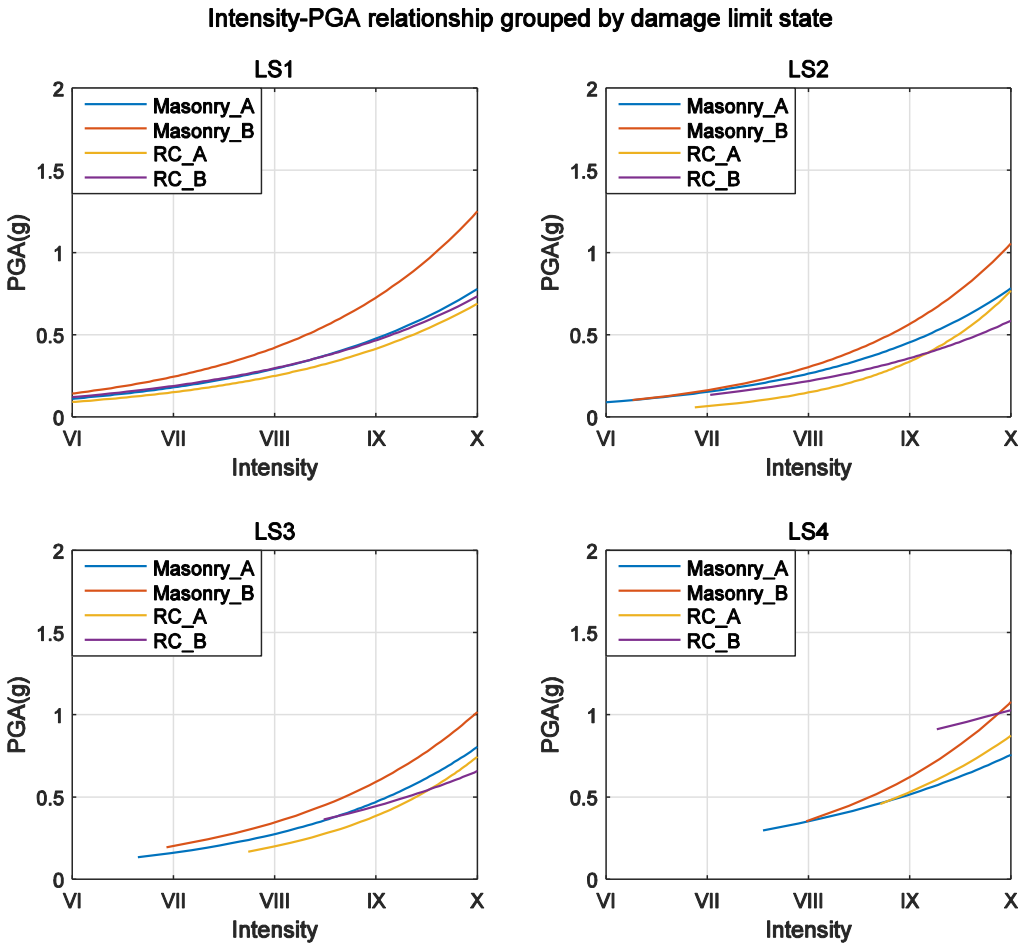

Figure 3-10: Intensity-PGA relations grouped by damage limit states. Only intensity and PGA values with truncated exceedance probability ≥1% for each damage limit state of each building type are plotted, since higher damage states can appear only for higher intensities or PGA values (see Section 3.5.2 for more details).

Actually in mainland China, the macro-seismic intensity level in post-earthquake filed surveys is determined by damage states of three reference buildings types, namely (1) Type A: wood-structure, soil/stone/brick-made old building; (2) Type B: single- or multi- storey brick masonry without seismic resistance; (3) Type C: single- or multi- storey brick masonry sustaining shaking of intensity degree VII. While in this study, buildings assigned as "Masonry_B" mainly refer to those constructed after 2001 with seismic resistance level VIII and above, and their seismic resistance capability is obviously much higher than all those three referred Type A/B/C building types. Therefore, intensity levels derived from damage to those less fragile "Masonry_B" buildings tend to be underdetermined. This may help explain why for the same intensity level, the corresponding PGA revealed by intensity-PGA relation of "Masonry_B" is higher than that of "Masonry_A".

Based on above discussion and the initial analysis in Section 3.4.1, it is clear that (a) Due to the high scatter in originally collected fragility database (as validated by the low R^2 values in Table 3-4), the intensity-PGA relations derived for LS1, LS2, LS3 of "RC_A" are of low robustness; (b) Due to the damage data scarcity, intensity-PGA relations for LS4 of "RC_A" and LS4 of "RC_B" are also not fully reliable; (c) Due to the high

seismic resistance capability attached to "Masonry_B", the intensity-PGA relations derived for all damage limit states of "Masonry_B" have the probability to underestimate intensity (or overestimate PGA) compared with "Masonry_A". Therefore, intensity-PGA curves derived for "Masonry_A" are of relatively highest robustness/reliability. Actually, the four intensity-PGA curves of "Masonry_A" do coincide very well as expected (Figure 3-9). According to Yuan (2008), those seriously damaged buildings in earthquake affected areas are mainly masonry buildings. Therefore, the median empirical and analytical fragility curves derived for "Masonry_A" (with uncertainties shown in Appendix Figure C1-C4 and Table B) are also considered to be the most representative ones for seismic prone areas in mainland China, compared with those developed for other buildings types in this study.

3.5.4 Average intensity-PGA relation derived for "Masonry_A"

According to the analysis in Section 3.5.3, intensity-PGA curves derived for four damage limit states of "Masonry_A" are of relatively highest robustness and have no such intensity underestimation problem as "Masonry_B". Therefore, I first focus only on building type "Masonry_A" and average its four PGA values for discrete intensity values, to derive the corresponding averaged PGA values, as listed in Table 3-5. If I match the data points in Table 5 with a linear relation between intensity and ln(PGA), I find Eq. (3.5):

$$\ln(PGA) = 0.521 * Int - 5.43 \pm \varepsilon \qquad (PGA: \mathrm{g}) \tag{3.5}$$

where ε follows the normal distribution, with 0 as the median value and the standard deviation is σ.

By integrating the uncertainty in both original empirical and analytical fragility data of "Masonry_A" (as shown in Appendix Figure C1-C4 and Table B) into the intensity-PGA relation, the averaged standard deviation σ in Eq. (3.5) is estimated to be 0.3 (*the detailed uncertainty transmission methodology is given in Appendix D*). As the "Masonry_A" type is the most common and relevant with buildings damaged in historical earthquakes (Section 3.5.3), I recommend using Eq. (3.5) for building damage assessment for earthquakes occurred in mainland China, especially in seismic active provinces e.g. Sichuan and Yunnan (Figure 3-2).

Table 3-5: The mean PGA values derived from intensity-PGA relations of "Masonry_A" based on the newly proposed approach.

intensity	VI	VII	VIII	IX	X
PGA(g)	0.1	0.16	0.3	0.48	0.78

3.5.5 Comparison with other intensity-PGA relations

Based on the analysis in Section 3.5.3, if I only remove those obviously unreliable intensity-PGA curves, namely LS1, LS2, LS3, LS4 of "RC_A" and LS4 of "RC_B", the range of PGA values derived from the remaining intensity-PGA relations are shown in Table 3-6. For comparison, the recommended PGA range for each intensity degree in the Chinese Official Seismic Intensity Scale (GB17742-2008) is listed in Table 3-7. The PGA values for intensity VI, VII in my results are higher than those in GB17742-2008; while for intensity VII, IX and X, the PGA values are quite comparable. It is also found that the recommended PGA ranges in GB17742-2008 are indeed the same as those given in GB17742-1980, which was issued in the 1980s

around four decades ago. At that time, available damage data used to derive the intensity-PGA relation in China was quite scarce. Therefore, damaging earthquakes occurred in the United States before 1971 were also largely used, which may not be representative of the situation in China today. Thus, one possible explanation for the relatively low PGAs for low intensity levels (VI, VII) in Table 3-7 (GB17742-1980/2008) is that, the buildings in the 1980s were more fragile than nowadays buildings. Since macro-seismic intensity is a direct macro indicator of building damage, nowadays buildings generally have better seismic resistance capacity and thus require higher ground motion (PGA) than buildings in the 1980s to be equally damaged.

Table 3-6: The PGA ranges derived from more intensity-PGA relations.

intensity	VI	VII	VIII	IX	X
PGA(g)	0.06-0.14	0.12-0.25	0.21-0.43	0.36-0.73	0.58-1.25

Table 3-7: The recommended intensity-PGA relations in China (GB17742-2008/1980).

intensity		VI	VII	VIII	IX	X
PGA (g)	mean	0.06	0.13	0.25	0.5	1.0
	range	0.05-0.09	0.09-0.18	0.18-0.35	0.35-0.7	0.7-1.4

Since the recommended PGA ranges in GB17742-2008 are not so representative of the current building status in mainland China, comparisons with the latest intensity-PGA relation developed in Ding et al. (2017) are also conducted. Ding et al. (2017) adopted traditional practice in regressing the macro-seismic intensities and instrumental PGA records within the same geographical range, by using records for 28 M$\geqslant$5 earthquakes occurred during 1994-2014 in mainland China. The PGA values for intensity VI-IX in Ding et al. (2017) are listed in Table 3-8. When comparing the results in Table 3-5 and Table 3-6 with that in Table 3-8, PGA values are quite consistent for both low intensity (VI, VII) and high intensity (VIII, IX) levels, though these data are separately developed by the new approach and by traditional practice. This congruence shows the reasonability of the new approach proposed here in developing intensity-PGA relation.

Table 3-8: The latest intensity-PGA relation derived by traditional practice for mainland China (Ding, 2017).

intensity		VI	VII	VIII	IX
PGA (g)	mean	0.09	0.16	0.3	0.55
	range	0.06-0.12	0.09-0.22	0.22-0.41	0.41-0.75

3.6 Conclusion

An empirical fragility database was established by evaluating 69 papers and theses, mostly from the Chinese literature, that document observations of macro-seismic intensities reflecting earthquake damage occurred in densely populated areas in mainland China over the past four decades. These publications provide empirical fragilities dependent on macro-seismic intensities for four damage limit states (LS1, LS2, LS3, LS4) of four building types (Masonry_A, Masonry_B, RC_A, RC_B). Analytical fragility database was

also established by scrutinizing 18 papers and theses with results on modeling fragilities for the nominally same building types and the same damage states either by response spectral methods or by time-history response analysis. These analytic methods provide fragilities as functions of PGA. From this wealth of data, the median fragility curves were derived for these building types by removing outliers. Based on the newly collected empirical and analytical fragility database, possible comparisons with several international projects including PERPETUATE, SYNER-G, PAGER, HAZUS, GEM were also conducted.

A new approach was proposed by using fragility as the bridge to derive intensity-PGA relations independently for each building type and each damage state. The potential sources of abnormalities in these newly derived intensity-PGA relations were discussed in detail. Ideally the individual intensity-PGA curves should all coincide and allow us to derive an average relation between intensity and PGA. The coincidence is not 100% perfect and deviations for the cases where they occur were discussed. Given the high damage data abundance and wide distribution of masonry buildings in mainland China, for studies referring to historical earthquakes and their losses in seismic active regions, e.g. Sichuan and Yunnan, I recommend utilizing the intensity-PGA relation derived from "Masonry_A" buildings in Eq. (3.5).

However, for engineering application, due to the scattering in original fragility datasets and simplification in using median fragility to derive intensity-PGA relation in the newly proposed approach, the use of the preliminary intensity-PGA relations developed here should be with caution. It's also worth to note that, buildings used for empirical intensity determination and for analytical studies do not coincide: a "Masonry_A" building in a post-event field survey may encompass a wider range than in an analytic study. Therefore, following the novel idea of using fragility as the bridge to develop intensity-PGA relation in this study, possible extensions in the future can be performing fragility analysis for more specifically designed building types that are more representative of those widely damaged building types in the fields.

3.7 Data/Code availability

More fragility extraction and building classification details are available from online supplement in:

https://www.jianguoyun.com/p/DaPyWSEQgPb4Bhi--NUB

(Filename: *Supplementary_building_classification_details.pdf*).

The earthquake catalog in plotting Figure 3-2 is in:

(Filename: *EQ_list_with_field_survey.xlsx*).

The empirical and analytical fragility data in Figure 3-3 and Figure 3-4 are available in:

(Folder name: *data_Fig3-4*).

4 Residential building stock modelling for mainland China

4.1 Background introduction

With the theme of last year's International Day for Disaster Reduction (IDDR2018) being "Target B: Reducing the number of affected people by disasters by 2030", the awareness of the impacts of natural disasters on human society has been increasing over the years. Demands from public sector for quantification of disaster risk is thus more urgent than before. As spoken by António Guterres, the current United Nations Secretary-General, in IDDR2018, that "Disasters cost hundreds of billions of dollars, hitting the poorest countries disproportionately and pushing millions into poverty. We must tackle disaster risks and leave a more resilient planet to future generations." To better cope with the frequent occurrence of earthquakes and other natural hazards (typhoon, flood, tsunami etc.), the development of sound hazard risk models should be given top priority, since these hazards can lead to tremendous and often crippling economic losses especially in the countries of the developing world. According to the estimation in Daniell et al. (2011), during 1900-2011, worldwide economic losses (direct and indirect) associated with the occurrence of over 7000 damaging earthquakes (amongst 1996 events caused fatalities) reached USD 2.1 trillion (in 2010 price level).

To develop a seismic risk model, three layers of information are essential: hazard, exposure and vulnerability. Hazard refers to the occurrence frequency and severity of earthquakes. Exposure captures the attributes of exposed elements in terms of value, location and relative importance (e.g. buildings, critical facilities and infrastructure) to potential earthquake. Vulnerability describes the susceptibility of those exposed elements to earthquake. Among the exposed elements, buildings are considered as the most important asset category in seismic risk assessment, since the major source of loss and fatality that occur during earthquakes are related to building damage and collapse (Neumayer and Barthel, 2011; Yuan, 2008). As such, estimation of the building stock and the value at risk is an important and integral part of any risk modeling effort. Specifically in developing and disaster vulnerable countries like China, rapid urbanization process has led to massive increase in both the asset value and population exposed to seismic hazards (Hu et al., 2010; Yang and Kohler, 2008). Therefore, a country-level modelling of the building stock and its spatial distribution across China is quite essential.

Ideally, if building stock value of the research portfolio is already known, e.g. in an insurance portfolio, building attributes (i.e. the location, geometry, height, construction age and material, occupancy type etc.) are used mainly for building vulnerability determination. However, in most cases, the building stock value is not available and obtaining such detailed information for every building in a large region is not practicable. Therefore, the aforementioned building attributes, which are usually provided in administrative level in census data, are also used to estimate the building stock value. In this case, appropriate proxy (e.g. population density) is required to disaggregate administrative level census data into finer scale. The use of proxy is quite a reasonable approach in dasymetric modelling and has been frequently adopted in previous studies (e.g. Gunasekera et al., 2015; Silva et al., 2015; Thieken et al., 2008).

When disaggregating census data into finer scale, it cannot be carried out by simply assuming that the assets within an administrative unit are evenly distributed, since in reality people and buildings tend to be concentrated in settlements e.g. along the riverside or within alluvial plains (Figueiredo and Martina, 2016). In regard of this, more sensible techniques have been applied and documented in the literature. For example, Silva et al. (2014) disaggregated the building stock at parish level for mainland Portugal based on the population density profile at 30×30 arc-sec resolution cells from LandScan. The LandScan population density profile was produced by apportioning best available census counts into cells based on probability coefficients, which in turn were derived from road proximity, slope, land cover and night-time lights (Dobson et al., 2000).

In mainland China, the modelling of building stock value and its spatial distribution across China is scarcely done at high-resolution (e.g. 1km×1km scale). In those published studies related to building stock model development, e.g. Yang and Kohler (2008) and Hu et al. (2010), the simulation and evolution of building stock value (taking the mainland China as a whole) were designed and targeted for resource consumption and environmental impacts purposes, which cannot meet the needs in risk analysis due to their coarse resolution. International projects e.g. PAGER (Jaiswal et al., 2010) and Gunasekera et al. (2015) also conducted global exposure modelling that covered the building stock value in mainland China. However, these global models cannot fully make use of the census data available in each country and usually assuming a uniform distribution of building stock value per capita for each province or even for each country, which might be convenient, but not realistic, especially for unevenly developed countries like China. A recent work of Wu et al. (2018) established a high-resolution (1km×1km scale) asset value model for mainland China based on the net capital stock value estimated for 344 prefectures in mainland China using the perpetual inventory method (Wu et al., 2014). However, their orginal asset data to be disaggregated into grid level was actually restricted to prefecture level. Furthermore, the extent of the natural hazards, in most cases, are dependent on the geological structure (earthquakes) or along the riverside (floods), instead of being restricted to administrative boundary. Therefore, to better cope with this spatial mismatch between natural hazards and administrative boundary, building stock model should be geocoded with relatively higher resolution and be disaggregated from more detailed census data.

The organization of this Chapter is as follows: the census data sources and methodology to develop the high-resolution building stock for mainland China will be firstly introduced. Then, to evaluate the model performance, provincial and district level comparison of the modelled results with that in previous studies and yearbook records will be conducted. An application of the building stock in seismic risk analysis will also be given. It is worth to note that the building types classified in the census data is different from that in Chapter 3 based on building vulnerability. Therefore, a recategorization process of the building types in this Chapter to the four major building types in Chapter 3 (Masonry_A, Masonry_B, RC_A, RC_B) will be introduced later in Chapter 5.

4.2 Data Sources and Methodology

This section will introduce the details of building related census data used to develop the building stock model and the methodology to disaggregate these administrative level census data into grid level. The census data used in this study for building stock modelling are extracted from the Tabulation of the 2010 Population Census of the People's Republic of China (hereafter abbreviated as "2010census", http://www.stats.gov.cn/tjsj/pcsj/rkpc/6rp/indexch.htm), particularly for residential buildings. Like in most countries of the world, the national level population and housing census are carried-out at 10-year

interval, and currently the latest version was issued in 2010. In 2010census, there are two types of tables: Long Table and Short Table. Long Table includes summaries based on the surveys of 10% of the overall population in mainland China, while in the Short Table summaries are based on the surveys of the whole population. Building stock model related census data (e.g. building occupancy type, height classes, construction material etc.) are extracted from the Long Table of 2010census. Supplementary demographic information (e.g. the overall population, the average number of person per family and average floor area per person) were extracted from the Short Table of 2010census. The numbering of these data in 2010census is summarized in Table 4-1.

Table 4-1: Main data sources used in this study.

Data source	Data description	Resolution	Data location	Indicator in the text	Notes
2010 China Sixth Census Short Table	overall population	urban/township/rural level for each of the 31 provinces/municipalities in mainland China; (the urbanity level in the census is defined according to the administrative belonging of the surveyed population)	Table 1-1a, 1-1b, 1-1c	N/A	Based on surveys of 100% of the population in mainland China
2010 China Sixth Census Long Table	Number of families living in buildings grouped by usage (purely residence, mixed with production/business, no residence)		Table 9-1a, 9-1b, 9-1c	N/A	Based on surveys of 10% of the overall population in mainland China
	Number of families dwelled in buildings grouped by storey number (1, 2-3, 4-6, 7-9, ≥10)				
	Number of families dwelled in buildings grouped by construction material (steel/RC, mixed, other, brick/wood)				
2010 China Sixth Census Short Table	Average population per family		Table 1-1a, 1-1b, 1-1c	D3 of Fig. 1	Based on surveys of 100% of the population in mainland China
	Average residential floor area per person (unit: square meter)		Table 1-14a, 1-14b, 1-14c	D4 of Fig. 1	
2015 GHS population density profile	provides the population density in each geo-coded grid	1km×1km	N/A	λ	The original resolution is 250m × 250m and was resampled to 1km×1km
2015 Shanghai Statistics Yearbook	GDP and population in each district	District level	Page 495-545	N/A	To derive the uniform construct cost (UCC)
2015 China Construction Yearbook	Yearly construction value added in each province	Provincial level	Table 1-2	N/A	These data are used to evaluate modelled building stock value

For each of the 31 provinces and municipalities in China, the building related census data in the Long Table are categorized into three urbanity levels (urban, township and rural), based on the administrative belonging of the surveyed population. The values of these building related census data for each urbanity level of each province are listed in Table 4-2. Compared with provincial level census data used in previous studies, one advantage of the 2010census data is its further categorization of data into three urbanity levels, which better reflects the regional difference within one province/municipality.

Table 4-2: Building related data extracted from the Tabulation of the 2010 Population Census of the People's Republic of China (abbreviated as "2010cencus").

Prov_ID	Province	2015 GHS pop.	floor area per capita	person per family	Number of families grouped by usage			Number of families grouped by building height (storey)					Number of families grouped by construction material				Amp. Factor (F2 in Fig.1)
					living	prod/comm	mixed	1	2-3	4-6	7-9	≥10	steel/RC	mixed	brick-wood	others	
URBAN																	
1001	Anhui	12162978	29.42	2.71	331730	9035	287	44093	82489	175486	20922	17775	135377	176462	26705	2221	1.32
1002	Beijing	18597540	27.81	2.40	517975	6482	988	127740	33290	193270	21919	148238	226367	212873	83192	2025	1.47
1003	Chong-qing	8391462	29.77	2.65	258417	3956	247	17185	39448	39087	85383	81270	131656	112494	13433	4790	1.21
1004	Fujian	12699884	30.29	2.70	360721	13488	736	30557	97680	135725	79915	30332	213350	124702	23948	12209	1.25
1005	Gansu	5282457	26.69	2.68	160717	3134	107	24489	21076	75051	34161	9074	78731	66665	15057	3398	1.20
1006	Guang-dong	56519993	26.37	2.63	1466895	34218	513	152601	299326	453172	412315	183699	748196	663772	76682	12463	1.43
1007	Guangxi	8478357	30.71	2.93	238044	5912	264	26305	53876	99335	52485	11955	86601	138730	16271	2354	1.18
1008	Guizhou	5485811	25.94	2.82	157713	5141	19	17373	38055	50766	49256	7404	78055	75834	7703	1262	1.19
1009	Hainan	2327452	25.42	3.17	56383	1602	68	9674	14288	13787	13124	7112	41510	10814	4948	713	1.26
1010	Hebei	14836541	30.10	2.95	419978	3950	96	100741	42944	230919	29889	19435	155581	211716	54745	1886	1.19
1011	Hei-longjiang	14367419	23.72	2.58	455996	6911	418	122051	20020	130862	173283	16691	163427	188650	104208	6622	1.20
1012	Henan	18527056	34.02	3.05	521036	7612	215	79535	122569	244091	64920	17533	190648	307902	28268	1830	1.15
1013	Hubei	17537483	33.22	2.82	502439	12733	349	40937	132838	179474	126270	35653	180316	298109	33900	2847	1.21
1014	Hunan	12911981	33.45	2.89	358447	9813	501	32935	92165	160007	62887	20266	132713	201615	31404	2528	1.21
1015	Jiangsu	30857658	33.86	2.81	876264	14961	802	129293	224580	412115	65052	60185	325288	469388	92721	3828	1.23
1016	Jiangxi	7844695	29.76	3.19	201690	3594	201	17052	46727	85663	48457	7385	111658	76679	15396	1551	1.20
1017	Jilin	10270924	25.21	2.62	329782	4910	1777	59861	13029	149906	96067	15829	175788	108325	48852	1727	1.17
1018	Liaoning	22172958	25.76	2.57	768884	7122	843	111439	28046	366106	211530	58885	321935	381031	71386	1654	1.11
1019	Inner Mongolia	8302698	24.86	2.67	251738	6951	631	84432	24977	133932	11690	3658	105902	87092	61924	3771	1.20
1020	Ningxia	2215109	28.38	2.71	64336	1829	29	10922	7958	44770	1313	1202	24606	34483	6352	724	1.23
1021	Qinghai	1470242	27.77	2.74	41342	1229	62	4877	8035	20737	6292	2630	13527	26113	2415	516	1.26
1022	Shaanxi	9021036	28.81	2.70	269044	4820	362	33723	56478	122687	37356	23620	89287	173753	8694	2130	1.22
1023	Shandong	28921044	32.41	2.80	855282	15616	242	252471	88326	432226	67205	30670	348873	356038	161295	4692	1.19
1024	Shanghai	20557127	25.11	2.52	604654	9991	928	60506	116799	304794	27780	104766	268377	249438	93734	3096	1.33
1025	Shanxi	9837996	25.77	2.88	282847	4319	87	53815	47879	157087	18683	9702	90187	163209	29124	4646	1.19
1026	Sichuan	15732199	30.70	2.67	499024	9628	630	47158	79975	198299	136824	46396	218827	247875	34088	7862	1.16

1027	Tianjin	10012251	25.51	2.65	237060	2606	167	34902	12083	143755	28570	20356	58333	156521	23467	1345	1.58
1028	Xinjiang	6578245	28.00	2.56	201621	2686	84	32261	24343	129144	12124	6435	88699	94628	18420	2560	1.26
1029	Tibet	289534	31.81	2.45	8394	973	7	2930	4798	1580	47	12	5449	2227	1020	671	1.26
1030	Yunnan	6531449	31.27	2.59	200602	7122	172	21262	45555	93027	36704	11176	102015	85386	13317	7006	1.21
1031	Zhejiang	21732071	30.97	2.54	675858	19305	774	80859	193447	332899	50666	37292	220048	393843	74559	6713	1.23
TOWNSHIP																	
2001	Anhui	13372970	32.20	2.95	355306	19130	477	144219	160370	67744	1426	677	95625	182264	91921	4626	1.21
2002	Beijing	1548053	33.20	2.52	41959	1129	143	21808	2812	16414	710	1344	6224	20550	15964	350	1.42
2003	Chong-qing	6393138	34.91	2.73	187287	7816	357	35957	71385	40448	41156	6157	46425	112018	23805	12855	1.20
2004	Fujian	8616342	37.67	3.09	224647	11851	318	44154	105240	65529	18822	2753	100650	83984	28551	23313	1.18
2005	Gansu	3949838	25.92	3.17	101071	5160	124	58128	13450	30226	4198	229	31721	30839	34944	8727	1.17
2006	Guang-dong	17954335	26.41	3.52	357650	15136	348	119634	161452	60743	27235	3722	124661	175520	63890	8715	1.37
2007	Guangxi	10216390	34.43	3.34	264485	12263	480	94666	111560	58971	11002	549	53729	175149	42500	5370	1.10
2008	Guizhou	6142030	28.39	3.12	159970	12522	41	65929	60006	34332	11785	440	44016	89287	28725	10464	1.14
2009	Hainan	1986929	23.78	3.42	45035	2592	51	26889	15458	4359	607	314	19912	12356	14449	910	1.22
2010	Hebei	17723090	30.74	3.40	454034	12232	203	338450	45232	73026	3484	6074	90952	165751	204531	5032	1.12
2011	Hei-longjiang	7326077	22.67	2.63	230438	7764	526	152211	13711	54825	16851	604	26869	70838	130084	10411	1.17
2012	Henan	18079108	32.04	3.60	435993	14307	304	242151	151413	53669	2676	391	91696	240373	114219	4012	1.11
2013	Hubei	10287748	38.10	3.12	267951	11284	318	65151	136106	59020	18152	806	75159	150951	47125	6000	1.18
2014	Hunan	15928705	36.74	3.18	413160	16084	1397	107304	216464	90305	12926	2245	103618	225168	92116	8342	1.16
2015	Jiangsu	17599234	39.53	3.00	493818	16021	436	194665	224247	86379	2299	2249	99148	264939	142526	3226	1.15
2016	Jiangxi	12539807	33.57	3.54	283781	10796	1125	57795	138466	80093	17102	1121	144491	98662	45425	5999	1.20
2017	Jilin	4483838	22.51	2.70	139477	4710	1966	90313	10161	37025	6460	228	34567	30467	73754	5399	1.14
2018	Liaoning	5202389	26.23	2.75	168663	5618	94	100064	11565	51923	9229	1500	51280	52098	69815	1088	1.08
2019	Inner Mongolia	5916056	24.38	2.74	172725	9637	1622	124351	14566	41832	1422	191	43195	35332	90983	12852	1.17
2020	Ningxia	1035570	24.82	3.14	25273	1397	58	16542	2590	7308	176	54	6140	7109	12255	1166	1.23
2021	Qinghai	1234007	21.94	3.06	28364	1806	1694	15491	4641	9622	386	30	8482	9814	8928	2946	1.27
2022	Shaanxi	8393227	28.85	3.05	218969	10349	295	103810	63776	53427	6133	2172	61288	115983	30075	21972	1.20
2023	Shandong	19633228	32.14	3.03	555539	16773	117	412345	53861	102936	2235	935	105549	177664	274908	14191	1.13
2024	Shanghai	3396024	30.25	2.45	100049	3066	715	24233	44272	29262	638	4710	35992	46750	19423	950	1.34
2025	Shanxi	8095334	25.43	3.24	208837	7124	292	128133	41454	42626	2929	819	49930	87194	66418	12419	1.16
2026	Sichuan	16239393	34.47	2.80	494678	24545	2048	133695	170345	141458	64579	9146	144800	259633	80423	34367	1.11
2027	Tianjin	1604748	29.64	2.98	36626	688	6	20978	1965	12727	559	1085	5896	13066	18217	135	1.44
2028	Xinjiang	3536191	26.04	2.75	95090	2368	50	57285	7087	32598	301	187	31109	21827	34576	9946	1.32
2029	Tibet	434071	33.52	2.89	10835	1334	69	5712	5333	1058	39	27	5633	2406	2961	1169	1.23
2030	Yunnan	9948973	30.04	3.29	249892	15089	538	95990	113777	49076	5598	540	85728	73181	58444	47628	1.14
2031	Zhejiang	14032915	38.53	2.66	435571	17019	321	78393	215994	143891	9590	4722	88524	262572	92204	9290	1.16

RURAL																	
3001	Anhui	33868749	34.04	3.12	972114	12697	1032	594442	384935	5062	259	113	122416	440296	399437	22662	1.10
3002	Beijing	3290554	35.39	2.76	85494	2139	89	81788	2698	2877	93	177	2991	19546	63298	1798	1.36
3003	Chong-qing	13097499	42.04	2.72	436237	8496	810	215548	219389	6337	3076	383	34275	160849	146892	102717	1.08
3004	Fujian	16023424	41.24	3.16	447940	13851	615	152099	279696	27946	1860	190	105558	152003	108638	95592	1.10
3005	Gansu	16457361	21.94	3.89	444734	2789	233	434394	12043	911	94	81	23583	50990	233241	139709	0.94
3006	Guang-dong	38073367	25.99	3.74	825588	7932	862	473821	328499	27016	3542	642	168179	388958	244088	32295	1.22
3007	Guangxi	28020960	28.82	3.47	788492	7837	834	494076	294396	7474	300	83	100152	424443	210891	60843	1.01
3008	Guizhou	22795976	27.92	3.29	657275	13176	244	526145	137494	5485	1206	121	80232	208026	247780	134413	1.03
3009	Hainan	4368909	21.29	3.63	109378	771	69	101212	8248	437	217	35	22309	16584	68949	2307	1.09
3010	Hebei	41534503	30.09	3.50	1138877	6755	525	1108487	32754	3591	510	290	65563	351042	689663	39364	1.04
3011	Hei-longjiang	17284909	20.92	3.19	472849	3926	1647	469755	3174	2668	1148	30	5933	44163	339849	86830	1.13
3012	Henan	58426898	32.23	3.58	1593259	18790	715	1263614	341472	6231	554	178	170146	778487	632719	30697	1.01
3013	Hubei	28165214	38.64	3.40	805308	11381	807	395220	405959	12191	2267	1052	87280	373421	286599	69389	1.01
3014	Hunan	37755133	34.27	3.54	1008324	9900	2170	496152	516168	5569	262	73	113888	408562	427367	68407	1.05
3015	Jiangsu	32006376	42.35	3.03	978352	13096	999	526012	444382	17344	893	2817	77218	494838	411206	8186	1.06
3016	Jiangxi	26204945	33.81	3.86	627420	6578	1410	251425	373710	8390	355	118	184327	209487	198186	41998	1.07
3017	Jilin	12897767	20.98	3.35	353543	2220	2523	347297	3170	4561	676	59	11283	35524	274007	34949	1.07
3018	Liaoning	16672483	25.95	3.12	519784	3994	237	512930	6643	3709	390	106	31856	123657	360371	7894	1.02
3019	Inner Mongolia	11385344	22.17	2.97	337168	4773	1167	331674	6301	3644	77	245	10616	34647	206674	90004	1.12
3020	Ningxia	3527454	22.12	3.54	86461	1371	35	80927	1965	4863	64	13	4944	9056	60381	13451	1.13
3021	Qinghai	3342860	18.51	4.06	71842	604	1521	69459	2789	181	7	10	2675	9718	36221	23832	1.11
3022	Shaanxi	20689727	31.22	3.54	572916	6711	497	481090	94599	3360	348	230	60338	235474	142395	141420	1.01
3023	Shandong	49116344	31.95	3.07	1549890	8748	182	1511164	40165	6807	399	103	77610	400711	1025247	55070	1.03
3024	Shanghai	2871449	38.83	2.37	90972	1752	1153	31644	57352	3415	49	264	8884	48551	33963	1326	1.29
3025	Shanxi	19386995	25.09	3.44	521669	4921	593	481296	38553	6348	290	103	34053	138101	243316	111120	1.07
3026	Sichuan	47518958	36.63	3.10	1625052	36122	3253	1067677	574735	16573	1425	764	147168	513785	611594	388627	0.92
3027	Tianjin	3007476	25.95	3.21	78318	570	30	74498	686	3345	110	249	2325	7772	68306	485	1.19
3028	Xinjiang	13521011	22.35	3.55	314397	2226	115	309505	2663	4345	82	28	11730	36704	207565	60624	1.20
3029	Tibet	2468309	27.55	4.95	44816	1260	718	27819	17858	360	26	13	2594	5152	23631	14699	1.07
3030	Yunnan	30987983	25.61	3.89	756974	10742	1276	461191	296513	6950	2470	592	68863	112129	239753	346971	1.04
3031	Zhejiang	22254831	49.12	2.67	740469	17587	807	152558	544733	58732	1649	384	60829	419761	236627	40839	1.10

To disaggregate the urbanity-level based census data into grid-level, population density is also used as the proxy, as is a common practice in risk analysis (Aubrecht et al., 2013). The population density profile chosen in this study is developed by Global Human Settlement (GHS) project of the European Union (http://data.europa.eu/89h/jrc-GHS-ghs_pop_gpw4_globe_r2015a) in 2015, which was disaggregated from census or administrative units to geo-girds, informed by the distribution and density of built-up area as mapped in the Global Human Settlement Layer (GHSL) global layer. In the 2015 GHS population density profile, the number of population in each geo-grid is given, which is proved to be of high resolution and accuracy when compared with real cases (Gunasekera et al., 2015). The original resolution of the 2015 GHS population density profile is 250m×250m, for calculation convenience it is resampled to 1km×1km resolution before further going analysis. The provincial/municipal boundary (level 1) vector layer dataset defining the spatial boundaries of mainland China is from the Global Administrative Areas (GADM, www.gadm.org).

After getting all the input data source (all with publicly available sources) ready for residential building stock modelling, a top-down spatial scaling method will be performed to disaggregate the urbanity-level based census data for each province/urbanity in mainland China into 1km×1km resolution grids. The flowchart in Figure 4-1 provides a brief overview of this modelling process. Detailed explanations of each component and step are as follows.

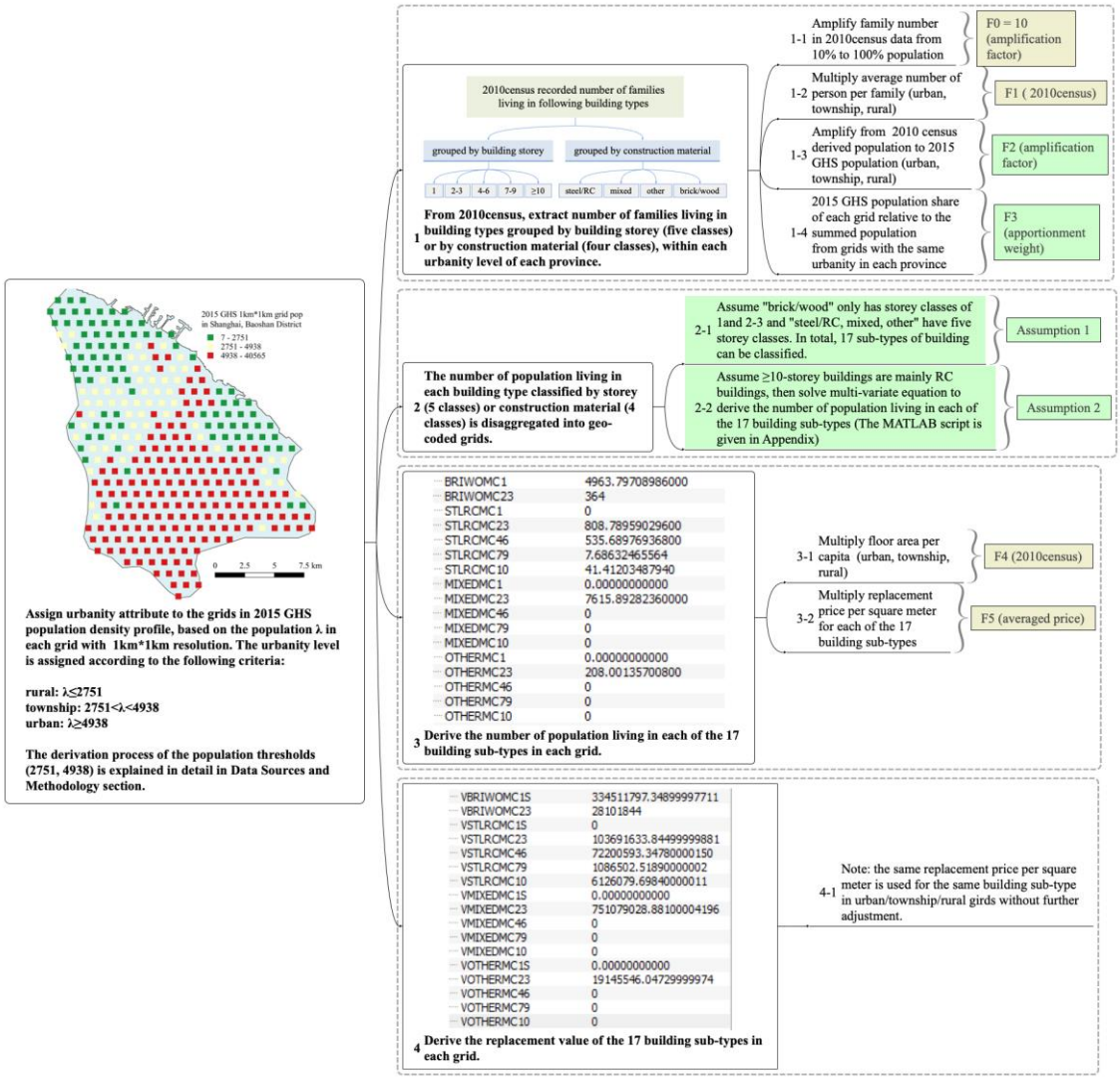

Figure 4-1: Flowchart of the residential building stock modelling process for mainland China.

4.2.1 Assign urbanity attribute (urban/township/rural) to the geo-coded grids in the 2015 GHS population density profile

As outlined above, the population and housing related census data for each of the 31 provinces/municipalities in mainland China are categorized into three urbanity levels: urban, township and rural. Therefore, the geo-coded grids in 2015 GHS population density profile should also be assigned with an urbanity attribute first, before disaggregating the urbanity-level based census data into each grid. For each province/municipality, this is achieved by applying the population reallocation approach developed by Aubrecht et al. (2015) and also illustrated in detail in Gunasekera et al. (2015).

Following this population reallocation approach, the urban/township/rural population proportion of each province can be derived from the Short Table of 2010census (as listed in Table 4-2). For example, in Shanghai City, the population proportion of urban/township/rural urbanity level is 76.64%, 12.66% and 10.7%, respectively. Then the grids (1km×1km) in 2015 GHS population density file of Shanghai are sorted from

the largest to the smallest, and the population in those largest and most populated geo-codes grids are summed up and selected until the 2010census urban population share (i.e. **76.64%** for Shanghai) is reached. These selected grids are thus assigned with urbanity attribute "urban". The smallest population of these selected grids is taken as the threshold to divide urban and non-urban grids (for Shanghai this urban/non-urban population density threshold is **4938** per km^2). For the remaining non-urban grids, the same process is repeated iteratively until the township population ratio (i.e. **12.66%** for Shanghai) is reached. These secondly selected grids are assigned with urbanity attribute "township" and the smallest population among these grids is taken as the threshold to divide township and rural grids (for Shanghai this township/rural population threshold is **2751** per km^2). The remaining grids are thus assigned with "rural" attribute. The distribution of the assigned urban/township/rural grids in Baoshan District of Shanghai is shown in Figure 4-1 as an example.

Reiterate the above calculations for all the 31 provinces/municipalities in mainland China, then all the geo-coded grids in the 2015 GHS population profile can be assigned with urban/township/rural attribute accordingly. The corresponding population urbanity thresholds for each province/municipality are provided in Appendix G.

4.2.2 Step 1----Extract the building related census data from the Long Table of 2010census (statistics derived from surveys of 10% population of mainland China

As in many other countries, the population and housing census data in mainland China are particularly surveyed for residential buildings. Therefore, accurately speaking, the building stock model to construct in this study is mainly for residential building stock. Related census data for assessment of residential building stock value include the number of families living in building types grouped by building occupancy (i.e. residential, commercial, other), by number of storey (i.e. 1, 2-3, 4-6, 7-9, ≥10), and by construction material (i.e. steel/reinforced-concrete, mixed, brick/wood, other). As already listed in Table 4-1, these data are extracted from the Long Table of the 2010census, based on the survey of 10% of the overall population in mainland China. Therefore, to evaluate the whole building stock value across China, these building related 2010census data should be extended from 10% to 100% population first by multiplying the factor of 10 (namely factor *F0* in Step 1-1 of Figure 4-1).

After multiplying the factor of 10, the overall number of families living in building types grouped by building storey or construction material is considered to be complete for each urbanity level of each province/municipality. With the family number living in each building type known, by multiplying the average number of population per family (namely factor *F1* in step 1-2 in Figure 4-1), which was also provided in the Short Table of 2010census, the overall population living in building types grouped by storey (1, 2-3, 4-6, 7-9, ≥10) or construction material (steel/RC, mixed, other, brick/wood) can thus be instantly derived for each province and each urbanity level.

Up to now, the geo-codes grids in the 2015 GHS population density profile have been assigned with urbanity attribute and the population living in each building type is also derived for each province and each urbanity level from the 2010census. It is noteworthy that the changes in population or building from 2010 to 2015 has not been considered yet. In rapid urbanization countries like China, the increasing construction of buildings and the population inflow from township/rural areas to urban areas are not negligible. Therefore, the population derived from 2010census needs to be further amplified to 2015 level, and

mathematically this amplification factor (factor *F2* in Step 1-3 of Figure 4-1) is assumed to be equal to the ratio between 2015 GHS population and 2010census derived population (already amplified from 10% to 100% population).

As listed in the last column in Table 4-2, the amplification factor *F2* varies for each urbanity level of each province (namely factor *F2* in Step 1-3 of Figure 4-1). For each province, *F2* in the urban area is generally higher than in township/rural area, which is quite reasonable. However, it should be noted that the increase in building construction area from 2010 to 2015 is also assumed to be equal to the population increase. The reasonability of such assumption and the performance of the residential building stock model will be further evaluated in the Results and Discussion section.

After getting the population living in each building type for each urbanity level of each province derived, the urbanity-level based population data can be disaggregated into the geo-coded grids with the same urbanity attribute in 2015 GHS population density profile, by multiplying the apportionment weight (namely factor *F3* in step 1-4 of Figure 1). *F3* is defined as the population share of each grid relative to the summed population from grids with the urbanity level for each province.

4.2.3 Step 2----Disaggregate population and building related census data from urbanity level into grid-level

As explained in Section 4.2.2, by multiplying the original building related records extracted from 2010census with factor *F0, F1, F2* and *F3* in Step 1 of Figure 1, the population in each grid living in building types grouped by storey (1, 2-3, 4-6, 7-9, ≥10) or by construction material (steel/RC, mixed, other, brick/wood) can be derived.

To further estimate the residential building stock value, more detailed building classification for construction pricing is needed. Therefore, the next step is to recategorize the building types classified by five storey classes and four construction material classes into sub-types in terms of both storey and construction material. Theoretically 20 building sub-types can be derived. Considering the fact that in real cases, most brick/wood buildings are with quite low height (1 or 2-3 storey), while steel/RC-made buildings are generally quite high with height of 10-storey and above. Therefore, it is further assumed for "brick/wood" building type, there are only two storey classes (1, 2-3). While for "steel/RC", "mixed", and "other" building types defined in 2010census, all five storey classes (1, 2-3, 4-6, 7-9, ≥10) are available (namely *Assumption 1* in Step 2-1 of Figure 4-1). Thus, the buildings in each grid can be further classified into 17 building sub-types (as listed in Table 4-3).

In each grid, the number of population living in buildings of five storey classes or four construction materials is already derived in Step 1. Thus, multi-variate equations can be established, in which 17 unknown variables need to be solved from 9 equations. Therefore, further reasonable approximations need to be made (namely *Assumption 2* in Step 2-2 of Figure 4-1), to make sure that in each grid the sum of population living in the 17 building sub-types is equal to the population living in building types grouped by construction material or by storey class. The MATLAB script illustrating the multi-variate equations' solving process is provided in Data/Code Availability section.

4.2.4 Step 3----Derive the number of population living in each of the 17 building sub-types

With necessary assumption and approximation and by solving the multi-variate equations mentioned in Section 4.2.3, the population living in each of the 17 building sub-types can be derived for each grid. In the Short Table of 2010census, the average residential floor area per capita is also provided for each urbanity level of each province (namely factor *F4* in Step 3-1 of Figure 4-1). Therefore, the floor area of the 17 building sub-types in each grid can be directly derived. Comparison between the modelled floor area with statistical yearbook recorded residential floor area for Shanghai will be performed in the Results and Discussion section.

With the building floor area known in each grid, to model the building stock value, another key component is the replacement value per square meter of each of the 17 buildings sub-types (namely factor *F5* in Step 3-2 of Figure 4-1). Given the specialty/uniqueness of the building classification in this study, there is no official construction prices evaluated for the building types used here. Therefore, the construction price per square meter for each of the 17 building sub-types is derived (as listed in Table 4-3) by averaging the values given from different sources (e.g. China Construction Statistical Yearbook, the World Housing Encyclopedia, real-estate agency reports etc.). It should be noted that, due to the disparity of urbanization level, the actual construction price varies across urbanity levels and provinces/municipalities in mainland China. Therefore, when applying the residential building stock model to target area for risk analysis, the construction price should be justified accordingly. In this study, the set of averaged construction prices in Table 4-3 for the 17 building sub-types is used mainly to initially evaluate the replacement value of the residential building stock in each geo-coded grid.

Table 4-3: Averaged construction price per square meter for each of the 17 building sub-types used in this study to estimate the building stock value in mainland China.

Construction material	Storey class	Building type abbreviation	Construction price (RMB/m^2) in 2015 current price)
brick/wood	1	BRIWOMC1	2050
	2-3	BRIWOMC23	2350
steel/RC	1	STLRCMC1	3700
	2-3	STLRCMC23	3900
	4-6	STLRCMC46	4100
	7-9	STLRCMC79	4300
	≥10	STLRCMC10	4500
mixed	1	MIXEDMC1	2800
	2-3	MIXEDMC23	3000
	4-6	MIXEDMC46	3200
	7-9	MIXEDMC79	3400
	≥10	MIXEDMC10	3600
others	1	OTHERMC1	2600
	2-3	OTHERMC23	2800
	4-6	OTHERMC46	3000
	7-9	OTHERMC79	3200
	≥10	OTHERMC10	3400

4.2.5 Step 4----Derive the replacement value of the 17 building sub-types in each grid

As elaborated in Step 3, after multiplying the floor area with construction price, the replacement value of the 17 building sub-types within each grid can be evaluated. By summing up the replacement value of all the geo-coded grids, the overall residential building stock value in mainland China can also be derived (in RMB of 2015 current price). It is worth to emphasize that in this residential building stock model, the term "building replacement value" is used, which refers to the amount that will be needed to rebuild a property exactly as it was prior to its destruction regardless of any depreciation due to its age (Gunasekera et al., 2015).

4.3 Results and Discussion

4.3.1 Results----urbanity-level (urban/township/rural) based sum of modelled floor area and replacement value

Following the efforts of extensive data survey, collection and processing, with the modelling components and steps being explained in detail in Data Sources and Methodology section, a high-resolution (with 1km×1km resolution) building stock model for mainland China targeted for future seismic risk assessment is established by disaggregating urbanity-level based census data into grid level. Since the census data are mainly related residential buildings, the model developed is thus particularly for residential buildings. As listed in Table 4-4, the modelled residential building floor area and replacement value (unit: RMB, in 2015 current price) in each grid are aggregated into urbanity level (urban/township/rural) for each province/municipality.

Table 4-4: Modelled residential building floor area and replacement value for urban/township/rural area of 31 provinces/municipalities in mainland China and comparison with net capital stock value estimated in Wu et al. (2014) using perpetual inventory method.

Prov_ID	Province	Initially modelled residential floor area (m^2)			(A): Initially modelled residential building stock replacement value (RMB in 2015 current price)			(C): Net capital stock value modelled in Wu et al. (2014, RMB in 2012 current price)	(A)/(C)
		urban	township	rural	urban	township	rural		
1	Anhui	3.57E+08	4.30E+08	1.15E+09	5.08E+11	4.97E+11	1.08E+12	3.86E+12	0.54
2	Beijing	5.16E+08	5.13E+07	1.16E+08	1.92E+12	1.48E+11	2.22E+11	3.85E+12	0.59
3	Chongqing	2.50E+08	2.23E+08	5.50E+08	5.63E+11	4.29E+11	8.25E+11	2.98E+12	0.61
4	Fujian	1.40E+08	2.46E+08	1.07E+09	3.61E+11	5.14E+11	2.02E+12	4.73E+12	0.61
5	Gansu	1.41E+08	1.02E+08	3.61E+08	2.31E+11	1.14E+11	2.71E+11	1.56E+12	0.39
6	Guangdong	1.11E+09	4.16E+08	1.40E+09	2.97E+12	8.05E+11	1.74E+12	1.07E+13	0.52
7	Guangxi	2.27E+08	2.94E+08	8.84E+08	5.42E+11	5.78E+11	1.29E+12	4.74E+12	0.51
8	Guizhou	1.42E+08	1.74E+08	6.36E+08	2.19E+11	1.98E+11	4.88E+11	2.08E+12	0.44
9	Hainan	1.82E+07	2.37E+07	1.43E+08	3.98E+10	3.87E+10	1.63E+11	7.86E+11	0.31
10	Hebei	3.90E+08	5.16E+08	1.33E+09	7.75E+11	8.23E+11	1.56E+12	6.82E+12	0.46
11	Heilongjiang	3.37E+08	1.65E+08	3.64E+08	8.39E+11	2.56E+11	3.68E+11	3.19E+12	0.46
12	Henan	6.30E+08	5.79E+08	1.88E+09	1.12E+12	1.02E+12	2.56E+12	9.30E+12	0.51
13	Hubei	5.82E+08	3.92E+08	1.09E+09	1.30E+12	6.09E+11	1.40E+12	5.44E+12	0.61
14	Hunan	4.31E+08	5.83E+08	1.29E+09	7.75E+11	7.86E+11	1.36E+12	5.22E+12	0.56
15	Jiangsu	8.27E+08	5.98E+08	1.73E+09	2.72E+12	1.67E+12	3.91E+12	1.27E+13	0.65
16	Jiangxi	2.33E+08	4.20E+08	8.84E+08	3.85E+11	5.35E+11	8.45E+11	2.93E+12	0.60
17	Jilin	2.48E+08	9.70E+07	2.79E+08	1.04E+12	2.60E+11	5.10E+11	4.52E+12	0.40
18	Liaoning	4.35E+08	1.14E+08	5.86E+08	1.68E+12	2.92E+11	1.07E+12	6.82E+12	0.45
19	Inner Mongolia	2.01E+08	1.38E+08	2.60E+08	1.20E+12	4.73E+11	5.94E+11	5.39E+12	0.42
20	Ningxia Hui	6.27E+07	2.57E+07	7.80E+07	1.83E+11	5.62E+10	1.22E+11	8.53E+11	0.42
21	Qinghai	4.07E+07	2.56E+07	6.07E+07	1.26E+11	5.47E+10	8.76E+10	6.26E+11	0.43
22	Shaanxi	2.59E+08	2.42E+08	6.46E+08	7.19E+11	5.22E+11	9.62E+11	4.25E+12	0.52

23	Shandong	7.49E+08	5.27E+08	1.85E+09	1.74E+12	1.05E+12	3.23E+12	1.32E+13	0.46
24	Shanghai	4.70E+08	1.10E+08	1.68E+08	1.99E+12	3.68E+11	3.92E+11	4.57E+12	0.60
25	Shanxi	2.53E+08	2.06E+08	4.86E+08	6.58E+11	3.61E+11	5.89E+11	3.27E+12	0.49
26	Sichuan	4.72E+08	5.51E+08	1.76E+09	7.95E+11	7.67E+11	1.81E+12	5.77E+12	0.58
27	Tianjin	2.19E+08	4.45E+07	1.18E+08	1.43E+12	1.90E+11	3.27E+11	3.88E+12	0.50
28	Xinjiang	1.81E+08	8.60E+07	3.10E+08	5.37E+11	1.96E+11	2.92E+11	2.19E+12	0.47
29	Tibet	8.73E+06	1.22E+07	6.92E+07	2.41E+10	3.06E+10	8.57E+10	3.37E+11	0.42
30	Yunnan	1.77E+08	2.33E+08	8.66E+08	2.83E+11	3.30E+11	8.14E+11	3.27E+12	0.44
31	Zhejiang	4.56E+08	4.10E+08	1.59E+09	1.20E+12	8.98E+11	2.84E+12	7.80E+12	0.63
In total:		1.06E+10	8.04E+09	2.40E+10	2.89E+13	1.49E+13	3.38E+13	1.48E+14	0.53

Note: (a) In this study, for each of the 17 building sub-types in each grid of urban/township/rural level in each province/municipality, the same unit construction price is used; (b) The modelled floor area and replacement value in this study are particularly for residential buildings; (c) The net capital stock value estimated in Wu et al. (2014) refers to the depreciated asset value of residential, non-residential buildings, and infrastructure as well; (d) The building construction price used in this study and that in Wu et al. (2014) are not equal.

As can be observed that up to year 2015, the total modelled residential building floor area for mainland China total reaches 42.64 billion m^2. By applying the same replacement price for the same building subtype (in total 17) in all the urban/township/rural areas of the 31 provinces/municipalities, the initially modelled residential building stock value in whole mainland China is approximately to be 77.6 trillion RMB (in 2015 current price). It is clear that, like all other building stock, the Chinese building stock is a complicated economic, physical and social system (Yang and Kohler, 2008). The economic disparity and geographic climatic diversity are widely spanned and the standardization in building construction also varies in different periods. Therefore, it is mainly for calculation convenience that this study applies the same unit construction price for all the provinces and all the urbanity levels. However, in future seismic risk assessment, to improve accuracy, the unit construction price of specific building types in the target study area should be adjusted accordingly.

4.3.2 Discussion

In this chapter, the building stock model is established through the disaggregation of urbanity-level based 2010census data into grid level by using 2015 GHS population density profile as the proxy. Due to the approximation and assumption made in this modelling process, the reasonability and consistency of the modelled results need to be cross validated. Due to the typical lack of officially accumulated building stock value from the government (Wu et al., 2018), direct comparison of the modelled floor area and replacement value with that from census or statistical yearbooks for whole mainland China is not availabl. Instead, the estimated stock value in previous studies is resorted to compare the modelled results with that in this study at provincial level.

4.3.2.1 Provincial-level based comparison between the modelled building value in this study and the net capital stock value estimated in Wu et al. (2014)

Previous studies on the capital stock estimation of mainland China mainly employed the perpetual inventory method (PIM), in which economy indicators e.g. gross fixed capital formation, total investment in fixed assets etc. were used. In general, these estimations are almost exclusively limited at national or provincial levels (Wu et al., 2014). Such coarse spatial resolution forms a major obstacle in applying the model in disaster loss estimation, due to the mismatch between the hazard extent and the administrative boundary. To better address this gap, Wu et al., (2014) estimated the net capital stock value (WKS) for 344 prefectures in mainland China by using the perpetual inventory method (PIM). In which, the WKS value (as listed in their Table A1) was calculated in 2012 current price, with the depreciation of all exposed assets (i.e. residential and non-residential building structures, tools, machinery, equipment and infrastructure) being considered.

To better evaluate the reliability and consistency of the modelled results in this study, the estimated net capital stock value in Wu et al. (2014) for prefectures within the same province is aggregated into provincial level first, as shown in Table 4-4. The ratio between the modelled residential building stock value in this study (represented by “A”) and net capital stock value (represented by “C”) in Wu et al. (2014) for each province is calcuated in column “(A)/(C)” of Table 4-4 for straightforward comparison. The value of (A)/(C) varies within the range of **0.31-0.65**, which indicates the high consistency between the residential building replacement value modelled in this study and the net capital stock value (for residential and non-residential buildings, infrastructure and other exposed elements) estimated in Wu et al. (2014), in spite of the differences in methodology and assumptions used in these two studies.

4.3.2.2 District-level based comparison between the modelled building floor area in this study and that recorded in statistical yearbook for Shanghai

It is found out a grid-level building stock model for Shanghai was developed in Wu et al. (2019), by disaggregating the census-level building floor area using building footprint map (extracted from high-resolution remote sensing data), combined with LandScan population density data as well as a financial appraisal of construction price according to building occupancy. Regretfully, Wu et al. (2019) did not separate residential floor area from non-residential floor area. Therefore, direct comparison of the modelled results with their outputs is not available. However, the district-level residential and non-residential floor area records used in their study for model performance evaluation, which were extracted from Shanghai 2015 Statistical Yearbook, turns out to be a good reference for this study to evaluate the modelled results at district-level.

To compare with the district-level residential floor area records in Shanghai statistical yearbook, the modelled floor area in each grid in Shanghai (Figure 4-2) is aggregated into district level (summarized in Table 4-5). As can be seen from Figure 4-2 that grids with high floor area typically cluster in downtown area (including eight administrative districts, namely Yangpu, Hongkou, Zhabei, Putuo, Changning, Xuhui, Jing'an and Huangpu) and in Pudong district. This corresponds to the fact that these districts are the most developed in Shanghai. As can be further validated from the 3D-view of population distribution in panel (d) of Figure 4-2, that these districts also have the highest population density in Shanghai.

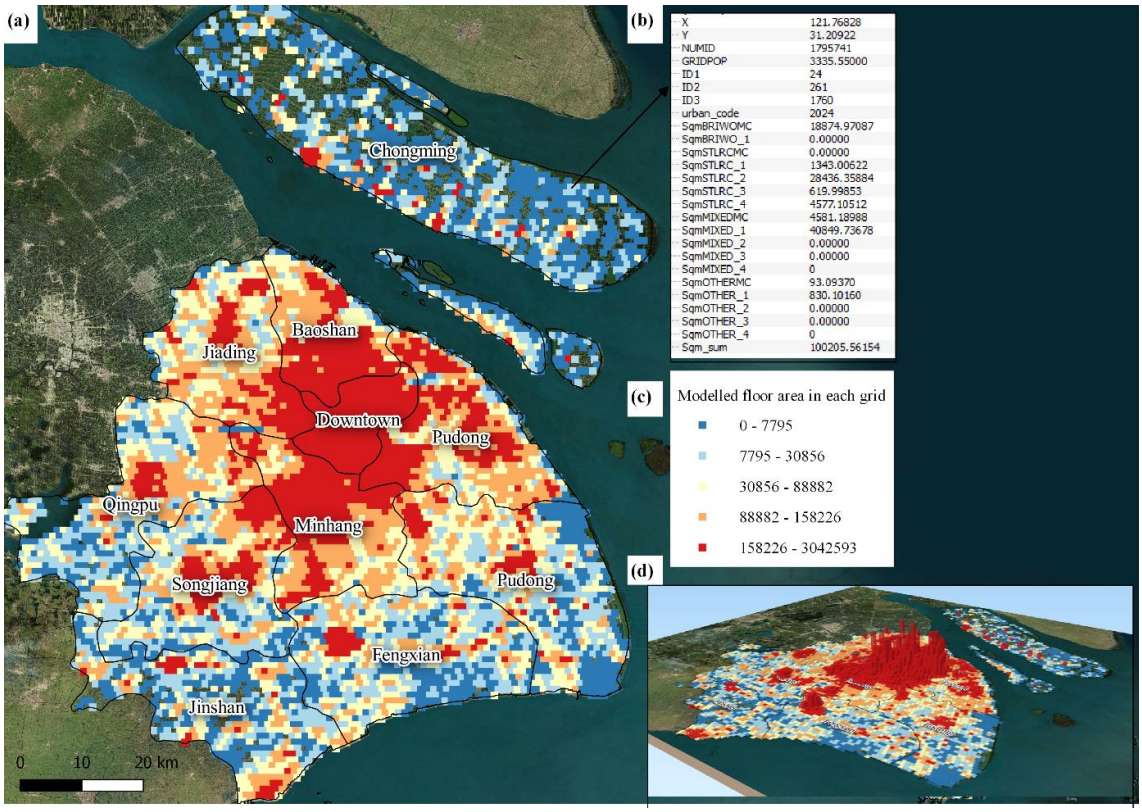

Figure 4-2: An example illustrating the modelled floor area for Shanghai: (a) the distribution of modelled floor area in each grid with resolution of 1km×1km; (b) in each grid, the floor area of the 17 building sub-types and the overall population "GRIDPOP" in each grid; (c) the legend of panel (a) and panel (d); (d) the 3D-view of the modelled floor area and the population distribution (the height of box in each grid is proportional to its population density). The background satellite map is provided by Bing map service that integrated in QGIS platform (https://qgis.org/en/site/).

Table 4-5 gives a summary of the population in 2015 GHS population density profile, the modelled floor area (classified by storey classes), as well as the 2015 statistical yearbook recorded population and floor area for districts/counties in Shanghai. For more direct comparison, the initially modelled floor area (without adjustment) and the yearbook recorded floor area in each district of Shanghai are plotted in Figure 4-3. The correlation between the initially modelled floor area and that recorded in yearbook turns out to be high, as indicated by the R^2 value (0.9103). However, when it comes to the absolute floor area value, the total residential floor area modelled in Shanghai is around 808 km^2, while the yearbook recorded residential floor area is 611 km^2, which means the initially modelled results is overpredicted (around 1.3 multiples of the yearbook records). Therefore, additional efforts are required to adjust the initially modelled results, to make the modelled floor area in each district more reasonably distributed and to de-amplify the overprediction of the overall modelled results.

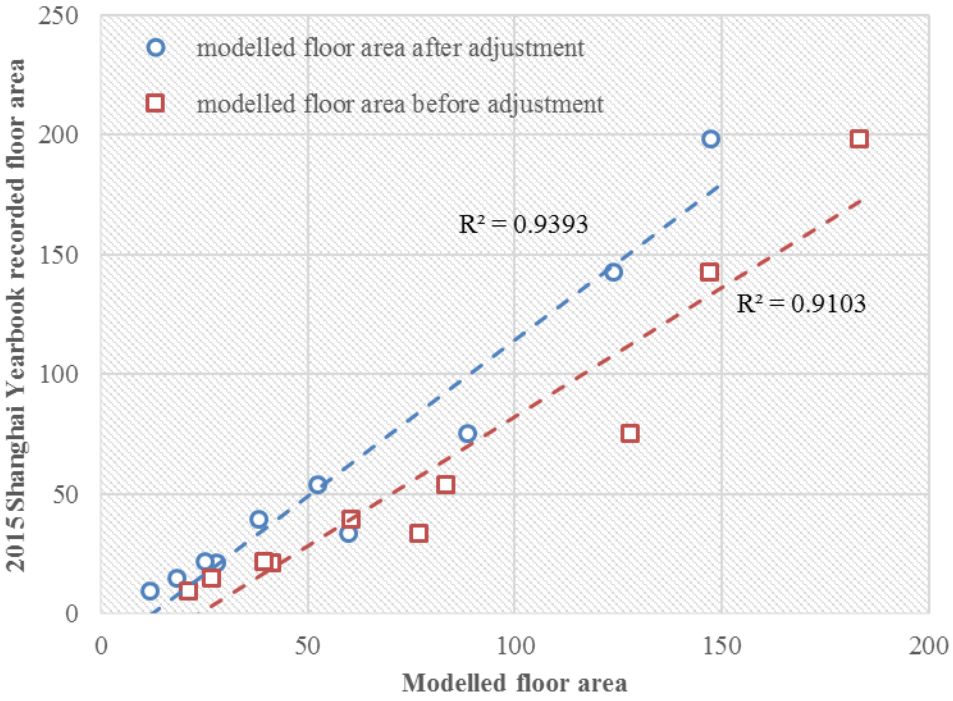

Figure 4-3: Comparison of the modelled floor area (before and after adjustment) with2015 Shanghai statistical yearbook recorded floor area in each district of Shanghai.

Table 4-5: Comparison of modelled floor area with Shanghai Statistical records in 2015.

District	Initially modelled population and floor area (km²)								Adjustment factor		adjusted floor area (km²)	2015 Shanghai Statistical Yearbook records			
	2015 GHS pop1	pop1. (%)	1	2-3	4-6	7-9	≥10	Sum of floor area in all storey classes	UCC	De-amp. factor		floor area diff. (%)	residential floor area (km²)	2015 statistics pop2	pop2 (%)
Baoshan	2.70E+06	10%	12.7	23.6	33.5	2.8	10.8	83.3	0.83	1.32	52.4	-3%	54	2.02E+06	8%
Chongming	6.67E+05	3%	7.0	12.6	1.4	0.0	0.2	21.3	0.74		12.0	23%	9.7	7.02E+05	3%
Fengxian	1.26E+06	5%	8.6	15.8	10.9	0.8	3.2	39.4	0.85		25.2	17%	21.6	1.17E+06	5%
Jiading	2.49E+06	9%	12.1	22.2	30.2	2.5	9.7	76.7	1.03		60.0	78%	33.6	1.57E+06	6%
Jinshan	8.54E+05	3%	5.7	10.5	7.8	0.5	2.2	26.7	0.91		18.4	25%	14.7	7.97E+05	3%
Minhang	4.20E+06	16%	15.3	29.0	58.9	5.1	19.6	127.9	0.92		88.6	18%	75.2	2.54E+06	10%
Pudong	4.74E+06	18%	27.6	51.1	49.5	3.9	15.2	147.2	1.11		124.0	-13%	142.9	5.45E+06	22%
Qingpu	1.33E+06	5%	8.5	15.6	12.5	0.9	3.6	41.1	0.90		27.9	32%	21.2	1.21E+06	5%
Songjiang	1.96E+06	7%	9.7	18.0	23.4	1.9	7.4	60.5	0.84		38.2	-3%	39.5	1.76E+06	7%
Downtown	5.99E+06	23%	22.9	43.3	82.5	7.2	27.5	183.4	1.06		147.3	-26%	198.5	7.05E+06	29%
	Sum: 2.62E+07							Sum: 807.5			Sum: 594.0	-3%	610.9	Sum: 2.43E+07	

Note: In "Adjustment factor", "UCC" is the abbreviation of Uniform Construction Price, derived in Table 4-7 and used to adjust the development disparity in districts of Shanghai; "De-amp. factor" is the averaged de-amplification factor, derived in Table 4-6 and used to adjust the amplification of population from 2010 census to 2015 GHS population; "Downtown" area includes eight administrative districts of Shanghai, namely Yangpu, Hongkou, Zhabei, Putuo, Changning, Xuhui, Jing'an and Huangpu.

Table 4-6: Derivation process of the de-amplification factor "1.32" in Table 4-5.

Shanghai urbanity	Modelled floor area (km²), without adjustment	Ratio (%)	Amp. Factor from 2010 census to 2015 GHS population	De-amp. factor
1024	469.6	63%	1.33	**1.32**
2024	110.4	15%	1.34	
3024	167.8	22%	1.29	

Looking backward the modelling process in Section 4.2, it is clear that the disaggregation of urbanity level floor area into each grid did not integrate the development disparity of districts/counties within the same province/municipality. Therefore, the initially modelled floor area is firstly rectified by using the index of Uniform Construction Cost (UCC) to reflect the development inequality across districts in Shanghai, which has been used in previous studies (e.g. Gunasekera et al., 2015). The UCC index of each district in Shanghai is developed from the population and per capita GDP in 2015, which is defined as the triple root of the ratio between each district's GDP/capita and the average GDP/capita of Shanghai in 2015. As listed in Table 4-7, the higher the UCC index value, the more developed the corresponding district.

Table 4-7: Derivation of Uniform Construction Cost (UCC) in Table 4-5 from Shanghai 2015 Statistical Yearbook, to reflect the development disparity among districts of Shanghai.

District	Population	District GDP	GDP/capita	UCC
Baoshan	202400	1.10E+11	54147	0.83
Chongming	70160	2.72E+10	38791	0.74
Fengxian	116760	6.68E+10	57246	0.85
Jiading	156620	1.63E+11	104084	1.03
Jinshan	79710	5.70E+10	71509	0.91
Minhang	253950	1.84E+11	72603	0.92
Pudong	545120	7.11E+11	130414	1.11
Qingpu	120830	8.27E+10	68476	0.90
Songjiang	175590	9.69E+10	55212	0.84
Downtown	704540	7.96E+11	113012	1.06
	sum: 2425680	sum: 2.29E+12	average: 94607	

Note: "Downtown" area includes eight districts of Shanghai located in the downtown area, namely Yangpu, Hongkou, Zhabei, Putuo, Changning, Xuhui, Jingan and Huangpu.

By multiplying the initially modelled floor area value with the UCC index in each district of Shanghai, the overall modelled floor area turns from 808 km^2 to 785 km^2. Although the overall floor area changes slightly, the application of UCC adjustment reallocates the floor area in each district, making it more proportionally related to the development level of each district. While, since compared with the yearbook recorded floor area 611 km^2 for Shanghai, the UCC index adjusted floor area 785 km^2 remains to be an obvious overprediction. Thus, de-amplification adjustment needs to be made as well. By checking the whole modelling process in Figure 4-1 carefully, it is found out that the overprediction of the modelled floor area for Shanghai may be attributed to the use of amplification factor F2 in Figure 4-1). F2 is used to synchronously amplify the building related census data from year 2010 to 2015 level. Mathematically it is equal to the ratio between 2015 GHS population and 2010census population for each urbanity level of each province. For example, the amplification factor F2 in Shanghai is 1.33/1.34/1.29 for urban/township/rural level, respectively.

In real cases, the increase of population in each urbanity level may not necessarily lead to the proportional increase of its residential floor area. Therefore, de-amplification of the initially modelled area for whole Shanghai is attempted here. The derivation of the de-amplification factor of Shanghai is achieved by summarizing the product between the amplification factor of each urbanity level (F2) and its modelled floor area proportion. As shown in Table 4-6, the final de-amplification of Shanghai is 1.32.

After applicating the de-amplification factor to the modelled floor area in Shanghai after UCC index adjustment (which is 785 km^2 in total), the final modelled floor area in each district of Shanghai is listed in Table 4-5. To better illustrate the difference between the initially modelled floor area and that adjusted by UCC index and de-amplification factor in each district of Shanghai, the comparison of modelled floor area (before and after adjustment) with statistical yearbook recorded floor area is plotted in Figure 4-3. As can be clearly seen from Figure 4-3, the value of the correlation indicator R^2 improves from 0.9103 (before adjustment) to 0.9393 (after adjustment). More importantly, after the adjustment of initially modelled floor area by UCC index and the de-amplification factor, the overall modelled floor area in Shanghai turns to 594 km^2, only a 3% difference compared with the statistical record of 610.9 km^2. This further indicates the reasonability of the adjustment made and the reliability of the modelled residential floor area in this study for Shanghai.

4.3.2.3 Application of the model to seismic loss estimation

Since the model developed in this study is mainly targeted for seismic risk analysis, the performance of the model is further evaluated by its application to the estimation of empirical loss in scenario earthquake. The hazard component to use for this loss assessment test is the macro-seismic intensity map of Wenchuan Ms8.0 earthquake (Figure 4-4), which was issued by China Earthquake Administration (CEA) based on the post-earthquake field investigations. The vulnerability function to use was the empirical loss function developed in Daniell (2014, Page 242) for mainland China. This empirical loss function was developed based on historical seismic damage and loss related to earthquakes occurred in mainland China. And such information was retrieved through extensive collection of damage and loss records from journals, books, reports, conference proceedings and even newspapers etc. Finally, based on the modelled residential building floor area in this study for Sichuan province and the unit construction price listed in Table 4-3, the estimated empirical loss to residential buildings caused by the recurrence of Wenchuan Ms8.0 earthquake is around 432 billion RMB (in 2015 current price). The distribution of loss ratio, i.e., the ratio between the estimated loss and the modelled residential building stock value, in counties/districts of Sichuan Province that damaged in Wenchuan Ms8.0 earthquake is shown in Figure 4-5.

In other reports and studies on the loss assessment of Wenchuan earthquake, e.g. in Yuan (2008), the estimated loss to residential buildings was around 170 billion RMB (in 2008 current price). The officially issued loss estimated by the Expert Panel of Earthquake Resistance and Disaster Relief (EPERDR, 2008) to residential buildings in Sichuan province was around 98.3-435.4 billion RMB, with the median around 212.32-247.25 billion RMB (in 2008 current price). It should be noted that in those studies, the unit construction price used for rural/urban/township building replacement was around 800-1500 RMB per square meter, which is 1/2.5-1/1.5 of the unit construction price used in this study as listed in Table 4-3. To lower down the gap in construction price used in this study and in previous studies, the estimated loss value (432 billion RMB) in this study is further divided by 1.5-2.5, then the rectified loss turns to be around 144-288 billion RMB. Then the estimated loss range based on the buildings stock model developed in this study and the empirical loss function developed in Daniell (2014) is quite compatible with that given in previous studies. This compatibility further validates the robustness of the residential building stock model. Therefore, the grid level building stock model developed in this study can be regarded as a reliable component input for further seismic risk assessment.

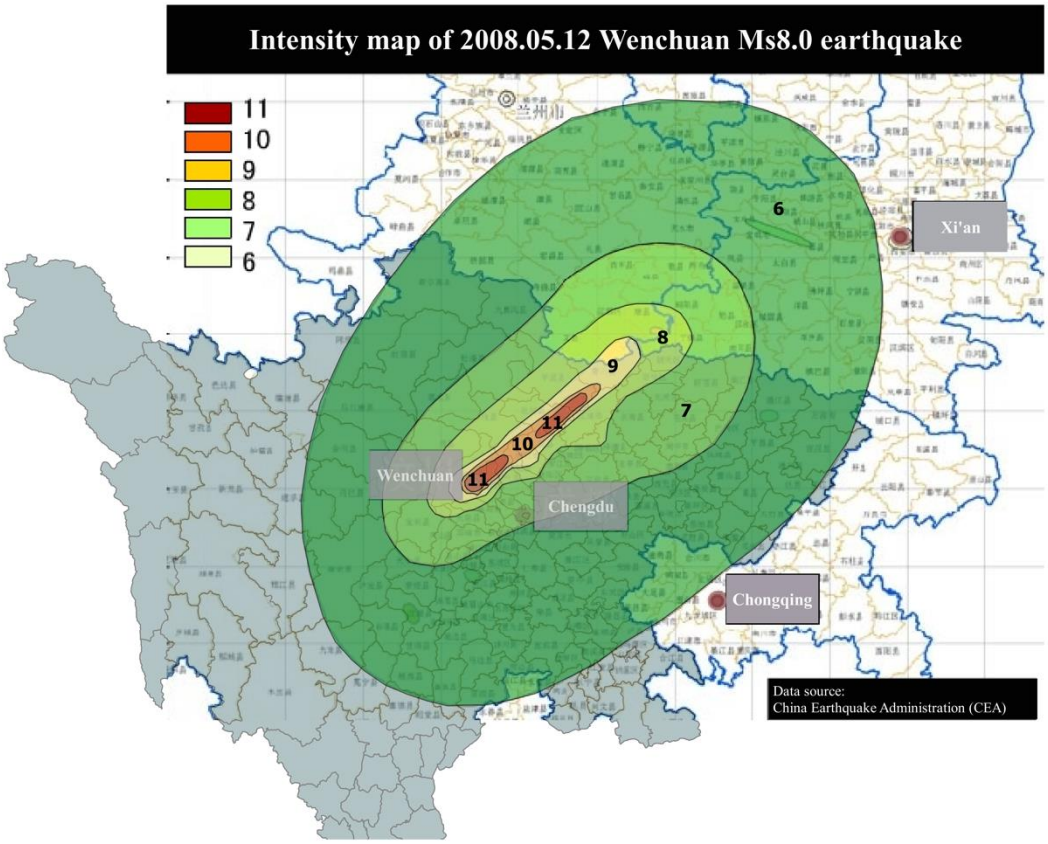

Figure 4-4: Macro-seismic intensity map of 2008 Wenchuan Ms8.0 earthquake, modified based on the version issued by China Earthquake Administration (CEA).

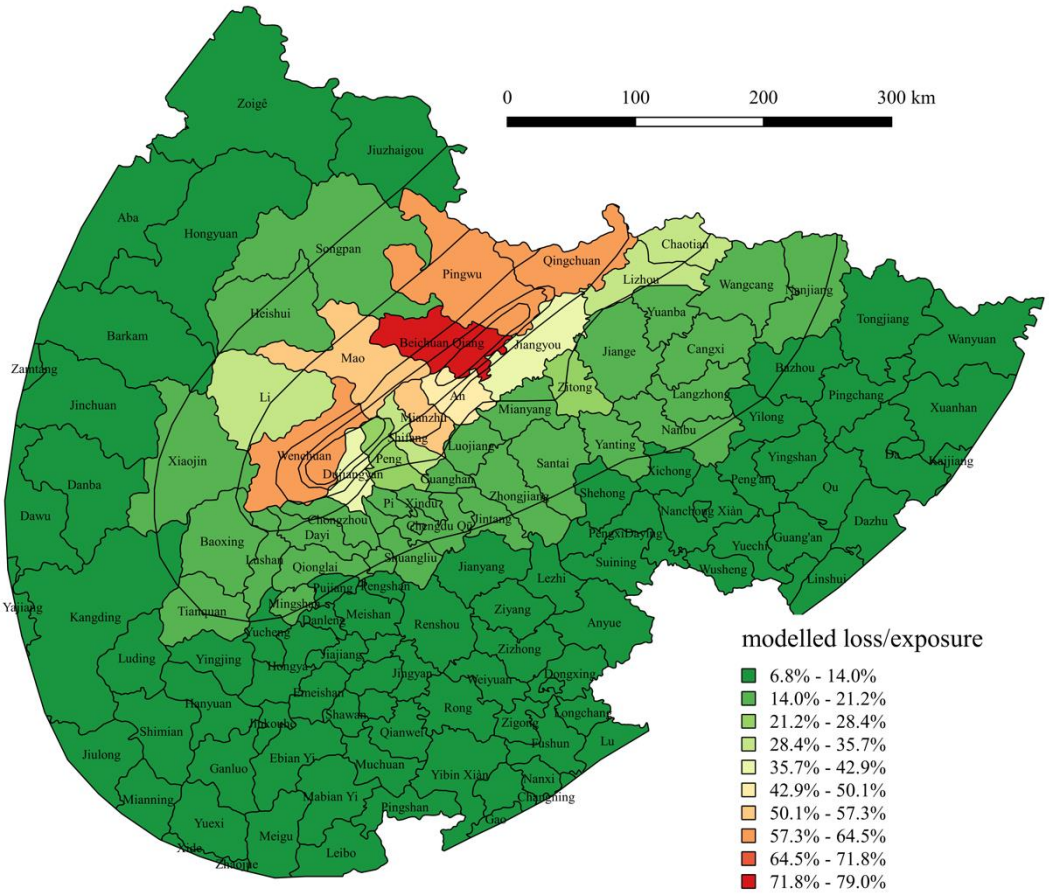

Figure 4-5: Distribution of estimated residential buildingloss ratio (the ratio between loss and exposed stock value) in affected districts/counties in Sichuan Province, by assuming the recurrence of the 2008 Wenchuan Ms8.0 earthquake.

4.4 Conclusion

In this Chapter, a grid-level residential building stock model (in terms of floor area and replacement value) targeted for seismic risk analysis for mainland China is developed, by using 2015 GHS population density profile as the proxy and by disaggregating the administrative level 2010census data into 1km×1km scale. To evaluate the model performance, the residential building stock value is compared with the net capital stock value estimated in Wu et al. (2014) using perpetual inventory method at provincial level. The modelled stock value in these two studies are indeed quite consistent for all the 31 provinces in mainland China. Furthermore, district level comparison of the residential floor area developed in this study with records from statistical yearbook of Shanghai is also conducted. It turns out that the floor area developed in this study is highly compatible with floor area recorded in the yearbook of Shanghai. Necessary adjustment to the modelled results is conducted to more reasonably reflect the development disparity among districts within Shanghai. To further validate the performance of the model in seismic risk assessment, an empirical loss estimation by assuming the recurrence of 2008 Wenchuan M8.0 scenario earthquake is performed. By lower down the gap in unit construction price used in this study and in previous studies, the overall estimated loss turns to be quite approximate to loss derived from damage reports based on

field investigation. These congruences indicate the reliability of the residential building stock model developed in this study.

The geo-coded grid-level residential building stock model developed here is flexible to update when more detailed census or statistics data are available. And it can also be conveniently combined with hazard data and vulnerability information for risk assessment to specific research area.

The limitation of this work is that, currently the modelling focus is only on residential building stock, given the availability of detailed census data. While, when disastrous earthquakes occur, although the damage to and the collapse of buildings is the main cause of fatality and economic loss, damages to those non-residential buildings (office, school, hospital, hotel, warehouse, factory, shop, cinema etc.) as well as life-line projects, infrastructures and the consecutive losses are not negligible. Therefore, in further work, more efforts should be made to estimate the stock value of non-residential buildings and infrastructures at risk. Furthermore, the replacement value developed in this study did not integrate the depreciation of the exposed buildings. These limitations also outline the optimization direction for future study.

4.5 Data/Code Availability

2015 GHS population density profile:

http://data.europa.eu/89h/jrc-GHS-ghs_pop_gpw4_globe_r2015a.

2010 China Sixth Population Census Tabulation: http://www.stats.gov.cn/tjsj/pcsj/rkpc/6rp/indexch.htm

2015 China Statistical Yearbook On Construction: http://tongji.cnki.net/kns55/navi/YearBook.aspx?id=N2017020307&floor=1

2015 Shanghai Statistics Yearbook: http://tjj.sh.gov.cn/html/sjfb/201701/1000201.html

An example illustrating the multi-variate equation solving process in Method section:

Input file: https://www.jianguoyun.com/p/DdOYRvoQgPb4Bhi-hdUB

MATLAB script: https://www.jianguoyun.com/p/DcAageEQgPb4BhjHhdUB

5 Comparison of modelled loss against historical damage information

Typically, the risk assessment of future potential seismic disasters entails three layers of information: hazard, exposure and vulnerability (Figure 5-1). Hazards refer to the distribution patterns and occurrence frequencies of various earthquake generated ground motions. Exposure captures the attributes of all exposed elements in terms of value, location and relative importance (e.g. critical facilities and infrastructure) to potential earthquakes. Vulnerability describes the susceptibility of those exposed elements to be damaged during an earthquake.

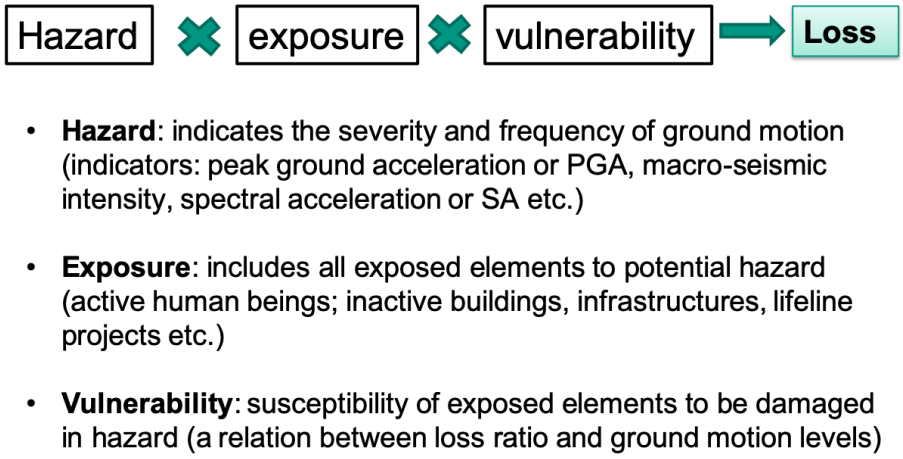

Figure 5-1: Layers of information in risk/loss assessment process.

Current earthquake risk/loss assessment methods can be divided into two types: the empirical method (e.g. ATC-13, 1985; Chen et al., 1997; Chan et al., 1998; Musson, 2000; Erdik et al., 2003; Jaiswal and Wald, 2013;) and the analytical method (e.g. Kircher et al., 1997; Bommer et al., 2002; Erdik et al., 2003; Cardona et al., 2008; FEMA, 2008). In empirical method, macro-seismic intensity is used as the ground shaking predictor, which is a natural choice for loss modelling application, since intensity is directly related to levels of damage in different categories of building (Musson, 2000). Furthermore, there are extensive databases of building damage and corresponding intensities, which permit the derivation of empirical damage functions (Bommer et al., 2002). Another key advantage of empirical loss estimation is that the exposed stock value of building and infrastructure can be represented by a macroscopic indicator e.g. Gross Domestic Product (GDP). This advantage allows the empirical method to be frequently used in post-earthquake rapid loss estimation.

The general form of analytical method for single scenario loss estimation was firstly proposed by Kircher et al. (1997) and elaborated in the HAZUS manual (FEMA, 1999), also called as the spectral displacement loss model (Spence et al., 2003). The analytical loss estimation method is considered to represent the state-of-the-art in earthquake loss estimation, at least for building damage due to ground shaking (Bommer et al., 2002). In this method, quantitative measures of ground shaking are used (e.g. peak ground acceleration, spectral acceleration, spectral displacement etc.); exposed building groups are analyzed in

a similar manner to the engineering analysis of a single structure. Thus, detailed information on building inventory (e.g. construction material, height, age, occupancy type, load-bearing structure etc.) needs to be known, which is not always straightforward to retrieve. Furthermore, building vulnerability function in analytical loss estimation method is derived from building capacity curve (based on engineering parameter to characterize the nonlinear behavior of each specific building type), fragility curve (relation of quantitative ground shaking and probability of being in each damage limit state given specific shaking), and the consequence model (relation between damage state and loss ratio). A summarization of the differences between empirical method and analytical method is listed in Figure 5-2.

Components	Analytical method	Empirical method
Hazard	instrumental ground motion indicator is used, e.g. PGA	macro-seismic intensity is used as the indicator
Exposure	In each grid, detailed building information (e.g. construction material, height, occupancy type) needs to be known	In each grid, only the overall building stock value is needed
Vulnerability	analyzed based on static/dynamic non-linear methods used in structure engineering	regressed from historical damage information (population, intensity map, loss, exposure)
Uncertainty source of loss	Uncertainty exists in every step of the loss modelling chain, since hazard, exposure and vulnerability are also modelled results	Intensity definition, exposure approximation, processing of historical damage information

Figure 5-2: Differences between loss estimation by using analytical method and empirical method.

The loss assessment can be performed for either one earthquake scenario or for multi-scenario (also distinguished by deterministic or probabilistic scenario, e.g. in Yeats et al., 1997). To validate the estimated loss for single earthquake scenario, the loss value derived from post-earthquake field surveys is considered to be the most reliable source. To validate the estimated loss for multi-scenario earthquakes, the empirical loss function is regarded as a representative of the historical damage information in this study, since the derivation of an empirical loss function entails a time-consuming and labor-intensive collection of historical earthquake related damage information that extensively distributed among papers, books, conference proceedings, newspapers etc.

In this chapter, probabilistic (single scenario based) and probabilistic (multi-scenario based) loss estimation will be presented by using both empirical and analytical loss estimation methods. Then, evaluation of these modelled loss will be given. For single scenario loss estimations, two sets of comparisons are to be conducted. Firstly, loss estimated with the empirical loss function developed by Daniell (2014) for mainland China will be compared with actual loss derived from field investigation, by using the macro-seismic intensity map of the 2008 Wenchuan Ms8.0 earthquake occurred in Sichuan province as the hazard input. Secondly, sensitivity tests of estimated loss to intensity-PGA conversion relations will be discussed. This starts from the fact that, after the occurrence of a damaging earthquake, to support the government in emergency response and disaster management, a rapid loss modelling result is required. In this case, a macro-seismic intensity map (required for empirical loss estimation) can only be converted from instrumental ground motion records (e.g. PGA, SA). Therefore, the difference between estimated loss by using different intensity-PGA conversion relations will be explored.

Multi-scenario based probabilistic loss to be estimated is mainly to quantitatively assess the socio-economic impact of potential earthquake hazard in a densely populated area, which is also of potential interest for insurance and reinsurance industries and helpful for governments to plan effective actions for seismic risk mitigation and preparedness. Since currently it is still not available to predict when and where future earthquakes will occur and how strong they will be, to evaluate the modelled probabilistic loss, a more practical way is to fully make use of the historical damage information, and try to derive a robust empirical loss estimation, which can be regarded as a tool to calibrate modelled probabilistic loss. In this regard, the empirical loss function developed in Daniell (2014) for mainland China has been validated to be a reliable source. Hence, the evaluation of modelled probabilistic loss for multi-scenario earthquake can be achieved by comparing loss estimated by using empirical method with the empirical loss function in Daniell (2014). Furthermore, sensitivity tests by changing the elements in hazard and vulnerability components (e.g. GMPE function, intensity-PGA relation) will also be conducted to quantify the sensitivity of the probabilistic loss to changes in these parameters.

To perform the loss estimation and evaluation above, the seismic source parameters in Chapter 2 to construct the hazard map for Shanxi Rift System in Northern China will be used to generate the earthquake scenarios (single earthquake scenario and multi probabilistic scenarios), i.e. as the “hazard” component of the loss estimation. The analytical fragility curves and the intensity-PGA relation developed in Chapter 3 for major building types in mainland China will be used to derive the “vulnerability” component. Meanwhile, the grid-level residential building stock model developed for mainland China in Chapter 4 will serve as the “exposure” component.

5.1 Single earthquake scenario loss estimation and evaluation

5.1.1 2008 Wenchuan Ms8.0 earthquake in Sichuan Province, China

Although the empirical loss function developed by Daniell (2014) has been proved to be excellent in predicating historical loss, to further validate the perfomance of this empirical loss function in estimating the seismic loss based on today’s exposure in China, a single scenario loss estimation and evaluation test will be presented by assuming the recurrence of the 2008 Wenchuan Ms8.0 earthquake in Sichuan Province, China. The estimated loss using the empirical loss function in Daniell (2014) will be compared with the loss estimated directly from damage reports, which are based on post-earthquake filed investigations and considered to be most reliable source of damage information.

The great Wenchuan Ms8.0 earthquake occurred on May 12, 2008 in the Sichuan Province of China. It is the most serious earthquake disaster in China since the great Tangshan Earthquake (*M*s=7.8, July 28, 1976). According to official reports, there were 69,225 deaths, 379,640 injuries and 17,939 missing as of Aug. 11, 2008. The China Earthquake Administration (CEA) quickly sent hundreds of experts to the field immediately after the event, to investigate the damage and assess the economic losses (Yuan, 2008). The macro-seismic intensity map and peak ground acceleration records in damaged area are shown in Figure 5-3.

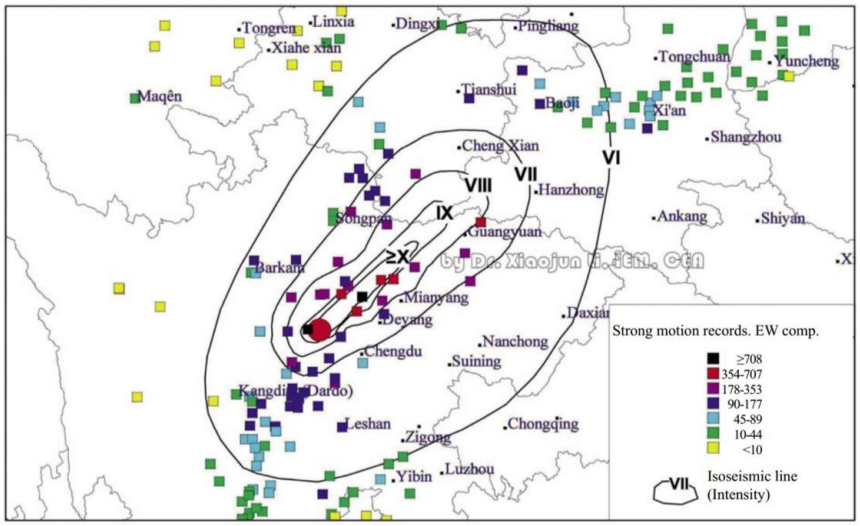

Figure 5-3: Comparison of PGA records with macro-seismic intensity map of Wenchuan earthquake (Li et al., 2008; note the extent of the intensity map is slightly different from the final intensity map issued by China Earthquake Administration).

5.1.2 Damage reports of Wenchuan earthquake based on post-earthquake investigation

In the post-earthquake damage reports (Chen and Tao, 2018; refer to their Table 6-1-61), the damaged buildings in Sichuan and its neighboring provinces were divided into rural and township/urban classes, but without further classification of building types. For rural buildings, the number of damaged rooms were recorded and for township/urban buildings, the total damage area of different damage states was given. The average size of a rural room is assumed to be 15 m^2 and the construction price is assumed to be around 1000 RMB/m^2. For township/urban buildings, the average construction price is assumed to be 2500 RMB/m^2. The direct loss to buildings in Sichuan Province is estimated to be around 169 billion RMB from these damage reports (Table 5-1, note this table does not include all the seriesly damage counties/districts, e.g. Wenchuan County). The distribution of loss proportion/quota (the percentage of loss in each county compared with the overall loss) estimated from damage reports for the 29 counties/districts in Sichuan Province in Table 5-1 is shown in Figure 5-4.

Table 5-1: Summary of damaged buildings in 29 seriously damaged counties/districts of Sichuan Province (data provided by Sichuan Earthquake Administration, through personal communication).

adm2_name	adm3_name	number of damaged township/urban buildings (unit: m^2)			number of damaged rural buildings (unit: room, 1 room=15m^2)			loss estimated from the damage reports (RMB)
		D4/D3	D2	D1	D4/D3	D2	D1	
Abazhou	Lixian	785700	77700	0	31306	16038	0	2.41E+09
Mianyang	Jiangyou	1470904	7018450	4032820	434096	354136	49212	2.17E+10
Guangyuan	Lizhou	6482800	4659400	0	422800	253500	0	2.80E+10
Guangyuan	Chaotian	485400	121300	0	27816	19555	5478	1.77E+09
Guangyuan	Wangcang	1577200	223000	0	84949	101918	170686	5.99E+09
Mianyang	Zitong	498000	1092000	827100	251687	235582	21525	7.89E+09
Mianyang	Youxian	903448	3018480	491760	161380	183697	95836	9.63E+09
Deyang	Jingyang	616300	396300	10491000	221100	147300	0	8.59E+09
Abazhou	Xiaojin	271000	61700	353100	40854	47377	0	1.68E+09

Mianyang	Fucheng	230194	1363295	2044943	28298	69664	29865	3.68E+09
Deyang	Luojiang	529400	260753	1171247	67100	134800	0	3.73E+09
Abazhou	Heishui	166300	10900	367900	27384	41327	0	1.16E+09
Chengdu	Chongzhou	13112	176749	373693	76040	151970	140000	2.72E+09
Guangyuan	Jiange	1491500	1012900	0	143100	341800	0	9.12E+09
Mianyang	Santai	1177820	5642140	5060860	427933	842074	561383	2.39E+10
Nanchong	Langzhong	525000	1120000	2630000	32554	0	0	3.68E+09
Mianyang	Yanting	320178	787212	707516	36448	62516	72111	2.95E+09
Abazhou	Songpan	84800	243300	360000	11808	64894	0	1.23E+09
Guangyuan	Cangxi	331600	1372400	0	145772	251692	176496	6.58E+09
Ya'an	Lushan	1680	12480	1062600	2300	44700	0	6.51E+08
Deyang	Zhongjiang	55160	247100	4012750	83498	202552	762188	5.23E+09
Guangyuan	Zhaohua	170600	235600	279200	48483	182925	30595	2.82E+09
Chengdu	Dayi	325000	347000	799000	5160	12445	27350	1.57E+09
Ya'an	Baoxing	4286	32467	173462	5300	36200	0	4.37E+08
Bazhong	Nanjiang	191300	106500	0	35300	46300	0	1.39E+09
Deyang	Guanghan	22400	126100	541547	65400	404900	0	4.26E+09
Ya'an	Hanyuan	115555	70935	180830	192100	76600	0	3.56E+09
Ya'an	Shimian	152600	167300	0	7500	22500	0	8.22E+08
Abazhou	Jiuzhaigou	167700	263100	543700	11291	55357	0	1.41E+09
In total:		19166937	30266561	36505028	3128757	4404319	2142725	**1.69E+11**

Note: D4, D3, D2, D1 refers to damage state of collapse, serious damage, moderate damage and slight damage, respectively; and the corresponding empirical loss ratio to estimate building loss from the damage reports is 0.9, 0.9, 0.5, 0.1.

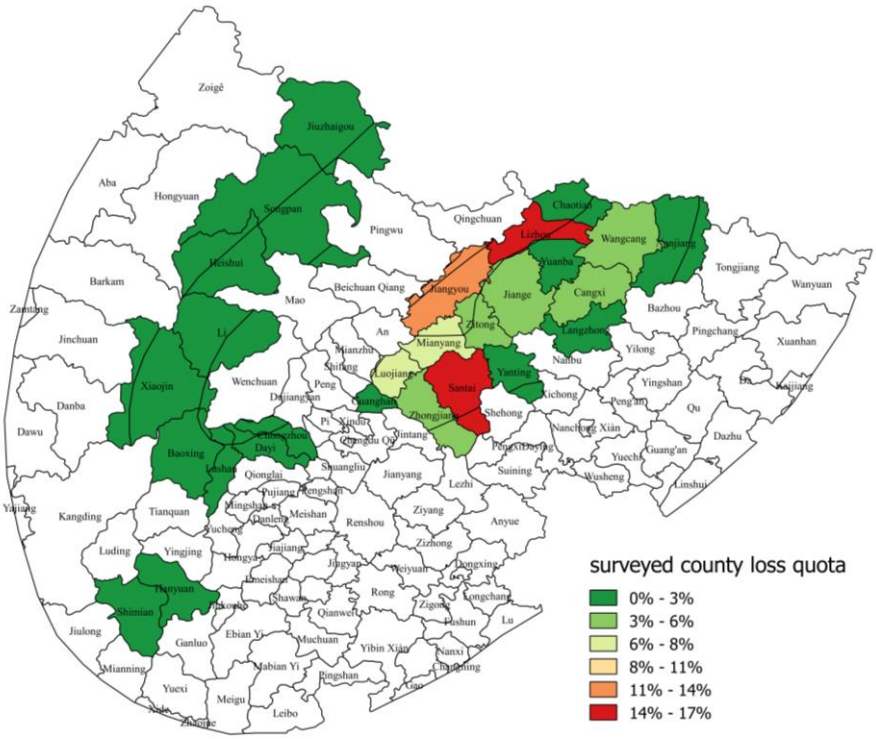

Figure 5-4: Distribution of building loss proportion/quota in counties/district of Sichuan Province with damage reports.

For comparison the county/district losses derived from damage reports in Table 5-1, the empirically estimated losses in these 29 counties/districts are shown in Figure 5-6, which is estimated based on the

official intensity map of Wenchuan earthquake issued by China Earthquake Administration (Figure 4-5) and the empirical loss function developed in Daniell (2014; Figure 5-5) as well as the residential building stock model developed in Chapter 4 for Sichuan Province.

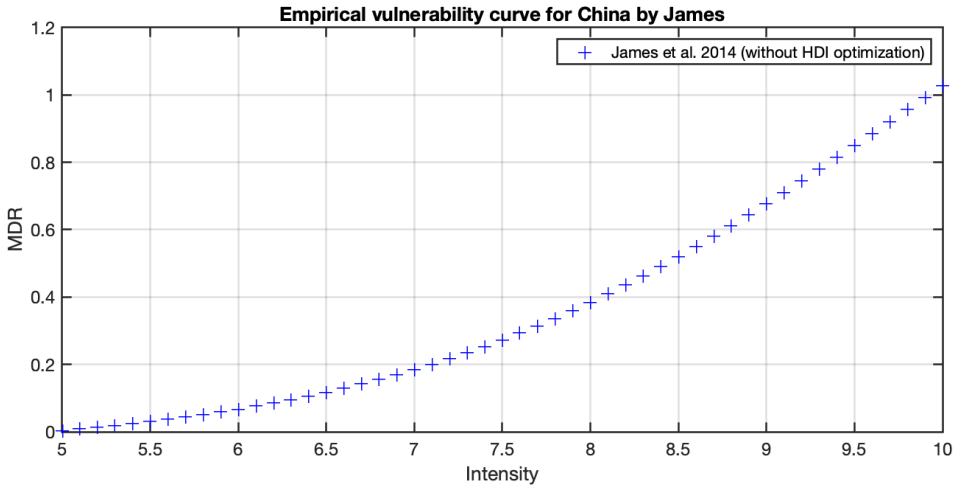

Figure 5-5: Empirical loss function developed in Daniell (2014) for mainland China, based on extensive collection of historical seismic damage information.

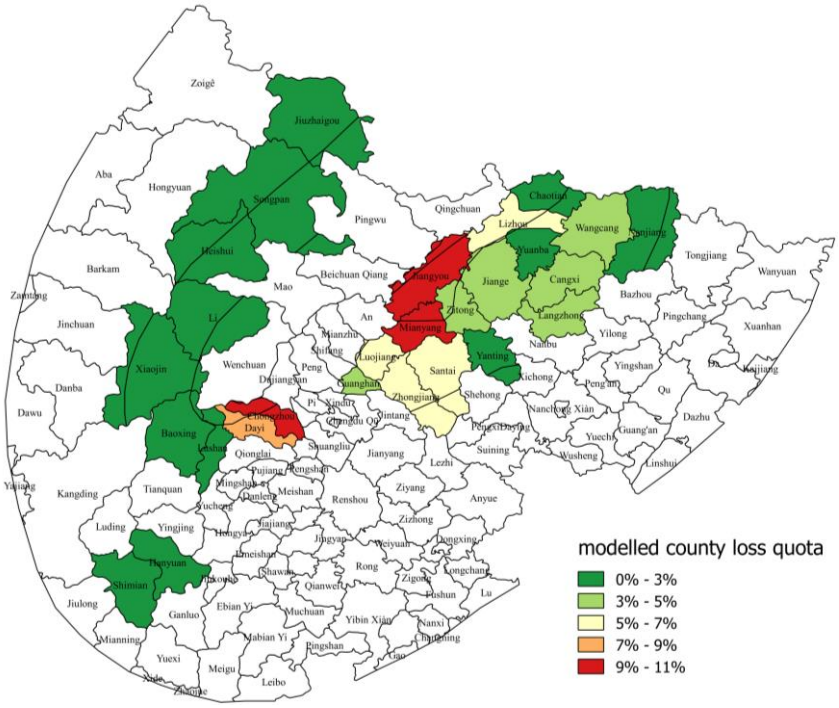

Figure 5-6: Distribution of estimated building loss proportion/quota for counties/districts in Table 5-1, based on the exposure model in Chapter 4, the empirical loss function in Daniell (2014) and the macro-seismic intensity map in Figure 4-5.

The misfit between damage reports based loss proportion/quota (or surveyed loss quota) in Figure 5-4 and empirically estimated loss quota in Figure 5-6 are illustrated in Figure 5-7. As can be clearly seen, the

estimated loss quota is highly consistent with the surveyed loss quota for most counties/districts, except in Santai and Lizhou, where surveyed loss quota is obviously higher than estimated; while in Chongzhou and Dayi, the surveyed loss is lower than estimated.

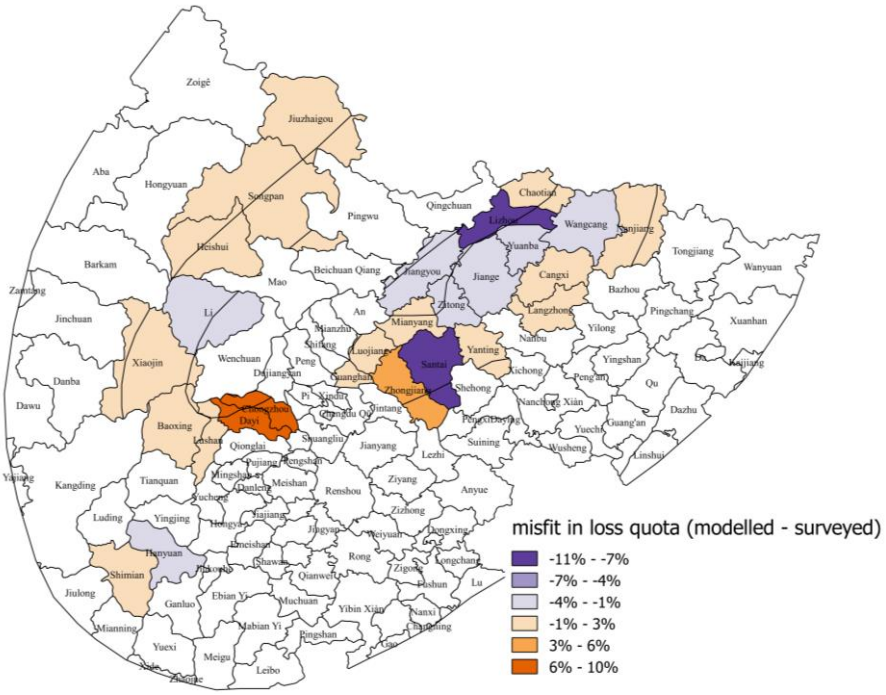

Figure 5-7: Misfit in loss quota for 29 counties/districts with damage reports in Sichuan Province.

According to field investigation, the southwestern rupture of the Longmenshan Fault (where the Wenchuan earthquake occurred) stopped at the intersection area between Chongzhou and Dayi, so the damage to buildings also stopped in between. This may explain why the empirically estimated ("modelled" in Figure 5-7) loss quota is higher than the actual surveyed loss quota ("surveyed" in Figure 5-7) in Chongzhou and Dayi. According to Ding (2017), abnormal high ground motions were recorded during Wenchuan earthquake in Lizhou and Sanzhou, which may lead to the higher surveyed loss quota ("surveyed" in Figure 5-7) than empirically estimated ("modelled" in Figure 5-7) in these two counties.

Generally, the loss proportion distribution based on field investigation is highly consistent with that based on the empirical loss function in Daniell (2014), the exposure model developed in Chapter 4 and the macro-seismic intensity map of Wenchuan earthquake issued by China Earthquake Administration. This consistency further validates the robustness of the empirical loss function in Daniell (2014) in evaluating the empirical loss based on today's exposure (as developed in Chapter 4, in 2015 price). Therefore, the empirical loss function develop for mainland China in Daniell (2014) is continuely regarded as a trustworthy representative of the historical seismic damage information, and can thus be used to calibrate/evaluate the seismic loss estimated by using other methods, e.g. the analytical method in both single-scenario based loss estimation and multi-scenario based probabilistic loss estimation.

5.2 Comparison of deterministic loss estimated by using empirical and analytical method

After validating the robustness of the empirical loss function developed in Daniell (2014) by comparing this empirical loss with filed investigation surveyed loss in Section 5.1, this empirical loss function is considered to be a reliable representative of the historical seismic damage information in mainland China. Therefore, in this section, loss estimated from empirical method will be compared with loss estimated from analytical method, based on several synthetic earthquake scenarios of different magnitudes for Shanxi Rift System (the ground shaking is in terms of PGA).

To calculate empirical loss, in which macro-seismic intensity map is used as the hazard input, conversion of the PGA values (in ground shaking maps of synthetic scenarios) to intensity is needed by using Intensity-PGA conversion relation. Such conversion is also quite necessary after the occurrence of a damaging earthquake. Since to support the government in emergency response and disaster management, a rapid loss modelling result is required. In this case, a macro-seismic intensity map (required for empirical loss estimation) can only be converted from instrumental ground motion records (e.g. PGA, SA). It is also obvious that using different Intensity-PGA relations will definitely lead to difference in modelled loss. Therefore, in this section, sensitivity tests to quantify the sensitivity of empirically estimated loss to changes in Intensity-PGA relation will be presented. Then, the components required to conduct analytical loss estimation will be illustrated in detail. Finally, comparison between the modelled loss using empirical and analytical method will be given.

5.2.1 Synthetic scenarios generated based on the seismic source parameters in Chapter 2 to construct the seismic hazard map in Shanxi Rift System

To quantify the sensitivity of the empirically modelled loss to changes in Intensity-PGA conversion relation, four synthetic earthquake scenarios are generated first (with magnitude of 6.3, 7.5, 8.2 and 9.8), based on the seismic source parameters in Chapter 2 to construct the seismic hazard map in Shanxi Rift System. The GMPE relation used to generate the ground shaking maps of these synthetic scenarios is developed by Yu et al. (2013) for Northern China, which is in terms of PGA. The PGA distribution of these four synthetic earthquake scenarios is shown in Figure 5-8.

Figure 5-8: PGA distribution map of the four synthetic earthquake scenarios with magnitude of 6.3, 7.5, 8.2 and 9.8 (the background layer represents the administrative extent of Shanxi Province).

5.2.2 Empirical loss estimation

To perform empirical loss estimation, the PGA related ground shaking map in the synthetic scenarios needs to be converted from PGA to macro-seismic intensity first. Therefore, a brief review of the existing Intensity-PGA conversion relations is necessary. As shown in Figure 5-9, among the scrutinized relations, three are developed for mainland China (Ma et al., 2014; Ding et al., 2017; Xin et al., 2019); two are for California, USA (Wald et al., 1999; Worden et al., 2012); three are for European countries (Ambraseys, 1975; Faccioli and Cauzzi, 2006; Tselentis and Danciu, 2008); and three are developed using data from different countries and regions, therefore tagged das “global“ (Medvedev and Sponheuer, 1969; Murphy and O‘Brien, 1977; Caprio et al., 2015).

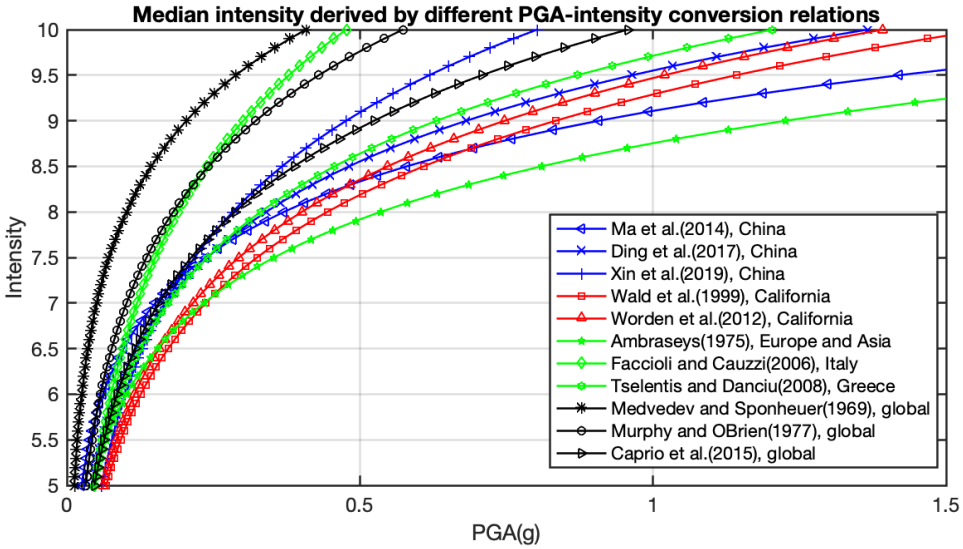

Figure 5-9: Comparison of different Intensity-PGA conversion relations.

5.2.2.1 Comparison of PGA-MDR relation (i.e. empirical loss function) derived from Intensity-PGA conversion relation

After the conversion of the PGA value in the synthetic ground shaking map in Figure 5-8 into intensity (using the relations in Figure 5-9), the derived intensity is then combined with the empirical loss function in Daniell (2014, Figure 5-5) to build the relation between PGA and the empirical mean damage ratio (MDR, i.e. loss ratio). A summarization of such PGA-MDR relations derived from different Intensity-PGA conversion relations is given in Figure 5-9. These PGA-MDR relations will be used later in Section 5.3 for probabilistic loss estimation.

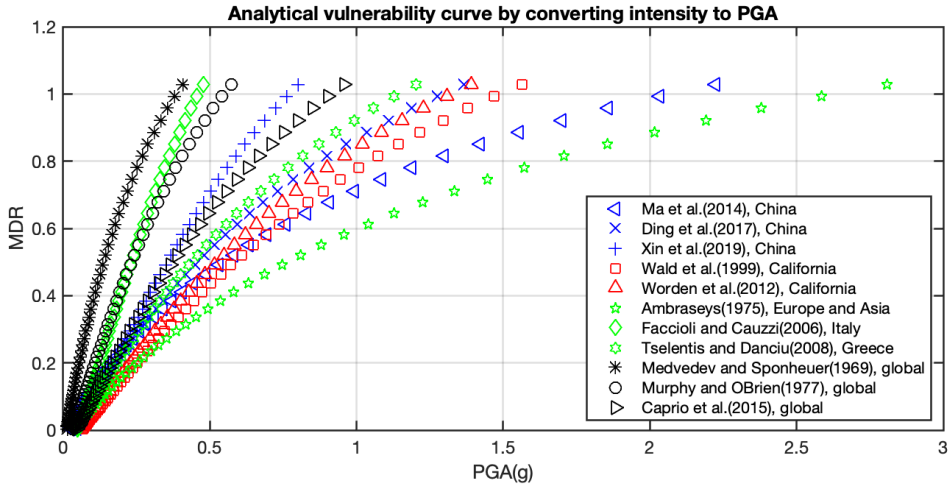

Figure 5-10: A summarization of PGA-MDR relations derived from different Intensity-PGA conversion relations, combined with the empirical loss function developed in Daniell (2014, Figure 5-5).

5.2.2.2 Empirical loss estimated by using median intensity derived from Intensity-PGA relation and by integrating the standard deviation of the derived intensity

After a visual comparison of the PGA-MDR relations in Figure 5-10, finally five of them are chosen to perform the empirical loss calculation for the four synthetic earthquake scenarios in Figure 5-8. The five PGA-MDR relations are derived based on the Intensity-PGA conversion relation in Ma et al. (2014), Ding et al. (2017), Xin et al. (2019; as explained in detail in Chapter 3), Worden et al. (2012) and Caprio et al. (2015). The empirical loss calculated using these PGA-MDR relations (based on the exposure model in Chapter 4) are summarized in Table 5-2 and Table 5-3, without or with the integration of variance in derived intensity, respectively. The integration of the variance in derived intensity in Table 5-3 is achieved by adding a random variable to the converted intensity from each PGA level, and this variable is assumed to follow the normal distribution, with zero as the expectation value and sigma of the Intensity-PGA relation as the sigma value.Then for the fixed PGA, the value of the converted intensity changes with the loop, thus the corresponding MDR also changes with the loop. Here, for better visualization, only ten loops of the modelled empirical loss are listed in Table 5-3.

Table 5-2: Empirically modelled median loss by using different Intensity-PGA conversion relations.

Mag	loss_Xin	loss_Ding	loss_Worden	loss_Caprio	loss_Ma
6.3	3.56E+09	4.64E+09	2.47E+09	4.58E+09	8.68E+09
order:	4	2	5	3	1
7.5	2.98E+10	3.58E+10	2.08E+10	3.6E+10	5.66E+10
order:	4	2	5	3	1
8.2	2.71E+11	2.28E+11	1.92E+11	2.63E+11	2.3E+11
order:	1	4	5	2	3
9.8	5.9E+11	4.82E+11	4.22E+11	5.66E+11	4.46E+11
order:	1	3	5	2	4

Table 5-3: Empirically modelled loss by using different Intensity-PGA conversion relations, with the variance of the converted intensity from fixed PGA level being considered.

Xin	loop											
0.58	1		3.85E+09	1.08		3.24E+10	1.09		2.78E+11	1.02		5.89E+11	1.00
	2		3.47E+09	0.98		3.54E+10	1.19		2.70E+11	1.00		5.94E+11	1.01
	3		3.97E+09	1.12		3.30E+10	1.11		2.80E+11	1.03		5.89E+11	1.00
	4		3.60E+09	1.01		3.46E+10	1.16		2.62E+11	0.97		6.06E+11	1.03
	5	6.3	4.06E+09	1.14	7.5	3.37E+10	1.13	8.2	2.81E+11	1.04	9.8	6.13E+11	1.04
	6		4.69E+09	1.32		3.51E+10	1.18		2.76E+11	1.02		6.15E+11	1.04
	7		4.02E+09	1.13		3.24E+10	1.09		2.78E+11	1.03		6.17E+11	1.05
	8		4.19E+09	1.18		3.44E+10	1.16		2.77E+11	1.02		5.99E+11	1.02
	9		4.02E+09	1.13		3.29E+10	1.11		2.97E+11	1.09		5.89E+11	1.00
	10		5.18E+09	1.46		3.98E+10	1.34		2.80E+11	1.03		6.11E+11	1.04
Ding	loop		4.64E+09	1.11		3.58E+10	1.06		2.28E+11	1.03		4.82E+11	1.01
0.31	1		5.24E+09	1.13		3.79E+10	1.06		2.34E+11	1.02		4.71E+11	0.98
	2		4.93E+09	1.06		3.77E+10	1.05		2.31E+11	1.01		4.83E+11	1.00
	3		5.71E+09	1.23		3.67E+10	1.02		2.35E+11	1.03		4.91E+11	1.02
	4		5.40E+09	1.16		3.74E+10	1.04		2.30E+11	1.01		4.94E+11	1.03
	5	7.5	4.61E+09	1.00	7.5	3.76E+10	1.05	8.2	2.26E+11	0.99	9.8	4.94E+11	1.03
	6		5.30E+09	1.14		3.91E+10	1.09		2.32E+11	1.02		4.91E+11	1.02
	7		5.24E+09	1.13		3.84E+10	1.07		2.33E+11	1.02		4.88E+11	1.01
	8		5.00E+09	1.08		3.77E+10	1.05		2.36E+11	1.04		4.71E+11	0.98
	9		4.77E+09	1.03		4.09E+10	1.14		2.41E+11	1.06		4.81E+11	1.00
	10		5.13E+09	1.11		3.72E+10	1.04		2.44E+11	1.07		4.92E+11	1.02
Worden	loop		2.47E+09	1.61		2.08E+10	1.39		1.92E+11	1.05		4.22E+11	1.06
0.73	1		4.71E+09	1.91		2.95E+10	1.42		1.92E+11	1.00		4.22E+11	1.00
	2	6.3	3.85E+09	1.56	7.5	3.00E+10	1.45	8.2	1.89E+11	0.99	9.8	4.37E+11	1.04
	3		4.08E+09	1.65		2.89E+10	1.39		2.11E+11	1.10		4.44E+11	1.05

	4		4.42E+09	1.79		3.10E+10	1.49		2.04E+11	1.06		4.62E+11	1.09
	5		3.81E+09	1.54		2.86E+10	1.38		2.03E+11	1.06		4.45E+11	1.05
	6		3.35E+09	1.35		2.75E+10	1.32		2.22E+11	1.16		4.49E+11	1.06
	7		3.34E+09	1.35		2.71E+10	1.31		1.93E+11	1.01		4.45E+11	1.05
	8		3.48E+09	1.41		3.14E+10	1.51		1.98E+11	1.03		4.48E+11	1.06
	9		5.17E+09	2.09		2.79E+10	1.34		2.05E+11	1.07		4.64E+11	1.10
	10		3.49E+09	1.41		2.67E+10	1.28		2.06E+11	1.07		4.53E+11	1.07
Caprio	loop		4.58E+09	2.57		3.60E+10	2.10		2.63E+11	1.24		5.66E+11	1.12
1.4	1		1.13E+10	2.47		8.25E+10	2.29		3.05E+11	1.16		6.31E+11	1.12
	2		1.18E+10	2.58		6.95E+10	1.93		3.01E+11	1.14		6.39E+11	1.13
	3		9.88E+09	2.16		8.09E+10	2.24		2.98E+11	1.13		6.38E+11	1.13
	4		1.19E+10	2.59		7.35E+10	2.04		3.40E+11	1.29		6.62E+11	1.17
	5	6.3	1.09E+10	2.38	7.5	7.76E+10	2.15	8.2	3.15E+11	1.19	9.8	6.33E+11	1.12
	6		1.11E+10	2.41		8.63E+10	2.39		3.61E+11	1.37		6.78E+11	1.20
	7		1.30E+10	2.83		7.23E+10	2.01		3.44E+11	1.31		5.82E+11	1.03
	8		1.05E+10	2.28		7.98E+10	2.21		3.48E+11	1.32		5.76E+11	1.02
	9		1.31E+10	2.87		6.89E+10	1.91		3.39E+11	1.29		6.34E+11	1.12
	10		1.45E+10	3.17		6.66E+10	1.85		3.18E+11	1.21		6.65E+11	1.18
Ma	loop		8.68E+09	1.47		5.66E+10	1.19		2.30E+11	1.06		4.46E+11	1.03
0.62	1		1.35E+10	1.56		6.54E+10	1.15		2.46E+11	1.07		4.57E+11	1.03
	2		1.29E+10	1.48		7.00E+10	1.24		2.37E+11	1.03		4.57E+11	1.03
	3		1.33E+10	1.53		6.79E+10	1.20		2.61E+11	1.13		4.49E+11	1.01
	4		1.30E+10	1.49		6.52E+10	1.15		2.38E+11	1.03		4.64E+11	1.04
	5	6.3	1.17E+10	1.35	7.5	6.63E+10	1.17	8.2	2.50E+11	1.09	9.8	4.57E+11	1.03
	6		1.34E+10	1.54		6.98E+10	1.23		2.54E+11	1.10		4.98E+11	1.12
	7		1.23E+10	1.41		6.57E+10	1.16		2.61E+11	1.13		4.55E+11	1.02
	8		1.23E+10	1.42		6.66E+10	1.18		2.30E+11	1.00		4.52E+11	1.02
	9		1.30E+10	1.49		6.79E+10	1.20		2.44E+11	1.06		4.46E+11	1.00
	10		1.27E+10	1.46		6.91E+10	1.22		2.25E+11	0.97		4.53E+11	1.02

Note: the value in red behind each author in the first column represents the sigma in each Intensity-PGA relation; the number in blue represents the average loss modelled in the following ten loops; the value filled in yellow represents the average amplification of the average loss in blue, compared with the median loss in Table 5-2.

Based on the empirically estimated loss values in Table 5-2 and Table 5-3, the following conclusions can be made:

1. Generally, the loss in Table 5-3 is higher than the median loss in Table 5-2, due to the integration of the variance of the converted intensity from PGA;

2. For each intensity-PGA relation, the overestimation of loss in Table 5-3 (compared with the median loss in Table 5-2) decreases with the increase of magnitude;

3. The loss overestimation factor (the ratio between the estimated loss in Table 5-3 and the median loss in Table 5-2) generally follows the order among different intensity-PGA relations:

Caprio > Worden > Ma > Xin >= Ding;

4. In Table 5-3, the higher the sigma value of the Intensity-PGA conversion relation, the higher the increase in estimated loss (compared with median loss in Table 5-2), since the variance of the converted intensity from PGA is integrated.

5.2.3 Analytical loss estimation

To perform analytical loss assessment, the PGA based ground shaking map in Figure 5-8 can be used directly as the hazard input. The exposure input to be used is the grid-level building stock model developed in Chapter 4. Within each grid of this exposure model, there are 17 building sub-types that derived from census data. To make use of the analytical fragility curves developed in Chapter 3, the 17 building sub-

types in the exposure model need to be recategorized into the four major buildings types classified in Chapter 3 (namely Masonry_A, Masonry_B, RC_A, RC_B), for which the analytical fragility curves have been derived. The analytical vulnerability curve to be used in analytical loss estimation method is derived from the fragility curve developed in Chapter 3 combined with the consequence model (relation between damage state and mean loss ratio) (Silva et al, 2015). The details of this building recategorization process are given as follows.

5.2.3.1 Recategorization of 17 building sub-types in the exposure model (Chapter 4) into the four building types classified by vulnerability (Chapter 3)

In the grid-level building stock model developed in Chapter 4, there are 17 specific buildings sub-types in each grid, classified by construction material and storey class given in 2010census data, as shown in 5-11.

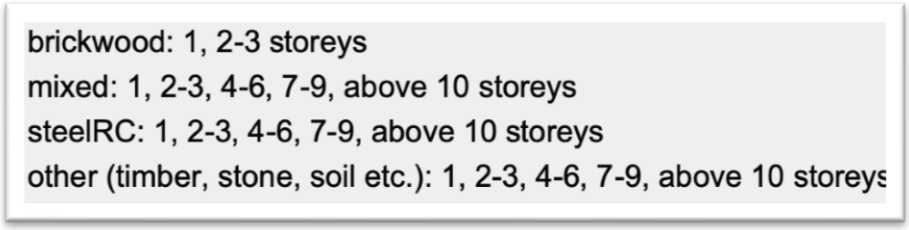

Figure 5-11: 17 building types in the building stock model developed in Chapter 4.

To perform the analytical loss assessment based on the analytical fragility curve developed in Chapter 3 for four major building types in mainland China, the 17 building sub-types in Figure 5-11 need to be recategorized into the four building types in Chapter 3 (namely Masonry_A, Masonry_B, RC_A, RC_B). Based on the similarity in seismic resistance capability among these 17 specific building types, the initially designed reclassification scheme is as follows:

- **Masonry_A**: brickwood (1,2-3); mixed (1,2-3,4-6, 7-9); other (1,2-3,4-6, 7-9)
- **Masonry_B**: mixed (⩾10); other (⩾10)
- **RC_A**: steel-RC (1,2-3,4-6, 7-9)
- **RC_B**: steel-RC (⩾10)

In each reclassified building type, the same fragility curve is to be used in analytical loss estimation. To derive the analytical vulnerability curve to be used in analytical loss modelling method, the fragility curves of the four reclassified building types need to be further combined with the consequence model (relation between damage state and loss ratio, as used in Silva et al, 2015). The consequence model used in this study is from Sun and Chen (2009), as listed in Table 5-4. The derived analytical vulnerability curves (relation between PGA and MDR/loss ratio) for Masonry_A, Masonry_B, RC_A and RC_B are plotted in Figure 5-12.

Table 5-4: The consequence model (relation between damage state and mean loss ratio) developed by Sun and Chen (2009).

Structure type	Damage state				
	Basically intact	Slight damage	Moderate damage	Serious damage	collapse

steel/RC	2-10	11-25	26-60	61-90	91-100
masonry	0-5	6-19	20-47	48-85	86-100

Note: the numbers in Table 5-4 are in percentage (%).

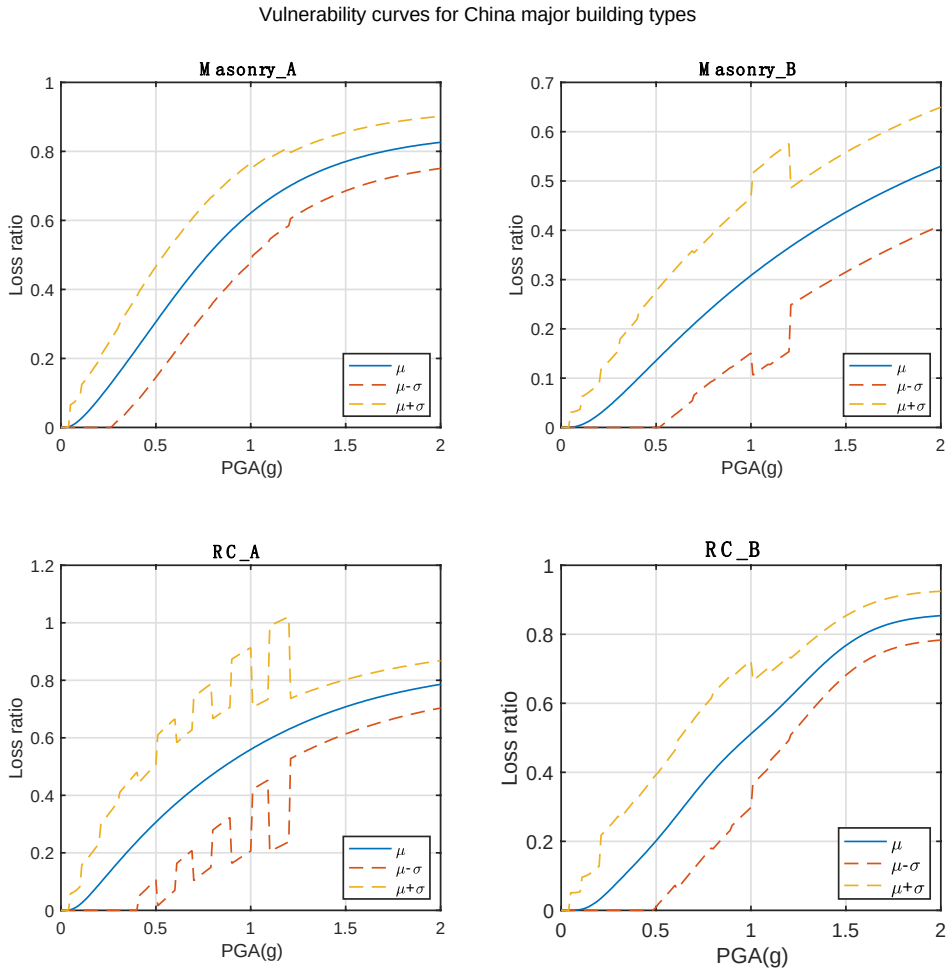

Figure 5-12: Vulnerability curves developed for building classes to estimate loss in analytical method.

5.2.3.2 Deterministic loss estimated using analytical method

After getting the hazard input, exposure model and analytical vulnerability curve ready, the loss calculation can be performed based on the open source platform CAPRA-GIS (Marulanda et al., 2013). It should be noted that, in analytical loss modelling method, the loss of each building type is calculated separately by multiplying the vulnerability curve of each building type with exposed building stock replacement value. In contrast, in empirical loss modelling method, only the replacement value of all exposed buildings is needed and the same empirical loss function is applied.

The deterministic (or single scenario based) loss estimated using the analytical method is shown in Table 5-5. The empirically modelled median loss in Table 5-2 by using the Intensity-PGA conversion relation in Xin et al. (2019, developed in Chapter 3) is listed in Table 5-5 for comparison. As can be observed, with the increase of magnitude, the empirically estimated median loss is increasingly larger than loss estimated

by using the analytical method, but still within the two times' difference (i.e. the empirical loss is lower than two times of the analytical loss). The change of difference in estimated loss might be ascribed to the increasing difference in vulnerability of different building types with magnitude increase, since the empirical method applies the same loss ratio to all building types, while the analytical method considers the difference in vulnerability of different building types.

Table 5-5: Comparison of loss estimated by analytical method with empirically estimated median loss listed in Table 5-2 (using the intensity-PGA conversion relation from Xin et al., 2019, as developed in Chapter 3) for the four synthetic earthquake scenarios in Figure 5-8.

Mag	median empirical loss (Xin et al, 2019)	analytical loss	empirical_loss/engineering_loss
6.3	3.56E+09	3.28E+09	1.09
7.5	2.98E+10	2.05E+10	1.45
8.2	2.71E+11	1.99E+11	1.36
9.8	5.9E+11	3.78E+11	1.56

It should be noted that when other intensity-PGA conversion relations are used in calculating empirical loss, the median empirical loss value will change accordingly (as shown in Table 5-2). And for the same magnitude, loss estimated by empirical method will not always higher than loss estimated by analytical method.

5.3 Multi-scenario based probabilistic loss estimation – a case study in Shanxi Rift System

To ensure a long-term security culture and economic prosperity especially in seismic active areas, the assessment of probabilistic loss is necessary. This allows the consideration of budget allocation and the implementation of an effective financial protection strategy, which in turn can protect government/private resources and safeguard socioeconomic development (Marulanda et al., 2013). The possibility of the occurrence of future highly destructive events in many areas of the world creates the need to focus risk estimation on probabilistic models, which can make full use of the limited available information of the historical data, given the low frequency of catastrophic seismic events. This fact also leads to the large uncertainties related to the severity and frequency characteristics of the events that must be considered in a probabilistic risk model. The development of earthquake prediction models uses seismological and engineering bases, which allows the assessment of the risk of loss for catastrophic events.

The probabilistic risk model quantifies potential losses arising from all the potential earthquake events to be occurred with the seismic source area and is built upon a sequence of modules (hazard, exposure, vulnerability, loss/risk). The hazard module in multi-scenario based probabilistic loss estimation defines the frequency and severity of earthquake to occur at different locations within the seismic sources and the ground shaking distribution of each event. For each earthquake, the annual probability of having a ground motion greater than some specified value is equal to the recurrence rate of the earthquake times the probability that the ground motion will be exceeded if that earthquake occurs (this probability is defined in the ground motion prediction equation, namely GMPE).

The seismic source parameters (e.g. the division of each area/fault source, the derivation of Gutenberg-Richter relation, the determination of maximum earthquake that can occur in each area/fault source) of

the hazard module are derived based the tectonic background, the historical earthquakes occurred and other geological information in scientific studies that performed in the region of interest. For Shanxi Rift System, these seismic hazard parameters are provided by Li (2015), with more details introduced in Chapter 2. Once these seismic source parameters are established, a series of synthetic events can be generated using open source software CRISIS (Aguilar-Meléndez et al., 2017). These sets of synthetic events represent all the possible hypocenters and the whole range of possible magnitudes associated with a specific hypocentral location. Each of these events or scenarios is associated with a specific frequency of occurrence. Naturally, the scenarios associated with low-magnitude earthquakes will have a higher probability of occurrence than those scenarios associated with high-magnitude earthquakes, which will have a relatively low probability of occurrence.

Based on the synthetic scenarios generated from the seismic source parameters to construct the seismic hazard map in Shanxi Rift System in Chapter 2, the grid-level residential building stock model developed in Chapter 4, and the empirical loss function and analytical vulnerability curve derived in previous sections of this chapter, the estimation of multi-scenario based probabilistic loss can be performed on the open source platform CAPRA (Comprehensive Approach to Probabilistic Risk Assessment). CAPRA is developed by ERN-AL Consortium (ERN-AL, 2010) with the support of the World Bank, the Inter-American Development Bank and the UN-ISDR. CAPRA is conceived as an open source model for the analysis and visualization of natural hazards, exposition and risks. Different activities of disaster risk management and not only for risk financing (Cardona et al., 2010) are integrated in this initiative. It also comprehends a training process that creates and enables an environment for the mainstreaming of disaster risk reduction.

5.3.1 Metrics to compare probabilistic loss

For proper comparison of estimated multi-scenario probabilistic loss by using empirical method and analytical method, the main metrics typically used are the loss exceedance curve (LEC) and the average annual loss (AAL), which provide loss comparison from a probabilistic view and from a deterministic view, respectively. The definitions of LEC and AAL in Marulanda et al. (2013) are modified and given as follows.

Loss exceedance curve (LEC): represents the annual frequency (or return period) of exceedance of a series of loss value. This is the most important catastrophe risk metric for risk managers, since it estimates the amount of funds required to meet risk management objectives. The *LEC* is calculated by considering the whole set of synthetic events generated in the hazard module, which comprises all the possible hypocenters and the whole range of possible magnitudes associated with a specific hypocentral location within the study region. Once the *LEC* is derived, it is possible to obtain other related metrics for the financial analysis of seismic loss such as the average annual loss of a region, the probable maximum loss at fixed return period.

Average annual loss (AAL): is the expected loss per year. Computationally, *AAL* is the sum of the product of the expected losses in a specific event and the annual occurrence frequency of that event, with all synthetic events generated in the hazard module being considered. The expected loss of one synthetic event includes losses from all buildings exposed to the hazard extent of the event, supposing that the process of occurrence of this synthetic event is stationary and that damaged buildings have their resistance immediately restored after an event.

5.3.2 Derivation of AAL and LEC in multi-scenario based probabilistic loss estimation

For building type k at grid i, the annual expected loss generated by earthquake j, marked as $Loss_{i,j,k}$, can be formulated as follows:

$$Loss_{i,j,k} = Vul\left(PGA_{i,j}\right) * Asset_{i,k} * Freq_j \tag{5.1}$$

In which, $Vul\left(PGA_{i,j}\right)$ represents the mean loss ratio given the median ground motion generated by earthquake j at grid i (defined by the GMPE equation used), which can be derived from the empirical/analytical vulnerability curve; $Asset_{i,k}$ is the asset value of building type k at grid i; $Freq_j$ is the annual occurrence frequency of synthetic event j, which is defined in the hazard module. By aggregating the loss generated by all synthetic events at all grids for all building types in the portfolio, the annual average loss can be derived.

For loss exceedance curve derivation, when uncertainties from the GMPE relation and from the vulnerability curve derivation process are considered, the annual frequency to exceed a loss ratio threshold l of building type k at grid i due to ground motions generated by earthquake j can be formulated as:

$$Freq(L > l|M_j, R_{i,j}) = Freq_j * \int_0^\infty \Pr\,(L > l|S_a)\Pr\,(S_a|M_j, R_{i,j})dS_a \tag{5.2}$$

Where M_j is the magnitude of earthake j, $R_{i,j}$ is the distance from earthquake j to grid i; $\Pr\,(S_a|M_j, R_{i,j})$ refers the probability to generate different ground motion level S_a by earthquake j at grid i, which is assumed to follow the lognormal distribution; $\Pr\,(L > l|S_a)$ refers to the probability of exceeding loss ratio threshold l given the ground motion level S_a, which is generally assumed to follow the beta distribution (Marulanda et al., 2013).

At different loss ratio thresholds, the corresponding loss generated by all synthetic events at all grids for all building types can be instantlys derived by multiplying the grid-level building stock model developed in Chapter 4. With the frequency to exceed such loss known from Eq. (5.2), the corresponding loss exceedance curve can be further developed. It is worth to note that, since the exposed residential building stock value is calculated using the replacement price, the loss estimated is the gross loss (different from net loss, in which the depreciation of the exposed stock value is considered).

5.3.3 Comparison of probabilistic loss estimated from empirical method and analytical method

The total number of synthetic earthquake events used in the hazard module of CAPRA is 10614. These events are generated by CRISIS, based on the seismic source parameters in constructing the seismic hazard map of Shanxi Rift System in Chapter 2. In CRISIS, the earthquakes to occur in each seismic source are assumed to follow a Poisson process and the epicenter of each synthetic event is assumed to be a point source. This means that the epicenter of the earthquake can not only occur in the center of the seismic source, but can also occur in any point inside the corresponding seismic source volume with equal probability. Thus, for the generation of synthetic events, sub-sources are defined by subdividing the seismic source, depending on hypocentral distance in diverse geometric shapes. For each subdivision, the seismicity of the sub-source is considered to be concentrated in its center of gravity (Cardona et al., 2008).

Fianlly, the whole set of 10164 synthetic events are generated, representing all the possible hypocenters and the whole range of possible magnitudes associated with a specific hypocentral location within Shanxi Rift System. Each of these events or scenarios is associated with a specific frequency of occurrence.

Then, to perform probabilistic loss estimation by using empirical method and analytical method, the ground shaking maps of these 10614 synthetic earthquake events (which are also generated by CRISIS in terms of PGA) will be used as the hazard input in CAPRA. The grid-level (1km×1km resolution) building stock model developed in Chapter 4 for Shanxi Province is to be used as the exposure input, in which the overall replacement value of the residential buildings in Shanxi Province reaches 1603.5 billion RMB (in 2015 current price).

For probabilistic loss estimation using empirical method, the PGA values in the synthetic ground shaking maps need to be converted into intensity values first, according to the Intensity-PGA conversion relation developed in Chapter 3. Then the empirical loss function developed in Daniell (2014) is used to calculate the empirical loss following the process described in Section 5.3.2. All the probabilistic loss calculations are performed on the CAPRA platform. The estimated AAL value using empirical method reaches **2.57 billion RMB**, which is around **1.61‰** of the whole exposed building stock value. The empirical loss exceedance curve derived by considering all the 10614 synthetic events is shown in Figure 5-13.

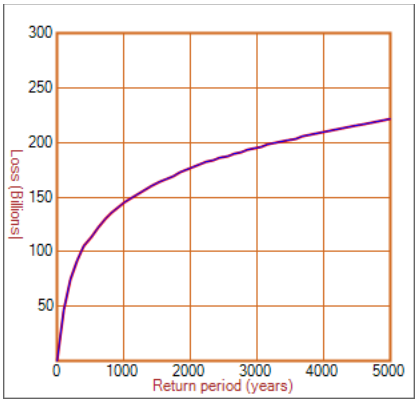

Figure 5-13: Loss exceedance curve derived using empirical loss estimation method.

For probabilistic loss estimation using analytical method, the same synthetic event sets and exposure model are to be used. The main difference in analytical loss estimation method, compared with empirical loss estimation method, is the derivation process of vulnerability curve. The analytical vulnerability curve in analytical loss estimation is derived from analytical fragility curve (developed in Chapter 3) combined with the consequence model (relation between damage state and loss ratio), following the method similar to Silva et al. (2015) in deriving the vulnerability curve for buildings in Portugal. The estimated AAL loss value using analytical method reaches **1.02 billion RMB**, which is **0.64‰** of the overall exposed building stock value and is 1/2.5 of the empirical AAL value. The analytical loss exceedance curve derived by considering all of the 10614 earthquake scenarios is shown in Figure 5-14.

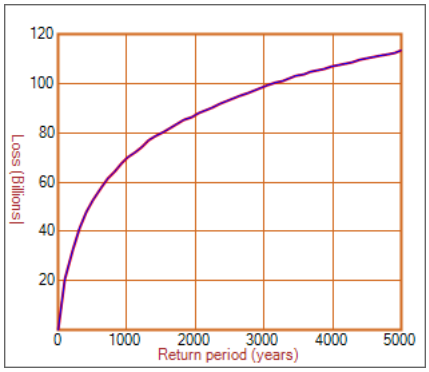

Figure 5-14: Loss exceedance curve derived from analytical loss estimation method.

For comparison from a deterministic view, the empirical AAL value is around 2.5 multiples of the engineering AAL value, which indicates a relatively good consistency compared with the usually large discrepancy (up to 10 times and even higher) among modelled losses from different sources (Chan et al., 1998; Spence et al., 2003). And for comparision from a probabilistic view based on the LEC curve in Figure 5-13 and Figure 5-14, it can be seen that for the same return period, the corresponding loss estimated from empirical method is also around two times of that estimated from analytical method.

5.3.4 Sensitivity test

It has been said that without a sensitivity analysis, a numerical model is not worth the computer it is written on. Any complex model, in which there are a large number of variables, warrants an exploration of the sensitivity of the output to variations in the various input parameters (Spence et al., 2003). The uncertainty in an earthquake loss model is obviously much greater than that in a seismic hazard model since it is compounded by the uncertainties associated with classification of the exposed building stock and the characteristic vulnerability of each class of building. Losses expressed in financial units are also subject to the uncertainty in assigning costs to physical damage. Therefore, in this section, several sensitivity tests are to be conducted by changing the inputs in hazard, exposure and vulnerability module. This is done for two purposes. The first purpose is to obtain an estimate of the confidence that can be associated with the loss modelling results. The second purpose is to identify which of the parameters should be prioritized if further investigative work is to be carried out to define their values with greater certainty.

5.3.4.1 Changing GMPE relation in generation of the ground shaking map

The uncertainty in the ground-shaking hazard arises from three main sources: the uncertainty in the model for earthquake occurrence, the scatter in the GMPE relation, and the uncertainty associated with the local site response. Among the earthquake scenarios used in this chapter, the local site response is set as the same as rock site for all sites. The uncertainty in the earthquake occurrence model is neglected, since such information was not provided in Li (2015) and detailed parameters in other alternative models (e.g. Li et al., 2018) are not shared. Therefore, the same set of seismic source parameters are applied in generating all the earthquake scenarios. In the probabilistic loss estimation process in Section 5.3.3, the GMPE relation used to depict ground motion attenuation is from Yu et al. (2013). Since variation in ground shaking map generated by using different GMPE relations will also affect the final estimated loss, here a different GMPE relation from Lu et al. (2009) is used to illustrate such effect. The comparison of PGA value generated by GMPE function in Lu et al. (2009) and in Yu et al. (2013) at magnitude 7.0 is shown in the

left panel of Figure 5-15. The median PGA value generated by these two GMPE relations are highly approximate. The main difference is that the sigma of the GMPE relation in Lu et al. (2009) is lower than the sigma of the GMPE relation in Yu et al. (2013). Following the same loss estimation process described in Section 5.3.2, the empirical AAL value, by changing GMPE from Yu et al. (2013) to Lu et al. (2009) in hazard map generation for all the 10614 synthetic earthquake scenarios, turns from **2.57 billion RMB** to **2.0 billion RMB**. The empirical loss exceedance curve of using GMPE relation in Lu et al. (2009) is shown in the right panel of Figure 5-15. Compared the loss exceedance curve in Figure 5-13, it can be concluded that the decrease in the estimated AAL value from 2.57 billion RMB to 2.0 billion RMB and the decrease in loss of the LEC curve for fixed return period in Figure 5-15 are mainly due to the higher sigma of the GMPE relation in Yu et al. (2013) than that in Lu et al. (2009), since the other input parameters for these two empirical loss estimations are the same.

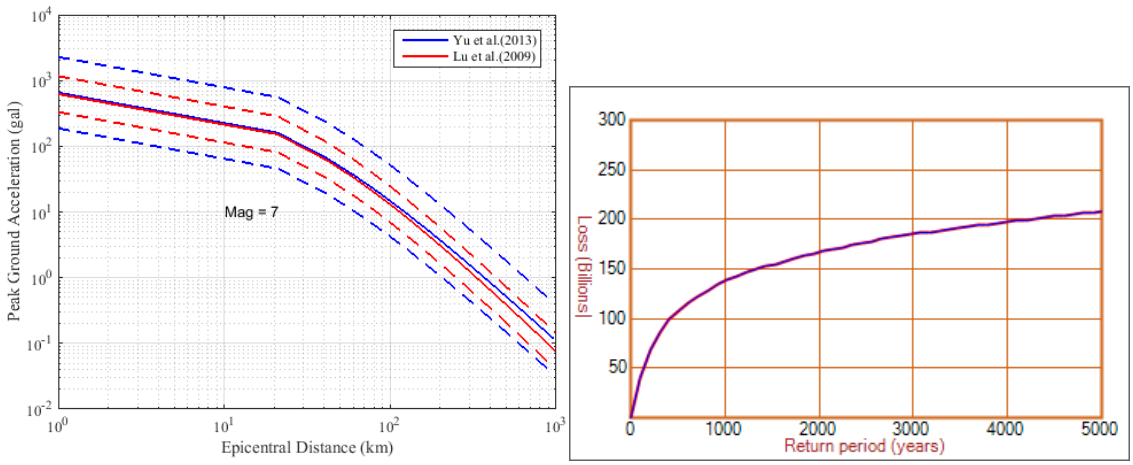

Figure 5-15: (left): Comparison of PGA generated by GMPE equations at magnitude 7 earthquake. (right): Empirical loss exceedance curve derived by changing the GMPE function from Yu et al. (2013) to Lu et al. (2009) in ground shaking map generation for the 10614 synthetic earthquake events. The decrease in estimated loss for fixed return period is obvious compared with the LEC in Figure 5-13.

5.3.4.2 Changing the Intensity-PGA conversion relation in empirical loss estimation

Another sensitivity test in empirical loss estimation is conducted by changing the Intensity-PGA conversion relation from Xin et al. (2019, Chapter 3) to that developed in Ding et al. (2017) for mainland China (both are shown in Figure 5-9). The corresponding AAL value turns from **2.57 billion RMB** to **2.71 billion RMB**. And the modified loss exceedance curve is shown in Figure 5-16.

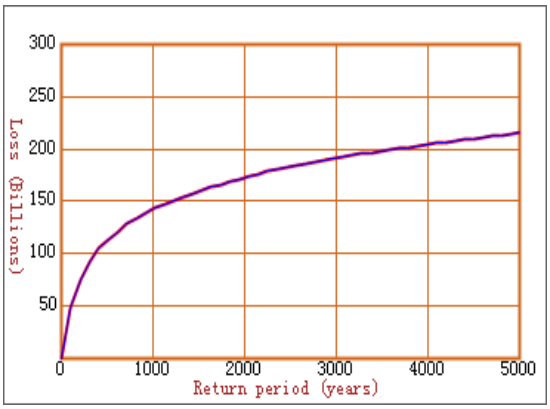

Figure 5-16: Empirical loss exceedance curve derived by using the changing the Intensity-PGA conversion relation from Xin et al. (2009, Chapter 3) to that in Ding et al. (2017) for mainland China.

The slight increase in the estimated loss by using the intensity-PGA conversion in Ding et al. (2017) can be explained based on Figure 5-9. When PGA level is lower than 0.17 g (as can be seen from Figure 5-17, which is the ampflified version of Figure 5-9), the corresponding intensity converted from the relation in Ding et al. (2017) is higher than that in Xin et al. (2019, developed in Chpater 3); when PGA level is higher than 0.17g, the converted intensity by Xin et al. (2019) is higher than by Ding et al. (2017). Thus, the final estimated loss by Ding et al. (2017) in Figure 5-16 is only slightly higher than by Xin et al. (2019) in Figure 5-13. Similar sentivity tests by using other intensity-PGA relations in Figure 5-9 can also be conducted and will not be presented in detail here.

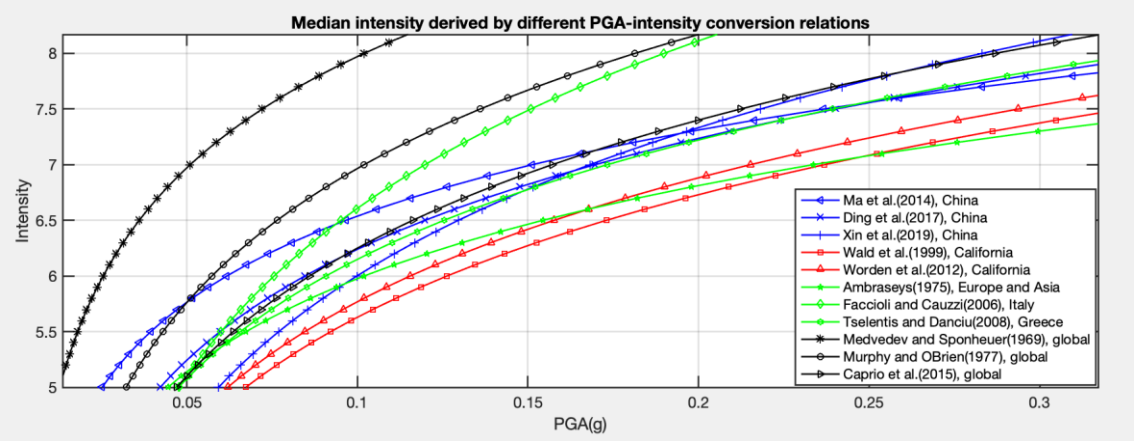

Figure 5-17: The amplified version of Figure 5-9.

5.3.4.3 Changing the empirical loss function

Currently the empirical loss function used in estimating single scenario and multi-scenario loss is from Daniell (2014), which is derived based on the extensive collection of historical damage information related to earthquakes occurred in mainland China. Besides the empirical loss function developed in Daniell (2014), there are also other available empirical loss functions (as summarized in Figure 5-18), which can be used to test the sensitivity of final estimated loss to variations in empirical loss function. It can be predicted from Figure 5-18 that, since the current empirical loss function (tagged as “China standard” in Figure 5-18) is the most “fragile” compared with others (for fixed intensity scale, the loss ratio is the highest), thus the empirically estimated loss will decrease if other empirical loss functions are used.

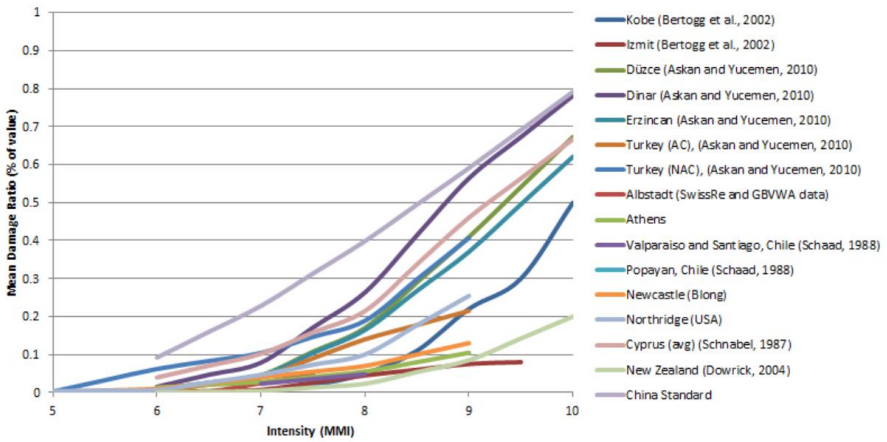

Figure 5-18: A collection of empirical loss functions (Daniell, 2014).

5.3.4.4 Changing the analytical vulnerability function in analytical loss estimation method

In this study, the derivation of analytical vulnerability function is based on the analytical fragility function combined with the relation between empirical loss ratio and damage state for each building type. There are also different approaches to derive the analytical vulnerability curves, as elaborated in e.g. Ordaz et al. (1998) and Marulanda et al. (2013). Since difference in fragility functions and empirical loss ratios can lead to direct increase or decrease in vulnerability curves, sensitivity tests by using different approaches in deriving analytical fragility functions and empirical loss ratios are thus necessary and will be conducted in the future.

5.3.4.5 Changing the unit replacement price of building types in exposure model development

It is straightforward that by using different unit construction price of the same building type, the modelled stock value will be different, so will the final estimation of loss. In the residential building stock model developed in Chapter 4 for mainland China, the same replacement price for the same building type is applied, without differentiation on the location difference of these buildings, which should be adjusted accordingly in the future.

5.4 Conclusion

This chapter presents in detail the deterministic (single scenario based) and probabilistic (multi-scenario based) loss estimation by using analytical method and empirical method, based on the hazard module constructed in Chapter 2, building fragility curve derived in Chapter 3 and the building stock model developed in Chapter 4.

For deterministic loss estimation using empirical method, when the actual macro-seismic intensity map of an earthquake is available, the robustness of the empirical loss function is evaluated through comparison with loss derived from post-earthquake damage reports. When intensity map needs to be converted from actual instrumental records (e.g. PGA, SA), sensitivity tests are conducted by using four synthetic earthquake scenarios to figure out the changes on estimated loss by using different Intensity-PGA conversion relations. It turns out the integration of the sigma of each Intensity-PGA conversion relation will increase the estimated empirical loss, especially for low magnitude events.

For deterministic loss estimation using analytical method, the analytical vulnerability curve is derived from the analytical fragility curve in Chapter 3 combined with the consequence model (relation between damage state and loss ratio). Losses estimated using analytical method are also given for those four synthetic earthquake scenarios, which are generally lower than losses estimated by using empirical method (as shown in Table 5-5), but still within the two times' difference (i.e. the empirical loss is lower than two times of the analytical loss). This difference might be ascribed to the difference in building vulnerability, since the empirical method applies the same loss ratio to all building types, while the analytical method considers the difference in building vulnerability by applying different fragility curves to derive different analytical vulnerability curves for specific building classifications.

For multi-scenario based probabilistic loss estimation, comparison between losses estimated from empirical and analytical method is conducted based on two metrics: the average annual loss (AAL) and the loss exceedance curve (LEC). Probabilistic loss estimated from empirical method is around 2.5 multiples of that estimated from analytical method. For fixed return period, the corresponding loss from the empirical LEC is generally two times of that in analytical method generated LEC, in which the uncertainties from GMPE and from vulnerability curve derivation process have been integrated into the loss calculation. Compared with the usually large discrepancy between modelled losses using different methods, which can reach a factor of 10 (Chan et al., 1998; Spence et al., 2003), the less than three times' difference between the probabilistic loss estimated by using empirical method and analytical method reveals indeed a relatively good consistency between these two methods, although quite different vulnerability functions are used and each method has its unique source of uncertainty.

Sensitivity tests to figure out the impact on the final estimated probabilistic loss are conducted, by changing the input parameters e.g. the GMPE function, the Intensity-PGA conversion relation etc. It turns out the usage of different inputs in the hazard, vulnerability and exposure module will change the final estimated loss accordingly. The study performed in this chapter is a new exploration in trying to fully make use of the historical damage information to calibrate the modelled loss from both deterministic and probabilistic view, with the purpose to develop a well-organized and robust rapid loss estimation method to better serve the needs in seismic risk assessment and post-earthquake mitigation.

6 Summary

In this thesis, a series of studies have been conducted to fully make use of the historical earthquake and damage information in a statistical way, and to check whether they can effectively constrain the predicted hazard and loss results by various models.

In Chapter 2, an area-based test of seismic hazard map is conducted to trade time with space by using a long historical earthquake catalogue, from which a database of peak ground acceleration (PGA) values is generated. Problems in current hazard map performance evaluation studies are summarized and discussed in detail. Different performance evaluation metrics and criteria are applied.

In Chapter 3, a literature review of the currently available building fragility analysis for major building types in China is conducted by collecting information from 87 papers, thesis, book, reports, conference proceedings etc. From these many studies the median fragility functions (dependent on intensity and PGA) were derived for four damage limit states of two most widely distributed building types: masonry and reinforced concrete. A solid fragility database based on both intensity and PGA is thus established for seismic prone areas in mainland China. A comprehensive view of the problems posed by the evaluation of fragility for different building types is given. Necessary comparisons with international projects with similar focus are conducted. Based on the newly collected fragility database, a new approach in deriving intensity-PGA relation is proposed by using fragility as the bridge and reasonable intensity-PGA relations are developed. This novel approach may shed light on new thought in decreasing the scatter in traditional intensity-PGA relation development, i.e., by further classifying observed macro-seismic intensities and instrumental ground motions based on difference in building seismic resistance capability.

In Chapter 4, a grid-level residential building stock model (in terms of floor area and replacement value) targeted for seismic risk analysis for mainland China is developed, by using 2015 Global Human Settlement population density profile as the proxy and disaggregating the administrative level 2010census data into 1km×1km scale. To evaluate the model performance, the residential building stock value is compared with the net capital stock value in Wu et al. (2014) using perpetual inventory method at provincial level. The modelled stocked value in these two studies are indeed quite consistent for all the 31 provinces in mainland China. Furthermore, district level comparison of the residential floor area developed in this study with records from statistical yearbook of Shanghai is also conducted. It turns out that the floor area developed in this study is highly compatible with floor area recorded in the yearbook of Shanghai. To further validate the applicability of the modelled results in seismic risk assessment, an estimation of the loss to residential buildings modelled in this study is performed, by assuming the recurrence of 2008 Wenchuan M8.0 scenario earthquake. The overall estimated loss is quite approximate to the loss value derived from damage reports based on field investigation. These congruences indicate the reliability of the residential building stock model developed in this study. The geo-coded grid-level residential building stock model developed here is flexible to update when more detailed census or statistics data are available. And it can also be conveniently combined with hazard data and vulnerability information for risk assessment to specific research area.

Chapter 5 performed the assessment of seismic loss by employing the hazard scenarios in Chapter 2, vulnerability curves in Chapter 3 and the residential building stock model developed in Chapter 4. The loss is estimated both for single scenario earthquake (from the deterministic view) and for multi-scenario

earthquakes (from the probabilistic view) by using both empirical method and analytical method. Empirically estimated losses are generally higher than losses estimated using analytical method and this estimated loss difference increases with magnitude, which may be ascribed to the assignment of the same loss ratio to all building types in the empirical method, thus the empirical loss is increasingly higher with magnitude increase. Sensitivity tests to quantify the sensitivity of estimated loss to parameters in hazard/vulnerability/exposure module are performed. The use of different GMPE relations in constructing the ground shaking of earthquake scenarios indicate that if the sigma of the GMPE is higher, the empirically estimated probabilistic loss will be also higher. For single scenario earthquake, when the sigma from the Intensity-PGA relation is considered in generating the macro-seismic intensity map from a PGA map, the higher the sigma in Intensity-PGA relation, the higher the deterministic loss. Finally, optimization directions for future loss assessment and sensitivity studies are briefly outlined.

7 Limitations and Outlook

With the target of this thesis being to fully make use of the historical earthquake and damage information to check whether they can effectively constrain the predicted hazard and loss results by various models, studies have been conducted focusing on the construction and validation of PSHA map, the review of empirical and analytical fragility database for major building types in China, the development and performance evaluation of the grid-level residential building stock model for mainland China, and the evaluation of estimated loss from deterministic and probabilistic view. In spite of the achievements have been made, the limitations of this thesis in its hazard and loss modelling process are also obvious.

One is the neglection of the dependence or spatial correlation of ground motion generated at multiple sites from one single earthquake in loss estimation. The open source software CRISIS and CAPRA used in constructing the hazard map and in calculation of loss provide no access to integrate such spatial correlation. In the future, when actual seismic assessment and loss estimation are to be performed, the OpenQuake engine (Pagani et al., 2014) developed by the Global Earthquake Model foundation (GEM) can be used to rectify the spatial correlation. As revealed in previous studies (e.g. Sokolov and Wenzel, 2003; Park et al., 2007), the higher the spatial correlation, the larger the variation in losses to a portfolio and the higher the probability of extreme loss values. For the case of a single scenario earthquake, intra-earthquake variability increases the possibility of obtaining extreme motion at one of the multiple locations compared with the single-site probability.

From a broad point of view, limitations of the framework of Probabilistic Seismic Hazard Analysis (PSHA) also entail more deep-going studies. Notwithstanding the current extensive acceptance and use of PSHA, there remain many challenges in the modelling process owing to the complexity of the underlying natural phenomena, the paucity of the information so far collected and the overall lack of standardization and consensus on techniques to be used in the construction of hazard models. Chapter 2 of this thesis has performed a systematic scheme in evaluating seismic hazard map performance with regard to the source model. The acceleration database was generated by historical earthquake plus an empirical ground motion attenuation relation, but not by real instrumental records. Thus, ground motion related effects have to be analysed separately.

The third limitation is related to the ground motion indicators (peak ground acceleration, macro-seismic intensity) used in this study for loss estimation. As summarized in Bommer et al. (2002), one shortcoming in loss modelling on the basis of intensity is the requirement of using attenuation equations that predict arithmetical values of intensity as if it were a continuous variable, whereas intensity values are discrete indices with non-uniform intervals. Another major shortcoming is that the use of intensity ignores entirely the relationship between the frequency content of the ground motion and the dominant period of buildings. PGA shares this second shortcoming with intensity but more importantly it has almost no correction with the damage potential of the ground motion. In recent years, the use of spectral displacement in determining damage levels due to earthquake shaking has increasingly populated, which is considered to be able to reflect the frequency difference and integrate the total energy in the ground motion. Therefore, in future actual loss estimation practices, the development of spectral displacement based ground motion indicator is preferred.

The fourth limitation is related to the grid-level exposure model developed in this study. Currently the modelling focus is only on residential building stock, given the availability of detailed census data to develop the model. While, when disastrous earthquakes occur, although the damage to and the collapse of buildings is the main cause of fatality and economic loss, damages to those non-residential buildings (office, school, hospital, hotel, warehouse, factory, shop, cinema etc.) as well as life-line projects, infrastructures and the consecutive losses are not negligible. Therefore, in further work, more efforts should be devoted to estimate the stock value of non-residential buildings and infrastructures at risk. Additionally, the replacement value developed in this study did not integrate the depreciation of the exposed buildings, which should be adjusted accordingly in further exposure modelling work.

Furthermore, although the loss assessment using the vulnerability curve and exposure model developed in this work can provide a reasonable loss estimation compared with reported loss based on field investigation for deterministic scenario, and consistency between probabilistic loss estimated by using empirical and analytical method is achieved, more deep-going sensitivity studies are still needed to have a thorough examination of the sensitivity of modelled loss to the changes in each parameter of the whole loss modelling chain.

Finally, the common aim of the various validation and optimization of seismic loss estimation model is to better serve the mitigation of future seismic risk and management of post-earthquake response. Therefore, in the future, another key issue should be kept in mind is related to the effective application of the loss modelling methodology and products. Global reinsurance companies reduce their risk by spreading it among policies in many countries, and by transferring some risk to the much larger capital markets by issuing insurance-linked securities, known as catastrophe bonds. These bonds pay a high rate of quarterly interest unless the specified catastrophe occurs, in which case the investor could lose his or her principal. An earthquake catastrophe bond could be 'triggered" by, among other things, an earthquake of a given magnitude falling into a specified location, or by exceeding a specified shaking threshold. Another option is to trigger by the exceedance of a specific loss value. Such bonds typically have maturities of less than a decade, and the investor must be able to assess the benefit of the high interest rate against the risk of losing the principal. With the optimization of seismic hazard and loss modelling for developing countries, such practice e.g. issuing of catastrophe bonds can be further studied and enhanced in those seismic active regions to mitigate government’s pressure in post-earthquake recovery and to better make use of the leverage effect of the capital market.

Appendix

A: Chinese Official Seismic Intensity Scale: GB17742-2008.

Macro Intensity	Senses by people on the ground	Degree of building damage			Other damages	Horizontal motion on the ground	
		Building type	Damages	Average damage index		Peak ground acceleration (m/s^2)	Peak speed (m/s)
I	Insensible						
II	Sensible by very few still indoor people						
III	Sensible by a few still indoor people		Slight rattle of doors and windows		Slight swing of suspended objects		
IV	Sensible by most people indoors, a few people outdoors; a few wake up from sleep		Rattle of doors and windows		Obvious swing of suspended objects; vessels rattle		
V	Commonly sensible by people indoors, sensible by most people outdoors; most wake up from sleep		Noise from vibration of doors, windows, and building frames; falling of dusts, small cracks in plasters, falling of some roof tiles, bricks falling from a few roof-top chimneys		Rocking or flipping of unstable objects	0.31 (0.22-0.44)	0.03 (0.02-0.04)
VI	Most unable to stand stably, a few scared to running outdoors	A	A few have D3 damage	0-0.11	Cracks in riverbanks and soft soil; occasional burst of sand and water from saturated sand layers; cracks on some standalone chimneys	0.63 (0.45-0.89)	0.06 (0.05-0.09)
		B	Very few have D3 damage, a few have D2 damage, most are intact				
		C	Very few have D2 damage, the majority are intact	0-0.08			
VII	Majority scared to running outdoors, sensible by bicycle riders and people in moving motor vehicles	A	A few have D4 and/or D5 damage, most have D3 and/or D2 damage	0.09-0.31	Collapse of riverbanks; frequent burst of sand and water from saturated sand layers; many cracks in soft soils; moderate destruction of most standalone chimneys	1.25 (0.90-1.77)	0.13 (0.10-0.18)
		B	A few have D3 damage, most have D2 and/or D1 damage				
		C	A few have D3 and/or D2, most are intact	0.07-0.22			
VIII	Most swing about, difficult to walk	A	A few have D5 damage, most have D4 and/or D3 damage	0.29-0.51	Cracks appear in hard dry soils; severe destruction of most standalone chimneys; treetops break; death of people and cattle caused by building destruction	2.50 (1.78-3.53)	0.25 (0.19-0.35)
		B	Very few have D5 damage, most have D3 and/or D2 damage				
		C	A few have D4 and/or D3 damage, most have D2 damage	0.2-0.4			

IX	Moving people fall	A	Most have D4 and/or D5 damage	0.49-0.71	Many cracks in hard dry soils; possible cracks and dislocations in bedrock; frequent landslides and collapses; collapse of many standalone chimneys	5.00 (3.54-7.07)	0.50 (0.36-0.71)
		B	A few have D5 damage, most have D4 and/or D3 damage				
		C	A few have D5 and/or D4 damage, most have D3 and/or D2 damage	0.38-0.6			
X	Bicycle riders may fall; people in unstable state may fall away; sense of being thrown up	A	Commonly have D5 damage	0.69-0.91	Cracks in bedrock and earthquake fractures; destruction of bridge arches founded in bedrock; foundation damage or collapse of most	10.00 (7.08-14.14)	1.00 (0.72-1.41)
		B	The majority have D5 damage				
		C	Most have D5 and/or D4 damage	0.58-0.8			
XI		A	Commonly have D5 damage	0.89–1.0	Earthquake fractures extend a long way; many bedrock cracks and landslides		
		B					
		C		0.78-1.0			
XII		A	Almost all have D5 damage	1.0	Drastic change in landscape, mountains, and rivers		
		B					
		C					

B: Statistics of fragility database for each damage limit state and each building type.

build_type	Int. or PGA (g)	Orig. Data No.	fragility number after removing outliers				median value of each fragility dataset with truncated exceed. prob. ≥ 1%				standard deviation of each fragility dataset with truncated median exceed. prob. ≥ 1%			
			LS1	LS2	LS3	LS4	LS1	LS2	LS3	LS4	LS1	LS2	LS3	LS4
Masonry_A	6	29	28	28	28	28	0.30	0.06	0.01		0.13	0.04	0.01	
	7	29	29	26	26	27	0.47	0.14	0.04		0.21	0.08	0.04	
	8	29	29	29	25	26	0.78	0.40	0.11	0.03	0.20	0.27	0.07	0.02
	9	28	28	28	28	25	0.91	0.64	0.36	0.11	0.14	0.27	0.27	0.06
	10	28	27	26	28	28	0.99	0.90	0.69	0.33	0.05	0.15	0.26	0.22
Masonry_B	6	21	21	21	21	21	0.15	0.02			0.09	0.02		
	7	21	21	20	18	18	0.26	0.08	0.02		0.21	0.10	0.03	
	8	21	21	21	21	18	0.66	0.17	0.07	0.01	0.30	0.24	0.16	0.01
	9	20	20	20	20	17	0.79	0.37	0.15	0.05	0.29	0.30	0.25	0.03
	10	20	20	20	20	20	0.96	0.74	0.39	0.15	0.24	0.31	0.30	0.22
RC_A	6	24	23	22	19	24	0.12				0.07			
	7	24	23	23	22	24	0.25	0.02			0.14	0.05		
	8	26	26	24	24	23	0.57	0.12	0.02		0.19	0.12	0.06	
	9	20	20	20	19	18	0.82	0.48	0.17	0.02	0.14	0.17	0.08	0.02
	10	16	16	16	16	14	0.98	0.84	0.55	0.16	0.10	0.16	0.26	0.10
RC_B	6	6	6	5	6	6	0.05				0.05			
	7	6	5	5	6	6	0.15	0.02			0.06	0.01		
	8	6	6	5	5	6	0.48	0.06			0.19	0.02		
	9	5	5	5	5	5	0.75	0.33	0.04		0.20	0.18	0.11	
	10	5	5	5	5	5	0.95	0.67	0.27	0.05	0.15	0.25	0.29	0.11
Masonry_A	0.1	6	6	6	5	6	0.22	0.06	0.02		0.14	0.06	0.01	
	0.2	6	6	6	6	6	0.60	0.25	0.08	0.02	0.15	0.13	0.06	0.01
	0.3	6	6	6	6	6	0.77	0.47	0.18	0.05	0.10	0.14	0.10	0.03
	0.4	6	6	6	6	6	0.86	0.60	0.29	0.09	0.07	0.14	0.14	0.07
	0.5	6	6	6	6	6	0.92	0.70	0.39	0.14	0.05	0.12	0.16	0.10
	0.6	6	6	6	6	6	0.95	0.77	0.50	0.20	0.04	0.10	0.16	0.13
	0.7	6	6	6	6	6	0.97	0.84	0.59	0.27	0.03	0.08	0.15	0.15
	0.8	6	6	6	6	6	0.98	0.88	0.66	0.34	0.02	0.07	0.15	0.17
	0.9	6	6	6	6	6	0.99	0.91	0.73	0.41	0.02	0.06	0.15	0.18
	1	6	6	6	6	6	0.99	0.94	0.78	0.47	0.02	0.05	0.14	0.19
	1.1	2	2	2	2	2	1.00	0.97	0.91	0.70	0.00	0.03	0.08	0.18
	1.2	2	2	2	2	2	1.00	0.98	0.93	0.74	0.00	0.03	0.05	0.16
Masonry_B	0.1	6	6	6	6	6	0.04	0.02			0.05	0.01		
	0.2	6	6	6	6	5	0.21	0.05	0.01		0.14	0.05	0.01	
	0.3	6	6	6	6	5	0.43	0.14	0.04		0.19	0.09	0.02	
	0.4	6	6	6	6	6	0.59	0.25	0.08	0.01	0.21	0.14	0.05	0.01
	0.5	6	6	6	6	6	0.69	0.37	0.13	0.03	0.20	0.17	0.07	0.02
	0.6	6	6	6	6	6	0.76	0.45	0.18	0.05	0.17	0.18	0.09	0.03
	0.7	6	6	6	6	6	0.81	0.53	0.22	0.07	0.14	0.18	0.11	0.04
	0.8	6	5	6	6	6	0.86	0.59	0.28	0.09	0.06	0.17	0.13	0.06
	0.9	6	5	6	6	6	0.89	0.65	0.33	0.11	0.05	0.16	0.14	0.08
	1	6	5	6	6	6	0.91	0.70	0.39	0.13	0.04	0.15	0.15	0.10
	1.1	3	3	3	3	3	0.93	0.70	0.42	0.15	0.09	0.20	0.23	0.17
	1.2	3	3	3	3	3	0.95	0.75	0.48	0.19	0.08	0.19	0.24	0.19
RC_A	0.1	20	18	18	20	17	0.07				0.07			
	0.2	20	20	18	19	20	0.42	0.13	0.01		0.32	0.12	0.03	
	0.3	22	22	22	21	20	0.72	0.45	0.05		0.29	0.35	0.09	
	0.4	20	20	20	20	18	0.78	0.48	0.10	0.02	0.26	0.36	0.21	0.02
	0.5	13	12	13	13	11	0.96	0.89	0.34	0.03	0.09	0.25	0.26	0.04
	0.6	22	22	22	22	19	0.93	0.82	0.33	0.05	0.30	0.41	0.32	0.05

	0.7	11	11	11	11	10	0.99	0.96	0.77	0.06	0.08	0.22	0.33	0.06
	0.8	17	17	17	17	15	0.88	0.64	0.37	0.15	0.38	0.36	0.37	0.08
	0.9	12	11	12	12	11	1.00	0.99	0.92	0.14	0.03	0.16	0.30	0.11
	1	16	16	16	16	15	0.91	0.70	0.41	0.25	0.49	0.38	0.34	0.13
	1.1	5	5	5	5	5	1.00	0.99	0.99	0.29	0.00	0.01	0.03	0.31
	1.2	14	14	14	14	14	0.61	0.68	0.67	0.39	0.47	0.43	0.34	0.27
RC_B	0.1	9	8	9	9	9	0.02				0.02			
	0.2	9	8	7	9	9	0.18	0.04			0.28	0.02		
	0.3	11	11	11	10	11	0.50	0.22			0.35	0.32		
	0.4	9	9	9	8	9	0.65	0.37	0.04		0.25	0.33	0.04	
	0.5	9	9	9	8	8	0.79	0.57	0.08		0.21	0.31	0.08	
	0.6	11	11	11	10	10	0.93	0.75	0.20	0.02	0.18	0.30	0.10	0.01
	0.7	9	9	9	9	8	0.93	0.81	0.37	0.03	0.15	0.29	0.22	0.02
	0.8	8	8	8	8	7	0.91	0.79	0.45	0.03	0.12	0.26	0.29	0.02
	0.9	10	10	10	10	9	0.99	0.93	0.68	0.03	0.12	0.25	0.33	0.03
	1	7	7	7	7	7	0.94	0.83	0.52	0.05	0.09	0.22	0.33	0.04
	1.1	4	4	4	4	4	1.00	0.97	0.89	0.08	0.02	0.05	0.19	0.07
	1.2	6	5	5	5	6	1.00	0.99	0.98	0.23	0.00	0.01	0.06	0.12

Note: “origin fragility number” refers to the number of original fragilities collected for each damage limit state of each building type from previous studies; “fragility number after removing outliers” refers to the remaining fragilities after removing outliers using box-plot check method. Only intensity and PGA values with truncated exceedance probability ≥1% for each damage limit state of each building type are given, since higher damage states can appear only for higher intensities or PGA values (see Sect. 5.2 for more details).

C: Supplementary figures in Chapter 3.

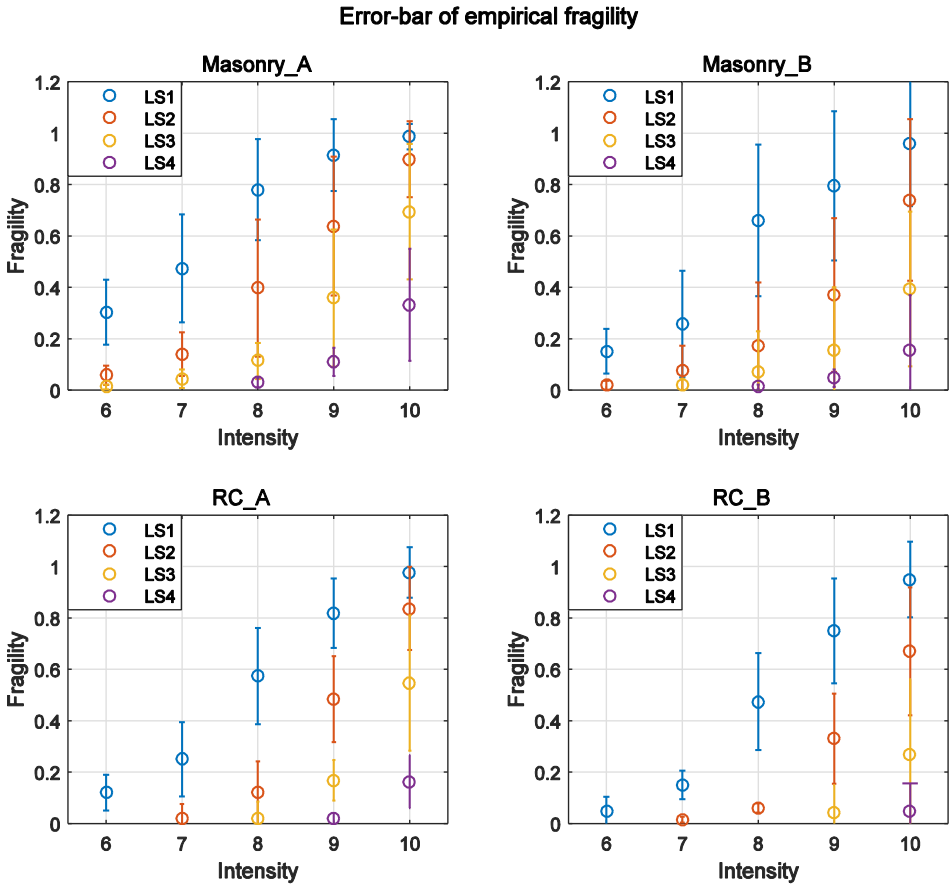

Figure C1: The error-bar of empirical fragility, namely the exceedance probability of each damage limit state (LS1, LS2, LS3, LS4) derived from empirical fragility datasets for each building type (Masonry_A, Masonry_B, RC_A, RC_B). Detailed values are given in Table B1. The circle within each bar represents the median exceedance probability of each damage limit state; the length of each bar indicates the value of the corresponding standard deviation. Only intensity and PGA values with truncated exceedance probability ≥1% for each damage limit state of each building type are plotted, since higher damage states can appear only for higher intensities or PGA values (see Sect. 5.2 for more details).

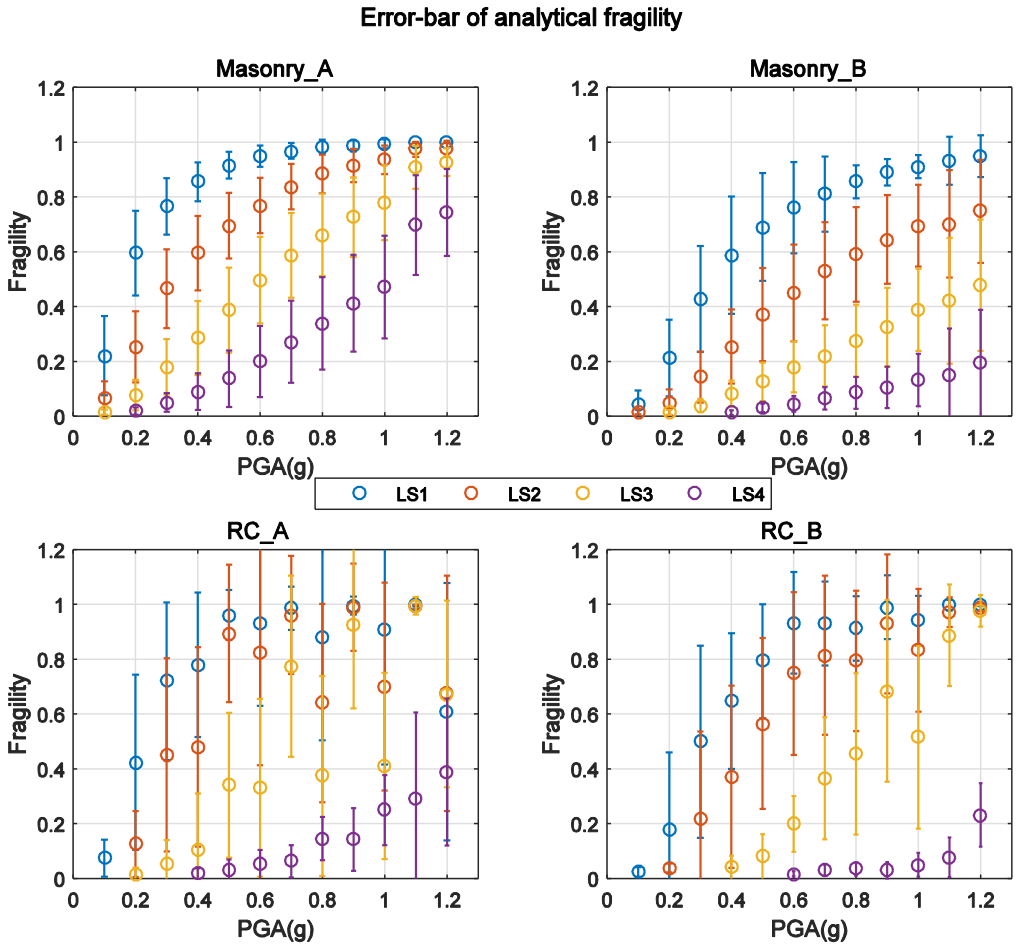

Figure C2: The error-bar of analytical fragility, namely the exceedance probability of each damage limit state (LS1, LS2, LS3, LS4) derived from analytical fragility datasets for each building type (Masonry_A, Masonry_B, RC_A, RC_B). Detailed values are given in Table B1. The circle within each bar represents the median exceedance probability of each damage limit state; the length of each bar indicates the value of the corresponding standard deviation. Only intensity and PGA values with truncated exceedance probability ≥1% for each damage limit state of each building type are plotted, since higher damage states can appear only for higher intensities or PGA values (see Sect. 5.2 for more details).

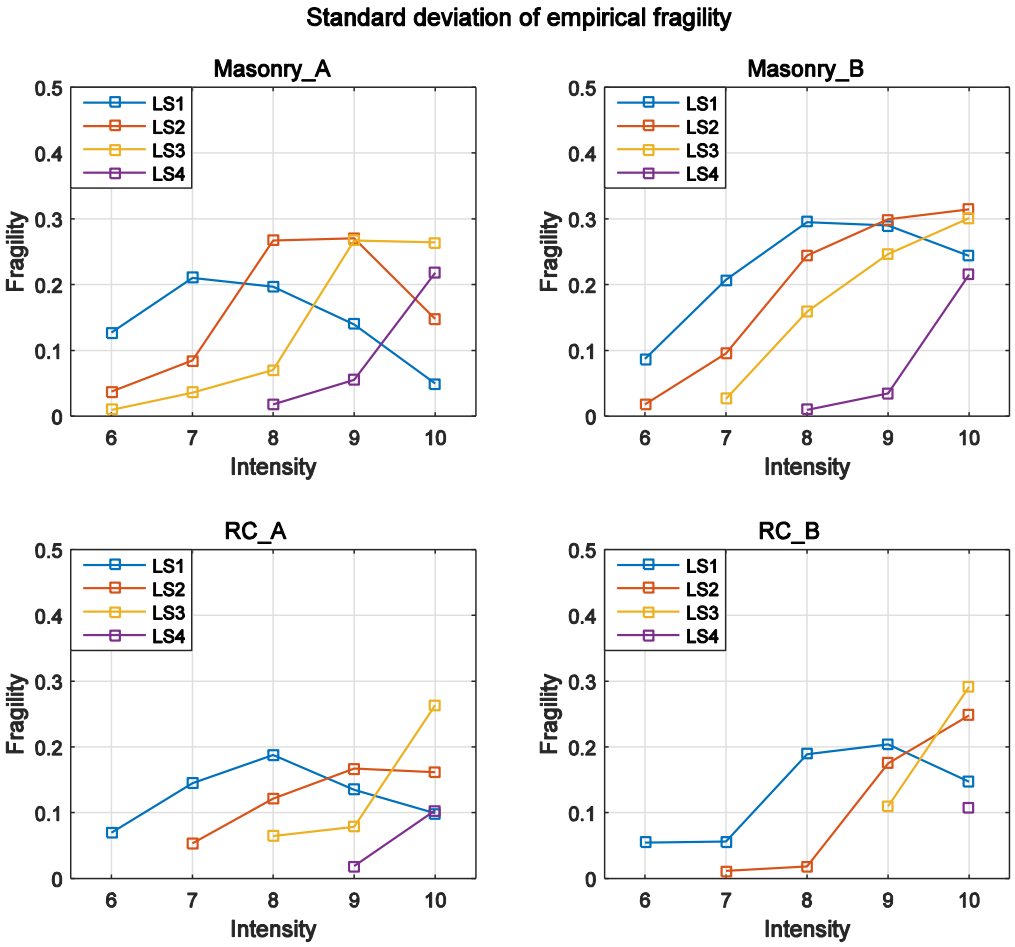

Figure C3: Standard deviation of empirical fragility, namely the exceedance probability of each damage limit state (LS1, LS2, LS3, LS4) derived based on empirical fragility datasets for each building type (Masonry_A, Masonry_B, RC_A, RC_B; detailed values are given in Table B1). Only intensity and PGA values with truncated exceedance probability ≥1% for each damage limit state of each building type are plotted, since higher damage states can appear only for higher intensities or PGA values (see Sect. 5.2 for more details).

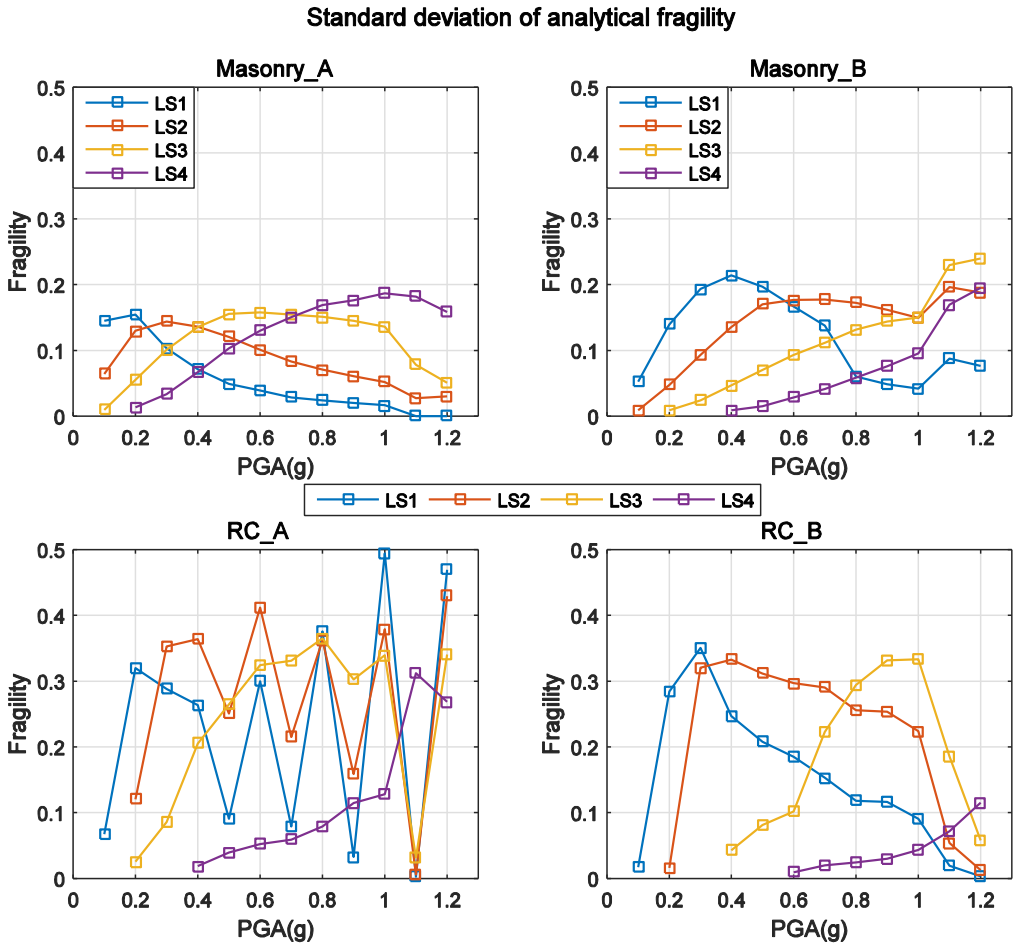

Figure C4: Standard deviation of analytical fragility, namely the exceedance probability of each damage limit state (LS1, LS2, LS3, LS4) derived based on analytical fragility datasets for each building type (Masonry_A, Masonry_B, RC_A, RC_B; detailed values are given in Table B1). Only intensity and PGA values with truncated exceedance probability ≥1% for each damage limit state of each building type are plotted, since higher damage states can appear only for higher intensities or PGA values (see Sect. 5.2 for more details).

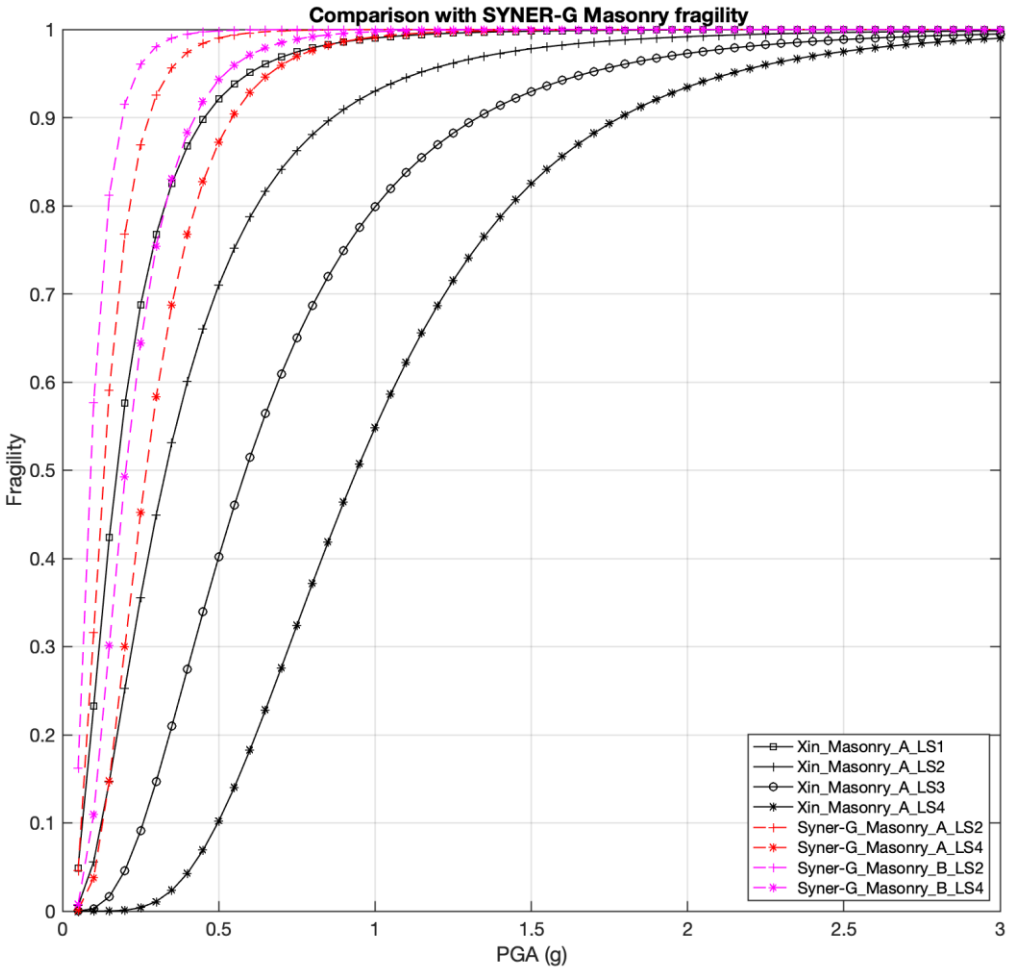

Figure C5: Fragility curve comparison between SYNER-G project mean outputs and our median results for masonry building type. In SYNER-G project, "Masonry_A", "Masonry_B" refer to the low-rise, mid-rise masonry building types, respectively; LS2 and LS4 refer to yielding state and collapse state (see Sect. 4.2.2 for more detailed discussion on sources of discrepancy).

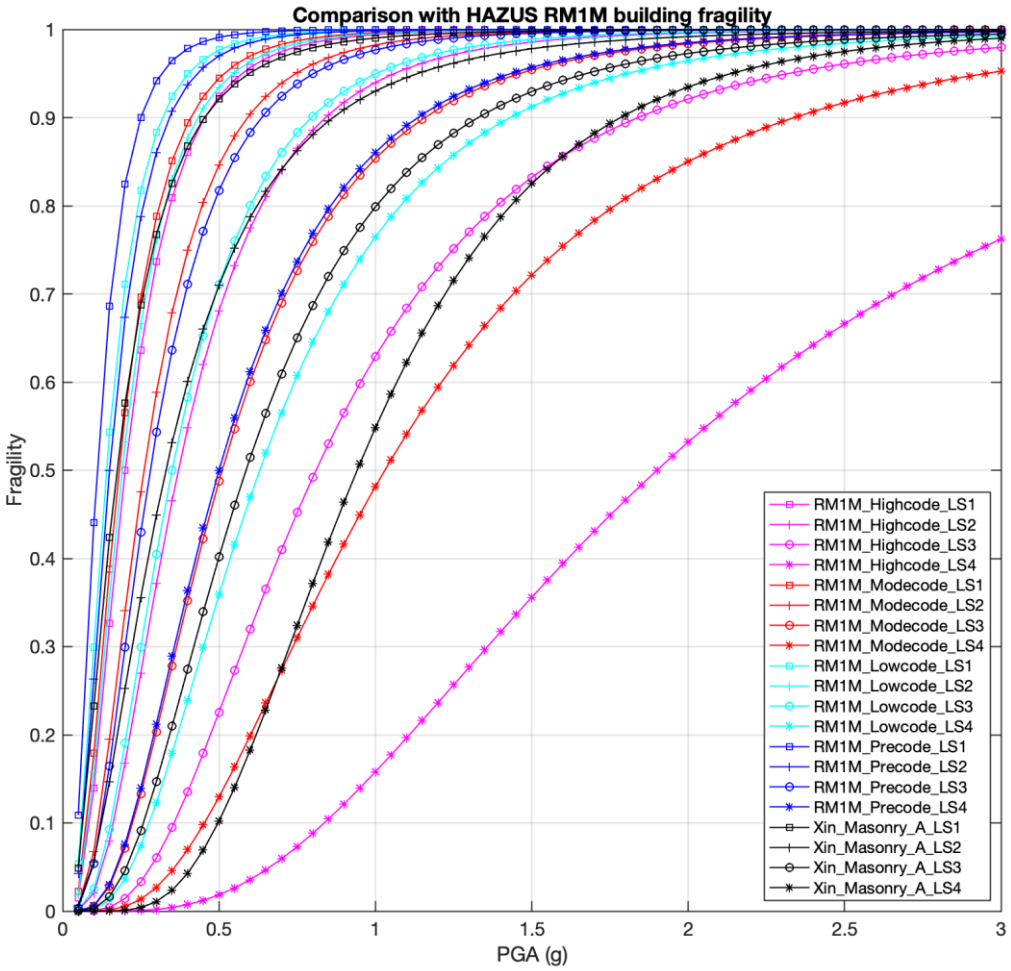

Figure C6: Median fragility curve comparison between HAZUS "RM1M" building type and our work for "Masonry_A". In HAZUS project, "RM1M" refers to "Mid-rise Reinforced Masonry Bearing Walls with Wood or Metal Deck Diaphragms" (see Sect. 4.2.4 for more details).

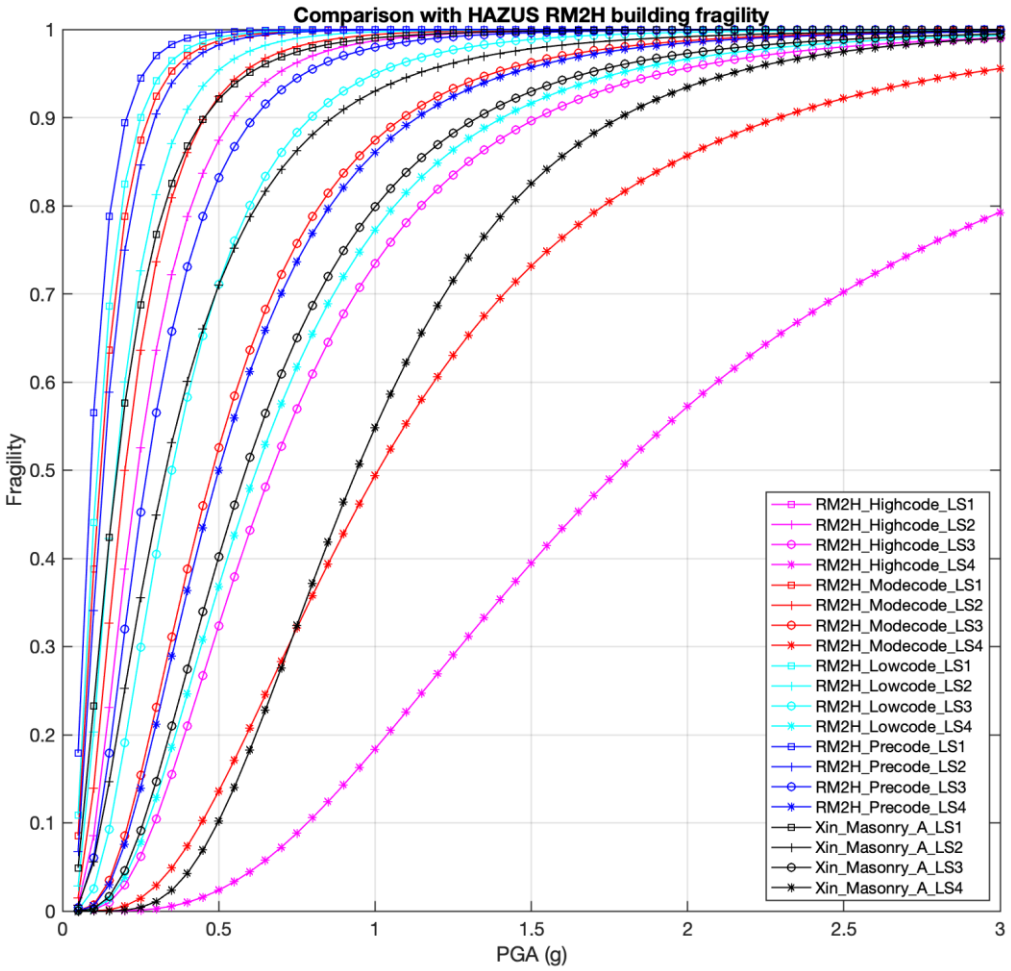

Figure C7: Median fragility curve comparison between HAZUS "RM2H" building and our work for "Masonry_A". In HAZUS project, "RM2H" refers to "High-rise Reinforced Masonry Bearing Walls with Precast Concrete Diaphragms" (see Sect. 4.2.4 for more details).

D: Methodology in Section 3.5.4 in characterization of uncertainty transmission from empirical/analytical fragility database to intensity-PGA relation

The estimation of the uncertainty of the intensity-PGA relation (Eq. (3-5)) is not a standard procedure like regression analysis. We have fragility as function of intensity with an error on the fragility so that fragility is a random variable. It is also a random variable when derived as function of *y* = ln(PGA). We express this as

$$f(y) = g(y) + \varepsilon_g \tag{D1}$$

$$f(i) = h(i) + \varepsilon_h \tag{D2}$$

With *i*: intensity, *y*: ln(PGA), f: fragility.

ε_g is a normally distributed random variable with zero mean, standard deviation σ_g.

ε_h is a normally distributed random variable with zero mean, standard deviation σ_h.

$g(y)$ and $h(i)$ are non-linear functions that can be modelled as cumulative normal distributions in intensity and ln(PGA) as fragility ranges between 0 and 1. Under this condition equating the expectation values of the fragilities

$$E[f(y)] = E[f(i)], g(y) = h(i) \tag{D3}$$

Leads to a linear relation between ln(PGA) and intensity. Including uncertainties in this relation leads to the hypothesis

$$\ln(PGA) = y = \alpha + \beta \cdot i + \varepsilon_y \tag{D4}$$

ε_y is a normally distributed random variable with zero mean, standard deviation σ_y and this is the quantity we want to determine. Note that with this relation y became a random variable. Its expectation value is related to intensity via

$$E[y] = \bar{y} = \alpha + \beta \cdot i \tag{D5}$$

We ask the question: If the above relation holds and intensity is fixed what range of values for y is possible so that

$$f\big(y(i)\big) = f(i) \tag{D6}$$

holds. Inserting above expressions provides

$$g\big(\alpha + \beta \cdot i + \varepsilon_y\big) + \varepsilon_g = h(i) + \varepsilon_h \tag{D7}$$

If we assume that the error term is small, we can write:

$$g\big(\alpha + \beta \cdot i + \varepsilon_y\big) \approx g(\alpha + \beta \cdot i) + g'\ (\alpha + \beta \cdot i) \cdot \varepsilon_y \tag{D8}$$

$g'\ (\alpha + \beta \cdot i)$ is the slope of the g(y) curve and has the unit 1/ln(PGA). The value changes along the curve so that we replace it by an average value $\bar{g}'$. Then,

$$\varepsilon_y = \frac{1}{\bar{g}'}(\varepsilon_h - \varepsilon_g) \quad \text{(D9)}$$

and under the assumption of independence of the two random terms we get

$$\sigma_y = \frac{1}{\bar{g}'}\sqrt{\sigma_h^2 + \sigma_g^2} \quad \text{(D10)}$$

In order to utilize this estimation scheme for our data we approximate $\bar{g}'$ by its value at the 0.5 value of the fragility function: $g(y_m) = 0.5$, so that $\bar{g}' = g'(y_m)$.When we do the estimates for each damage class and each building type we find the standard deviations for ln(PGA) according to the following table. The values do vary. A representative/average value appears to be 0.3.

Table D1: The standard deviation in intensity-PGA relation for each damage limit state of each building type.

Build_Type	LS1	LS2	LS3	LS4
Masonry_A	0.29	0.34	0.27	0.20
Masonry_B	0.48	0.49	0.44	0.25
RC_A	0.44	0.59	0.42	0.16
RC_B	0.27	0.32	0.24	0.05

E: Digitalized historical isoseismal maps in mainland China

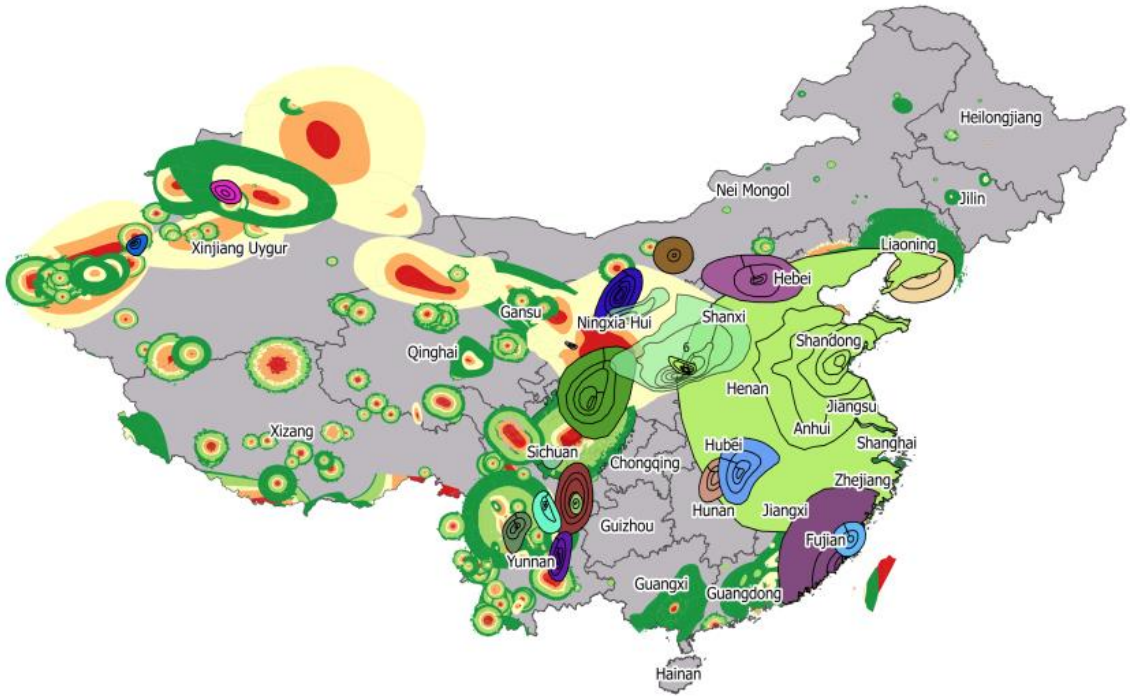

Figure E1: Distribution of digitalalized isoseismal maps.

F: Digitalized China 5th National Peak Ground Acceleration Zonation Map

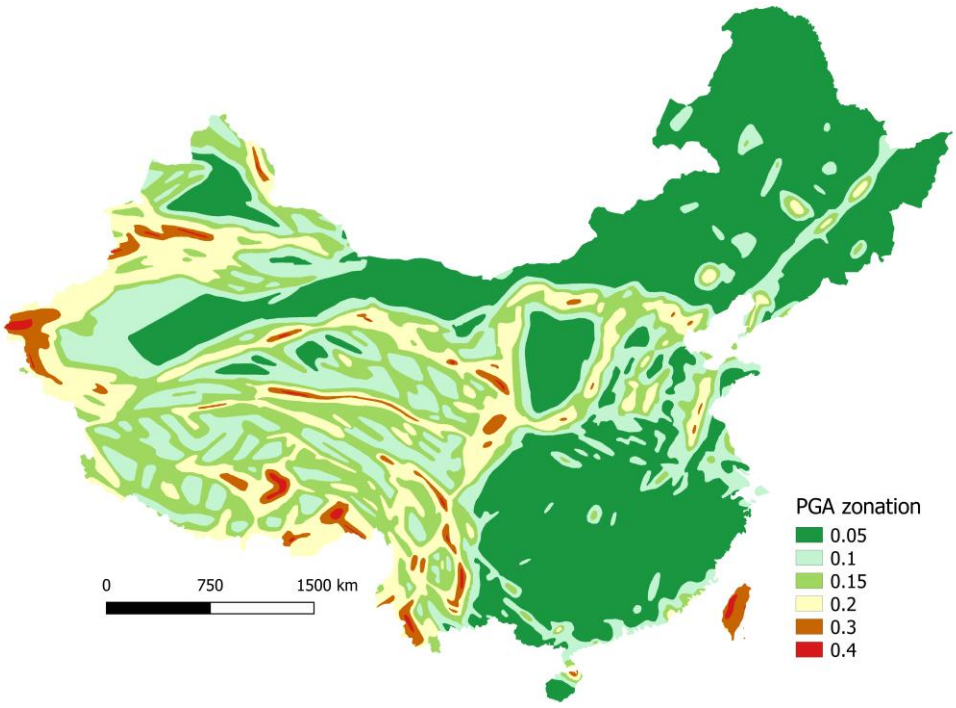

Figure F1: Digitalized China fifth National Peak Ground Acceleration Zonation Map.

G: The population threshold used in 31 provinces/municipalities in mainland China to assign urban/township/rural urbanity attribute in Chapter 4

Province	Province ID	Population of each urbanity level in 2010-census				Population share (%)			Population threshold	
		urban	township	rural	sum	urban	township	rural	Pop1 (urban/township)	Pop2 (township/rural)
Anhui	1	12182587	13394530	33923351	59500468	20.47%	22.51%	57.01%	13991	6908
Beijing	2	15563215	1295477	2753676	19612368	79.35%	6.61%	14.04%	2709	1784
Chongqing	3	8681611	6614192	13550367	28846170	30.10%	22.93%	46.97%	11194	5415
Fujian	4	12548384	8513556	15832277	36894217	34.01%	23.08%	42.91%	6177	2621
Gansu	5	5258935	3932250	16384078	25575263	20.56%	15.38%	64.06%	15175	9350
Guangdong	6	52388382	16641873	35290204	104320459	50.22%	15.95%	33.83%	4427	2521
Guangxi	7	8352777	10065066	27605918	46023761	18.15%	21.87%	59.98%	11711	5087
Guizhou	8	5537562	6199971	23011023	34748556	15.94%	17.84%	66.22%	18126	10384
Hainan	9	2324288	1984228	4362969	8671485	26.80%	22.88%	50.31%	8098	3658
Hebei	10	14388021	17187307	40278882	71854210	20.02%	23.92%	56.06%	5670	2402
Heilongjiang	11	14122516	7201199	16990276	38313991	36.86%	18.80%	44.34%	3845	1483
Henan	12	18331493	17888274	57810172	94029939	19.50%	19.02%	61.48%	15203	8451
Hubei	13	17928160	10516925	28792642	57237727	31.32%	18.37%	50.30%	11667	6345
Hunan	14	12738442	15714621	37247699	65700762	19.39%	23.92%	56.69%	13563	5881
Jiangsu	15	30166466	17205022	31289453	78660941	38.35%	21.87%	39.78%	6554	3341
Jiangxi	16	7504291	11995669	25067837	44567797	16.84%	26.92%	56.25%	11309	3403
Jilin	17	10196745	4451454	12804616	27452815	37.14%	16.21%	46.64%	6150	2849
Liaoning	18	22021184	5166779	16558360	43746323	50.34%	11.81%	37.85%	3486	1874
Inner Mongolia	19	8011564	5708610	10986117	24706291	32.43%	23.11%	44.47%	11152	5041
Ningxia	20	2059295	962727	3279328	6301350	32.68%	15.28%	52.04%	11659	7624
Qinghai	21	1368033	1148221	3110469	5626723	24.31%	20.41%	55.28%	11850	5088
Shaanxi	22	8837175	8222162	20268042	37327379	23.67%	22.03%	54.30%	13716	6862
Shandong	23	28364984	19255743	48171992	95792719	29.61%	20.10%	50.29%	6587	3373
Shanghai	24	17640842	2914256	2464098	23019196	76.64%	12.66%	10.70%	4938	2751
Shanxi	25	9414053	7746486	18551562	35712101	26.36%	21.69%	51.95%	8763	3873
Sichuan	26	15915660	16428768	48073100	80417528	19.79%	20.43%	59.78%	14668	8133
Tianjin	27	8858126	1419767	2660800	12938693	68.46%	10.97%	20.56%	3141	1868
Xinjiang	28	6071803	3263949	12480063	21815815	27.83%	14.96%	57.21%	10473	3618
Tibet	29	272322	408267	2321576	3002165	9.07%	13.60%	77.33%	9751	4483
Yunnan	30	6324830	9634242	30007694	45966766	13.76%	20.96%	65.28%	18128	8118
Zhejiang	31	20386294	13163915	20876682	54426891	37.46%	24.19%	38.36%	5594	2504

Note: For each province, Pop1 and Pop2 are two population thresholds used to assign the grids in 2015 GHS population density profile with urban, township and rural attributes, according to the population density λ in each grid with 1km×1km resolution . The detailed criteria are that: if $\lambda \geqslant Pop1$, the grid is assigned as **urban**; if $Pop1 > \lambda \geqslant Pop2$, **township**; *if* $\lambda < Pop2$, **rural**.

Bibliography

(References in Chapter 1)

Brooks, E. M., Stein, S. and Spencer, B. D.: Comparing the performance of Japan's earthquake hazard maps to uniform and randomized maps, Seismological Research Letters, 87(1), 90–102, doi:https://doi.org/10.1785/0220150100, 2016.

Frankel, A.: Comment on "Why earthquake hazard maps often fail and what to do about it" by S. Stein, R. Geller, and M. Liu, Tectonophysics, 592, 200–206, doi:https://doi.org/10.1016/j.tecto.2012.11.032, 2013a.

Frankel, A.: Corrigendum to comment on "Why Earthquake Hazard Maps Often Fail and What to do About It''' by S. Stein, R. Geller, and M. Liu [TECTO 592 (2013) 200-206]," Tectonophysics, 608, 1453–1454, doi:https://doi.org/10.1016/j.tecto.2013.08.010, 2013b.

Frankel, A. D.: [Comment on "Should Memphis build for California's earthquakes?"] from AD Frankel, Eos, Transactions American Geophysical Union, 84(29), 271–273, doi:https://doi.org/10.1029/2003EO190002, 2003.

Gu, G.: Catalogue of Chinese Earthquakes, Science Press, Beijing, China., 1989.

Gülkan, P.: A dispassionate view of seismic-hazard assessment, Seismological Research Letters, 84(3), 413–416, doi:https://doi.org/10.1785/0220130005, 2013.

Gunasekera, R., Ishizawa, O., Aubrecht, C., Blankespoor, B., Murray, S., Pomonis, A. and Daniell, J.: Developing an adaptive global exposure model to support the generation of country disaster risk profiles, Earth-Science Reviews, 150, 594–608, 2015.

Hanks, T. C., Beroza, G. C. and Toda, S.: Have recent earthquakes exposed flaws in or misunderstandings of probabilistic seismic hazard analysis?, Seismological Research Letters, 83(5), 759–764, doi:https://doi.org/10.1785/0220120043, 2012.

Hu, M., Bergsdal, H., Voet, E. van der, Huppes, G. and Müller, D. B.: Dynamics of urban and rural housing stocks in China, Building Research & Information, 38(3), 301–317, doi:10.1080/09613211003729988, 2010.

Jaiswal, K., Wald, D. and Porter, K.: A global building inventory for earthquake loss estimation and risk management, Earthquake Spectra, 26(3), 731–748, 2010.

Maio, R. and Tsionis, G.: Seismic fragility curves for the European building stock, Brussels: JRC Technical Report, European Commission, 2015.

Mak, S. and Schorlemmer, D.: A comparison between the forecast by the United States National Seismic Hazard Maps with recent ground-motion records, Bulletin of the Seismological Society of America, 106(4), 1817–1831, doi:https://doi.org/10.1785/0120150323, 2016.

Musson, R.: Objective validation of seismic hazard source models, in 13th World Conference on Earthquake Engineering, vol. 2492., 2004.

Stein, S., Tomasello, J. and Newman, A.: Should Memphis build for California's earthquakes?, Eos, Transactions American Geophysical Union, 84(19), 177–185, doi:https://nehrp.gov/pdf/ACEHRNov2010_NMSZ_Tomasello.pdf, 2003.

Stein, S., Geller, R. and Liu, M.: Bad assumptions or bad luck: Why earthquake hazard maps need objective testing, Seismological Research Letters, 82(5), 623–626, doi:https://doi.org/10.1785/gssrl.82.5.623, 2011.

Stein, S., Geller, R. J. and Liu, M.: Why earthquake hazard maps often fail and what to do about it, Tectonophysics, 562, 1–25, doi:https://doi.org/10.1016/j.tecto.2012.06.047, 2012.

Stein, S., Geller, R. J. and Liu, M.: Reply to comment by Arthur Frankel on "Why earthquake hazard maps often fail and what to do about it," Tectonophysics, 592, 207–209, doi:http://sci-hub.tw/10.1016/j.tecto.2013.01.024, 2013.

Stirling, M. W.: Earthquake hazard maps and objective testing: The hazard mapper's point of view, Seismological Research Letters, 83(2), 231–232, doi:https://doi.org/10.1785/gssrl.83.2.231, 2012.

Wong, I. G.: How big, how bad, how often: are extreme events accounted for in modern seismic hazard analyses?, Natural hazards, 72(3), 1299–1309, 2014.

Yang, W. and Kohler, N.: Simulation of the evolution of the Chinese building and infrastructure stock, Building Research & Information, 36(1), 1–19, doi:10.1080/09613210701702883, 2008.

(References in Chapter 2)

Aguilar-Meléndez, A., Ordaz Schroeder, M. G., De la Puente, J., González-Rocha, S. N., Rodriguez-Lozoya, H. E., Córdova-Ceballos, A., García-Elías, A., Calderón-Ramón, C., Escalante-Martínez, J. E., Laguna-Camacho, J. R. and others: Development and validation of software CRISIS to perform probabilistic seismic hazard assessment with emphasis on the recent CRISIS2015, Computacióny Sistemas, 21(1), 67–90, 2017.

Albarello, D. and D'Amico, V.: Testing probabilistic seismic hazard estimates by comparison with observations: An example in Italy, Geophysical Journal International, 175(3), 1088–1094, https://doi.org/10.1111/j.1365-246X.2008.03928.x, 2008.

Albarello, D., Peruzza, L. and D'Amico, V.: A scoring test on probabilistic seismic hazard estimates in Italy, Natural Hazards and Earth System Sciences, 15(1), 171–186, http://sci-hub.tw/10.5194%2Fnhess-15-171-2015, 2015.

Atkinson, G. M.: Challenges in seismic hazard analysis for continental interiors, Geological Society of America Special Papers, 425, 329–344, https://doi.org/10.1130/2007.2425(21), 2007.

Beauval, C., Hainzl, S. and Scherbaum, F.: The impact of the spatial uniform distribution of seismicity on probabilistic seismic-hazard estimation, Bulletin of the Seismological Society of America, 96(6), 2465–2471, https://doi.org/10.1785/0120060073, 2006.

Beauval, C., Bard, P.-Y. and Douglas, J.: Comment on "Test of seismic hazard map from 500 years of recorded intensity data in Japan" by Masatoshi Miyazawa and Jim Mori, Bulletin of the Seismological Society of America, 100(6), 3329–3331, https://doi.org/10.1785/0120100065, 2010.

Beauval, C. E. L., Bard, P.-Y., Hainzl, S. and Gueguen, P.: Can strong-motion observations be used to constrain probabilistic seismic-hazard estimates?, Bulletin of the Seismological Society of America, 98(2), 509–520, https://doi.org/10.1785/0120070006, 2008.

Brooks, E. M., Stein, S. and Spencer, B. D.: Comparing the performance of Japan's earthquake hazard maps to uniform and randomized maps, Seismological Research Letters, 87(1), 90–102, https://doi.org/10.1785/0220150100, 2016.

Brooks, E. M., Stein, S. and Spencer, B. D.: Investigating the effects of smoothing on the performance of earthquake hazard maps, International Journal of Earthquake and Impact Engineering, 2(2), 121–134, http://sci-hub.tw/10.1504/IJEIE.2017.089039, 2017.

Cornell, C. A.: Engineering seismic risk analysis, Bulletin of the seismological society of America, 58(5), 1583–1606, 1968.

Frankel, A.: Comment on "Why earthquake hazard maps often fail and what to do about it" by S. Stein, R. Geller, and M. Liu, Tectonophysics, 592, 200–206, https://doi.org/10.1016/j.tecto.2012.11.032, 2013a.

Frankel, A.: Corrigendum to comment on``Why Earthquake Hazard Maps Often Fail and What to do About It''by S. Stein, R. Geller, and M. Liu [TECTO 592 (2013) 200-206], Tectonophysics, 608, 1453–1454, https://doi.org/10.1016/j.tecto.2013.08.010, 2013b.

Frankel, A. D.: [Comment on “Should Memphis build for California’s earthquakes?”] from AD Frankel, Eos, Transactions American Geophysical Union, 84(29), 271–273, https://doi.org/10.1029/2003EO190002, 2003.

Fujiwara, H., Morikawa, N., Ishikawa, Y., Okumura, T., Miyakoshi, J., Nojima, N. and Fukushima, Y.: Statistical comparison of national probabilistic seismic hazard maps and frequency of recorded JMA seismic intensities from the K-NET strong-motion observation network in Japan during 1997–2006, Seismological Research Letters, 80(3), 458–464, https://doi.org/10.1785/gssrl.80.3.458, 2009.

Gardner, J. K. and Knopoff, L.: Is the sequence of earthquakes in Southern California, with aftershocks removed, Poissonian?, Bulletin of the Seismological Society of America, 64(5), 1363–1367, 1974.

Goda, K., Aspinall, W. and Taylor, C. A.: Seismic hazard analysis for the UK: Sensitivity to spatial seismicity modelling and ground motion prediction equations, Seismological Research Letters, 84(1), 112–129, https://doi.org/10.1785/0220120064, 2013.

Gülkan, P.: A dispassionate view of seismic-hazard assessment, Seismological Research Letters, 84(3), 413–416, https://doi.org/10.1785/0220130005, 2013.

Gutenberg, B. and Richter, C. F.: Magnitude and energy of earthquakes: Annali di Geofisica, Annali di Geofisica, 9(1), 7–12, https://doi.org/10.4401/ag-5590, 1956.

Hanks, T. C., Beroza, G. C. and Toda, S.: Have recent earthquakes exposed flaws in or misunderstandings of probabilistic seismic hazard analysis?, Seismological Research Letters, 83(5), 759–764, https://doi.org/10.1785/0220120043, 2012.

Huang, W., Li, W. and Cao, X.: Study of seismic catalog completeness of mainland China: Part 1-a case study in Northern China, Acta Seismologica Sinica, 16(3), 273–280, 1994a.

Huang, W., Li, W. and Cao, X.: Study of seismic catalog completeness of mainland China: Part 2-the distribution of starting year of catalog completeness of each seismic zone, Acta Seismologica Sinica, 16(4), 423–432, 1994b.

Iervolino, I.: Probabilities and fallacies: Why hazard maps cannot be validated by individual earthquakes, Earthquake Spectra, 29(3), 1125–1136, 2013.

Leonard, M.: Earthquake fault scaling: Self-consistent relating of rupture length, width, average displacement, and moment release, Bulletin of the Seismological Society of America, 100(5A), 1971–1988, https://doi.org/10.1785/0120090189, 2010.

Li, B.: Seismotectonics and seismic hazard of the Shanxi Rift System, North China, PhD Thesis, University of Bergen, Bergen, Norway., 2015.

Li, C., Xu, W., Wu, J. and Gao, M.: Time-dependent probabilistic seismic hazard assessment for Taiyuan, Shanxi Province, China, and the surrounding area, Journal of Seismology, 21(4), 749–757, http://sci-hub.tw/10.1007/s10950-016-9633-1, 2017.

Liu, J., Wang, Z., Xie, F. and Lv, Y.: Seismic hazard assessment for greater North China from historical intensity observations, Engineering Geology, 164, 117–130, http://sci-hub.tw/10.1016/j.enggeo.2013.07.002, 2013.

Mak, S. and Schorlemmer, D.: A comparison between the forecast by the United States National Seismic Hazard Maps with recent ground-motion records, Bulletin of the Seismological Society of America, 106(4), 1817–1831, https://doi.org/10.1785/0120150323, 2016.

Mak, S., Clements, R. A. and Schorlemmer, D.: The statistical power of testing probabilistic seismic-hazard assessments, Seismological Research Letters, 85(4), 781–783, https://doi.org/10.1785/0220140012, 2014.

McGuire, R. K.: FORTRAN computer program for seismic risk analysis, US Geological Survey. [online] Available from: https://doi.org/10.3133/ofr7667, 1976.

McGuire, R. K.: Probabilistic seismic hazard analysis and design earthquakes: closing the loop, Bulletin of the Seismological Society of America, 85(5), 1275–1284, 1995.

Mezcua, J., Rueda, J. and Blanco, R. G. I. A.: Observed and calculated intensities as a test of a probabilistic seismic-hazard analysis of Spain, Seismological Research Letters, 84(5), 772–780, https://doi.org/10.1785/0220130020, 2013.

Miyazawa, M. and Mori, J.: Test of seismic hazard map from 500 years of recorded intensity data in Japan, Bulletin of the Seismological Society of America, 99(6), 3140–3149, https://doi.org/10.1785/0120080262, 2009.

Musson, R.: Objective validation of seismic hazard source models, in 13th World Conference on Earthquake Engineering, vol. 2492., 2004.

Ren, X.: Study on the estimation of b value on seismic zonation, Institute of Geophysics, China Earthquake Administration, Beijing, China., 2011.

Ren, X., Gao, M. and Feng, J.: Effect of Completeness of Earthquake Catalogue on Calculating b Value, Technology for Earthquake Disaster Prevention, 6(3), 257–268, http://dx.china-doi.cn/10.3969/j.issn.1673-5722.2011.03.005, 2011.

Scherbaum, F., Cotton, F. and Smit, P.: On the use of response spectral-reference data for the selection and ranking of ground-motion models for seismic-hazard analysis in regions of moderate seismicity: The case of rock motion, Bulletin of the seismological society of America, 94(6), 2164–2185, https://doi.org/10.1785/0120030147, 2004.

Sørensen, M. B., Spada, M., Babeyko, A., Wiemer, S. and Grünthal, G.: Probabilistic tsunami hazard in the Mediterranean Sea, Journal of Geophysical Research: Solid Earth, 117(B1), http://dx.doi.org/10.1029/2010JB008169, 2012.

Stein, S., Tomasello, J. and Newman, A.: Should Memphis build for California's earthquakes?, Eos, Transactions American Geophysical Union, 84(19), 177–185, https://nehrp.gov/pdf/ACEHRNov2010_NMSZ_Tomasello.pdf, 2003.

Stein, S., Geller, R. and Liu, M.: Bad assumptions or bad luck: Why earthquake hazard maps need objective testing, Seismological Research Letters, 82(5), 623–626, https://doi.org/10.1785/gssrl.82.5.623, 2011.

Stein, S., Geller, R. J. and Liu, M.: Why earthquake hazard maps often fail and what to do about it, Tectonophysics, 562, 1–25, https://doi.org/10.1016/j.tecto.2012.06.047, 2012.

Stein, S., Geller, R. J. and Liu, M.: Reply to comment by Arthur Frankel on "Why earthquake hazard maps often fail and what to do about it," Tectonophysics, 592, 207–209, http://sci-hub.tw/10.1016/j.tecto.2013.01.024, 2013.

Stein, S., Spencer, B. D. and Brooks, E. M.: Metrics for assessing earthquake-hazard map performance, Bulletin of the Seismological Society of America, 105(4), 2160–2173, https://doi.org/10.1785/0120140164, 2015.

Stirling, M. and Gerstenberger, M.: Ground motion–based testing of seismic hazard models in New Zealand, Bulletin of the Seismological Society of America, 100(4), 1407–1414, https://doi.org/10.1785/0120090336, 2010.

Stirling, M. and Petersen, M.: Comparison of the Historical Record of Earthquake Hazard with Seismic-Hazard Models for New Zealand and the Continental United States, Bulletin of the Seismological Society of America, 96(6), 1978–1994, https://doi.org/10.1785/0120050176, 2006.

Stirling, M. W.: Earthquake hazard maps and objective testing: The hazard mapper's point of view, Seismological Research Letters, 83(2), 231–232, https://doi.org/10.1785/gssrl.83.2.231, 2012.

Tasan, H., Beauval, C. E. L., Helmstetter, A. E. S., Sandikkaya, A. and Gu E Guen, P.: Testing probabilistic seismic hazard estimates against accelerometric data in two countries: France and Turkey, Geophysical Journal International, 198(3), 1554–1571, https://doi.org/10.1093/gji/ggu191, 2014.

Wang, Y.-J., Lee, Y.-T., Chan, C.-H. and Ma, K.-F.: An investigation of the reliability of the Taiwan Earthquake Model PSHA2015, Seismological Research Letters, 87(6), 1287–1298, https://doi.org/10.1785/0220160085, 2016.

Ward, S. N.: A multidisciplinary approach to seismic hazard in southern California, Bulletin of the Seismological Society of America, 84(5), 1293–1309, 1994.

Ward, S. N.: Area-based tests of long-term seismic hazard predictions, Bulletin of the Seismological Society of America, 85(5), 1285–1298, 1995.

Xie, F., Wang, Z. and Liu, J.: Seismic hazard and risk assessments for Beijing–Tianjin–Tangshan, China, area, Pure and applied geophysics, 168(3–4), 731–738, http://sci-hub.tw/10.1007/s00024-010-0115-z, 2011.

Xu, W.-J. and Gao, M.-T.: Statistical analysis of the completeness of earthquake catalogues in China mainland, China Journal of Geophysics, 57(9), 2802–2281, http://dx.doi.org/10.6038/cjg20140907, 2014b.

Yu, Y. X., Li, S. Y. and Xiao, L.: Development of ground motion attenuation relations for the new seismic hazard map of China, Technol. Earthq. Disaster Prev., 8(1), 24–33, 2013.

(References in Chapter 3)

In English:

Antoniou, S. and Pinho, R.: Development and verification of a displacement-based adaptive pushover procedure, Journal of Earthquake Engineering, 8, 643-661, https://doi.org/10.1080/13632460409350504, 2004.

Bilal, M. and Askan, A.: Relationships between Felt Intensity and Recorded Ground-Motion Parameters for Turkey, B SEISMOL SOC AM, 104, 484-496, https://doi.org/10.1785/0120130093, 2014.

Billah, A. H. M. M. and Alam, M. S.: Seismic fragility assessment of highway bridges: A state-of-the-art review, Structure and Infrastructure Engineering, 11, 804-832, https://doi.org/10.1080/15732479.2014.912243, 2015.

Calvi, G. M., Pinho, R. and Magenes, G.: Development of seismic vulnerability assessment methodologies over the past 30 years, ISET journal of Earthquake Technology, 43, 75-104, https://www.researchgate.net/publication/241826044, 2006.

Caprio, M., Tarigan, B. and Worden, C. B.: Ground motion to intensity conversion equations (GMICEs): A global relationship and evaluation of regional dependency, Bulletin of the Seismological Society of America, 105, 1476-1490, https://doi.org/10.1785/0120140286, 2015.

CSIS: China seismic intensity scale, a non-official English translation based on contents in Wikipedia, https://en.wikipedia.org/w/index.php?title=China_seismic_intensity_scale&oldid=812457225, last access: 21 May 2019.

Crowley, H., Colombi, M., Silva, V., Ahmad N., Fardis M., Tsionis G., Papailia A., Taucer F., Hancilar U., Yakut A., Erberik M.A.: D3.1. Fragility functions for common RC building types in Europe, Pavia, Italy, 223 pp., http://www.vce.at/SYNER-G/files/dissemination/deliverables.html, 2011a.

Crowley, H., Colombi, M., Silva, V., Ahmad N., Fardis M., Tsionis G., Karatoni T., Lyrantazaki F., Taucer F., Hancilar U., Yakut A., Erberik M.A.: D3.2. Fragility functions for common masonry building types in Europe, Pavia, Italy, 177 pp., http://www.vce.at/SYNER-G/files/dissemination/deliverables.html, 2011b.

Draper, N. R., Smith, H: Applied Regression Analysis, 3rd ed., John Wiley & Sons, New York, United States, 2014.

Del Gaudio, C., Ricci, P. and Verderame, G. M.: Development and urban-scale application of a simplified method for seismic fragility assessment of RC buildings, Engineering Structures, 91, 40-57, https://doi.org/10.1016/j.engstruct.2015.01.031, 2015.

Dumova-Jovanoska, E.: Fragility curves for reinforced concrete structures in Skopje (Macedonia) region, Soil Dynamics and Earthquake Engineering, 19, 455-466, https://doi.org/10.1016/S0267-7261(00)00017-8, 2000.

EMS1998: European Macro-seismic Scale 1998, European Seismological Commission, sub commission on Engineering Seismology, Working Group, Macro-seismic Scales, Conseil de l'Europe, Cahiers du Centre Européen de Géodynamique et de Séismologie, Vol. 15, Luxembourg, 1998.

Fajfar, P.: A nonlinear analysis method for performance-based seismic design, Earthquake spectra, 16, 573-592, https://doi.org/10.1193/1.1586128, 2000.

FEMA: HAZUS®MH estimated annualized earthquake losses for the United States, FEMA 366, Washington DC, United States, https://secure.madcad.com/media/fema/FEMA-366-2008.pdf, 2008.

FEMA: Multi-hazard loss estimation methodology: earthquake model (HAZUS-MH-MR3), Technical Report, Washington DC, USA, https://www.fema.gov/media-library/assets/documents/24609, 2003.

Freeman, S. A.: The capacity spectrum method, in Proceedings of the 11th European conference on earthquake engineering, Paris., http://citeseerx.ist.psu.edu/viewdoc/summary?doi=10.1.1.460.2405, 1998.

Freeman, S. A.: Review of the development of the capacity spectrum method, ISET Journal of Earthquake Technology, 41(1), 1–13, http://citeseerx.ist.psu.edu/viewdoc/download?doi=10.1.1.451.9286, 2004.

GEM Fragility Database: https://platform.openquake.org/vulnerability/list?type_of_assessment=1, last access: 30 January 2019.

GEM Vulnerability Database: https://www.ucl.ac.uk/epicentre/resources/gem-vulnerability-database, last access: 30 January 2019.

Hariri-Ardebili, M. A. and Saouma, V. E.: Seismic fragility analysis of concrete dams: A state-of-the-art review, Engineering structures, 128, 374-399, https://doi.org/10.1016/j.engstruct.2016.09.034, 2016.

HAZUS User & Technical Manuals: https://www.fema.gov/hazus-mh-user-technical-manuals, last access: 30 January 2019.

Kaynia, A. M., Fardis, M. and Pitilakis, K.: D3.12: SYNER-G fragility functions of elements at risk, SYNER-G Deliverable 3.12, Norwegian Geotechnical Institute, Norway, 145 pp., http://www.vce.at/SYNER-G/files/dissemination/deliverables.html, 2013.

Maio, R. and Tsionis, G.: Seismic fragility curves for the European building stock, Brussels: JRC Technical Report, European Commission, https://sci-hub.tw/10.2788/586263, 2015.

Medvedev, S. and Sponheuer, W: Scale of seismic intensity (MSK1969), in proceedings of the 4th World Conference on Earthquake Engineering, Chilean Association of Seismology and Earthquake Engineering, Santiago, vol 1, 143-153 pp., http://www.iitk.ac.in/nicee/wcee/article/4_vol1_A2-143.pdf, 1969.

Nakamura, H.: Preliminary report on the great Hanshin Earthquake January 17, 1995 (AIJ1995), Japan Society of Civil Engineers, Tokyo, Japan, http://resolver.tudelft.nl/uuid:96f94279-326a-483c-ac1d-c7f9e9226342, 1995.

Ogweno, L. P. and Cramer, C. H.: Improved CENA regression relationships between Modified Mercalli Intensities and ground motion parameters, Bulletin of the Seismological Society of America, 107, 180-197, https://doi.org/10.1785/0120160033, 2017.

PAGER Scientific Background: https://earthquake.usgs.gov/data/pager/background.php, last access: 30 January 2019.

PERPETUATE Project Report Summary: https://cordis.europa.eu/result/rcn/57689_en.html, last access: 30 January 2019.

Pitilakis, K., Crowley, H. and Kaynia, A. M.: SYNER-G: typology definition and fragility functions for physical elements at seismic risk, Geotechnical, Geological and Earthquake Engineering, 27, 432 pp., https://link.springer.com/content/pdf/10.1007/978-94-007-7872-6.pdf, 2014.

Rossetto, T. and Elnashai, A.: Derivation of vulnerability functions for European-type RC structures based on observational data, Engineering structures, 25, 1241-1263, https://doi.org/10.1016/S0141-0296(03)00060-9, 2003.

Rota, M., Penna, A. and Magenes, G.: A methodology for deriving analytical fragility curves for masonry buildings based on stochastic nonlinear analyses, Engineering Structures, 32, 1312-1323, https://doi.org/10.1016/j.engstruct.2010.01.009, 2010.

Silva, V., Crowley, H. and Colombi, M.: Fragility function manager tool, in SYNER-G: Typology Definition and Fragility Functions for Physical Elements at Seismic Risk, 385-402 pp., Springer., https://doi.org/10.1007/978-94-007-7872-6_13, 2014.

SYNER-G Project Deliverables: http://www.vce.at/SYNER-G/files/dissemination/deliverables.html, last access: 30 January 2019.

Tang, B., Lu, X., Ye, L. and Shi, W.: Evaluation of collapse resistance of RC frame structures for Chinese schools in seismic design categories B and C, Earthq. Eng. Eng. Vib., 10(3), 369, http://sci-hub.tw/10.1007/s11803-011-0073-1, 2011.

Vamvatsikos, D. and Cornell, C. A.: Incremental dynamic analysis, Earthquake Engineering & Structural Dynamics, 31, 491-514, https://doi.org/10.1002/eqe.141, 2002.

Vamvatsikos, D. and Fragiadakis, M.: Incremental dynamic analysis for estimating seismic performance sensitivity and uncertainty, Earthquake Engineering and Structural Dynamics, 39, 141-163, https://doi.org/10.1002/eqe.935, 2010.

Worden, C. B., Gerstenberger, M. C. and Rhoades, D. A.: Probabilistic relationships between Ground-Motion parameters and modified Mercalli intensity in California, Bulletin of the Seismological Society of America, 102, 204-221, https://doi.org/10.1785/0120110156, 2012.

Yepes-Estrada, C., Silva, V., Rossetto, T., D'Ayala, D., Ioannou, I., Meslem, A. and Crowley, H.: The global earthquake model physical vulnerability database, Earthq. Spectra, 32(4), 2567–2585, https://doi.org/10.1193/011816EQS015DP, 2016.

Yuan, Y.: Impact of intensity and loss assessment following the great Wenchuan Earthquake, Earthquake Engineering and Engineering Vibration, 7(3), 247–254, http://dx.chinadoi.cn/10.1007/s11803-008-0893-9, 2008.

In Chinese:

A, N.: Simplified Prediction Methods of Earthquake Disaster Losses in Hohhot, M.S. Thesis, Inner Mongolia Normal University, Inner Mongolia, China, 45 pp., 2013.

Bie, D., Feng, Q. and Zhang, T.: A Research on Vulnerability of Brick-Concrete Buildings in Fujian Based on Partition of Region Characteristics, Journal of Catastrophe, 25(S0), 254-257, http://sci-hub.tw/10.3969/j.issn.1000-811X.2010.z1.054, 2010.

Chang, X., Alimujiang, Y. and Gao, C.: Disaster Loss Assessment and Characteristic of Seismic Hazard of Heshuo Earthquake with Ms5.0 in Xinjiang on Jan 8th, 2012, Inland Earthquake, 26(3), 279-285, http://sci-hub.tw/10.3969/j.issn.1001-8956.2012.03.012, 2012.

Chen, H.: Study on Earthquake Damage Loss Assessment of Urban Buildings' Decorations, M.S. Thesis, Institute of Engineering Mechanics, China Earthquake Administration, Harbin, China, 108 pp., 2008.

Chen, X., Sun, B. and Yan, P.: The characteristics of earthquake disasters distribution and seismic damage to structures in Kangding Ms 6.3 earthquake, Earthquake Engineering and Engineering Dynamics, 37(2), 1-9, http://dx.doi.org/10.13197/j.eeev.2017.02.1.chenxz.001, 2017.

Chen, Y., Chen, Q. and Chen, L.: Vulnerability Analysis in Earthquake Loss Estimate, Earthquake Research in China, 15(2), 97-105, 1999.

Chinese Seismic Intensity Scale: GB17742-2008, issued by General Administration of Quality Supervision, Inspection and Quarantine of the People's Republic of China (AQSIQ) and Standardization Administration of the People's Republic of China (SAC), Beijing, China, 2008.

Cui, Z. and Zhai, Y.: Research on Effects of Provincial Characteristic on Architecture, Journal of Catastrophe, 25(S0), 271-274, 2010.

Ding, B., Sun, J., Li, X., Liu, Z. and Du, J.: Research progress and discussion of the correlation between seismic intensity and ground motion parameters, Earthquake Engineering and Engineering Vibration, 34(5), 7–20, http://dx.doi.org/10.13197/j.eeev.2014.05.7.dingbr.002, 2014.

Ding, B.: Study on Related Quantitative Parameters of Seismic Intensity Scale, Ph.D. Thesis, Institute of Engineering Mechanics, China Earthquake Administration, Harbin, China, 195 pp., 2016.

Ding, B., Sun, J. and Du, K.: Study on relationships between seismic intensity and peak ground acceleration, peak ground velocity, Earthquake Engineering and Engineering Dynamics, 37(2), 26-36, http://dx.doi.org/%2010.13197/j.eeev.2017.02.26.dingbr.004, 2017.

Fang, W., Wang, J. and SHI, P.: Comprehensive Risk Governance: Database, Risk Map and Web Platform, Science Press, Beijing, China., 2011.

Gan, P.: Research on the Vulnerability and Damage Index of Seismic Building, M.S. Thesis, Institute of Engineering Mechanics, China Earthquake Administration, Harbin, China, 70 pp., 2009.

Gao, H., Bie, D. and Ma, J.: A Research on Vulnerability for Brick-Residence Buildings in Wenchuan Earthquake Areas, World Earthquake Engineering, 26(4), 73-77, 2010.

Ge, M., Chang, X. and Yiliyaer, A.: Direct Economic Loss and Post-earthquake Recovery and Reconstruction Fund Evaluation of Yutian Ms7.3 Earthquake on Feb.12, 2014, Inland Earthquake, 28(2), 104-112, http://dx.doi.org/10.16256/j.issn.1001-8956.2014.02.003, 2014.

Guo, X., Wang, Z. and Duan, C.: Earthquake Damage Assessment Method for Rural Timber Buildings, Building Science, 27(S2), 64-67, http://dx.doi.org/10.13614/j.cnki.11-1962/tu.2011.s2.035, 2011.

Han, X., Wang, Y. and Zeng, J.: The Seismic Damage Assessment of M4.4 Earthquake of Yuncheng Saline Lake District in March 12, 2016, Shanxi Architecture, 43(15), 21-22, 2017.

He, J. and Kang, R.: The Prediction of Seismic Hazard of Multi-Floor Brick Buildings in Weifang Area of Shandong Province, North China Earthquake Sciences, 17(1), 18-28, 1999.

He, J., Pan, W. and Zhang, J.: Study on the Vulnerability of Buildings in Rural Areas of Yunnan Province Based on Seismic Damage Statistics Since 1993, Building Structure, 46(S1), 379-383, 2016.

He, P. and Fu, G.: Initial Research on Seismic Loss Prediction for Cities in Zhujiang Delta, South China Journal of Seismology, 29(4), 114-126, http://dx.doi.org/10.13512/j.hndz.2009.04.015, 2009.

He, S., Wang, Q. and Gong, P.: Seismic Damage Prediction of Rural Houses in Shiyan City, China Earthquake Engineering Journal, 39(S), 195-201, http://sci-hub.tw/10.3969/j.issn.1000-0844.2017.Supp.0195, 2017.

He, Y., Li, D. and Fan, K.: Research on the Seismic Vulnerabilities of Building Structure in Sichuan Region, Earthquake Research in China, 18(1), 52-58, http://sci-hub.tw/10.3969/j.issn.1001-4683.2002.01.005, 2002.

Hu, S., Sun, B. and Wang, D.: Approach in Making Empirical Earthquake Damage Matrix, Journal of Earthquake Engineering and Engineering Vibration, 27(6), 46-50, http://dx.doi.org/10.13197/j.eeev.2007.06.010, 2007.

Hu, S., Sun, B. and Wang, D.: A Method for Earthquake Damage Prediction of Building Group Based on Building Vulnerability Classification, Journal of Earthquake Engineering and Engineering Vibration, 30(3), 96-101, http://dx.doi.org/10.13197/j.eeev.2010.03.009, 2010.

Hu, Y.: Earthquake Engineering, Seismological Press, Beijing, China, 1988.

Li, J., Li, Y. and Zhou, R.: Characteristics of Surface Rupture and Building Damage by Ms 6.3 Earthquake in Kangding of Sichuan, China, Mountain Research, 33(2), 249-256, http://sci-hub.tw/10.16089/j.cnki.1008-2786.000032, 2015.

Li, P.: Research on Evaluation and Comparison of Seismic Performance in China's Rural Residential Buildings, M.S. Thesis, Ocean University of China, Qingdao, China, 106 pp., 2014.

Li, S., Tan, M. and Wu, G.: Disaster Loss Assessment and Building Seismic Damage Characteristic of Atushi Earthquake with Ms5.2 in Xinjiang on March 11th, 2013, Inland Earthquake, 27(4), 341-347, http://dx.doi.org/10.16256/j.issn.1001-8956.2013.04.007, 2013.

Lin, S., Xie, L. and Gong, M.: Methodology for estimating seismic capacity of city building, Journal of Natural Disasters, 20(4), 31-37, http://dx.doi.org/10.13577/j.jnd.2011.0405, 2011.

Liu, H.: Seismic Disaster of Tangshan Earthquake, Seismological Press, Beijing, China, 1986.

Liu, J., Liu, Y. and Yan, Q.: Performance-based Seismic Fragility Analysis of CFST Frame Structures, China Civil Engineering Journal, 43(2), 39-47, http://dx.doi.org/10.15951/j.tmgcxb.2010.02.017, 2010.

Liu, J.: Performance-based Seismic Design and Seismic Vulnerability Analysis for Isolated High-rise Buildings, M.S. Thesis, Guangzhou University, Guangzhou, China, 111 pp., 2014.

Liu, Y.: Research on Vulnerability of RC Frame-core Wall Hybrid Structures Subjected to the Bidirectional Earthquake, M.S. Thesis, Xi'an University of Architecture and Technology, Xi'an, China, 80 pp., 2014.

Liu, Z.: Study on Seismic Fragility of Tall Reinforced Concrete Structures, Ph.D. Thesis, Institute of Engineering Mechanics, China Earthquake Administration, Harbin, China, 184 pp., 2017.

Lv, G., Zhang, H. and Sun, L.: The Vulnerability Analysis of Important Buildings in Langfang City, Journal of Seismological Research, 40(4), 638-645, 2017.

Ma, K. and Chang, Y.: Earthquake Disaster Prediction of Multistorey Masonry Building, Journal of Hefei University of Technology, 22(6), 58-61, 1999.

Meng, L., Zhou, L. and Liu, J.: Estimation of near-fault strong ground motion and intensity distribution of the 2014 Yutian, Xinjiang, Ms7.3 earthquake, Acta Seismologica Sinica, 36(3), 362-371, http://dx.doi.org/10.3969/j.issn.0253-3782.2014.03.003, 2014.

Meng, Z., Guo, M. and Zhao, H.: Seismic Damage Evaluation of the Important Multi-Storey Brick Concrete Buildings in Baoding, Technology for Earthquake Disaster Prevention, 7(4), 397-403, http://sci-hub.tw/10.3969/j.issn.1673-5722.2012.04.008, 2012.

Meng, Z., Zhao, H. and Guo, M.: Research on Seismic Damage Prediction of the Building Complex in Baoding, Journal of Seismological Research, 36(2), 202-206, http://sci-hub.tw/10.3969/j.issn.1000-0666.2013.02.011, 2013.

Ming, X., Zhou, Y. and Lu, Y.: Evaluation of Building Features and Seismic Capacity in Northwest Yunnan, Journal of Seismological Research, 40(4), 646-654, http://sci-hub.tw/10.3969/j.issn.1000-0666.2017.04.017, 2017.

Piao, Y.: Study on Housing Seismic Vulnerability of Yunnan and Qinghai Province, M.S. Thesis, Institute of Engineering Mechanics, China Earthquake Administration, Harbin, China, 72 pp., 2013.

Qiu, S. and Gao, H.: The Research of Rural Dwelling's Seismic Vulnerability in Qinghai, Technology for Earthquake Disaster Prevention, 10(4), 969-978, http://sci-hub.tw/10.11899/zzfy20150415, 2015.

Shi, W., Chen, K. and Li, S.: Hazard Index and Intensity of the 2007 Ning'er, Yunnan, Ms6.4 Earthquake, Journal of Seismological Research, 30(4), 379-383, http://sci-hub.tw/10.3969/j.issn.1000-0666.2007.04.012, 2007.

Shi, Y., Gao, X. and Tan, M.: Disaster Loss Assessment of the Minxian-Zhangxian Ms6.6 Earthquake, 2013, China Earthquake Engineering Journal, 35(4), 717-723, http://sci-hub.tw/10.3969/j.issn.1000-0844.2013.04.0717, 2013.

Song, L., Tang, L. and Yin, L.: Method for Establishing Fragility Matrix of Groups of Buildings in Shihezi City and its Earthquake Disaster Prediction, Inland Earthquake, 15(4), 320-325, http://sci-hub.tw/10.3969/j.issn.1001-8956.2001.04.005, 2001.

Sun, B. and Chen, H.: Urban Building Loss Assessment Method Considering the Decoration Damage due to Earthquake, Journal of Earthquake Engineering and Engineering Vibration, 29(5), 164-169, 2009.

Sun, B. and Zhang, G.: Statistical Analysis of the Seismic Vulnerability of Various Types of Building Structures in Wenchuan M8.0 Earthquake, China Civil Engineering Journal, 45(5), 26-30, http://dx.doi.org/10.15951/j.tmgcxb.2012.05.015, 2012.

Sun, B., Chen, H. and Yan, P.: Research on Zoned Characteristics of Buildings Seismic Capacity along North South Seismic Belt-take Sichuan Province as an Example, China Civil Engineering Journal, 47(S), 6-10, http://dx.doi.org/10.15951/j.tmgcxb.2014.s1.002, 2014.

Sun, B., Wang, M. and Yan, P.: Damage Characteristics and Seismic Analysis of Single-storey Brick Bent Frame Column Industrial in Lushan Ms7.0 Earthquake, Journal of Earthquake Engineering and Engineering Vibration, 33(3), 1-8, http://sci-hub.tw/10.11810/1000-1301.20130301, 2013.

Sun, L.: Research on the Earthquake Disaster Loss Assessment Method for Urban Areas and System Development, Ph.D. Thesis, Xi'an University of Architecture and Technology, Xi'an, China, 171 pp., 2016.

Wang, G.: The Performance-based Fragility Analysis of Base-isolated RC Frame Structure, M.S. Thesis, Lanzhou University of Technology, Lanzhou, China, 75 pp., 2013.

Wang, H., Huang, H. and Yu, W.: Analysis on the Regional Building Vulnerability Based on the Damage Influencing Factors, Inland Earthquake, 25(3), 275-282, http://dx.doi.org/10.16256/j.issn.1001-8956.2011.03.001, 2011.

Wang, Y., Shi, P. and Wang, J.: The Housing Loss Assessment of Rural Villages Caused by Earthquake Disaster in Yunnan Province, Acta Seismologica Sinica, 27(5), 551-560, http://sci-hub.tw/10.3321/j.issn:0253-3782.2005.05.010, 2005.

Wang, D. L., Wang, X. Q. and Dou, A. X.: Primary study on the quantitative relationship between the typical building structures in western China, Earthquake, 27(3), 105-110, http://sci-hub.tw/10.3969/j.issn.1000-3274.2007.03.014, 2007.

Wang, Y.: The Research and Manufacture of Urban Buildings Seismic Disasters Prediction Information System Based on ArcGIS, M.S. Thesis, Jiangxi University of Science and Technology, Ganzhou, China, 99 pp., 2007.

Wei, F., Cai, Z. and Jiao, S.: A Fast Approach to Regional Hazard Evaluation Based on Population Statistical Data, Acta Seismologica Sinica, 30(5), 518-524, http://sci-hub.tw/10.3321/j.issn:0253-3782.2008.05.010, 2008.

Wen, H., Hu, W. and Tan, M.: Preliminary Analysis on Earthquake Disaster of Building in Two Destructive Earthquakes of Xinjiang, Inland Earthquake, 31(4), 325-334, http://dx.doi.org/10.16256/j.issn.1001-8956.2017.04.001, 2017.

Wenliuhan, H., Zhang, Y. and Wang, D.: Review on Seismic Vulnerability and Economic Loss Assessment of Engineering Structures, Journal of Architecture and Civil Engineering, 32(6), 17-29, http://sci-hub.tw/10.3969/j.issn.1673-2049.2015.06.003, 2015.

Wu, S.: Seismic Vulnerability Analysis of Masonry Buildings, M.S. Thesis, Institute of Engineering Mechanics, China Earthquake Administration, Harbin, China, 85 pp., 2015.

Xia, S.: Assessment of Seismic Intensity with Mean Damage Index in an Earthquake-resistant Region, M.S. Thesis, Institute of Geophysics, China Earthquake Administration, Beijing, China, 128 pp., 2009.

Xu, W. and Gao, M.: Statistical analysis of the completeness of earthquake catalogues in China mainland, China Journal of Geophysics, 57(9), 2802–2281, http://dx.doi.org/10.6038/cjg20140907, 2014.

Yang, G.: The study of vulnerability analysis of existing buildings under earthquake disaster, M.S. Thesis, Shenyang Jianzhu University, Shenyang, China., 78 pp., 2015.

Yang, X.: Rapid Loss Assessment for Earthquake Disaster Using Seismic Spatial Information Grid, Ph.D., Thesis, Huazhong University of Science and Technology, Wuhan, China, 121 pp., 2014.

Yang, X., Yang, J. and Che, W.: Seismic Vulnerability Study of Buildings in Different Enforcing Zones in Yunnan Province, Value Engineering, 229-232, http://dx.doi.org/10.14018/j.cnki.cn13-1085/n.2017.12.095, 2017.

Ye, Z., Yan, J. and Yang, L.: Study on the Earthquake Damage Characteristics of Tibetan Dwellings in Sichuan Province, Earthquake Research in Sichuan, (4), 24-29, http://dx.doi.org/10.13716/j.cnki.1001-8115.2017.04.007, 2017.

Yin, Z.: Classification of Structure Vulnerability and Evaluating Earthquake Damage from Future Earthquake, Earthquake Research in China, 12(1), 49-55, 1996.

Yin, Z., Li, S. and Yang, S.: Estimating Method of Seismic Damage and Seismic Loss, Earthquake Engineering and Engineering Vibration, 10(1), 99-108, http://dx.chinadoi.cn/10.13197/j.eeev.1990.01.010, 1990.

Yu, X., Lv, D. and Fan, F.: Seismic Damage Assessment of RC frame Structures Based on Vulnerability Index, Engineering Mechanics, 34(1), 69-75, http://dx.doi.org/10.6052/j.issn.1000-4750.2015.09.0731, 2017.

Zeng, Z.: Fragility Analysis and Seismic Reliability of the Isolated Structure, M.S. Thesis, Guangzhou University, Guangzhou, China, 110 pp., 2012.

Zhang, G. and Sun, B.: A Method for Earthquake Damage Prediction of Building Groups Based on Multiple Factors, World Earthquake Engineering, 26(1), 26-30, 2010.

Zhang, J., Pan, W. and Song, Z.: An Assessment of Seismic Vulnerability of Urban Structures Based on the Intensity Gap, Earthquake Engineering and Engineering Dynamics, 37(4), 77-84, http://dx.doi.org/10.13197/j.eeev.2017.04.77.zhangj.009, 2017.

Zhang, Q., Cheng, M. and Niu, L.: Seismic Vulnerability Analysis of Masonry Structures after Earthquake in Panzhihua Area, Architecture Application, (10), 110-112, http://dx.doi.org/10.16001/j.cnki.1001-6945.2016.10.023, 2016.

Zhang, T., Gao, H. and Huang, H.: Study on Regional Factors that Influence the Results of Vulnerability Analysis - A Case Study in Fujian, Journal of Catastrophe, 26(3), 73-77, http://sci-hub.tw/10.3969/j.issn.1000-811X.2011.03.015, 2011.

Zhang, Y., Kang, J. and Wei, M.: Seismic Damage Evaluation of Building Based on GIS in Changchun, Journal of Northeast Normal University, 46(3), 124-131, http://sci-hub.tw/10.11672/dbsdzk2014-03-024, 2014.

Zheng, S., Yang, W. and Yang, F.: Seismic Fragility Analysis for RC Core Walls Structure Based on MIDA Method, Journal of Vibration and Shock, 34(1), 117-123, http://dx.chinadoi.cn/10.13465/j.cnki.jvs.2015.01.021, 2015.

Zhou, G., Fei, M. and Xie, Y.: Discussion of the Intensity VIII of the Ms5.8 Yingjiang Earthquake on Mar. 10, 2011, Journal of Seismological Research, 34(2), 207-213, http://dx.chinadoi.cn/10.3969/j.issn.1000-0666.2011.02.017, 2011.

Zhou, G., Hong, L. and Liu, C.: Research on Assessment of Building Direct Economic Loss of Earthquake Based on GIS, Geomatics and Spatial Information Technology, 36(10), 56-59, http://dx.doi.org/10.3969/j.issn.1672-5867.2013.10.017, 2013.

Zhou, G., Tan, W. and Shi, W.: Seismic Hazard Matrix of House Construction in Yunnan, Earthquake Research in China, 23(2), 115-123, http://dx.chinadoi.cn/10.3969/j.issn.1001-4683.2007.02.001, 2007.

Zhou, W. and Wang, S.: Investigation and Vulnerability Analysis of the Dwellings in South Fujian Province, Journal of Fuzhou University, 43(1), 123-128, http://dx.chinadoi.cn/10.7631/issn.1000-2243.2015.01.0123, 2015.

Zhu, J.: Seismic Fragility and Risk Analysis of RC Buildings, Ph.D. Thesis, Xi'an University of Architecture and Technology, Xi'an, China, 153 pp., 2010.

(References in Chapter 4)

Aubrecht, C., Steinnocher, K., K O Stl, M., Z U Ger, J. and Loibl, W.: Long-term spatio-temporal social vulnerability variation considering health-related climate change parameters particularly affecting elderly, Natural hazards, 68(3), 1371–1384, 2013.

Aubrecht, C., Gunasekera, R., Ishizawa, O. and Pita, G.: The flipside of "urban"—A novel model for built-up-adjusted rural-urban pattern identification and population reallocation, in CDRP Working Paper (Country Disaster Risk Profiles Initiative), The World Bank-Social, Urban, Rural & Resilience (GSURR), Disaster Risk Management (DRM) Washington DC, USA., 2015.

Aubrecht, C., Steinnocher, K., K O Stl, M., Z U Ger, J. and Loibl, W.: Long-term spatio-temporal social vulnerability variation considering health-related climate change parameters particularly affecting elderly, Natural hazards, 68(3), 1371–1384, 2013.

Aubrecht, C., Gunasekera, R., Ishizawa, O. and Pita, G.: The flipside of "urban"—A novel model for built-up-adjusted rural-urban pattern identification and population reallocation, in CDRP Working Paper (Country Disaster Risk Profiles Initiative), The World Bank-Social, Urban, Rural & Resilience (GSURR), Disaster Risk Management (DRM) Washington DC, USA., 2015.

Daniell, J.: Development of socio-economic fragility functions for use in worldwide rapid earthquake loss estimation procedures, Ph.D. Thesis, Karlsruhe Institute of Technology, Karlsruhe, Germany., 2014.

Daniell, J. E., Khazai, B., Wenzel, F. and Vervaeck, A.: The CATDAT damaging earthquakes database, Natural hazards and earth system sciences, 11(8), 2235–2251, doi:https://doi.org/10.5194/nhess-11-2235-2011, 2011.

Dobson, J. E., Bright, E. A., Coleman, P. R., Durfee, R. C. and Worley, B. A.: LandScan: a global population database for estimating populations at risk, Photogrammetric engineering and remote sensing, 66(7), 849–857, 2000.

Expert Panel of Earthquake Resistance and Disaster Relief (EPERDR): Comprehensive Disaster and Risk Analysis of Wenchuan Earthquake, Science Press, Beijing, China., 2008.

Figueiredo, R. and Martina, M.: Using open building data in the development of exposure data sets for catastrophe risk modelling, Natural Hazards and Earth System Sciences, 16(2), 417–429, 2016.

Gunasekera, R., Ishizawa, O., Aubrecht, C., Blankespoor, B., Murray, S., Pomonis, A. and Daniell, J.: Developing an adaptive global exposure model to support the generation of country disaster risk profiles, Earth-Science Reviews, 150, 594–608, 2015.

Hu, M., Bergsdal, H., Voet, E. van der, Huppes, G. and Müller, D. B.: Dynamics of urban and rural housing stocks in China, Building Research & Information, 38(3), 301–317, doi:10.1080/09613211003729988, 2010.

Jaiswal, K., Wald, D. and Porter, K.: A global building inventory for earthquake loss estimation and risk management, Earthquake Spectra, 26(3), 731–748, 2010.

Kleist, L., Thieken, A. H., K O Hler, P., M U Ller, M., Seifert, I., Borst, D. and Werner, U.: Estimation of the regional stock of residential buildings as a basis for a comparative risk assessment in Germany, Natural Hazards and Earth System Science, 6(4), 541–552, 2006.

Neumayer, E. and Barthel, F.: Normalizing economic loss from natural disasters: a global analysis, Global Environmental Change, 21(1), 13–24, 2011.

Silva, V., Crowley, H., Varum, H. and Pinho, R.: Seismic risk assessment for mainland Portugal, Bulletin of Earthquake Engineering, 13(2), 429–457, 2015.

Song, C.: Whole life and highgrade quality—stick to the idea of giving first consideration for the people and implement housing performance certification, Housing Science, 9(000), 2004.

Thieken, A. H., Olschewski, A., Kreibich, H., Kobsch, S. and Merz, B.: Development and evaluation of FLEMOps–a new Flood Loss Estimation MOdel for the private sector, WIT Transactions on Ecology and the Environment, 118, 315–324, 2008.

Wu, J., Li, N. and SHI, P.: Benchmark wealth capital stock estimations across China's 344 prefectures: 1978 to 2012, China Economic Review, 31, 288–302, doi:10.1016/j.chieco.2014.10.008, 2014.

Wu, J., Li, Y., Li, N. and Shi, P.: Development of an asset value map for disaster risk assessment in China by spatial disaggregation using ancillary remote sensing data, Risk analysis, 38(1), 17–30, 2018.

Wu, J., Ye, M., Wang, X. and Koks, E.: Building asset value mapping in support of flood risk assessments: A case study of Shanghai, China, Sustainability, 11(4), 971, 2019.

Yang, W. and Kohler, N.: Simulation of the evolution of the Chinese building and infrastructure stock, Building Research & Information, 36(1), 1–19, doi:10.1080/09613210701702883, 2008.

Yuan, Y.: Impact of intensity and loss assessment following the great Wenchuan Earthquake, Earthquake Engineering and Engineering Vibration, 7(3), 247–254, 2008.

Wu, J., Ye, M., Wang, X. and Koks, E.: Building asset value mapping in support of flood risk assessments: A case study of Shanghai, China, Sustainability, 11(4), 971, 2019.

Yuan, Y.: Impact of intensity and loss assessment following the great Wenchuan Earthquake, Earthquake Engineering and Engineering Vibration, 7(3), 247–254, 2008.

(References in Chapter 5)

Ambraseys, N. N., Simpson, K. u and Bommer, J. J.: Prediction of horizontal response spectra in Europe, Earthquake Engineering & Structural Dynamics, 25(4), 371–400, 1996.

ATC-13: Earthquake Damage Evaluation Data for California, 1985.

Bommer, J., Spence, R., Erdik, M., Tabuchi, S., Aydinoglu, N., Booth, E., Del Re, D. and Peterken, O.: Development of an earthquake loss model for Turkish catastrophe insurance, Journal of Seismology, 6(3), 431–446, 2002.

Caprio, M., Tarigan, B., Worden, C. B., Wiemer, S. and Wald, D. J.: Ground motion to intensity conversion equations (GMICEs): A global relationship and evaluation of regional dependency, Bulletin of the Seismological Society of America, 105(3), 1476–1490, 2015.

Cardona, O. D., Ordaz, M. G., Marulanda, M. C. and Barbat, A. H.: Estimation of probabilistic seismic losses and the public economic resilience—an approach for a macroeconomic impact evaluation, Journal of Earthquake Engineering, 12(S2), 60–70, 2008.

Cardona, O. D., Ordaz Schroder, M. G., Reinoso, E., Yamín, L. and Barbat Barbat, H. A.: Comprehensive approach for probabilistic risk assessment (CAPRA): international initiative for disaster risk management effectiveness, in 14th European Conference on Earthquake Engineering, pp. 1–10., 2010.

Chan, L. S., Chen, Y., Chen, Q., Chen, L., Liu, J., Dong, W. and Shan, H.: Assessment of global seismic loss based on macroeconomic indicators, Natural Hazards, 17(3), 269–283, 1998.

Chen, Q.-F., Chen, Y., Liu, J. I. E. and Chen, L.: Quick and approximate estimation of earthquake loss based on macroscopic index of exposure and population distribution, Natural Hazards, 15(2–3), 215–229, 1997.

Chen, J. and Tao, L.: Damage of the Great Wenchuan Earthquake----Records of the Seismic Damage Mitigation Efforts in Sichuan (汶川特大地震四川抗震救灾志-灾情卷), Sichuan People Press, Sichuan, China., 2018.

Daniell, J.: Development of socio-economic fragility functions for use in worldwide rapid earthquake loss estimation procedures, Ph.D. Thesis, Karlsruhe Institute of Technology, Karlsruhe, Germany., 2014.

Ding, B., Sun, J., Du, K. and Luo, huan: Study on relationships between seismic intensity and peak ground acceleration, peak ground velocit, Earthquake Engineering and Engineering Dynamics, 37(2), 26–36, doi:http://dx.doi.org/%2010.13197/j.eeev.2017.02.26.dingbr.004, 2017.

Erdik, M., Aydinoglu, N., Fahjan, Y., Sesetyan, K., Demircioglu, M., Siyahi, B., Durukal, E., Ozbey, C., Biro, Y. and Akman, H.: Earthquake risk assessment for Istanbul metropolitan area, Earthquake Engineering and Engineering Vibration, 2(1), 1–23, 2003.

ERN-AL: CAPRA: Comprehensive Approach for Probabilistic Risk Assessment. [online] Available from: http://www.ecapra.org/, 2010.

Faccioli, E. and Cauzzi, C.: Macroseismic intensities for seismic scenarios estimated from instrumentally based correlations, in Proc. First European Conference on Earthquake Engineering and Seismology, paper., 2006.

FEMA2008: HAZUS-MH estimated annualized earthquake losses for the United States, Department of Homeland Security, Federal Emergency Management Agency, Mitigation Division, Washington DC, United States. [online] Available from: https://secure.madcad.com/media/fema/FEMA-366-2008.pdf, 2008.

Jaiswal, K. and Wald, D. J.: Estimating economic losses from earthquakes using an empirical approach, Earthquake Spectra, 29(1), 309–324, 2013.

Kircher, C. A., Nassar, A. A., Kustu, O. and Holmes, W. T.: Development of building damage functions for earthquake loss estimation, Earthquake spectra, 13(4), 663–682, 1997.

Li, B.: Seismotectonics and seismic hazard of the Shanxi Rift System, North China, PhD Thesis, University of Bergen, Bergen, Norway., 2015.

Li, X., Yu, A., Gan, P., Li, M. and Liu, L.: Survey and analysis of the disaster and engineering damage of Beichuan County in Ms8.0 Wenchuan Earthquake, Technology for Earthquake Disaster Prevention, 3(4), 352–263, 2008.

Lu, J. Q., Li, S. Y. and Li, W.: Study on ground motion attenuation relationship of moderate earthquake risk areas, World Earthquake Engineering, 25(4), 33–43, 2009.

Ma, Q., Li, S., Li, S. and Tao, D.: On the correlation of ground motion patterns with seismic intensity, Earthquake Engineering and Engineering Dynamics, 34(4), 83–92, doi:10.13197/j.eeev.2014.04.83.maq.011, 2014.

Marulanda, M. C., Carreno, M. L., Cardona, O. D., Ordaz, M. G. and Barbat, A. H.: Probabilistic earthquake risk assessment using CAPRA: application to the city of Barcelona, Spain, Natural hazards, 69(1), 59–84, 2013.

Medvedev, S. V. and Sponheuer, W.: Scale of seismic intensity, in Proc. IV World Conference of the Earthquake Engineering, Santiago, Chile, A-2, pp. 143–153., 1969.

Murphy, J. u and O'brien, L. J.: The correlation of peak ground acceleration amplitude with seismic intensity and other physical parameters, Bulletin of the Seismological Society of America, 67(3), 877–915, 1977.

Ordaz, M., Miranda, E., Reinoso, E. and Pérez-Rocha, L. E.: Seismic loss estimation model for Mexico City, Universidad Nacional Autónoma de México, México DF, 1998.

Silva, V., Crowley, H., Varum, H., Pinho, R. and Sousa, L.: Investigation of the characteristics of Portuguese regular moment-frame RC buildings and development of a vulnerability model, Bulletin of Earthquake Engineering, 13(5), 1455–1490, 2015.

Spence, R., Bommer, J., Del Re, D., Bird, J., Aydinoğlu, N. and Tabuchi, S.: Comparing loss estimation with observed damage: a study of the 1999 Kocaeli earthquake in Turkey, Bulletin of Earthquake Engineering, 1(1), 83–113, 2003.

Sun, B. and Chen, H.: Urban Building Loss Assessment Method Considering the Decoration Damage due to Earthquake, Journal of Earthquake Engineering and Engineering Vibration, 29(5), 164–169, 2009.

Tselentis, G.-A. and Danciu, L.: Empirical relationships between modified Mercalli intensity and engineering ground-motion parameters in Greece, Bulletin of the Seismological Society of America, 98(4), 1863–1875, 2008.

Wald, D. J., Quitoriano, V., Heaton, T. H., Kanamori, H., Scrivner, C. W. and Worden, C. B.: TriNet "Shake-Maps": Rapid generation of peak ground motion and intensity maps for earthquakes in southern California, Earthquake Spectra, 15(3), 537–555, 1999.

Worden, C. B., Gerstenberger, M. C., Rhoades, D. A. and Wald, D. J.: Probabilistic Relationships between Ground-Motion Parameters and Modified Mercalli Intensity in California, Bulletin of the Seismological Society of America, 102(1), 204–221, doi:10.1785/0120110156, 2012.

Xin, D., Daniell, J. and Wenzel, F.: Review of fragility analyses for major building types in China with new implications for intensity-PGA relation development, Nat. Hazards Earth Syst. Sci, 2019.

Yeats, R. S., Sieh, K. E. and Allen, C. R.: The geology of earthquakes, Oxford University Press, USA., 1997.

Yu, Y. X., Li, S. Y. and Xiao, L.: Development of ground motion attenuation relations for the new seismic hazard map of China, Technol. Earthq. Disaster Prev., 8(1), 24–33, doi:http://dx.china-doi.cn/10.3969/j.issn.1673-5722.2013.01.003, 2013.

Yuan, Y.: Impact of intensity and loss assessment following the great Wenchuan Earthquake, Earthquake Engineering and Engineering Vibration, 7(3), 247–254, 2008.

(References in Chapter 7)

Bommer, J., Spence, R., Erdik, M., Tabuchi, S., Aydinoglu, N., Booth, E., Del Re, D. and Peterken, O.: Development of an earthquake loss model for Turkish catastrophe insurance, Journal of Seismology, 6(3), 431–446, 2002.

Pagani, M., Monelli, D., Weatherill, G., Danciu, L., Crowley, H., Silva, V., Henshaw, P., Butler, L., Nastasi, M. and Panzeri, L.: OpenQuake engine: An open hazard (and risk) software for the global earthquake model, Seismological Research Letters, 85(3), 692–702, 2014.

Park, J., Bazzurro, P. and Baker, J. W.: Modeling spatial correlation of ground motion intensity measures for regional seismic hazard and portfolio loss estimation, Applications of statistics and probability in civil engineering, 1–8, 2007.

Sokolov, V. and Wenzel, F.: Influence of spatial correlation of strong ground motion on uncertainty in earthquake loss estimation, Earthquake Engineering & Structural Dynamics, 40(9), 993–1009, 2011.